SYNTHESIS AND CHARACTERIZATION OF CATALYSTS FOR DIMETHYL CARBONATE PRODUCTION

Ph.D. THESIS

by

PRAVEEN KUMAR

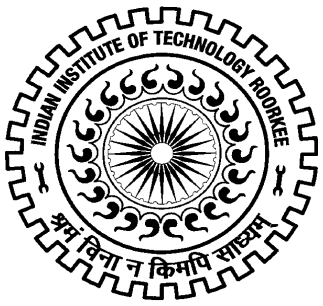

DEPARTMENT OF CHECHICAL ENGINEERING
INDIAN INSTITUTE OF TECHNOLOGY ROORKEE
ROORKEE - 247 667 (INDIA)

June, 2015

SYNTHESIS AND CHARACTERIZATION OF CATALYSTS FOR DIMETHYL CARBONATE PRODUCTION

A THESIS

Submitted in partial fulfilment of the requirements for the award of the degree

of

DOCTOR OF PHILOSOPHY

in

CHEMICAL ENGINEERING

by

PRAVEEN KUMAR

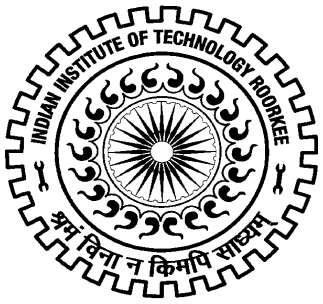

DEPARTMENT OF CHEMICAL ENGINEERING
INDIAN INSTITUTE OF TECHNOLOGY ROORKEE
ROORKEE - 247 667 (INDIA)

June, 2015

INDIAN INSTITUTE OF TECHNOLOGY ROORKEE
ROORKEE

CANDIDATE'S DECLARATION

I hereby certify that the work which is being presented in this thesis entitled **"SYNTHESIS AND CHARACTERIZATION OF CATALYSTS FOR DIMETHYL CARBONATE PRODUCTION**" in partial fulfilment of the requirement for the award of the Degree of Doctor of Philosophy and submitted in the Department of Chemical Engineering of the Indian Institute of Technology Roorkee is an authentic record of my own work carried out during a period from December, 2010 to June, 2015 under the supervision of Dr. V. C. Srivastava, Associate Professor and Dr. Indra Mani Mishra, Professor, Department of Chemical Engineering, Indian Institute of Technology Roorkee, Roorkee.

The matter presented in this thesis has not been submitted by me for the award of any other degree of this or any other Institute.

(PRAVEEN KUMAR)

This is to certify that the above statement made by the candidate is correct to the best of our knowledge.

(V. C. Srivastava) (I. M. Mishra)

Date: June , 2015 Supervisor Supervisor

ABSTRACT

The need for eco-friendly fuels for transport vehicles has spurred the search for new molecules and their viable and cost-effective synthesis method. Several research groups are working on the production techniques of dimethyl carbonate (DMC) and its usage as a fuel additive for vehicles. DMC can also be used as a reactant for the synthesis of diphenyl carbonate, glycerol carbonate, etc. DMC is commercially synthesized by using various methods, such as phosgenation, oxidative carbonylation, methyl nitrite carbonylation, etc. Although each production method has its own drawbacks, transesterification of propylene carbonate (PC) with methanol is considered to be a promising and feasible method for the synthesis of DMC. This route is sustainable, clean, with no formation of any harmful or waste by-product. Recently, utilization of CO_2 for the synthesis of chemicals has attracted a lot of attention. DMC can also be produced from CO_2, although this route has thermodynamic limitations.

An exhaustive review of the literature reveals that only a few catalysts have been tested for the DMC production via transesterification and direct CO_2 conversion reactions. Considering various possibilities, the main aim of the present work was to prepare and characterize various catalysts (CeO_2-based mixed oxide, hydrotalcites and supported catalysts) with different physico-chemical and textural characteristics; and to evaluate catalytic activity for the synthesized catalysts for DMC synthesis via transesterification and direct conversion of CO_2 reactions. It was also aimed to optimize the operating conditions such as temperature, pressure, molar ratio, amount of catalyst and to study the kinetics and thermodynamics of the DMC synthesis; and to explore the catalytic stability and recyclability of the synthesized catalysts, and to investigate the possible mechanism, kinetics and thermodynamics of DMC synthesis with different reactions.

Work of the transesterification reaction of PC for DMC production

Transesterification reaction of PC with methanol for the DMC production was studied with four different sets of catalysts, namely: Ce-M (M=Co, Fe, Cu and Zn), Ceria-Lanthanum, Ceria-Zinc-support mixed metal oxide and copper-zinc-aluminium hydrotalcite catalysts.

Ce–M catalysts (M=Co, Fe, Cu and Zn) were synthesized by sol-gel method and characterized by various techniques. BET surface area of CeCo, CeCu, CeFe and CeZn catalysts was found to be 40, 46, 24, and 37 m^2/g, respectively. CeCu catalyst having highest basicity was found to be most effective during transesterification of PC to form DMC. Highest DMC yield of 71.9% and PC conversion of 65.4% was obtained with CeCu catalyst at the optimum reaction condition.

A series of cerium-lanthanum catalysts were prepared using co-precipitation method. Catalytic activity was found to increase with an increase in the reaction temperature, reaction time and methanol/PC molar ratio and was found to be maximum in terms of DMC yield=74%, propylene glycol (PG) yield=65% and PC conversion=72% at optimum reaction conditions of reaction temperature=170°C, reaction time=6 h and methanol/PC molar ratio=10. Best catalytic activity was found for the catalyst having Ce/La molar ratio of 1/4.

Ceria and zinc oxide were impregnated onto various oxide supports such as alumina (Al_2O_3), silica (SiO_2) and titania (TiO_2) in the molar ratio of 1:1:2 by deposition-coprecipitation method (CZA, CZS and CZT having supports Al_2O_3, TiO_2 and SiO_2, respectively). CZS having highest basicity and surface area showed best catalytic activity. The basic strength of SiO_2 also helps in improving the highest catalytic activity.

Cu-Zn-Al (CZA) hydrotalcite catalysts prepared by the co-precipitation method and calcined at 300°C, 500°C and 800°C (named as CZA300, CZA500 and CZA800) were used

for the synthesis of DMC from methanol and PC. Pore volume distribution analysis revealed that the CZA300 and CZA500 have bimodal pore distribution with pores centered at 36±1 Å and 131±2 Å. Overall, an increase in the calcination temperature decreased the quantity of basic and acidic sites. Values of specific rate of reaction with CZA300 catalysts at 120°C, 140°C and 160°C were found to be 0.56, 0.58 and 0.65 h^{-1}, respectively. PC conversion of 70% and DMC selectivity of 94% was observed at the optimum operating condition of reaction time=4 h, methanol/PC molar ratio=10, catalyst dose=3 wt.% of PC and temperature=160 °C.

Values of the frequency factor (k_o) and the activation energy (E_a) were found to be 0.375 h^{-1} and 2.294 kJ/mol for CeCu catalyst, whereas respective values for CZA300 catalyst were found to be 0.225 h^{-1} and 12.72 kJ/mol. Among all the catalysts tested, Ce-Zn/SiO_2 showed highest PC conversion of 89% and DMC yield of 78%. Overall supported catalysts seem to be better option for use in the transesterification reaction of PC with methanol for DMC synthesis.

Work of the direct conversion of CO_2 to DMC

DMC synthesis via direct conversion of CO_2 was studied with different sets of catalysts namely: ceria-zirconium, ceria-manganese and ceria-calcium catalysts.

The catalysts CeO_2, ZrO_2 and $Ce_{0.5}Zr_{0.5}O_2$ were synthesized by hydrothermal method. The basic sites density and the acidic site density of synthesized catalysts were in the order: $ZrO_2 < CeO_2 < Ce_{0.5}Zr_{0.5}O_2$. Under optimized reaction condition of reaction temperature=120 °C, reaction time=24 h, catalysts dose=1.25 g and pressure=150 bar, the optimum yield of DMC was obtained as 2.56 mmol/g-cat for $Ce_{0.5}Zr_{0.5}O_2$ catalyst.

Cerium-zirconium mixed oxide catalysts were also synthesized using an exo- and endo-templating method applying different Ce_x-Zr_{1-x} (x=0 to 1) molar ratios. Polymer based activated carbon spheres were used as exo-template, and pluronic was used as endo-template. The Ce_x-Zr_{1-x} (x=0.5) catalyst showed the highest basic sites and acidic site among all the catalysts, and giving the highest DMC yield.

MnO_x-CeO_2 catalysts were synthesized by surfactant-template method with different ratio of Mn/Ce. The optimum yield of 2.514 mmol was found with Ce_1-$Mn_{0.125}$ at a pressure of 150 bar, reaction temperature 140°C, catalysts dose 1.25 g and reaction time 24 h. A series of CeO_2-CaO catalysts with different Ce/Ca ratio (Ce_3-Ca_1, Ce_1-Ca_1, and Ce_1-Ca_3) were synthesized by surfactant-template method. Hexadecyltrimethyl ammonium bromide (CTAB) was used as the template. Ce_1-Ca_1 catalyst was found to possess highest activity owing to its high surface area, acidity and basicity as compared to other catalysts.

Basic thermodynamic calculation shows that DMC synthesis from CO_2 and methanol at 393 K becomes spontaneous at pressure $\geq 6.3\times10^4$ MPa which is very difficult to achieve. The Peng–Robinson–Stryjek–Vera equation of state (PRSV-EoS) along with the van der Waals one-fluid (1PVDW) mixing rule, were used to calculate the fugacity coefficient of species in the mixture which in turn was used to calculate equilibrium conversion at various temperatures. The values of the heat of reaction (ΔH_r^o) and Gibbs free energy change (ΔG_r^o) for $Ce_{0.5}Zr_{0.5}O_2$ (hydrothermal method) using the data points at T=120-150°C were found to be -45.66 kJ/mol and 25.04 kJ/mol, respectively. Similarly, for $Ce_{0.5}Zr_{0.5}O_2$ (templating method), the respective values were found to be -139.76 kJ/mol and 1.54 kJ/mol, respectively.

Overall, $Ce_{0.2}$-$La_{0.8}$ and Ce-Zn/SiO_2 were found to be the best catalysts for DMC production via transesterification reaction, whereas Ce_1-Ca_1 and $Ce_{0.5}Zr_{0.5}O_2$ were the best catalysts for direct CO_2 conversion reaction for DMC production.

ACKNOWLEDGEMENT

I would like to express my sincere gratitude to my both the thesis supervisors Prof. I. M. Mishra, Professor and Dr. V. C. Srivastava, Associate Professor, Department of Chemical Engineering, Indian Institute of Technology Roorkee, for their guidance, enthusiasm and insight in supervising the thesis. They provided a motivating, enthusiastic and critical atmosphere during discussions. I thank them for their immense support, outstanding guidance and encouragement. It was a great pleasure for me to conduct this thesis under their supervision. I owe them lots of gratitude for giving the freedom of thought, amiable environment and motivation which provided in me a confidence in analysing my research problems. The enormous knowledge that I gained during their inspiring guidance would be enormously valuable to me for all my future endeavors.

I am also thankful to Prof. Roger Gläser, who kindly agreed to be my host supervisor at Institute of Chemical Technology, University of Leipzig, Germany for my DAAD fellowship stay. He was always excited about my projects and was interested in discussions despite of his busy schedule. I would like to extend my thanks to Prof. Dirk Enke, Dr. Patrick With, Dr. M.M. Azim, Dr. Michael Kästetoast, Ms. Erissa Saraci, Ms. Sepideh Banakhojasteh and Ms. Katrin Kunze.

I wish to express my sincere thanks to Prof. I. D. Mall, Prof. Basheshwar Parsad and Dr. Vimal Kumar, Department of Chemical Engineering, IIT Roorkee, and their invaluable and unconditional support. His inspiration provided me the strength to carry out this research. I wish to express my sincere gratitude to the members of advisory committee namely Prof. Mala Nath for her encouragement and critical input to work hard during the course of my Ph.D. degree.

I would like to take this opportunity to put on record my gratitude to Head, Prof. C. B. Majumder, Department of Chemical Engineering, IIT Roorkee for providing the various basic facilities for carrying out the present research work. My sincere thanks are also for Prof. V. K. Agarwal, Prof. Bikash Mohanty and Prof. Shri Chand, Prof. Shishir Sinha and all faculty members of the Department of Chemical Engineering, IIT, Roorkee for their kind assistance and encouragement. I am also thankful to Prof. Ramesh Chandra, Head, Institute Instrumentation Centre, IIT Roorkee for his generous assistance and facilitation in the analysis of the samples.

I owe my grateful thanks to my friends, especially Jyoti Sharma, Parth Kundu, Nilamber and many others who generously helped and encouraged me during my research work. I am also greatly indebted to Ravikant Gupta, Vijay Verma, Anil Verma,

Satyanarayana Murthy, Nitin Pandhare, Seema Singh, T. Sandeep Kumar, Ajay Hiwarkar, Ranvir Singh, Kartikeya Shukla and Kaushal Kishor for their moral encouragement. I would like to extend my thanks to Shivam Kumar, Subham Kumar Jain, Sumukh Verma for their help during thermodynamics and kinetics study.

I would like to thank all employees and former employees of the Department: Dr. Rajendra Bhatnagar, Shri Satyapal Singh, Shri Arvind Kumar, Shri Vipin Ikka, Shri Tara Chand, Shri Ayodhya Prasad, Shri Suresh Sani, Shri S.K. Susodia, etc., who helped me during the course of my experimental work and analysis of the samples. Finally my warm thanks to Shri Arun Kumar, Shri Shadab Ali and Shri Sudesh.

I am also very thankful to Mrs. Kanchan Lata Srivastava and beloved Bhavishya for their cooperation and warm-hearted nature, whenever I went to Dr. V.C. Srivastava residence.

I sincerely thank the Indian Institute of Technology, Roorkee and the Ministry of Human Resource and Development, Government of India, for providing financial support to undertake the work. The Institute is great and the environment is supportive to the research activities. I am also thankful to DAAD (German Academic Exchange Service) for a short term doctoral fellowship.

I would like to express my sincere love and affection to my father Shri Satbir Singh, mother Shrimati Saroj Bala, my sister Rashmi, Jiju Varun Singh and all my family members, for their persistent love, support and encouragement in my life. I have no any suitable word for my mother and father, for their everlasting love and blessing to me. I am extremely conscious of the crucial role played by Ms. Ramanpreet Kaur during my research work. Without his support it is simply impossible for me to complete my doctoral research work. I thank her from the bottom of my heart for her patience and support at each step of this journey.

I would like to thank am thankful to all of them and extremely sorry if anyone is left out in the acknowledgement. I thank God for helping me in one way or the other and providing strength to me and to my family members to bear the pains of remaining away from them for long duration.

PRAVEEN KUMAR

CONTENT

LIST OF FIGURES

LIST OF TABLES

ABBREVIATIONS AND NOTATIONS

ABBRIVATIONS

AAS	Atomic absorption spectrometer
ABMDFP	ammonium bromide/dicyandiamide–formaldehyde polymer
AFM	Atomic force microscopy
AR	Analytical grade
BET	Brunauer-Emmett-Teller
BisAG	Bisphenol A diglycidyl ether
BJH	Barrett-Joyner-Halenda
bmimBr	1-Butyl-3-methylimidazolium bromide
BO	butylene oxide
Cal	Calcination temperature
cat.	Catalyst
Cat/CH_3OH	Catalyst dose with respect to methanol
CH_3OK	Potassium Methoxide
CHD	1,2-cyclohexanediol
CHNS	Elemental analysis
CHO	Cyclohexane oxide
CIPO	Epi-chlorohydrin
C_{MC}	Conversion methyl carbamate
C_{MeOH}	Conversion of methanol
CO	Carbon monoxide
CO_2-TPD	CO_2-temperature programmed desorption
CP	2-cyanopyridine
C_{PO}	Conversion of PO
C_{SO}	Conversion of SO
CTAB	hexadecyltrimethyl ammonium bromide
DABCO	1,4-Diazabicyclo[2.2.2]octane
DBU	1,8-Diazabicyclo-[5.4.0]undec-7-ene
DCC	Dicyclohexylcarbodiimide
DFT	Density functional theory
DMC	Dimethyl carbonate
DME	Dimethyl ether
DMM	Dimethoxy methane
DMO	Dimethyl oxalate
DTA	Differential thermal analysis

DTG	Differential thermal gravimetery
EC	Ethylene carbonate
EDBS	Electron backscatter diffraction
EDX	Energy-dispersive X-ray spectroscopy
$EMImBF_4$	1-Ethyl-3-Methylimidazolium Tetrafluoroborate
EMImCl	1-Ethyl-3-methylimidazolium chloride
EO	Ethylene oxide
EOS	Equations of state
EPR	Electron paramagnetic resonance
ESR	Electron spin resonance
fcc	Face-centered cubic
FHH	Frenkel-Halsey-Hill
FID	Flame ionization detector
FTIR	Fourier transformed infrared spectroscopy
FWHM	full width of the reflection at half maximum
GC	Gas chromatograph
GHSV	Gas hourly space velocity
hcp	Hexagonal close-packed
He	Helium
HP-NMR	High performance-nuclear magnetic resonance
HTLc	Hydrotalcite-like compounds
ICDD	International centre for diffraction data
ICP-AES	Inductively coupled plasma atomic emission spectroscopy
IR	Infrared spectroscopy
IUPAC	International union of pure and applied chemistry
JCPDS	Joint committee on powder diffraction standards
LD_{50}	Lethal dose
LHSV	Liquid hourly space velocity
MC	Methyl carbonate
MCM-41	Mobil composition of matter-41
MeOH	Methanol
MF	Methyl formate
MF	Methyl formate
MTBE	Methyl tert-butyl ether
$n\text{-}Bu_3N$	n-butylamines
n-Bu4NBr	Tetra-n-butylammonium bromide
NMR	Nuclear magnetic resonance

NO	Nitrogen monoxide
OSC	Oxygen storage capacity
PBSAC	Polymer-based spherical activated carbon
PC	Propylene carbonate
P_{CO}	Pressure of CO (continuous flow)
PDF	Powder diffraction file
PG	Propylene glycol
PO	Propylene oxide
P_{O2}	Pressure of O_2 (continuous flow)
PP	Polypropylene
PPA	Polyphosphoric acid
PRSV EoS	Peng–Robinson–Stryjek–Vera equation
SBA-15	Santa Barbara amorphous-15
SCI	Science citation index
S_{CO}	Selectivity of CO
S_{DMC}	Selectivity of DMC
S_{DMO}	Selectivity of DMO
SEAD	Selected area electron diffraction
SEM	Scanning electron microscopic
SEM-EDX	Scanning electron microscope-energy dispersive atomic spectra
S_{MN}	Selectivity of methyl formate
SO	Styrene oxide
S_{PC}	Selectivity of PC
S_{PG}	Selectivity of PG
Stirr	Stirring speed
STY	Space time
SV	Space velocity
t	Reaction time
TBC	Triblockcopolymer
TCD	Thermal conductivity detector
TEM	Transmission electron microscopy
TGA	Thermogravimetric analysis
TMP	Trimethyl phosphate
TOF	Turn over frequency
TPD	Temperature programmed desorption
TPD-Methanol	Temperature programmed desorption-Methanol
TPR	Temperature programmed oxidation

XPS	X-ray photoelectron spectroscopy
XRD	X-ray diffraction
Y_{CHO}	Yield of cyclohexane oxide
Y_{DMC}	Yield of DMC
Y_{DMO}	Yield of DMO
Y_{DMO}	Yield of DMO.
ZrPP	Zirconium phenylphosphonate phosphate
1PVDW	van der waals One-Fluid

NOTATIONS

a	Mixture parameter in PRSV
A_{cat}	Mass of catalyst
a_{ij} , b_{ij}	UNIQUAC binary interaction parameter
b	Mixture parameter in PRSV
$C_{MeOH,e}$	Concentrations of methanol at equilibrium
$C_{MeOH,o}$	Initial concentration of methanol
$C_{MeOH,t}$	Concentrations of methanol at time t
C_p	Heat capacity
$C_{PC,e}$	Concentrations of PC at equilibrium
$C_{PC,o}$	Initial concentration of PC
$C_{PC,t}$	Concentrations of PC at time t
D	Fractal dimension
E_a	Activation energy
g	Gram
G	Gibbs free energy
H	Enthalpy
i,j	Interaction between components i and j
K	Scherrer's constant
k	Rate constant
k'	Specific kinetic constant
K_C	Reaction equilibrium constant
K_{eq}	Equilibrium constant
K_{FHH}	Constant
k_o	Initial rate of reaction
L	Crystallite size
l_{ij}, k_{ij}	Binary interaction parameter in 1PVDW mixing rule
mL	Mili litter

m_{PC}	Initial mole
M_{PC}	Molecular weight of PC
n	Number of experimental points
P	Pressure or Partial vapour pressure
P_c	Critical pressure
P_{CO}	Pressure of CO (continuous flow)
P_o	Saturated pressure
P_{O2}	Pressure of O_2 (continuous flow)
P_{total}	Total pressure
q	Amount of N_2 adsorbed at equilibrium pressure
Q_1	Heat of liquefaction
Q_a	Heat of adsorption
q_e	Amount adsorbed filling micropore volume
q_i	Area parameter
r	Reaction rate according to PC
R	Ideal gas constant
r_i	Volume parameter
r_k	Kelvin' radius
rpm	Rate per minute
S	Entropy
T	Temperature
t	Time
T_c	Critical temperature
V	Volume, vapor
V_a	Volume of gas adsorbed
V_m	Monolayer volume
x	liquid molar fraction
x_i	Mole fraction
X_{PC}	Conversion of PC
y	Vapour molar fraction
B	Full width of the reflection at half maximum angle
θ	Scattering angle
θ`	Wetting angle
λ	Wavelength of X-ray radiation
σ	Surface tension
τ_{ij}	Binary interaction coefficient
υ_i	Stoichiometric coefficient at equilibrium

γ_i	Activity coefficient
ΔH_r^o	Enthalpy of reaction
ΔG_r^o	Gibbs energy of reaction
ΔH_f^o	Enthalpy of reaction of product
ΔG_f^o	Gibbs free energy change of product
$\Delta_r H^{Ø}$	Reaction heats
$\Delta_r G^{Ø}$	Gibb's function change
ΔH_r	heat of reaction
°C	Degree centigrade temperature

Subscripts

o or 0	Initial
e	Element
eq	At equilibrium
f	Formation
i,j	Component
k	Group number in Bension's method
rex	Reaction

Greek Letters

Δ	Change
Θ	CO_2/CH_3OH feed molar ratio
$Ø_{\text{or }\theta}$	UNIQUAC parameter
ω	Accentric factor
Φ_i	Fugacity coefficient of vapor
γ_i	Activity coefficient of liquid

Chapter-1

INTRODUCTION

1.1. GENERAL

In the last few decades, environmental impact of chemical substances and their effect on human health has become a critical issue. Owing to this problem, the environmentally benign clean processes and green chemicals are being developed. Green chemistry is one of the approaches which can help in achieving this goal. Synthesis of green organic chemicals must avoid use of toxic raw material and chemicals, must be atom efficient and use renewable materials, eco-compatible solvents and avoid auxiliary substances, use catalysts rather than stoichiometric reagents, produce compounds better than existing ones which are biodegradable and non-toxic, reduce energy requirements and produce no waste [Tundo, 2001; Tundo and Selva, 2002]. The need for eco-friendly fuels for transport vehicles has spurred the search for new molecules either as a fuel or an additive to fuels, and methods for their viable and cost-effective synthesis, purification and scale-up design for commercial production. For gasoline as a motor fuel, a number of additives as an oxygenate are being used. For example, methanol, ethanol, dimethyl ether (DME) and methyl tert-butyl ether (MTBE). Dimethyl carbonate (DMC) has also emerged as an alternative oxygenate. Several research groups are working on the production of DMC and its usage as a fuel additive for vehicles [Keller et al., 2010].

CO_2, a green house gas, is considered to be largely responsible for the phenomena of global warming and as an agent of climate change. Over the last two decades, mitigation of CO_2 emission has become an important area of research. CO_2 has a number of useful industrial and domestic applications. All the application of CO_2 can be classified into two categories namely physical and chemical applications. Physical applications include its usage in enhanced oil recovery, beverage industry, supercritical CO_2 extraction, etc. It should be noted that these applications do not directly reduce the emission in most of the cases.

Chemical application involves use of CO_2 as a raw material for its chemical conversion for the production of useful materials and molecules. Thus Chemical applications directly contribute to reduction of CO_2 emission.

CO_2 is available as an abundant, cheap, non-toxic and inexpensive renewable resource which can be utilized for the synthesis of a variety of chemicals. However, the transformation of CO_2 to valuable products requires high energy. Therefore, this transformation can be based on choosing high energy reactants or by selecting less energized products. Various catalysts are also being used to lower this energy requirement barrier and enhance the productivity using different routes.

CO_2 behaves as Lewis acid because of the lower electron density of the carbonyl group in CO_2. Methods are being developed to transform of CO_2 into DMC in the presence of a catalyst. It may be denoted that CO_2 utilization requires intensive research as it gives a very low DMC yield because of thermodynamic constraints [Cui et al., 2013]. The research has to focus on the reaction schemes so as to shift the equilibrium of the reaction towards the product side [Delledonne et al., 2001].

1.2. DIMETHYL CARBONATE

DMC is considered as an environment friendly green chemical which is widely used in the synthesis of polymers, pesticides, flavoring agents, foodstuff, solvents, dyestuff and composite materials due to its high versatility, excellent biodegradability, high oxygen content and low bioaccumulation [Pacheco and Marshall, 1997; Ono, 1997; Delledonne et al., 2001; Keller et al., 2010;]. Synthesis and application of DMC for various usages has attracted considerable attention in recent years.

1.2.1. Properties of DMC

DMC is a transparent liquid with melting point of 4.6°C, boiling point of 90.3°C, flash point of 21.7°C, auto-ignition temperature of 458°C, cetane number of 45, lower heating value of 55.6 MBtu/gal, heat of combustion of 3452 kcal/kg, and specific gravity of

1.07 [Keller et al., 2010]. It is miscible in organic solvents such as ketones, acetate esters and water. It has excellent blending properties with gasoline. It has low toxicity with its lethal dose (LD_{50}) for rats being 13.8 g/kg. Thus, the DMC is practically a non-toxic, volatile and flammable organic compound, and is easily biodegradable.

1.2.2. Uses of DMC

DMC is used in the synthesis of diphenyl carbonate, glycerol carbonate and methyl propionate. It contains high oxygen content on weight basis (53.3%) as compared to other fuel additives such as methanol (50%), ethanol (34.89%), DME (35%) and MTBE (17.6%), and is consequently used as an oxygenate in the gasoline-based fuels. Thus, DMC is a more effective oxygenates then others, and it produces less CO emission and total hydrocarbons as compared to traditionally used MTBE. High dielectric constant of DMC allows it to be used as an electrolyte too [Wei et al., 2003; Keller et al., 2010].

DMC is used as a methylation agent for carbon, nitrogen and sulfur. It is used as an alternative and replacement of phosgene for aromatic polycarbonate and isocyanate synthesis. It is also used as an alternative compound to dimethyl sulfate or methyl iodide. DMC is used as replacement to ketones and acetates in paints and adhesives due to its strong salvation power. It is also used as a solvent in organic chemistry, polymer synthesis (polycarbonates, polyurethanes, non-isocyanate polyurethanes), beauty and personal care products and as a carrier in lithium-ion batteries, in the pharmaceutical preparations and detergent compositions, etc.

1.3. METHODS FOR DMC SYNTHESIS

Various methods are used for the synthesis of DMC. These methods include phosgenation, oxidative carbonylation, methylnitrite carbonylation urea methanolysis, transesterification, CO_2 utilization process, etc. Phosgenation has been abandoned due to extremely hazardous nature of phosgene. Methanol oxidative carbonylation, and methylnitrite carbonylation are industrially developed processes for the synthesis of DMC.

Transesterification of ethylene carbonate (EC), propylene carbonate (PC) and urea with methanol; and direct CO_2 conversion techniques are in the developing stage for the synthesis of DMC.

Methanol oxidative carbonylation process was commercialized for DMC production by Enichem Company, Italy. In this process, DMC is produced via catalytic reaction between carbon monoxide (CO), liquid methanol and oxygen in the presence of catalysts. Excess of CO is used in this reaction and oxygen is the limiting reagent. This reaction is highly exothermic (heat of reaction, ΔH_r=-318 kJ/mol) and therefore, the temperature must be carefully controlled. Reaction temperature is in the range of 100-140°C with the optimum reaction temperature of 130°C and pressure in the range of the 20-40 bar with the optimum pressure being 24 bar. Copper chloride is used as a catalyst. During this process, CO_2 and water are produced as by-products. CO_2 is recycled as a carbonaceous source for the carbon monoxide synthesis and methanol is recycled back to the reactor. At the end of the reaction, the reaction mixture contains 30–40% DMC, 50–70% methanol and 2–5% water.

Methylnitrite carbonylation process was commercialized for DMC and dimethyl oxalate (DMO) production by UBE group, Japan [Keller et al., 2010]. For this synthesis route, nitrogen monoxide (NO), oxygen and methanol are used as feed materials and various catalysts such as activated charcoal supported palladium chloride ($Pd^{II}Cl_2$) is used in a fixed-bed reactor. The nitrogen oxide reacts with O_2 to form methyl nitrite (CH_3ONO), which reacts further with CO in the second step, in presence of bimetallic catalyst at 100-120°C and 5-10 bar to produce DMC and original nitric oxide [Uchiumi et al., 1999; Keller et al., 2010]. It is necessary to remove the water formed in the first step from the reaction media in order to carry out the DMC synthesis in a fully anhydrous media, in order to maximize the activity of the catalyst in the second step. Contact between water, methanol and DMC is to be avoided which results in separation problems because of the azeotrope formation. Strong toxicity of the methylnitrite reactant and safety issue arising out of the probability of explosion due to the use of the $Pd/NO/O_2$ mixture is major disadvantages of this process [Keller et al., 2010].

Alcholysis of urea to produce DMC is a developing process which is not commercialized yet. In this process, urea reacts with methanol in the presence of a catalyst at 160-190°C to produce DMC. Ammonia is obtained produced as a coproduct. No water is formed in the process, and therefore, the separation and purification of DMC becomes simple since no ternary azeotrope (DMC–methanol–water) is formed. This route of DMC production has both ecological and economical benefits. Another advantage for this process is that the ammonia, as a co-product, can be used as the starting material for the production of urea [Hou et al., 2014]. Figure 1.3.1. shows the reaction steps involved in various routes for DMC synthesis.

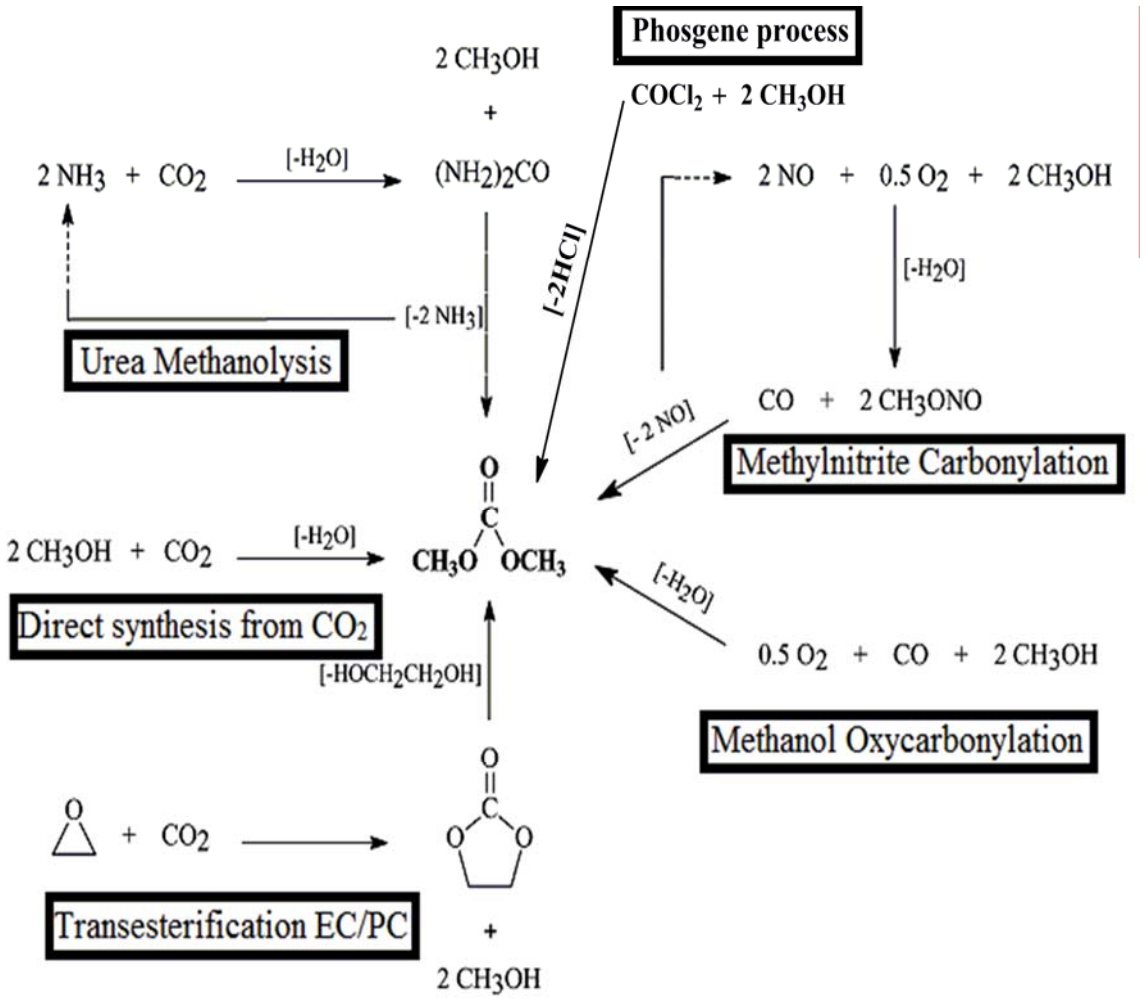

Figure 1.3.1. Reaction steps involved in various methods of synthesis of DMC.

Transesterification of PC or EC with methanol in the presence of catalysts is a promising, clean and sustainable route for the DMC synthesis. DMC is the main product in the transesterification of PC with methanol. Propylene glycol (PG) is obtained as a co-product. In this reaction, the yield of DMC is higher than other routes. Also, the numbers of byproducts are less. Therefore, the separation of components from the reaction mixture is easy and economical as compared to other routes of DMC production. Although each production method has its own drawbacks, transesterification of PC with methanol is a promising and feasible method for the synthesis of DMC, especially in the framework of green chemistry and environmentally benign production route as compared to other routes. This route is sustainable, clean with no formation of any harmful or waste byproduct. However, this route has associated complex thermodynamics and unfavorable chemical equilibrium. A wide variety of catalysts such as ion exchange resins [Pyrlik et al., 2012], pure metal oxide [Wei et al., 2003a], basic ionic liquids [Yang et al., 2010], mixed metal oxide [Wang et al., 2006] and double metal cyanide [Srivastava et al., 2006] have been used for the synthesis of DMC using transesterification reaction.

Several technologies are being used for synthesis of DMC. Among these technologies, reaction of methanol with CO_2 is the most preferred route for DMC synthesis. This route is very promising and sustainable as this eliminates the toxic feed stock such as phosgene and carbon monoxide. Utilization of CO_2 generates economic benefits and helps in managing green-house gas emission [Delledonne et al., 2001]. Synthesis of DMC from CO_2 and methanol is an attractive method in which reaction occurs at 110-150°C temperature and 50 bar pressure in the presence of catalyst [Honda et al., 2014]. This route eliminates the toxic feed stock such as phosgene and carbon monoxide. Although, this route is environmentally friendly, the activation of CO_2, thermodynamical limitations and low yield of DMC are some of the major drawbacks associated with this route for DMC production [Cui et al., 2013]. Deactivation of catalyst, difficult separation process, and recovery of catalyst, etc. are some of the drawbacks of homogeneous catalytic systems.

In another method, epoxide reacts with CO_2 to produce alkylene carbonates. In the presence of methanol, in-situ ester exchange occurs with the formation of DMC. The reaction is fast and exothermic, and epoxide itself works as the dehydrating agent. Various types of side reactions also occur in which such coproducts as 1, 2 diols are formed [Sakakura et al., 2007].

A comparative assessment of reaction condition, advantages and disadvantages of various DMC synthesis methods is given in Table 1.3.1.

1.4. AN OVERVIEW OF RESEARCH WORK ON DMC SYNTHESIS

The critical literature review (chapter 2) focuses on the traditional and developing technologies for the DMC synthesis. A search in the science citation index (SCI) database was performed through SCOPUS with such keywords search as "dimethyl carbonate, DMC, propylene carbonate, ethylene carbonate, urea, methyl carbamate, transesterification, carbon dioxide, phosgenation, oxidative carbonylation, carbonylation of methylnitrite and CO_2 conversion, etc. Conferences publications were excluded in this literature search. Figures 1.1.2a and 1.1.2b show the number of research publications and citations there on for various processes employed for DMC synthesis in the last 20 years (1995-2015). This figure indicates a spread of approaches undertaken by scientist and engineers for DMC synthesis. In the time period 2010-2015, out of the total 148 papers published on DMC synthesis, papers on phosgenation, methylnitrile carbonylation, oxidative carbonylation and CO_2 conversion are 2, 2, 29 and 52, respectively. Similarly, papers on transesterification of urea, EC and PC are 27, 23 and 13, respectively. Analysis of number of citations and publication data shows growing interest for the DMC synthesis by oxidative carbonylation of methanol, transesterification of PC with methanol and direct conversion of CO_2 to DMC.

Table 1.3.1. Comparative assessment of DMC synthesis methods.

Synthesis Methods	Method Conditions	Advantages	Disadvantages	Reference
Phosgenation	Single step Reaction: T=50-150°C	High yield of DMC and cyclic and activated carbonates produced	High energy requirement, extremely hazardous phosgene, and purification, etc	Shaikh and Sivaram, 1996
Oxidative carbonylation	Two step commercial process, T=130°C, P=24 bar, low-grade thermal energy	Productivity is high	Selectivity and decreases the formation of water, separation is difficult, deactivate catalysts	Ding et al., 2014
Methylnitrite carbonylation	Two step commercial process, T=100-120°C and P=5-10 bar,	No azeotropes used for separation, Catalysts regeneration is easy	Productivity is low	Yamamoto, 2010
Urea Methanolysis	Two steps via a methyl carbonate (MC) process P=92 bar, T=265°C, t=2 h	Low cost of starting material (eg. urea), no water formation and easily separation	Produced NH_3 shift the reaction, second rate-controlled step and chemical equilibrium formation	Hou et al., 2014
Conversion of CO_2	High pressure is required	Low cost of CO_2, very promising, sustainable and eliminating the toxic feed stock	Thermodynamics limitation and deactivate catalysts	Keller et al., 2010
Transesterification	Temp=170°C, P=21 bar (CO_2) MeOH/PC=10,	Co-product mono ethylene glycol formed no waste and renewable route and environment friendly	Thermodynamic equilibrium shift major problem	Srivastava et al., 2006

T=Temperature, P=Pressure

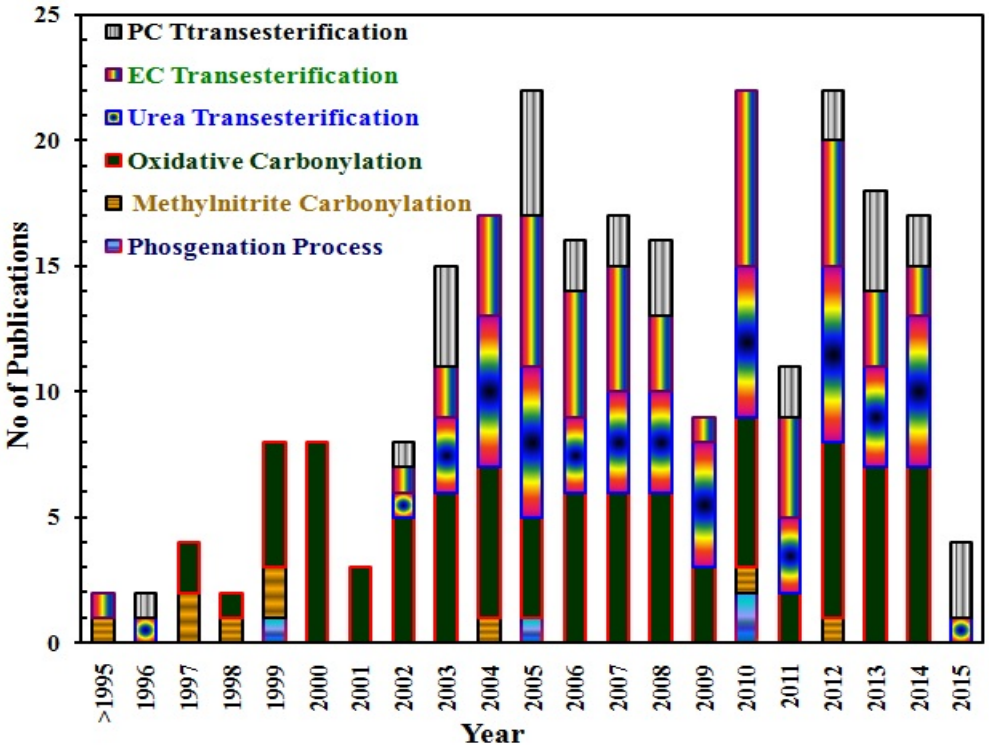

(a)

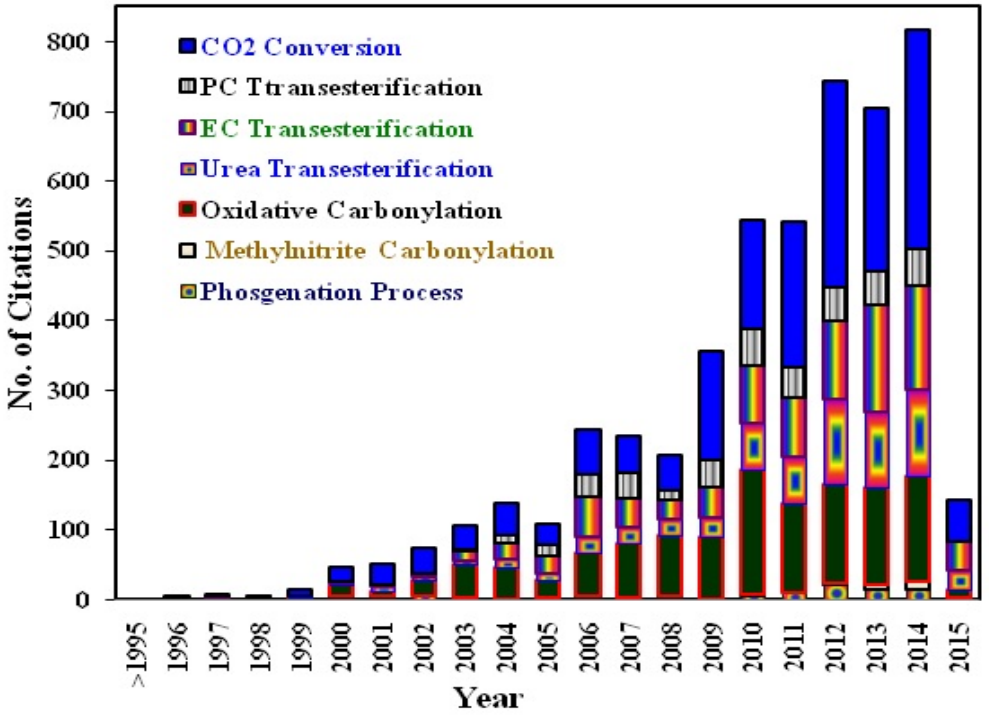

(b)

Figure 1.1.2. (a) Number of research articles published and (b) number of citations on DMC synthesis processes by phosgenation, methylnitrile carbonylation, oxidative carbonylation and PC, EC and urea transesterification (Scopus database search on June 10, 2015).

1.5. OBJECTIVES OF THE PRESENT STUDY

Based on the critical review of the literature and research gaps identified, it is found that only a few catalysts have been tested for the DMC production via transesterification and direct CO_2 conversion routes. Considering various possibilities, the following objectives are set for the present study:

- To prepare various catalysts (CeO_2-based mixed oxide, hydrotalcites and supported catalysts).
- To perform physio-chemical characterization of the synthesized catalysts by using N_2 sorption, X-ray diffraction, temperature programmed oxidation and reduction (H_2-TPR), temperature programmed desorption (TPD) of NH_3 and CO_2, atomic force microscopy (AFM), Fourier transform infrared spectroscopy (FTIR), scanning electron microscopic-energy dispersive atomic spectra (SEM-EDAX), transmission electron microscopy (TEM), inductively coupled plasma atomic emission spectroscopy (ICP-OES), atomic absorption spectroscopy (AAS), thermogravimetric analysis (TG), etc.
- To evaluate catalytic activity of the synthesized catalysts for DMC synthesis via transesterification and direct conversion of CO_2 routes.
- To optimize the operating conditions such as temperature, pressure, molar ratio, amount of catalyst, and to study the thermodynamics and kinetics of the DMC synthesis.
- To test the stability and recyclability of the synthesized catalysts, and to investigate the possible mechanism of DMC synthesis.

Chapter –2

LITERATURE REVIEW

2.1. GENERAL

Many techniques have been developed for the synthesis of dimethyl carbonate (DMC). These include commercially developed technologies and newer alternative techniques which are in the developing stages. The main aim of this chapter is to critically review the literature on the synthesis of DMC using various techniques and the established technologies. This chapter also aims to sean the available literature on the catalysts used for the synthesis of catalysts used in the DMC production and their characterization. DMC synthesis by transesterification reaction with propylene carbonate (PC); and by direct conversion of carbon dioxide (CO_2) have been exhaustively reviewed.

2.2. TRADITIONAL AND DEVELOPING METHODS FOR THE SYNTHESIS OF DMC

Various traditional and developing methods are used for the synthesis of DMC. The methanol oxidative carbonylation, methylnitrite carbonylation and old phosgenation processes are full-scale commercial methods used for the DMC synthesis. Phosgenation process is now abandoned because of the hazards associated with it and banned in the United States and Europe. Transesterification of ethylene carbonate (EC), PC and urea with methanol and conversion of CO_2 are in the developing stage for the synthesis of DMC. Consequently, transesterification reaction and direct CO_2 conversion reaction are being developed for their industrial feasibility. Transesterification and direct CO_2 conversion to DMC have been proved to be the most effective methods for the synthesis of DMC. These methods are environment-friendly and alternative method for the replacement of hazardous and undesirable compounds, green chemistry, low cost and easy case of availability of the

materials [Keller et al., 2010]. Methods used for the commercial production of DMC are methanol oxidative carbonylation and methylnitrite carbonylation.

2.2.1. Phosgenation Process

This technology was used earlier for large scale production of DMC, however, it has now been abandoned because of inherent toxic use of raw material. In this process, phosgene and alcohols (methanol) react in two steps to produce DMC. First, phosgene reacts with methanol to form chloroformates which react further with another molecule of methanol to form DMC [Leino et al., 2010].

$$COCl_2 + CH_3OH \rightarrow CH_3COOCl + HCl \quad (2.2.1)$$

$$CH_3COOCl + CH_3OH \rightarrow (CH_3O)_2CO + HCl \quad (2.2.2)$$

Overall reaction can be written as:

$$COCl_2 + CH_3OH \rightarrow (CH_3O)_2CO + 2HCl \quad (2.2.3)$$

Among many acid acceptors (pyridine, dimethyl aniline, quaternary ammonium bases or inorganic bases such as oxides, hydroxides and carbonates), pyridine is preferred one [Leino et al., 2010]. This reaction occurs below room temperature using anhydrous solvent (such as toluene, benzene, dichloromethane and chloroform) in the presence of excess pyridine or in excess of sodium hydroxide so as to trap the hydrochloric acid formed in the reaction. Excess amount of pyridine, or sodium hydroxide shift the equilibrium of the reaction towards DMC formation as well [Sheikh and Sivaram, 1996]. The temperature of the reaction depends on the nature of the alkaline reagent. In the presence of pyridine or caustic soda, a temperature below room temperature is required, whereas, the reaction temperature should be above 50°C when calcium carbonate is used. In the absence of base, the reaction requires high temperature (50–150°C) to occur, however, it results in poor carbonate yields [Leino et al., 2010].

Reactivity of phosgene is high, unwanted monomers also get produced [Keller et al. 2010]. Recovery and disposed of by product is additional step required in this reaction. Overall, DMC production from methanol and phosgene as a reactant is about 82-85% [Aresta and Galatola, 1999; Keller et al., 2010]. The main disadvantage of this method is that phosgene as a reactant is extremely hazardous.

2.2.2. Methanol Oxidative Carbonylation

Synthesis of DMC using non-phosgene routes was developed in 1980 and industrialized by EniChem Company, Italy in 1983. This industrial process was based on methanol oxidative carbonylation with copper chloride as a catalyst. After completion of this reaction, separation of DMC was done using distillation process [Romanao et al., 1980]. CO_2 and water are by-products in which CO_2 is recycled for synthesis of CO. Product stream contains ~50-70% methanol, 30-40% DMC, and 2-5% water [Keller et al., 2010].

Synthesis of DMC by methanol oxidative carbonylation method is completed in two step oxidation and reduction. In the first step, cupric chloride reacts with oxygen in presence of methanol and copper methoxychloride is formed. In the second step, copper methoxychloride react with CO and DMC is formed, copper chloride is regenerated and then used in new catalytic cycle.

$$2CH_3OH + 2CuCl + \frac{1}{2}O_2 \rightarrow 2Cl(CH_3O)Cu + H_2O \qquad (2.2.4)$$

$$CO + 2Cl(CH_3O)Cu \rightarrow (CH_3O)_2CO + 2CuCl \qquad (2.5)$$

The overall reaction is given below:

$$CO + 2CH_3OH + \frac{1}{2}O_2 \rightarrow (CH_3O)_2CO + H_2O \qquad (2.2.6)$$

Excess of CO is used in this reaction and oxygen is the limiting reagent, which must be fed at carefully controlled rate. This reaction is highly exothermic (~76 kcal/mol of DMC) and takes place at 100-140°C and 20-40 bar [Delledonne et al., 2001; Leino et al., 2010].

Various types of bimetallic chloride, single metal chlorides are used as catalyst for this reaction.

In this reaction, DMC selectivity is low due to formation of dimethyl ether, methyl chloride and water. Dimethyl oxalate (DMO) is produced as a coproduct [Matsuzaki and Nakamura, 1997; Romano et al., 1980]. Methanol oxidative carbonylation process suffers from various problems such as low per-pass conversion from formation of chlorine gas which causes corrosion in the reactor section, and separation problem due to formation of azeotropes between DMC, water and methanol.

Table 2.2.1 gives literature review on the synthesis of DMC by methanol oxidative carbonylation process using various catalysts, process parameters and reaction conditions. Many authors have worked on different catalysts which were synthesized using different methods, different calcination temperatures and DMC/methanol azeotropes. Furthermore, many authors studied the effect of temperature, total pressure, amount of catalysts, etc. Some of the authors worked on increasing the selectivity and decreasing the formation of water. Various authors used Cu-NaOH/activated carbon [Han et al., 2001], $CuCl_2$ immobilized on MCM-41/ MCM-48 [Cao et al., 2003], $CuBr_2$–PyIL/SBA-15 [Wang et al., 2010], Cu-SiO_2-TiO_2 cogelled xerogel [Ren et al., 2011] and $PdCl_2$–$CuCl_2$–KOAc/AC@Al_2O_3 [Ding et al., 2014] for the synthesis of DMC. Anderson and Root [2004] used Cu^+X and Cu^+ZSM-5 based catalysts synthesized by solid–state exchange method and reported a rate equation for DMC synthesis. Engeldinger et al. [2010] synthesized reduced CuY (copper with NH_4-Y-zeolite) catalyst by incipient wetness impregnation method and used it for the DMC synthesis in micro flow reactor at a low pressure (P=3 bar) and 130-150°C temperature. Funakawa et al. [2005] used Au/carbon catalysts for the electrochemical carbonylation of methanol to produce DMC.

Table 2.2.1. Oxidative carbonylation of methanol.

Catalyst	Method	Reactor/Reaction Condition	Process parameter and brief description	Yield (%)	Reference
Cu/MWCNT and Cu–Ni/MWCNT	Conventional incipient wetness impregnation	Continuous flow, H_2-Reduced catalyst, T=120°C, Flow rate=16 ml/min	➢ Methyl formate (MF), DMC and CO_2 formed in this reaction as product. ➢ Molar ratio of $CH_3OH/CO/O_2$=2/1/1, ➢ Proposed possible reaction mechanism	S_{DMC}=30 Y_{DMC}=1.2	Merza et al., 2014
$PdCl_2$–$CuCl_2$–KOAc/AC@Al_2O_3	impregnating active carbon	Continuous flow, T-160°C, GHSV=7100 h^{-1}, P=3 bar,	➢ $PdCl_2$–$CuCl_2$–KOAc/AC@Al_2O_3 catalyst showed high DMC selectivity, ➢ Molar ratio of $CH_3OH/CO/O_2$=3.6/2.3/1, ➢ The catalytic mechanism catalyst was proposed	S_{CO}=71 Y_{CH3OH}=97	Ding et al., 2014
Cu-clinoptilolite	Cation exchange and impregnation	Continuous flow, T=150°C, GHSV=7100 h^{-1}, P=3 bar,	➢ Dimethoxy methane (DMM) and MF produced as product and no DMC was formed	-	Vélez et al., 2012
Cu-SiO_2-TiO_2 cogelled xerogel	Sol-gel method	Batch reaction, T=120°C, P_{co}=2 bar, P_{O2}=1 bar, 10 ml methanol, t=1.5 h, Continuous flow	➢ Synthesis of Silica–Titania matrix using sol-gel method. ➢ Proposed structure of Silica–Titania matrix and study for DMC synthesis	S_{DMC}=97 C_{MeoH}=13 S_{DMM}=3.2	Ren et al., 2011
Cu^+/SiO_2-ZrO_2	Sol-gel and ion-exchange method	Batch reaction, T=140°C, Pco=1.6 bar, Po_2=0.8 bar, 10 ml methanol, t=1.5 h, Stirr=500 rpm	➢ Molar ratio of CO/O_2=2/1, ➢ silica-zirconia mixed oxide ➢ Calcined -450°C	S_{DMC}=79 C_{MeoH}=10	Hua-Yan et al., 2011
Cu^IY ($CuCl_2$ with Zeolite)	Solid-state ion-exchanged reaction	Continuous flow, T=140°C, SV=5600 h^{-1},	➢ Molar ratio of $CH_3OH/CO/O_2$=4/10/1, ➢ Calcined =300-500°C	S_{DMC}=75 C_{MeoH}=4.4 S_{DMM}=26	Zhong et al., 2010
$CuBr_2$–PyIL/SBA-15	Conventional impregnation method	Batch reaction, T=120°C, methanol=10 ml, P_{CO}=24 bar, t=2 h,	➢ Synthesis of SBA-15 and ionic liquid. ➢ P_{CO} /P_{O2}=2:1	S_{DMC}=98 C_{MeoH}=9.5 S_{DMM}=0.5	Wang et al., 2010
CuY (Copper with NH_4-Y-zeolite)	Incipient-wetness-impregnation	Flow micro-reactor, T=130-150°C, P=3 bar, H_2-Reduced catalyst	➢ Molar ratio of $CH_3OH/CO/O_2$=15/30/1 or 15/30/0 ➢ Calcined temperature=400°C	S_{DMC}=12 S_{DME}=77 S_{DMM}=17 S_{MF}=1 C_{MeOH}=10	Engeldinger et al., 2010
Co-Schiff Base/ Zeolite	Stepwise method	T-120°C, P_{total}=30 bar, t=4 h, P_{CO}=20 bar, P_{O2}=10 bar	➢ Molar ratio of CO/O_2=2/1, ➢ Calcination temperature=400°C, ➢ Amount of catalyst=1 g, ➢ Acetonitrile=25 mL, ➢ Methanol=40 mmol	C_{MeOH}=25.4 S_{DMC}=99.5	Zhu et al., 2009
$CuCl/SiO_2$–TiO_2	Conventional & microwave heating methods	Batch reactor, T-120°C, P_{total}=30 bar, t-1.5 h, P_{CO}=20 bar, P_{O2}=10 bar	➢ Studies on quantum-chemical calculations and Cu-O corridation. ➢ Calcination temperature=550°C. ➢ Optimized geometry of the clusters calculated by DFT	S_{DMC}=96.5 S_{DMM}=3.2 S_{MF}=0.3	Ren et al., 2009
Cu-exchanged zeolite Y	Solid-state ion exchange of H-Y zeolite	T=130°C	➢ Proposed Mechanism for DMC synthesis, $CH_3OH/CO/O_2/He$=4.0/9.0/1.0/19.3, ➢ Calcination temperature=650°C,	-	Zhang and Bell, 2008a

Catalyst	Method	Reactor/Reaction Condition	Process parameter and brief description	Yield (%)	Reference
Ionic liquid	-	Batch reactor, T=120 ^{o}C, P_{total}=24 bar, t=2 h, P_{CO}=20 bar, P_{O2}=10 bar	➢ Effect of molar ratio of CO/O_2, ➢ CO/O_2=2/1, ➢ Methanol=4 g	S_{DMC}=97.8 C_{MeoH}=17.2 S_{DMM}=2.8	Dong et al., 2008
Cu-Y Zeolite	-	-	➢ DFT study for DMC synthesis, ➢ Proposed reaction mechanism	-	Zheng and Bell, 2008b
CuCl/1,10-phenanthroline immobilized on polystyrene	Conventional impregnation method	Batch reactor, T-120°C, P_{total}=30 bar, t=5 h, P_{CO}=20 bar, P_{O2}=10 bar	➢ Molar ratio of CO/O_2=9/1, ➢ Methanol=60 mL, ➢ Stirring speed=1000 rpm/min. ➢ Polymer supported catalysts synthesis	S_{DMC}=96.8 C_{MeoH}=15.5 Y_{DMC}=78.2	Mo et al., 2007
Cu-impregnated zeolite Y	Incipient wetness impregnation	Continuous flow, T=140-170°C, Space velocity=6250 h^{-1}, P=12 bar,	➢ Molar ratio of $CH_3OH/CO/O_2$=6.67/3.33/1, Calcination temperature=650°C, ➢ Proposed reaction mechanism	S_{DMC}=96.8 C_{MeoH}=12 $_{YDMC}$=78.2	Richter et al., 2007a
Cu-precipitated zeolite Y	Incipient wetness impregnation	Continuous flow, T=140-170°C, Space velocity=3000 h^{-1},	➢ $CH_3OH/CO/O_2$=6/8/1, Cal- 700–750 ^{o}C for 15 h, Synthesis. Proposed reaction mechanism. Normal pressure	S_{DMC}=52 C_{MeoH}=12	Richter et al., 2007b
Cu-exchanged Y, ZSM-5, and Mordenite	Solid-state ion exchange method	Continuous flow, T=130°C	➢ Effect of catalysts activity, ➢ Selectivity as Cu-Y > Cu-ZSM-5 > Cu-MOR, ➢ Molar ratio of $CH_3OH//CO/O_2/He$=4/9/1/19.3, ➢ To study the effect of reactant	-	Zhang et al., 2007
Cu-Y Zeolite	Vapor-phase exchange method	Catalysts characterization	➢ Possible locations for Cu+ in faujasite by DFT study. ➢ DFT simulation of DMC, DMM, and MF, ➢ To study the amount of DME produced	-	Drake et al., 2006
CuCl/Schiff base		Batch reactor, T=120 ^{o}C, P=24 bar, t=2 h, Stirr=1000 rpm	➢ Molar ratio of CO/O_2=2/1, ➢ Study of Schiff base promoters with different-donor abilities effect the catalytic performances	S_{DMC}=98.3 C_{MeoH}=23.7	Mo et al., 2006
Cu-ZSM-5	Solid-state ion exchange	Continuous flow, T=130°C	➢ Proposed reaction mechanism for DMC synthesis	-	Zhang et al., 2006
Cu/SiO_2	Chemical vapor deposition	Continuous flow, T=130°C, residence time=3.5 s,	➢ To study the molar ratio of $CH_3OH/CO/O_2$=4/9/1, ➢ High DMC activity correlated with Cu dispersion.	S_{DMC}=90	Drake et al., 2005
Au/Carbon anode by electrochemical potential	-	-	➢ Unique electrocatalysis for the electrochemical carbonylation of methanol to DMO and DMC. ➢ DMC found higher potential and DMO found lower potential	-	Funakawa et al., 2005
Cu^{+}Xand Cu^{+}ZSM-5 Zeolite	Solid-state ion exchange	Continuous flow, T=130°C, P_{CO}=0.4-2.0 bar	➢ Proposed reaction mechanism and pathways for DMC synthesis from oxidative carbonylation of methanol using CuZSM-5, ➢ Finding rate equation expression.	-	Anderson and Root, 2004

Catalyst	Method	Reactor/Reaction Condition	Process parameter and brief description	Yield (%)	Reference
Carbon-supported Wacker-type ($CuCl_2$-$PdCl_2$-KOAc/AC)	Impregnation Method	Continuous flow, T=140°C, P_{CO}=0.4-2.0 bar, t=1.2 h^{-1}, GHSV=1680 h^{-1}	➢ Vapor-phase oxidative carbonylation of methanol, ➢ Molar ratio of CO/O_2=3.67/1	$S_{DMC/MeOH}$=96 C_{MeoH}=18	Cao et al., 2004
Copper chloride hydroxides ($CuCl_2$/NaOH/AC)	Conventional impregnation method	Continuous flow, T=130°C, P=1 bar,	➢ MeOH/CO/O_2=4/16/1, ➢ OH/Cu molar ratio depends upon the DMC yield.	S_{DMC}=89.3 C_{MeoH}=23.7 Y_{DMC}=20.9	Han et al., 2003
$CuCl_2$-$PdCl_2$	Impregnating method	Continuous flow, T=140°C, P_{CO}=0.4-2.0 bar, t=1.2 h^{-1}, GHSV=700 h^{-1}	➢ Effect of Cu/Pd on DMC synthesis ➢ CO/O_2=2/1	S_{DMC}=89.3 C_{MeoH}=9 Y_{DMC}=20.9	Yang et al., 2003a
$CuCl_2$-$PdCl_2$-Activated carbon	Impregnating method	Continuous flow, T=130°C, P_{CO}=0.4-2.0 bar, t=1.2 h^{-1}, GHSV=4300 h^{-1}	➢ MeOH/CO/O_2=7.34/3.67/1	S_{DMC}=97.7 C_{MeoH}=7.3	Yang et al., 2003b
$CuCl_2$ immobilized on MCM-41/ MCM-48	Conventional impregnation method	Continuous flow, P=10 bar, T=130°C, GHSV=1200 h^{-1}	MeOH/$CO/O_2/N_2$=4/18/1/2	S_{DMC}=97.5 C_{MeoH}=12.6	Cao et al., 2003
$CuCl_2$-$PdCl_2$/ Activated carbon	Conventional impregnation method	Continuous flow, P=10 bar, T=150°C, GHSV=1500 h^{-1}	➢ CO/O_2=2.8/1, ➢ Effect of K, Na and Li on DMC synthesis, Reasons of deactivation of catalyst, activity and stability	-	Ruixia et al., 2003
$PdCl_2$–$CuCl_2$–CH_3COOK/A.C.	Impregnation method	Continuous flow, P=10 bar, T=150°C, GHSV=1500 h^{-1}, LHSV=4 h^{-1},	➢ CO/O_2=2.8/1, ➢ Proposed reaction mechanism, Effect of K on DMC synthesis	-	Jiang et al., 2002
poly (N-vinyl-2-pyrrolidone)-$CuCl_2$	Combination of an alcoholic solutions method	Batch reactor, T=120°C, P_{CO}=27.6 bar, P_{O2}=2.4 bar, t=5 h,	➢ CO/O_2=11.5/1, ➢ Proposed reaction mechanism	S_{DMC}=98.3 C_{MeoH}=12.09 Y_{DMC}=61	Hu et al., 2002
Cu-NaOH/Activated Carbon	Conventional impregnation method	Continuous flow, P=10 bar, T=120°C,	➢ MeOH/CO/O_2=4/16/1, ➢ Effect of Cu and NaOH on DMC synthesis	S_{DMC}=83 C_{MeoH}=13	Han et al., 2001

Stirr=Strring speed, T=Temperature, P=pressure, S_{DMC}=Selectivity of DMC, Y_{DMC}= Yield of DMC, C_{MeOH}= Conversion of methanol, Cal=Calcination temperature.

2.2.3. Methanol Carbonylation of Methylnitrite

This process was commercialized for DMC production by Ube Industries Ltd. Japan. In this process, nitric oxide (NO) is used as a redox coupling agent for the synthesis of DMC and dimethyl oxalate (DMO) is formed as a coproduct [Pacheco and Marshall, 1977]. Presently the carbonylation of methylnitrite is mainly used for the synthesis of DMO.

In this process, CO and O_2 are also used as raw materials. DMC formation takes place in two steps. In the first step, nitrogen oxides react with O_2 to form methyl nitrite (CH_3ONO) and water. This step is completed without catalyst at a temperature of 60°C.

$$2NO + \tfrac{1}{2}O_2 \rightarrow N_2O_3 \qquad (2.2.7)$$

$$N_2O_3 + 2CH_3OH \rightarrow 2CH_3ONO + H_2O \qquad (2.2.8)$$

Overall reaction of methyl nitrite production is as follows:

$$2NO + \tfrac{1}{2}O_2 + 2CH_3OH \rightarrow 2CH_3ONO + H_2O \qquad (2.2.9)$$

In the second step, CO reacts with methyl nitrite in the presence of bimetallic catalyst at 100-120°C temperature and 5-10 bar pressure to produce DMC and original nitric oxide [Uchiumi et al., 1999; Keller et al., 2010].

$$CO + 2CH_3ONO \xrightarrow{PdCl_2} (CH_3O)_2CO + 2NO \qquad (2.2.10)$$

After completion of the reaction, the water formed is removed. Methanol carbonylation of methylnitrite process suffers from various problems such as difficulty in separation of produced DMC, NO toxicity and CH_3ONO reactivity [Pacheco and Marshall, 1997; Keller et al., 2010].

Some authors used this reaction for the DMC synthesis using various catalysts such as Pd/NaY [Yamamoto et al., 1997], copper impregnated on activated carbon or supported catalyst [Tomishige et al., 1999a], Pd catalyst [Matsuzaki, 2003], Pd-(AC/Si/Al/NaY/Si-Al) [Yamamoto, 2010] and a combination of palladium and copper oxide ($CuCl_2$-$PdCl_2$/Li-Al-O) [Ge et al., 2012]. Table 2.2.2 summarizes the literature on the synthesis of DMC using methanol oxidative carbonylation by methylnitrite process using various catalysts.

Table 2.2.2. Oxidative carbonylation process.

Catalyst	Method	Reactor/Reaction Condition	Process parameter and brief description	Yield (%)	Reference
Pd/NaY	Ion-exchange technique	Fixed bed flow reactor, Cat=5.0 g, T=110°C, $CO/CH_3ONO/CH_3OH/N_2$= 3/18/5/74, GHSV=8000 h^{-1},	➢ Characterization of synthesized catalysts, ➢ Effect of Pd loading on zeolite for DMC synthesis, ➢ Effect of calcinations temperature, Proposed mechanism of DMC synthesis	S_{DMC}= > 85% S_{MN}=76% S_{CO}=88%	Yamamoto et al., 1997
Pd catalyst	Conventional method	Fixed bed flow reactor, Cat=1 wt%, T=120°C, $CO/MN/N_2$=20/10/70, GHSV=4000 h^{-1},	➢ Effect of support in fixed bed reactor for DMC synthesis, ➢ Proposed a reaction mechanism using Pd catalysts, ➢ Comparison to other method in DMC	Y_{DMC}=6.14 Y_{DMO}=0.25 mol/1 Cat h	Matsuzaki and Nakamura, 1997
$CuCl_2$/Activated Carbon (AC)	Impregnation method	Fixed bed flow reactor, Cat=0.93 g, P=5 bar, T=110°C, GHSV=10000 h^{-1}, or $CH_3OH/CO/N_2/O_2$=2/2/0.8/0.2, $CH_3OH/CO/Air$=2/2/1,	➢ Activity of $CuCl_2$/AC catalysts for DMC synthesis, ➢ Study of rate of formation of DMC, ➢ Effect of Cu loading on AC,	S_{DMC}=2.5 $mmol.h^{-1}$ S_{MN}=0.9 $mmol.h^{-1}$ S_{CO}=0.4 $mmol.h^{-1}$	Tomishige et al., 1999a
Pd catalyst	Impregnation method	Fixed bed flow reactor,	➢ Study of catalysts deactivation, ➢ High DMC selectivity.	-	Matsuzaki, 2003
Pd-(AC/Si/Al/NaY/Si-Al)	Impregnation method	Fixed bed flow reactor, Cat=0.5 g, P=2-5 bar, T=120°C, $CO/MN/N_2$=20/10/70, GHSV=4000 h^{-1},	➢ Effect of support on catalytic activity and stability, ➢ Effect of pressure on DMC synthesis, ➢ Proposed a reaction mechanism for DMC in absence/presence of chlorine ion.	Y_{DMC}=6.14 Y_{DMO}=0.25 mol/1 Cat h	Yamamoto, 2010
$CuCl_2$-$PdCl_2$/Li-Al-O	Ceramic method and impregnation method	Fixed bed flow reactor, Cat=0.93 g, P=2 bar, T=120°C, $CO/MN/N_2$=5/80/15, CH_3OH=10 mL GHSV=8000 h^{-1},	➢ Effect of support and calcinations temperature on the catalytic properties and used for DMC synthesis	S_{MN}=95%,	Ge et al., 2012

*DMM=dimethoxy methane, MF=Methyl formate, DME=Dimethyl ether, STY=Space time yield, S_{MN}= Selectivity of MN, S_{CO}=Selectivity of CO, Y_{DMC}=Yield of DMC, Y_{DMO}=Yield of DMO.

2.2.4. Transesterification of Urea with Methanol

Synthesis of DMC from urea and methanol is a two-step process. First urea is converted to methyl carbamate at low temperature and without any catalyst. In the second step, methyl carbamate reacts with methanol at 160-190°C temperature in the presence of a catalyst to produce DMC and ammonia.

$$NH_2CONH_2 + CH_3OH \rightarrow NH_2COOCH_3 + NH_3 \qquad (2.2.11)$$

$$CH_3OCOCH_3 + NH_3 \rightarrow CH_3OCOOCH_3 + NH_3 \qquad (2.2.12)$$

Ammonia is removed from the reaction and no azeotrope forms between the methanol and water. Thus, the separation of DMC is easy as compared to other processes. This route is cheap and environment-friendly, as no toxic gas forms.

However, this process suffers from the requirement of high molar ratio of methanol/urea, unfavorable thermodynamics and low product selectivity due to formation of various byproducts such as N-methyl carbamate, N-methyl urea and methyl carbamate.

A number of investigations have been reported recently which have tried to overcome these limitations. Work done by various authors is summarized in Table 2.2.3. Various types of catalysts such as mixed metal oxide [Wu et al., 2014b; Wu et al., 2014a; Wang et al., 2012a; Joe et al., 2012; Wang et al., 2009], pure metal oxide [Wang et al., 2010; Zhang et al., 2010; Wang et al., 2006; Wang et al., 2005; Wang et al., 2004], ionic liquids [Wang et al., 2009] and hydrotalcites [Wang et al., 2010] have been used for the DMC production from urea and methanol.

2.2.5. Transesterification of EC or PC with Methanol

DMC can be produced by the transesterification reaction between methanol and PC or methanol and EC. During transesterification of PC with methanol, DMC is the main product and propylene glycol (PG) is a co-product.

$$C_4H_6O_3 + CH_3OH \rightarrow H_3COCOOCH_3 + CH_3CHOHCH_2OH \qquad (2.2.13)$$

This process of DMC formation is sustainable and clean and environmentally benign as compared to other routes, and has gained the attention of a number of researchers. This route has these advantages: first, it is free from corrosion of equipment; second, there is no waste formation; and the third, it has higher conversion.

Table 2.2.3. Literature review of transesterification activity of urea methanolysis with various catalysts.

Catalyst	Reactor and Method of catalyst	Reaction condition	%Y_{DMC} / %C_{PC}/ %S_{DMC}*	References
Zn/Al mixed metal	Stainless steel autoclave with a magnetic stirrer. (batch reactor)	T-180°C, MeOH/urea=20, C/U=8.33 wt%, t=10 h. Cal=350-1000°C	Y_{DMC}=31.4 Y_{MC}=66.6 T_Y=98.0	Wu et al., 2014a
No catalysts	Stainless steel autoclave (batch reactor)	T-265°C, MeOH/urea=14, C/U=8.33 wt%, t=2h., P=92 bar, Solvent=Acetone	Y_{DMC}=98	Hou et al., 2014
ZnO–CaO	Stainless steel autoclave with a magnetic stirrer. (batch reactor)	T-180°C, MeOH/urea=20, C/U=8.33 wt%, t=10 h. Cal=1000 °C,	Y_{DMC}=41 Y_{MC}=51 T_Y=92	Wu et al., 2014b
ZnO–Al_2O_3	Batch and continuous Reactor	T-180°C, MeOH/urea=20, C/U=25.3 wt%, t=10 h. Cal=600°C, P=15 bar	Y_{DMC}=35 C_{MC}=55 Y_{NMMC}=7	Wang et al., 2012
Fe_2O_3/HMCM-49	Stainless steel autoclave with a magnetic stirrer. (batch reactor)	T-180°C, MeOH/urea=12, C/U=160 wt%, t=8 h. Cal=1000°C,	Y_{DMC}=34 C_{MC}=34 S_{DMC}=98	Zhang et al., 2012
ZnO (X)–CeO_2 (1-X)	Stainless steel autoclave with a magnetic stirrer with reflux column.	T-170°C, MeOH/urea=20, C/U=8.3 wt%, t=4 h. Cal=500 °C, P=20 bar @CO_2	Y_{DMC}=29	Joe et al., 2012a
ZnO–CeO_2–MO (MO-Single metal)	Stainless steel autoclave with a magnetic stirrer with reflux column.	T-170°C, MeOH/urea=20, C/U=25 wt%, t=4 h. Cal=500°C, P=20 bar @CO_2	Y_{DMC}=50 C_{MC}=40 Y_{NMMC}=7	Joe et al., 2012b
Zn/Fe mixed oxide	Stainless steel autoclave with a magnetic stirrer with reflux column.	T-190°C, MeOH/urea=20, C/U=13.3 wt%, t=10 h. Cal=500°C, P=20 bar @CO_2	Y_{DMC}=31 C_{MC}=46 Y_{NMMC}=7	Wang et al., 2010b
La $(NO_3)_3$ based oxides	Stainless steel autoclave with a magnetic stirrer with reflux column.	T-190°C, MeOH/urea=20, C/U=13.3 wt%, t=8 h. Cal=800°C, P=20 bar @CO_2	Y_{DMC}=54 C_{MC}=85 Y_{NMMC}=14	Wang et al., 2010
ZnO	Isothermal fixed-bed reactor Kinetics Study using MATLAB	T-180-200°C, t=4.7 mol/h		Zhang et al., 2010
Zn/Al, Zn/Cr and Zn/Fe (HTLc)	Stainless steel autoclave with a magnetic stirrer with reflux column.	T-190°C, MeOH/urea=20, C/U=13.3 wt%, t=10 h. Cal=500°C,	Y_{DMC}=32 C_{MC}=67 Y_{NMMC}=9	Wang et al., 2010d
ZnO composite	Stainless steel autoclave with a magnetic stirrer	T-170°C, Stirr-650, Cal-500°C, t=8 h.,MeOH/urea=20, C/U=16.6 wt%,	Y_{DMC}=43 C_{MC}=60	Wang et al., 2010e
Ionic liquids	500 mL stainless steel reactor with a mechanical stirrer and electric heater.	T-160°C, MeOH/urea=37, C/U=16.6 wt%, t=4 & 8 h. (liquid emimBr–$ZnCl_2$)	Y_{DMC}=26 S_{DMC}=100	Wang et al., 2009
Compounds of Zinc	350 mL stainless steel reactor with a mechanical stirrer and electric heater.	T-190°C, Stirr-650, MeOH/MC=20, C/U=135 wt%, t=10 h. Cal-500°C,	Y_{DMC}=31 C_{MC}=51 Y_{NMMC}=9	Zhao et al., 2008
CaO, MgO, ZrO_2	Stainless steel autoclave with a magnetic stirrer with reflux column.	T-200°C, MeOH/MC=8 wt%, C/U=6.67 wt%, t=10 h, Stirr-650.	Y_{DMC}=17.5 C_{MC}=44.3 S_{DMC}=39.5	Wang et al., 2006a
CaO,TiO_2, $CaCl_2$, MgO	Stainless steel reactor with a mechanical stirrer and electric heater.	T-150°C, Stirr-1000 rpm, MeOH/urea=15 molar ratio, C/U=18 wt%, t=10 h.	Y_{DMC}=28	Yang et al., 2006

Catalyst	Reactor and Method of catalyst	Reaction condition	%Y_{DMC} / %C_{PC}/ %S_{DMC}*	References
polyphosphoric acid (PPA)	750 mL-stainless steel reactor with a mechanical stirrer and electric heater.	T-140°C, MeOH/urea=14 molar ratio, C/U=18 wt%, t=4 h. P=8 bar @CO_2, Stirr-1000 rpm,	Y_{DMC}=67.4 C_{MC}=44.3 S_{DMC}=39.	Sun et al., 2005
ZnO	250 mL Stainless steel autoclave with a magnetic stirrer with reflux column.	T-170°C, MeOH/urea=20 molar ratio, C/U=25 wt%, t=8 h. P=8 bar @CO_2, Stirr-1000 rpm,	Y_{DMC}=70 C_{MC}=48 Y_{NMMC}=15	Wang et al., 2005a
CaO, ZnO, MgO, ZrO_2	Stainless steel autoclave with a magnetic stirrer with reflux. (batch reactor)	T-180°C, stirr=500 rpm, MeOH/urea=8, C/U=8.33 wt%, t=10 h. Cal=600°C,	Y_{DMC}=37 Y_{MC}=99 C_{MC}=42	Wang et al., 2004

*T=Temperature, P=Pressure, Stirr=Strring, MeOH/urea=Methanol/urea molar ratio, C/U=wt% of urea, Y_{DMC}=DMC Yield (%), S_{DMC}=DMC Selectivity (%), C_{MC}=methyl carbamate conversion (%), S_{EG}=EG Selectivity (%), Y_{EG}=EG Yield (%), t=reaction time.

Transesterification of PC/EC with methanol for the production of DMC has been investigated using various homogeneous and heterogeneous catalytic reactions. Previous studies showed that the surface acid and base functionalities play major role during the transesterification reaction for the DMC production. A comparative assessment of the transesterification of PC/EC with methanol using catalysts is given in Tables 2.2.4 and 2.2.5.

Some investigators have reported on the favorable activity of CaO and CaO-ZrO_2 based catalysts for the transesterification of PC/EC with methanol. However, the regeneration and reusability of the catalysts was found to be poor [Wang et al., 2005a; Wang et al., 2005b; Wang et al., 2005c]. The decrease in the CaO specific surface area due to agglomeration and blockage of the active sites caused appreciable decrease in the catalytic activity of CaO during its reuse in the transesterification reaction. Other catalysts such as quaternary ammonium salt, [Jeong et al., 2005], ion exchange resins [Pyrlik et al., 2012], ionic liquids [Ju et al., 2007; Dharman et al., 2009; Yang et al., 2010], ionic liquid supported on metal oxide [Kim et al., 2010a; Kim et al., 2010b; Kim et al., 2011], and mixed metal cyanide [Srivastava et al., 2006] have also been used for the transesterification of PC/EC with methanol. Many of these catalysts take long reaction times, and the addition of more than one solvent and requirement of high temperature during synthesis of DMC. The reusability of the catalysts is also not satisfactory.

Table 2.2.4. Literature review of transesterification activity of PC with various catalysts.

Catalyst	Reactor and Method of catalyst	Reaction condition	$\%Y_{DMC}$ / $\%C_{PC}$/ $\%S_{DMC}$*	References
CaO/C and CaO	250 mL flask equipped with reflux condenser,	T-50°C, MeOH/PC=4, CaO/C C=1.8 wt% and CaO=0.90 wt%, t=1 h.	Y_{DMC}=43	Wei et al., 2003a
MgO and CaO	batch reactor and direct use after heating	T-20°C, MeOH/PC=4, CaO/C C=1.8 wt% and CaO=0.90 wt%, t=2 h.	S_{DMC}=80 Y_{DMC} =46 C_{PC} =55	Wei et al., 2003b
$CaO-ZrO_2$	Reactive distillation reactor and co-precipitation method	T=150°C, P=5 bar (N_2), MeOH/PC=4, C=15g rate of methanol=15 ml/h, t=12h,	C_{PC} =97	Wang et al., 2005a
Quaternary ammonium salt	Stainless steel autoclave equipped with a magnetic stirrer, Commercial use	T-140$^{°C}$, P=21 bar using CO_2 MeOH/PC=8, C/PC=8 wt%, t=6 h.	S_{DMC}=81 S_{PG}=70.4 C_{PC} =59	Jeong et al., 2005
$CaO-ZrO_2$	Batch reactor/distillation reactor and co-precipitation	T-160°C, P=5 bar (N_2) MeOH/PC=6, C=0.5g/15g, LHSV=0.03 h^{-1}, t=2 h/12 h.	C_{PC} =56/97	Wang et al., 2006b
Fe-Zn double metal cyanide	Teflon-lined steel autoclave	T-170°C, P=21 bar (CO_2) MeOH/PC=10, C=24.5 wt% of PC t=8 h.	Y_{DMC}=87	Srivastava et al., 2006
$CaO-ZrO_2$	Batch reactor /distillation reactor and co-precipitation, physical mixing, impregnation methods	T-150$^{°C}$, P=5 bar (N_2) MeOH/PC=6, C=0.5g/15g, LHSV=0.03 h^{-1}, t=2 /12 h.	C_{PC} =56/97	Wang et al., 2006c
Ionic liquids (cations and anions)	50 mL Stainless steel autoclave equipped with a magnetic stirrer and Commercial used	T-180$^{°C}$, P=35.5 bar (CO_2) MeOH/PC=8, C/PC=8 wt%, t=6 h.	S_{DMC} =81 S_{PG}=91 C_{PC} =75	Ju et al., 2007
Au/CeO_2	Autoclave reactor and Deposition-precipitation method	T=140°C, MeOH/PC=10, C/PC=11 wt%, t=6 h.	Y_{DMC} =35 S_{DMC} =55 C_{PC} =63	Juárez et al., 2009
Verkade bases	Autoclave and commercial sources	T=40°C, MeOH/PC=16, C/PC=1 wt%, t=1 h.	-	Williams et al., 2009
KF/Al_2O_3	Double necked round bottom flasks equipped with condenser	T=80°C, MeOH/PC=10, C/PC=1.22 wt%, stirr-300 rpm, t=4 h.	S_{DMC} =98 C_{PC} =71	Murugan et al., 2010a
$Mg-Al-CO_3$	25mL-Round bottom flask and Coprecipitation	T=130°C, MeOH/PC=10, C/PC=4 wt%, stirr-500 rpm, t=4 h.	S_{DMC} =97 C_{PC} =72	Murugan et al., 2010b
Ion exchange resins	Autoclave/continuous flow fixed bed reactor	T=130°C, MeOH/PC=8, C/PC=7 wt%, t=2 h.	S_{DMC} =95 S_{PG} =20 C_{PC} =55	Pyrlik et al., 2012
Waste eggshell	Round bottom flask	T=25°C, P=1 bar MeOH/PC=8, C/PC=0.8 wt%, t=2 h.	Y_{DMC} =80 Y_{PG} =66 $C_{PC=}$83	Gao and Xu, 2012

*T=Temperature, P=Pressure; Stirr=Strring; MeOH/PC=Methanol/PC molar ratio; C/PC: wt% of PC, Y_{DMC}=DMC Yield (%),S_{DMC}=DMC Selectivity (%); C_{PC}: PC conversion (%); S_{PG}=PG Selectivity (%); Y_{PG}=PG Yield (%); t: reaction time.

Table 2.2.5. Literature review of transesterification activity of EC with various catalysts.

Catalyst	Reactor and Method of catalyst	Reaction condition	$\%Y_{DMC}$ /$\%C_{EC}$/ $\%S_{DMC}$*	References
Mg–Al (HTLc)	Flask with reflux	T=100-160°C, MeOH/EC=4, C=89 mg, t=3 h.	S_{DMC}=40 S_{EG} =99 C_{EC}=54	Watanabe et al., 1998
K_2CO_3, KOH, LiOH and NaOH	Stainless steel autoclave	T=25°C, MeOH/EC=4, C=0.1g, P=50 Psig using N_2, t=2 h.	S_{DMC}=61 C_{EC} =62	Han et al., 2001
Mg-/Ni Smectite	Stainless steel autoclave	T=150°C, MeOH/EC=8, C=0.45 g, t=4 h.	S_{DMC}=89 S_{EG} =96 C_{EC} =62	Bhanage et al., 2002
Amberlyst A-21	SS-316 high-pressure reactor	T=90-120°C, MeOH/EC=4,16, C=11.24-44.97 kg/m^3g, t=4 h.	S_{DMC}=95 C_{EC} =36	Dhuri and Mahajani, 2006
Ionic liquid (EMImCl, $EMImBF_4$)	Stainless steel autoclave	T=100-160°C, MeOH/EC=8, C=2 mmol, P=100-400Psig using CO_2, t=6 h.	S_{DMC}=99 S_{EG} =100 C_{EC}=61	Ju et al., 2007
Poly-4-vinyl pyridine	Stainless steel autoclave	T=140-150°C, MeOH/EC=8, C=20 wt of EC, t=4 h.	Y_{DMC}=82 Y_{EG} =75 C_{EC} =96	Jagtap et al., 2008
Ionic liquid	Multimode microwave reactor	T=80-120°C, MeOH/EC=8, C=2 mmol, t=0.5-6 h.	Y_{DMC}=82 Y_{EC} =85	Dharman et al., 2009
$Na/NH_4/Mg/K$ Dawsonites	2 L glass batch reactor	T=70 °C, MeOH/EC=4, C=10 wt%, t=6 h.	Y_{DMC}=65	Stoica et al., 2009
DABCO/ basic ionic liquids	-	T=70°C, MeOH/EC=15, C=1 mol%, t=6 h.	Y_{DMC}=81 C_{EC} =90	Yang et al., 2010
Ionic liquid /amorphous silica	Stainless steel autoclave	T=160°C, MeOH/EC=8, C=0.2 g, P=13.4 bar, t=6 h.	Y_{DMC}=86 Y_{EG} =84 C_{EC} =93	Kim et al., 2010a
Ionic liquid /commercial silica	Stainless steel autoclave with magnetic stirrer	T=160°C, MeOH/EC=8, C=0.2 g, P=13.4 bar using CO_2, t=6 h.	Y_{DMC}=74 Y_{EG} =73 C_{EC} =81	Kim et al., 2010b
Zinc-yttrium oxides	50 ml flask as reactor	T=65°C, MeOH/EC=8, C=2.5 wt% of EC, t=2 h.	Y_{DMC}=72 Y_{EG} =70 C_{EC} =71	Wang et al., 2011
Ionic liquids on MCM-41	50-mL Stainless steel autoclave	T=180°C, MeOH/EC=8, C=0.2 g, P=11.7 bar using CO_2, t=4 h.	Y_{DMC}=76 Y_{EG} =76 C_{EC} =78	Kim et al., 2011
Imidazolium on poly- styrene resin	Fixed bed reactor/ 50 mL st ainless-steel reactor	T=110°C, MeOH/EC=10, C=0.2 mmol or 1 mol%, t=1.2 h. Fixed bed reactor -200 h	Y_{DMC}=82 S_{DMC} =99 C_{EC} =84	Wang et al., 2012
MgO with mesoporous silica	Flask as a reactor	T=140°C, MeOH/EC=8 (5mL), C=30 mg, P=12 bar@CO_2, t=6 h.	S_{DMC}=96 C_{EC} =92	Cui et al., 2013
Mesostructured graphitic carbon nitride	80 mL stainless steel autoclave,	T=160°C, MeOH/EC=10, C=0.1 g, P=6 bar using CO_2, t=6 h.	Y_{DMC}=81 S_{DMC} =99 C_{EC} =82	Xu et al., 2013
N-hetero- cyclic carbene	-	T=180°C, MeOH/EC=3, C=5 mol%, t=10 h.	Y_{DMC}=86	Du et al., 2015
Ceria mesoporous	80-mL Stainless steel autoclave	T=140°C, MeOH/EC=10, C=0.1 g, P=6 bar using CO_2, t=2 h.	Y_{DMC}=73 S_{DMC} =96 C_{EC} =76	Xu et al., 2014

*T=Temperature, P=Pressure, Stirr=Strring, MeOH/EC=Methanol/EC molar ratio, C/EC=catalyst dose wt.% of EC, Y_{DMC}=DMC Yield (%), S_{DMC}=DMC Selectivity (%), C_{EC}=EC conversion (%), S_{EG}=EG Selectivity (%), Y_{EG}=EG Yield (%), t=reaction time.

2.2.6. Direct Synthesis Processes

2.2.6.1. Direct conversion of CO_2 to DMC

Utilization of CO_2 and reducing CO_2 emission are important issues from the sustainability point of view. CO_2 along with alcohol was used for the direct synthesis of carbonates in 1980 [Delledonne et al., 2001]. This route for the synthesis of DMC using CO_2 and methanol seems to be an attractive method, and is currently pursued very vigorously:

$$2CH_3OH + CO_2 \rightleftharpoons CH_3OCOOCH_2 + H_2O \qquad (2.2.14)$$

The above reaction occurs at a temperature of 110-150°C and a pressure of 50 bar in the presence of a catalyst [Honda et al., 2014]. To overcome the problem of limited equilibrium conversion, application of dehydrating agents, use of highly effective catalysts and high CO_2 pressure have been used to shift the thermodynamic equilibrium towards DMC side. Synthesis of DMC from CO_2 without use of a dehydrating agent leads to very low DMC yield and low CO_2 conversion. Two types of dehydration systems (namely reactive and non-reactive) are being investigated. Inorganic absorbent system, membrane separation and gas-phase system are non-reactive dehydration systems. Butylene oxide, acetals, ortho ester, trimethyl phosphate (TMP), dicyclohexylcarbodiimide (DCC) and CH_3I are used as reactive dehydration reagents[Honda et al., 2014].

Although this route is environmentally friendly, the, low yield of DMC is the major drawback. Various homogeneous catalysts such as thallium(I)hydroxide, tin(IV)tetralkoxides, dialkytin dialkoxides, bases, C, N-chelated organotin(IV)trifluoro methane sulfonates [Svec et al., 2012] and titanium(IV)tetralkoxides have been studied for increasing the DMC yield. [Knifton and Duranleau, 1991; Kizlink, 1993; Kizlink and Pastucha, 1995; Fang et al., 1996]

Deactivation of catalyst, difficult separation process, and recovery of catalyst, etc. are some of the drawbacks of the homogeneous systems. Subsequently, various heterogeneous catalysts have been investigated for DMC synthesis such as CeO_2 [Chen et al., 2014], ZrO_2 [Chen et al., 2014], $Ce_{0.5}Zr_{0.5}O_2$ [Zhang et al., 2009; Lee et al., 2012], Gd-$Ce_{0.4}Zr_{0.6}O_2$ [Lee et

al., 2012], Cu-CeO_2 [Wada et al., 2013], Sn-SBA-15 [Ballivet-Tkatchenko et al., 2011], and C, N-chelated organotin(IV)trifluoro methane sulfonates [Svec et al., 2012] have been reported for DMC synthesis.

Various types of catalysts have been synthesized by various routes and tested for their catalytic activity at varied conditions for this reaction. Several authors have worked on supported catalysts such as Cu-Fe/SiO_2, graphene/Cu-Ni, Sn-SBA-15, SnO_2 and ZrO_2 supported on silica, Cu-activated carbon at different pressures and temperatures [Bian et al., 2011; Tkatchenko et al., 2011; Ballivet-Tkatchenko et al., 2011; Zhou et al., 2012]. Some authors used ionic liquid supported on metal oxide and tested for DMC synthesis [Yuan et al., 2009; Zhang et al., 2011]. CeO_2 synthesis using different methods such as Ce-Zr synthesized by sol-gel, complex decomposition and conventional methods have also been used for the DMC synthesis by this route [Tomishige et al., 2002; Zhang et al., 2009; Hofmann et al., 2012]. In other studies, CeO_2 was tested in batch and continuous reactors under 200 bar pressure and 125°C temperature [Santos et al., 2013; Wang et al., 2013; Honda et al., 2014]. Ce-Zr catalyst was synthesized by sol-gel, complex decomposition and conventional methods and was tested in a batch reactor under 60-200 bar pressure, 80-160°C temperature [Hofmann et al., 2012; Zhang et al., 2009; Tomishige et al., 2002]. Table 2.2.6 provides a comparative assessment of work done on DMC synthesis by CO_2 conversion.

Few investigators have proposed a possible mechanism for the synthesis of DMC from CO_2 with methanol [Bian et al., 2010]. Initially, methanol is activated to CH_3O^- in the presence of base catalyst. CH_3O^- further reacts with CO_2 to produce methoxide which reacts with methyl iodide dehydrating agent and HI and DMC gets formed. Regeneration of dehydrating agent to form a water molecule is an important step in this reaction. In this mechanism, some side reactions may also be forced to reduce the water formation. Methyl iodide was used as a dehydrating agent [Fang and Fujimoto, 1996; Honda et al., 2014].

$$Base + CH_3OH \rightarrow CH_3O^- + H\text{-}Base$$

(2.2.15)

$$CH_3O^- + CO_2 \rightarrow CH_3OCOO^- \quad (2.2.16)$$

$$CH_3OCOO^- + CH_3I \rightarrow DMC + I^- \quad (2.2.17)$$

$$I^- + H - Base \rightarrow HI + Base \quad (2.2.18)$$

$$HI + CH_3OH \leftrightarrow CH_3I + H_2O \quad (2.2.19)$$

$$K_2CO_3 + 2HI \rightarrow KI + CO_2 + H_2O \quad (2.2.20)$$

Currently, the focus of research is on the development of highly efficient heterogeneous catalysts, maximization of CO_2 conversion, increasing DMC yield, overcoming thermodynamic limitations, reducing the severing of reaction conditions, etc.

2.2.6.2. Reaction of epoxide and CO_2

In this process, epoxide reacts with CO_2 to produce alkylene carbonates followed by in-situ ester exchange in the presence of excess methanol to form DMC.

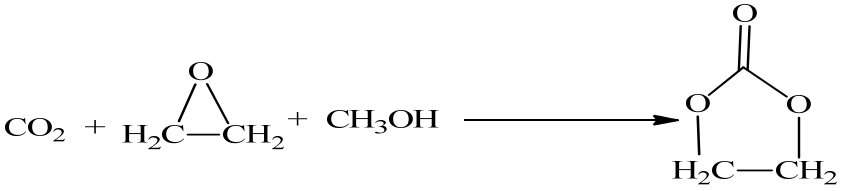

(2.2.21)

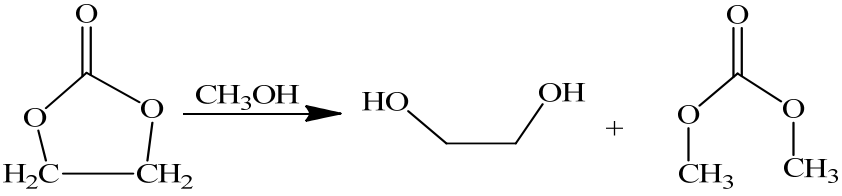

(2.2.22)

This process does not require a dehydrating agent. In this reaction, coproduct 1,2-diols gets formed which is recycled. However, excess methanol is required in this reaction which is not favorable for ester exchange between DMC and methanol. Also, various types of side reactions such as ring opening of epoxide by methanol also occurs [Sakakura et al., 2007].

Table 2.2.6. DMC synthesis from CO_2 with methanol.

Catalyst	Method	Reactor/Reaction Condition	Process parameter and brief description	Yield (%)	Reference
bis [2-(1H-benzimidazol-2-yl) benzoato] nickel (II) (NiL2)	Polyphosphoric acid (PPA)-catalyzed condensation	Stainless steel autoclave T-80°C, P-10 bar, t=6 h, MeOH/ DCC=100, Catalyst dose=1 mmol,	➢ Dicyclohexyl carbodiimide as promoter ➢ Effect of temp, pressure, time, catalyst amount and reusability. ➢ Proposed mechanism for DMC synthesis	Y_{DMC}=58	Shi et al., 2014
CeO_2	Conventional method	Stainless steel autoclave T=110-150°C, P=50 bar, t=24 h, MeOH/CP=2, Catalyst dose=0.34 g,	➢ 2-cyanopyridine (CP) as hydration agent, ➢ Proposed mechanism for DMC synthesis with DFT	Y=1.4 C_{MeOH}=1.7	Honda et al., 2014
KBr-Polyethylene glycol	Conventional method	Stainless steel autoclave, T=100°C, P=200 bar, t=2 h,	➢ Effect of temp, pressure, catalysts amount, reaction time, catalyst amount and reusability	Y_{DMC}=12.8 S_{DMC} =98	Kumar et al., 2014
CeO_2 versus over ZrO_2	Sol-gel Method	Stainless steel autoclave, T=140°C, P=50 bar, t=2 h, Catalyst dose=0.1 g	➢ Studies of DMC formation using FTIR with intermediates. ➢ Formation of mechanism using FTIR	-	Chen et al., 2014
K_2CO_3	-	Stainless steel autoclave, CH_3OH/ CHO=5, T=150°C, P=26, t=6h, Catalyst dose=0.28 g/2.0 mmol	➢ 1,2-cyclohexanediol (CHD) and DMC synthesis from Cyclohexane oxide (CHO) and CO_2, ➢ Optimization of reaction and proposed reaction mechanism	Y_{DMC}=55.4 Y_{CHD} =63.40	Yang et al., 2013
CeO_2	-	Continuous and batch steel autoclave, T=125°C, P=200 bar, stir=200 rpm, Catalyst dose=4.6 g, CO_2/CH_3OH=1.1-4,	➢ Proposed Eley–Rideal and Langmuir–Hinshelwood mechanisms, ➢ Fitting the reaction data in models, ➢ Finding and Optimization of activation, enthalpy and Gibbs energy using reaction parameter	-	Santos et al., 2013
CeO_2 nanocrystals	Template-free hydrothermal method	Stainless steel autoclave, T=140°C, P=50 bar, CH_3OH=15 mL, t=2 h, Catalyst dose=0.1 g	➢ Proposed a mechanism over CeO_2 catalyst, ➢ Morphology correlated with acidity and basicty and used for DMC synthesis	Y_{DMC}=1.382 mmol	Wang et al., 2013
Zirconium phenylphosphonate phosphate (ZrPP)	Conventional method	Stainless steel autoclave, T=170°C, P=50 bar, CH_3OH=16 mL, t=8 h, Catalyst dose=0.16 g	➢ Proposed a mechanism over ZrPP catalyst, ➢ To check the reusability of the catalyst\	Y_{DMC}=26 mmol/g, C_{MeOH}=31.8 mol%	Unnikrishna et al., 2013
Mg-Al hydrotelcite-silica lyogels	Sol-gel method	Continuous flow reactor, T=130°C, P=50 bar, CH_3OH=16 mL, t=8 h, Catalyst dose=0.16 g	➢ Design of more-efficient heterogeneous catalysts and reaction systems for valorizing CO_2 as a potential source of economic	Y_{DMC}=12%	Stoian et al., 2013

Catalyst	Method	Reactor/Reaction Condition	Process parameter and brief description	Yield (%)	Reference
Ionic liquid	-	Stainless steel autoclave, T=140°C, P=30 bar, CH_3OH=25 mL, t=6 h, Catalyst dose=0.066 mol	➢ Optimization of DMC using Pressure, amount of catalysts, amount of ionic liquid, reaction time, and recyclability of catalyst. ➢ Proposed a reaction mechanism using ionic liquid.	Y_{DMC}=1.5 mmol S_{DMC}=95%	Sun et al., 2013
CeO_2	Conventional method	Stainless steel autoclave, Catalyst dose=0.34 g, CH_3OH/Nitrile=2/1, P=50 bar, T=100$^{°C}$	➢ Effect of presence of nitrile in the direct synthesis of DMC.	Y_{DMC}=94 mmol	Honda et al., 2013
Cu-Ce oxide	Coprecipitation Method	Stainless steel autoclave, T=80°C, P=13 bar, CH_3OH=25 mL, t=2 h, Catalyst dose=0.10 g	➢ Effect of Cu on DMC synthesis, ➢ Optimization of reaction parameter for DMC synthesis, ➢ Proposed reaction mechanism	Y_{DMC}=0.4 mmol	Wada et al., 2013
Ce-Zr	Oxalate gel method	Batch reactor with Teflon, P=65 bar, T=160°C, Catalyst dose=0.05 g,	➢ Proposed reaction mechanism. ➢ Kinetics study using thermodynamic models, ➢ Study of enthalpies of the reaction component	Y_{DMC}=0.65 % mass fraction	Hofmann et al., 2012
C,N-chelated organotin (IV) trifluoromethanesulfonates	-	Stainless steel autoclave, CH_3OH=20 mL, DMC/Cat=1.15, CO_2=32.7 g	➢ Synthesized and their characterization such as NMR, XRD etc.	Y_{DMC}=2.3 mmol	Svec et al., 2012
Cu-Fe/SiO_2	Impregnated method	Continuous flow reactor, T=120°C, P=120 bar, t=6 h, Space velocity=360 h^{-1}, Catalyst dose=0.16 g	➢ Catalytic performances on time, reduction temperature. ➢ Correlated with catalytic properties such as acidity, basicty	S_{DMC}=85.9 %, C_{MeOH}=5.37%	Zhou et al., 2012
ZrO_2–MgO	Co-precipitation	Stainless steel autoclave, T=120°C, P=80 bar, CH_3OH=10 mL, t=9 h, Catalyst dose=0.5 g, ionic liquid=3.2 g,	➢ Effect of the catalyst and the ionic liquid on DMC synthesis, ➢ Effect of temperature and ionic liquid loading, ➢ recyclability of ionic liquid	Y_{DMC}=1.32 mmol	Eta et al., 2011
Graphene /Cu-Ni	Modified Staudenmaier method	Stainless steel autoclave, T=120°C, P=12 bar, CH_3OH /CO_2=2 mL, t=3 h, Catalyst dose=3.0 g,	➢ Synthesis of DMC using CO_2 and methanol.	S_{DMC}=92%	Bian et al., 2011
$Ga_2O_3/Ce_{0.6}Zr_{0.4}O_2$	Sol-gel/ Impregnation method	Stainless steel autoclave, CH_3OH=30 mL, T=170°C, P=60 bar, t=3 h, Catalyst dose=0.7 g,	➢ Synthesis of catalyst and characterized. ➢ DMC yield correlated with catalysts acidity and basicity.	Y_{DMC}=0.7 to 2.4 mmol	Lee et al., 2011

Catalyst	Method	Reactor/Reaction Condition	Process parameter and brief description	Yield (%)	Reference
Di-n-butyltin (IV)-catalyzed	-	-	➢ Proposed mechanism for direct organic carbonate synthesis promoted by di-n-butyltin (IV) species and molecular representation, ➢ Possible monomeredimer equilibria and HP-NMR spectroscopy.	-	Laurenczy et al., 2011
Sn-SBA-15	Templating method	Stainless steel autoclave, CH_3OH=16 mL, T=150°C, P_{CO2}=40g/200 bar, t=15 h, catalyst dose=0.1 g,	➢ Synthesis of DMC using supported catalysts with turnover number	Y_{DMC}=8 mmol	Tkatchenko et al., 2011
$Ce_xZr_{1-x}O_2$ and [EMIM]Br /$Ce_{0.5}Zr_{0.5}$ O_2	Sol-gel method	Stainless steel autoclave, CH_3OH=8 mL, T=150°C, P=200 bar, t=24 h, Catalyst dose=0.1 g,	➢ Effect of molar ratio of Ce/Zr metal on DMC synthesis, ➢ Trimethoxymethane used for removal of formed water, ➢ Optimization of reaction conditions	C_{MeOH}=11 %	Zhang et al., 2011
SnO_2 and ZrO_2 as support Silica		Stainless steel autoclave, CH_3OH=20 mL, T=150°C, P=200 bar, t=2 h, catalyst dose=0.55 g,	➢ Effect of silica as support on DMC synthesis, ➢ Recyclability of catalysts used for DMC.		Ballivet-Tkatchenko et al., 2011
Organotin compound immobilized on mesoporous silicas	-	Stainless steel autoclave, CH_3OH=20 mL, T=180°C, P=180 bar, t=10 h, catalyst dose=0.1 g,	➢ Effect of Sn on the catalytic reaction for DMC synthesis. ➢ Optimization of DMC yield using temperature, pressure and methanol amount. Catalytic stability	Y_{DMC}=0.4 mmol	Fan et al., 2010
Cu-Activated Carbon	Incipient wetness impregnation	Fixed bed flow, CH_3OH=20 mL, T=120°C, P=12 bar, CH_3OH/CO_2=2/1, t=4 h, Catalyst dose=3.0 g,	➢ Effect of calcinations temperature, reaction time, reaction temperature, Some byproduct was formed as MF and DME.	S_{DMC}=90.1 %	Bain et al., 2010
$Co_{1.5}PW_{12}$ O_{40}	-	Stainless steel autoclave, CH_3OH=20 mL, T=80°C, P=2.5 bar, t=5 h, catalyst dose=0.1 g,	➢ Higher temperatures favour the formation of dimethoxymethane (DMM) and methyl formate (MF), ➢ Effect of calcinations temperature, reaction temperature, pressure	S_{DMC}=69% S_{MF}=14% S_{DMM}=17%	Aouissi et al., 2010
Cu–Ni/thermally expanded graphite	-	Continuous Flow reactor, CH_3OH=20 mL, T=100°C, P=12 bar, t=5 h, catalyst dose=0.1 g, CH_3OH/CO_2=2/1,	➢ Proposed reaction mechanism, Effect of temperature, pressure, time, etc. ➢ Stability of catalyst in this reaction.	S_{DMC}=89.3 % C_{MeOH}=4.97%	Bian et al., 2009
Cu–Ni/Natural expanded graphite	Traditional wetness impregnation method	Continuous tubular fixed-bed reactor, CH_3OH=20 mL, T=140°C, P=16 bar, CH_3OH/CO_2=2, t=5 h, catalyst dose=1g,	➢ Proposed reaction mechanism, Effect of temperature, pressure, time, etc. ➢ Stability of catalyst in this reaction and investigation of support and catalysts structure.	S_{DMC}=90.2 % C_{MeOH}=10.13%	Bian et al., 2009

Catalyst	Method	Reactor/Reaction Condition	Process parameter and brief description	Yield (%)	Reference
Ionic Liquid	Conventional method	Cyclic voltammetry of CO_2 in ionic liquid, electrochemical reaction	➢ Proposed electrochemical reaction mechanism, ➢ Effect of temperature, time. Influences of CH_3OK and Ionic liquid and electrochemical synthesis.	Y_{DMC}=3.9 %, S=88.4%	Yuan et al., 2009
$Ce_{0.5}Zr_{0.5}O_2$	Complex-decomposition method	Stainless-steel autoclave reactor, CH_3OH=8 g, Cat=0.5g, T=80-180°C, P=200 bar, t=24h.	➢ Effect of complex for synthesis of catalysts, ➢ Proposed structure of complex for salicylic acid, ➢ Correlated with catalysts properties	Y_{DMC}=1.75 mmol	Zhang et al., 2009
V-doped Cu-Ni/AC	co-impregnation	Continuous tubular fixed-bed reactor, CH_3OH=8 g, Catalyst dose=1 g, T=110°C, P=12 bar, t=3h. CH_3OH/CO_2=2	➢ Synthesis of bimetallic catalyst and supported activated carbon. ➢ Reduced catalysts used for synthesis of DMC with low pressure.	S_{DMC}=89.9 % C_{MeOH}=7.76%	Bian et al., 2009
Cu–Ni/Carbon nanotube	Incipient impregnation	Continuous reactor CH_3OH=8 g, Catalyst dose=1 g, T=120°C, P=12 bar, t=3 h. CH_3OH/CO_2=2	➢ Interaction between the metal particles and the supports, ➢ Proposed reaction mechanisms using Cu-Ni catalyst	S_{DMC}=92% C_{MeOH}=4.5 %	Bian et al., 2009
Sn- SBA-15	Wetness impregnation	Stainless-steel autoclave reactor, T=200°C, P=180 bar, t=10 h, Catalyst dose=0.1 g, CH_3OH=16g	➢ Effect of Sn on SBA-15 and their characterization, ➢ Effect of CO_2 pressure and reusability of catalysts	-	Fan et al., 2008
$H_3PW_{12}O_{40}/Ce_xTi_{1-x}O_2$	Sol-gel method	Stainless-steel autoclave reactor, T=170°C, P=50 bar, CH_3OH=6.4 g, t=12 h, Catalyst dose =0.5 g	➢ Correlated with acidic and basic properties of catalysts with DMC synthesis,	Y_{DMC}=5 mmol	La et al., 2007
Cu/ (Ni,V,O) semiconductor complex	Impregnation method	Continuous reactor CH_3OH=8 g, catalyst dose=1 g, T=120-140°C, P=12 bar, t=3h.	➢ Photo catalytic synthesis of DMC from CO_2 with methanol, ➢ Effect of temperature on DMC synthesis,	Y_{DMC}=4%, S_{DMC}=90%	Wang et al., 2007
CeO_2	-	Stainless-steel autoclave reactor, T=130°C, t=2 h, CH_3OH/CO_2=1, catalyst dose=0.05 g,	➢ Rate of DMC synthesis and activity over surface area and low temperature reaction with ethanol and methanol over CO_2	Y_{DMC}=0.3 mmol	Yoshida et l., 2006
n-$Bu_2Sn(OCH_3)_2$ [n-$Bu_2(CH_3O)Sn]_2O$	-	Stainless-steel autoclave reactor, T=110°C, P=200 bar, t=16 h, CH_3OH/CO_2=1, catalyst dose=0.05 g,	➢ Given a molecular structure of catalyst, ➢ IR and NMR study of catalysts. Kinetics study of synthesis of DMC.	Y_{DMC}=0.02 mmol	Ballivet-Tkatchenko et al., 2006
Cu-Ni/VSO	Conventional method	Continuous tubular fixed-bed reactor, T=100-180°C, P=9 bar, t=16 h, catalyst dose=0.5 g, CH_3OH/CO_2=2	➢ Drift study of the CO_2 and methanol with catalyst. ➢ Effect of crystalline structure, ➢ Optimization of condition such as temperature,	Y_{DMC}=6 mmol S_{DMC}=90%	Wu et al., 2006

Catalyst	Method	Reactor/Reaction Condition	Process parameter and brief description	Yield (%)	Reference
Potassium methoxide	Commerciall y	Stainless-steel autoclave reactor, T=80°C, P=73 bar, t=10 h, catalyst dose=0.05 g,	➢ Reaction kinetics and mechanism, ➢ Effect of reaction conditions such as temperature, ➢ Given activation energy for DMC synthesis.	Y_{DMC}=16.2 % or 0.071 mmol S_{DMC}=100 %	Cai et al., 2005
H_3PO_4/V_2O_5	Impregnation method	Continuous tubular fixed-bed micro-gaseous reactor, T=140°C, P=6 bar, t=10 h, Cat=0.5 g, CH_3OH/CO_2=2	➢ Optimum composition of $H_3PO_4/V_2O_5$with P/V=0.15–0.50 showed effective activation of both CO_2 and CH_3OH. ➢ Direct interaction between V and P is essential for the formation acidic sites.	Y_{DMC}=4.5 % S_{DMC}=92.1 2%	Wu et al., 2005
Cu–KF/MgSiO	Ions exchange/im pregnating method	Membrane catalytic reactor, T=130°C, P=10 bar, CH_3OH/CO_2=2	➢ Influences of operating conditions on the conversion of methanol and the selectivity.	S_{DMC}=89.9 %, C_{MeOH}=4.8 3%	Li et al., 2003
CeO_2-ZrO_2	Calcining the hydroxides	Stainless steel autoclave reactor, CH_3OH=6.1 g, Cat=0.5 g, T=110°C, P=60 bar, t=2 h,	➢ Model scheme of DMC formation from methanol, ➢ DMP adding for the formation of DMC	Y_{DMC}=0.73 mmol,	Tomishige et al., 2002
H_3PO_4/ZrO_2	Impregnation method	Stainless steel autoclave reactor, CH_3OH=6.1 g, Cat=0.5 g, T=170°C, P=40 bar@ room temp, t=2 h,	➢ Proposed a reaction mechanism using H_3PO_4/ZrO_2 catalyst, ➢ Effect of P/Zr molar ratio and effect of acidity of the reaction	Y_{DMC}=0.3 mmol,	Ikeda et al., 2001
Ni $(CH_3OO)_2.4H_2O$	-	Stainless steel autoclave reactor, CH_3OH=6.1 g, Cat/CH_3OH=1.25 M, T=32°C, P=93 bar, t=12 h,	➢ Calculated equilibrium conversion of methanol ➢ Proposed reaction mechanism, ➢ Influences of methanol on supercritical synthesis, ➢ FTIR used for estimation of DMC	S_{DMC}=100 %	Zhao et al., 2000
Zirconia	Commercial	Stainless steel autoclave reactor, CH_3OH=6.1 g, T=190°C, P=50 bar, t=16 h, Catalyst dose=0.5 g,	➢ Acid-Base Properties by TPD correlated by DMC synthesis,	Y_{DMC}=0.42 mmol,	Tomishige et al., 2000
Polymer-Supported Iodide	Ion exchange method	Stainless steel autoclave reactor, CH_3OH=6.1 g, T=150°C, P=35 bar, t=6 h, Cat-3 g,	➢ DMF used as solvent, ➢ Proposed reaction mechanism	Y_{DMC}=19 mmol,	Chu et al., 2000
Zirconia	Commercial	Stainless steel autoclave reactor, CH_3OH=6.1 g, T=160°C, P=66 bar, t=16 h, Catalyst dose=0.04 g,	➢ Effect of reaction temperature, reaction time, ➢ Correlated with acidic-basic and surface area catalysts.	Y_{DMC}=0.42 mmol,	Tomishige et al., 1999
Basic oxide metals	Commercial	Stainless steel autoclave reactor, CH_3OH=6.1 g, T=100°C, P=66 bar, t=2 h, Cat=0.04 g,	➢ Proposed reaction mechanism, ➢ effect of CH_3I as a promoter	Y_{DMC}=11.2 mmol,	Fang et al., 1996

*DMM=dimethoxy methane, DMM= Dimethoxy methane, DCC=Dicyclohexyl carbodiimide, DFT=Density functional theory, CHO= Cyclohexane oxide, CHD=1,2-cyclohexanediol , MF=Methyl formate, S_{MN}= Selectivity of MN, DME=Dimethyl ether, STY=Space time yield, S_{CO}=Selectivity of CO, Y_{DMC}=Yield of DMC, Y_{DMO}=Yield of DMO, S_{DMC}=Selectivity of DMC, Y_{CHD}=Yield of CHO, Cat/CH_3OH=Catalyst dose with respect to methanol.

Table 2.2.7. Synthesis of DMC from epoxide with CO_2

Catalyst	Reactor and Method of catalyst	Solvents	Reaction condition	%Y_{DMC} / %C_{PO}/ %S_{DMC}*	References
Ammonium bromide/dicyandiamide–formaldehyde polymer (ABMDFP)	Fixed-bed continuous flow reactors, For PO conversion: PO=14.3 mmol, T=130°C, P=20 bar, Cat=2.0 mol% on ILs, t=3.5 h, For DMC synthesis: CH_3OH/EC =10, t=6 h, T=150 ^oC, catalyst dose=2.5 mol% (0.1 g).	PO	➢ Effect of reaction parameter such as temperate, pressure, catalyst dose and time. ➢ Recyclability of catalysts also study on optimum reaction condition. ➢ Proposed a reaction mechanism using catalysts and DFT study.	C_{PO}=96 S_{PC}=99 S_{DMC}=99	Meng et al., 2014
2-hydroxymethyl-functionalized ionic liquids	Fixed-bed continuous flow reactors, For PO conversion: PO=14.3 mmol, T=110°C, P=20 bar, catalyst dose=1.0 mol% on ILs, t=1 h, For DMC synthesis: CH_3OH=8 g, t=6 h, T=120°C, catalyst dose=1.5 mol% (Ils=1 mol%+ K_2CO_3=0.5%0.1), P=10-20 bar.	PO and EO	➢ Effect of reaction parameter such as temperate, pressure, catalyst dose and time. ➢ Recyclability of catalysts also study on optimum reaction condition. ➢ Proposed a reaction mechanism using catalysts with CO_2, EC and EO fixation also find out using DFT model.	C_{PO}=90 Y_{PC}=90 S_{DMC}=99	Wang et al., 2014
C60 fullerenol	Stainless-steel reactor, P=20 bar, PO=100 mmol, Catalyst dose=100 mg, T=120°C, t=5-22 h.	PO	➢ To study of optimization of reaction condition such as temp, pressure, catalysts amount and time. ➢ Proposed a reaction mechanism using epoxide. ➢ To study of reusability of catalyst under optimum condition 10 times.	Y_{PC}=94	Sun et al., 2014
Zn-CO (double metal cyanide)	Stainless-steel reactor, P=40 bar, PO=100 mmol, Cat=100 mg, T=120°C, t=9 h.	PO	➢ The effect of additional solvent on BisAG/CO_2 coupling reaction.	C_{PO}=93.6	Wei et al., 2013
Triazine frameworks	Stainless-steel reactor, catalyst dose=100 mg, T=130°C, t=4 h, P=69 bar, epichlorohydrin =18 mmol.	CIPO, PO, SO, CHO	➢ Effect of different solvent (epoxide) for DMC yield, recyibility of catalyst upto 8 times. ➢ Synthesized catalysts were characterizing various methods	C_{PO}=86, S_{DMC}=15.2	Roger et al., 2012
Quaternary Ammonium Ionic Liquids	Stainless-steel reactor, catalyst dose=0.6 mmol, CH_3OH/EO=12.5, T=150°C, t=4-8 h, P=40-50 bar,	EO	➢ Synthesized various type of ionic liquid as bi-functional catalyst and their characterization using various techniques. ➢ Optimization of reaction condition such as temperature, reaction time, pressure, molar ratio of CH_3OH/EO, ➢ To study of recyclability of catalyst upto 8 times.	C_{EO}=99 S_{DMC}=74 S_{EG}=72, S_{EC}=22	Li et al., 2011

Catalyst	Reactor and Method of catalyst	Solvents	Reaction condition	%Y_{DMC} / %C_{PO}/ %S_{DMC}*	References
Ionic liquid (bmimBr)	Cyclic voltammograms in bmimBr, CH_3OH=0.489 mol, PO=0.43, catalyst dose=0.059 mol, T=30°C, t=48 h.	PO	➢ DMC synthesized by electrochemical method using various types of electrodes such as graphite, Pt, glass–carbon, optimization of reaction condition, ➢ In this article shows the electrolysis, redox reaction ➢ Proposed reaction mechanism	Y_{DMC}=75.5 S_{EG}=72, S_{EC}=22	Yan et al., 2011
Choline hydroxide/MgO	Stainless-steel reactor, catalyst dose=0.6 mmol, CH_3OH/EO=12.5, T=120°C, t=6 h, P=25 bar,	PO	➢ Synthesized catalysts and their characterization ➢ Influence of various reaction conditions such as temperature, molar ratio CH_3OH/PO, pressure and catalyst dose, reaction time and reusability of catalysts.	Y_{DMC}=65.4 S_{DMC}=66.9 C_{PO}=98	De et al., 2009
Tungstate-based ($Na_2WO_4.2H_2O$)	Stainless-steel reactor, catalyst dose=0.2 g, CH_3OH/PO or BO=10, T=150°C, t=15 h, P=34 bar,	PO, BO	➢ Optimization of reaction condition such as catalysts amount, molar ratio CH_3OH/EC, temperature and reaction time, ➢ Proposed a reaction mechanism with intermediates	C_{PO}=92 Y_{DMC}=24	Sankar et al., 2006
n-Bu_4NBr/n-Bu_3N	Stainless-steel reactor, catalyst dose=0.2 g, CH_3OH/SO=40, T=150°C, t=8 h, P=150 bar,	SO	➢ Study the effect on catalyst precursors, reaction time and temperature, methanol/epoxide feed ratio in moles, and CO_2 pressure. ➢ A proposed a possible mechanism for the present n-Bu_4NBr/n-Bu_3N catalyst	Y_{DMC}=84 C_{SO}=98	Tian et al., 2006
KOH/4A	Stainless-steel reactor, catalyst dose=5 g, CH_3OH/PO=0.86, T=180°C, t=6 h, P=30 bar,	PO	➢ Effects of various conditions, such as reaction time, reaction temperature, molar ratio of the reactants and KOH loading, and stability of KOH/4A catalyst on the yield of DMC were investigated, ➢ Effect of catalyst support on catalytic activity.	Y_{PC}=58.7 Y_{DMC}=16.8 S_{DMC}=16.8	Li et al., 2005
Double metal (Metal halide and inorganic alkali)	Stainless-steel reactor, CH_3OH/PO=4, P=25 bar, T=160°C, catalyst dose=5 wt%,	PO	➢ Synthesized single metal and supported catalyst and their characterization, ➢ Effect of reaction temperature, calcinations of temperature on DMC yield, ➢ The reusability of the catalyst upto 6 times	C_{PO}=82.4 S_{DMC}=22.4 S_{PG}=24.9 S_{PC}=42 Y_{DMC}=18	Jiang and Yang, 2004
KI supported on ZnO (KI/ZnO) and KI/ZnO with K_2CO_3	Stainless-steel reactor, CH_3OH/PO=4, P=165 bar, T=150°C, catalyst dose=0.25 g, t=4 h,	EO	➢ Effect of different supports and effect of reaction temperature, pressure, reaction time and molar ratio of CH_3OH/EO, Proposed a reaction mechanism	C_{PO}=98.6.4 Y_{DMC}=37.5	Chang et al., 2004

Catalyst	Reactor and Method of catalyst	Solvents	Reaction condition	%Y_{DMC} / %C_{PO}/ %S_{DMC}*	References
KI and K_2CO_3	Stainless-steel reactor, P=80 bar, T=160°C, CH_3OH/EO=10, catalyst dose=1.0 g,	EO	➢ Kinetics of DMC synthesis using EO methanol and CO_2. ➢ An isothermal kinetics model and an isobaric kinetics model for the one-pot synthesis of DMC were developed. ➢ Effect of temperature, pressure and CO_2 density on the rate of reaction and selectivity	-	Cui et al., 2004
1,8-Diazabicyclo-[5.4.0] undec-7-ene (DBU)	Stainless-steel reactor, P=150 bar, T=150°C, CH_3OH/EO=10, catalyst dose=1.0 g, t=5 h	SO,	➢ Effect of catalysts amount, reaction temperature, pressure, ➢ Study on phase behaviour, ➢ Effect of epoxide and alcohol.	Y_{DMC} > 96	Kishimoto and Ogawa, 2004
Metal oxide (MgO, CaO, ZnO, ZrO_2, La_2O_3, CeO_2 & Al_2O_3)	Stainless-steel reactor, P=80 bar, T=150°C, CH_3OH/EO=10, catalyst dose=1.0 g, t=15 h EO+PO+SO=100 mmol, CH_3OH200 mmol.	All EO, SO and PO	➢ Effect of different alcohol, Proposed a reaction mechanism, ➢ Catalyst was characterized and correlated with their properties. ➢ To study the recyclability of the catalyst.	C_{PO}=82.3 Y_{DMC}=60	Bhanage et al., 2001

*PC=Propylene Carbonate, BO=Butylene oxide, EO=Ethylene oxide, PO=Propylene oxide, PG=Propylene glycol, PC=propylene carbonate, CIPO= Epi-chlorohydrin, SO=Styrene oxide, CHO=Cyclohexane oxide, DMC=Dimethyl carbonate, Y_{DMC}=Yield of DMC, C_{PO}=Conversion of PO, S_{PC}=Selectivity of PC, S_{PG}=Selectivity of PG.

Various types of heterogeneous catalysts have been used for the production of DMC from CO_2 and epoxide. Meng et al. [2014] synthesized ammonium bromide/dicyandiamide–formaldehyde polymer (ABMDFP) and used it in continuous flow system and optimized the reaction conditions such as temperate, pressure, catalyst amount and time and recyclability of catalysts. Various authors have synthesized ionic liquid-based catalysts used for the synthesis of DMC from CO_2 with epoxide [Li et al., 2011; Yan et al., 2011; Wang et al., 2014]. Some of the authors also worked on the mixed metal oxide based catalysts and optimized the reaction conditions [Bhanage et al., 2001; Jiang and Yang, 2004; Wei et al., 2013]. Few studies are reported on the supported catalysts for synthesis of DMC [Chang et al., 2004; Sankar et al., 2006]. Table 2.2.7 compares various types of catalysts, operating conditions, etc.

Many patents have been granted on the synthesis of DMC using different processes. Table 2.2.8 complies different patents available on transesterification of EC, transesterification of urea and direct conversion of CO_2 to DMC.

Table 2.2.8. List of patents on DMC production.

Title	Patent No	Organization	Authors and Year
Synthesis of dimethyl carbonate and related compounds	WO2014072802A2	CSIR, New Delhi	Ranade et al., 2014
Process for making dimethyl carbonate	WO2013175510A1	CSIR, New Delhi	Srinivas et al., 2013
Methods for dimethyl carbonate synthesis	EP1623758B1	Mitsubishi Heavy Industries Ltd.	Osora et al., 2012
Process for the production of high-purity dimethyl carbonate	US20120283464A1 EP20100790588	San Donato Milanese (Milano)	Ghirardini et al., 2012
Synthesis of dimethyl carbonate carbon dioxide and methanol	US20110196167A1	King Abdulaziz City Science and Technology	Almusaiteer et al., 2011
Process for producing dimethyl carbonate containing compositions	US20100099806A1	E. I. Du Pont De Nemours and Company, Delaware	Houze et al., 2010
Catalysts for dimethyl carbonate synthesis	US7674742B2	Mitsubishi Heavy Industries Ltd.	Osora et al., 2010
Method and device for manufacturing dimethyl carbonate	US7605285B2 US20070037998A1	Mitsubishi Heavy Industries Ltd.	Kobayashi et al., 2009, 2007
Catalyst for the synthesis of dimethyl carbonate from urea and methanol, preparation and use thereof	US7271120B2 US20060047136A1 EP1629888A1	Institute of coal, chemistry; and Feicheng acid chemical Co. Ltd.	Sun et al., 2007
Method and device for manufacturing dimethyl carbonate.	WO2004092109A1 EP1616855A4	Mitsubishi Heavy Industries Ltd.	Kobayashi et al., 2004
Process for the preparation of dimethyl carbonate	US005498744A	Bayer Aktiengesellschaft	Jentsch et al., 1996
Process for the preparation of dimethyl carbonate	US005543548A	Bayer Aktiengesellschaft	Landscheidt et al., 1996
Process for cosynthesis of ethylene glycol and dimethyl carbonate	US004661609	Taxaco Inc.	Knifton, 1987

2.3. MIXED OXIDE AND HYDROTALCITE CATALYSTS

In recent years there has been a strong interest in obtaining a fundamental understanding of the chemical behavior of mixed-metal oxides at the nanometer size range. Various types of mixed metal oxide-based catalysts are synthesized using various techniques such as sol-gel, co-precipitation, hydrothermal, combustion, surfactant templating and templating methods. These methods play very important role in the morphological, functional and structural properties of mixed metal oxide catalyst.

Ceria (CeO_2) and CeO_2-based catalysts play a vital role in the emerging technologies for energy-related and environmental applications. CeO_2 is a chemically stable oxide, with an outstanding capacity to store or release oxygen due to the variation of the oxidation state of cerium between +3 and +4, under various reductive or oxidizing conditions, and CeO_2 spread over the high surface area is thermally stable. Ceria-based mixed oxides exhibit improved oxygen storage capacity (OSC) and lower reduction temperatures as compared to pure ceria.

Catalytic performance can be compared by changing the properties of the metals by doping the active cerium phase with metal (zirconium, zinc, yttrium, lanthanum, cobalt, copper, iron, etc.) oxide nanoparticles. Ce-Zn mixed metal oxides are synthesized by various methods, and preparation strategies (impregnation, grafting, co-precipitation, chemical vapor deposition methods, hydrothermal synthesis, and sol–gel process). Ce-Zn mixed metal oxide catalysts are widely used in the industrial production of chemicals, and intermediates. Major applications include the oxidation CO to CO_2, produced [Xie et al.,2014], esterification [Wang et al., 2011], cyclo-hexanol dehydrogenation [Mishra and Rao, 2006], oxidative reaction of CO_2 to produce C_2 hydrocarbons [He et al., 2013], oxidative steam reforming to produce hydrogen [Ying et al., 2012], etc. Table 2.2.8 presents a comparative assessment of the characteristics of Ce-Zn catalysts and their applications.

Hydrotalcite-like compounds (HTLc) have been used in various applications because of their unique acid–base properties and their utility as bi-functional redox-base catalyst [Centi et al., 2008]. HTLc can be represented in terms of composition by the following

general formula: $[M(II)_{1-x}M(III)_x(OH)_2]^{x+}(A^{n-})_{x/n}.mH_2O$, where M(II), M(III) are divalent and trivalent citations in the octahedral position in hydrotalcite layers, x is the molar ratio of M(III)/M(II) and A^{n-} is the interlayer exchangeable anion [Zhao et al., 2013]. Thus, M(II) can be Mg(II), Zn(II), Ni(II), Ca(II), Cu(II), Co(II), etc. M(III) is mostly Al(III), however, Fe(III), Mn(III), La(III), etc. can also be used. Thus, a number of combinations of HTLc can be prepared. Calcinations of these materials results in the loss of crystal water, hydroxyl, interlayer anions and destroy hydrotalcite-like layered structures along with the formation of metal oxides [Zhao et al., 2013].

Only a few authors have synthesized Cu-Zn-Al (hydrotalcites) based catalysts earlier. They used these catalysts for different applications such as CO_2 or CO hydrogenation to produce methanol or higher alcohol [Gao et al., 2013; Heracleous et al., 2013], hydrogenation of fatty acid ester or dimethyl oxalate or glycerol [He et al., 2013; Zhang et al., 2012; Mehar et al., 2009], steam reforming of methanol or ethanol [Cunha et al., 2012; Busca et al., 2006] etc.

Table 2.2.9 presents in brief the work reported on the characterization of Cu-Zn/Al (HTLc) catalysts and their applications.

2.4. RESEARCH GAPS

A critical literature review on DMC production from various routes shows that the maximum work has been reported on the oxidative carbonylation of methanol, transesterification and direct CO_2 conversion methods. For transesterification and direct CO_2 conversion methods, one of the major challenges is to synthesize catalysts which have high physcio-chemical and thermal stability during time-on-stream experiments and their regeneration and reusability for the DMC production.

Various types of catalysts such as single metal oxides, mixed metal oxides, etc. have been used in the DMC synthesis by transesterification of PC with methanol (chapter 2), Table 2.2.7. Only one study on the use of pure ceria is reported for the DMC synthesis by transesterification with EC [Xu et al., 2014]. However, no study is reported on the use of

ceria-based catalyst for the DMC synthesis by transesterification with PC. It may also be seen in the literature review presented in Chapter 2, that the mixed oxides of metals Ce and La have been used previously individually or in combination with other metals, however, mixed oxides of Ce and La together have not been used for the DMC synthesis, although the ceria-lanthanum based catalysts were prepared and used in various other applications.

Similarly, ceria-zinc oxide-based catalysts have been used in CO oxidation, steam reforming, methanolysis, desulfurization, etc. (as shown in chapter 2, Table 2.2.8). Comparative assessment of the characteristics of the ceria-zinc based catalysts and their applications are (given in the Table 2.2.8). Shows table that the ceria-zinc oxide supported on $Al_2O_3/SiO_2/TiO_2$ has never been used for the synthesis of DMC using transesterification reaction. Most of the researchers also did not characterize the ceria-zinc catalyst. Thus, it is found that the use of the ceria-zinc oxide catalyst supported on $Al_2O_3/SiO_2/TiO_2$ for the transesterification of PC with methanol is not reported till date.

Few authors have previously synthesized copper-zinc-aluminum hydrotalcite (HTLc)-based catalysts and used them for different applications. Table 2.2.10 shows a comparative assessment of the characteristics of copper-zinc-aluminum HTLc and their applications. It may be seen that only a limited numbers of research articles are available on the use of HTLc for DMC production [Watanabe et al., 1998; Stoica et al., 2009; Murugan and Bajaj, 2010b; Wu et al., 2013]. Only Unnikrishnan and Srinivas [2012] and Murugan and Bajaj [2010b] have used PC as a raw material for the synthesis of DMC using any type HTLc as catalyst. It may be seen in Tables 2.2.6 and 2.2.7 that the copper-zinc-aluminum HTLc hasn‘t been used for the synthesis of DMC using transesterification reaction. Thus, it is seen that no studies are reported on the transesterification of PC by C-M, Ce-La, Ce-Zn mixed oxides and Cu-Zn-Al HTLc catalyst.

During the synthesis of DMC by direct CO_2 conversion reaction, deactivation of catalyst, difficult separation process, and recovery of catalyst, etc. are some of the drawbacks of the homogeneous systems. Subsequently, various heterogeneous catalysts have been investigated for DMC synthesis. Among these studies, only few studies are reported on Ce-Zr

catalysts. Zhang et al. [2009] synthesized and characterized $Ce_{0.5}Zr_{0.5}O_2$ catalyst and used it for the DMC synthesis from CO_2. However, Lee et al. [2012] synthesized $Ce_{0.4}Zr_{0.6}O_2$ catalysts by sol-gel method and transition metal oxides (Ga_2O_3, La_2O_3, Ni_2O_3, Fe_2O_3, Y_2O_3, Co_3O_4, and Al_2O_3) were further supported on $Ce_{0.6}Zr_{0.4}O_2$ by an incipient wetness impregnation method and used as catalysts for the DMC synthesis. These authors correlated the amount of DMC formed in mmol/g-catalyst with basicity and acidity of the catalysts. Chen et al. [2014] used CeO_2 and ZrO_2 catalysts individually for the direct conversion of CO_2 with methanol into DMC, and studied their reaction mechanism. Thus, neither the effect of operating parameters such as catalyst dose, reaction temperature and reaction time have been studied earlier nor were these parameters optimized for the synthesis of DMC using CeO_2-ZrO_2 catalysts. Reusability of the catalysts has also not been studied. Also, a comparative study on CeO_2, ZrO_2 and combined CeO_2-ZrO_2 catalysts for the synthesis of DMC from CO_2 has also not been performed. Moreover, no studies are reported on Ce-Mn and Ce-Ca catalysts for the DMC synthesis. In addition, thermodynamics and kinetic studies on transesterification and direct CO_2 conversion methods using non-ideal conditions are not reported much.

Table 2.2.9. A brief summary of work done on the characterization of ceria-zinc based catalysts for various applications.

Characterization technique	Xie et al. 2014	Rajgure et al. 2014	Mi et al. 2012	Joe et al. 2012	Zhong et al. 2012	Ying et al. 2012	Wang et al. 2011	Ma et al. 2010	Mishra and Rao 2006	He et al. 2006	This Work
	CeO_2-ZnO	CeO_2–ZnO	Ce-ZnF_2O_3	ZnO (X) – CeO_2 (1-X)	$Ce_{1-x}Zn_xO_{2-\delta}$ oxide	$Ce_{1-x}Zn_xO_y$	$S_2O_8^{2-}$/Al_{-x} wt% Ce–Zn–O	ZnO-CeO_2	CeO_2-ZnO	CeO_2/ZnO	CeO_2-ZnO/support Al_2O_3/SiO_2/TiO_2
XRD	X	X	X	X	X	X	X	X	X	X	X
N2-sorption	X		X	X				X		X	X
SEM	X	X	X		X		X	X	X	X	X
FTIR	X						X				X
TPD-NH_3				X					X		X
TPD-CO_2				X						X	X
TEM	X	X			X			X			
CHNS									X		
TPD-Methanol						X					
Process	CO Oxidation	Gas sensor	Desulfurization	Urea methanolysis	CO Oxidation	Oxidative stem reforming	Esterification	Photocatalytic oxidation	Cyclohexanol dehydrogenation	Oxidative reaction of CO_2	Synthesis
End Products	CO_2, H_2, H_2O			Dimethyl carbonate	CO_2, H_2, H_2O	Hydrogen	n-butyl acetate			C_2 Hydrocarbons	Dimethyl carbonate

*X denotes that particular study reported in the study. XRD=X-ray powder diffraction; SEM=Scanning electron microscope; FTIR=Fourier transform infrared spectroscopy; TPD= Temperature-programmed desorption; TEM=Transmission electron microscopy; CHNS=Elemental analysis.

Table 2.2.10. A summary of work done on the synthesis and characterization of synthesis and characterization of Cu-Zn-Al hydrotalcite catalysts for various applications.

Characterization technique and application	Gao et al., 2013	He at al., 2013	Cunha et al., 2012	Zhang et al., 2012	Kaluza et al., 2011	Heracleous et al., 2013	Mehar et al., 2009	Venugopa et al., 2009	This Work
	Cu/Zn/Al/Zr	Cu/Zn/Al	Cu/Zn/Al	Cu/Zn/Al	Cu/Zn/Al	Cu/Zn/Al	Cu/Zn/Al	Cu/Zn/Al/M	Cu/Zn/Al
Cu:Zn:Al ratio	2/1/0.7/0.3	2/1/1	1.5/0.5/1	1/1/1	1/1/1	1.5/1.5/1; to 2/2/0	1/1/1	6/2.5/1:0/0.5	1/1/1
Calcination temp. (°C)	500	350	200, 600	500,600, 700	320	300	450, 600	400	300, 500, 800
XRD	X	X	X	X	X	X	X	X	X
N2-sorption	X	-	X	X	X	X	X	X	X
SEM/TEM*	X	-	X/X*	X*	-	X	-	X	X
FTIR	-	-	-	-	-	-	-	-	X
TPD-NH_3	-	-	-	-	-	X	X	-	X
TPD-CO_2	X	-	-	-	-	-	X	-	X
TPR-H_2	X	X	X	X	X	X	-	X	-
TGA	X	X	X	-	X	-	-	-	X
ICP-AES	-	-	X	-	-	X	X	-	-
XPS	X	X	-	X	-	-	-	X	-
ESR/ Chemisorption*	X	-	-	-	-	-	-	X*	-
Process	CO_2 hydrogenation	Hydrogenation of fatty acid ester	Ethanol Steam Reforming	Hydrogenation of dimethyl Oxalate	Synthesis	CO Hydrogenation	hydrogenolysis of glycerol	Synthesis	Synthesis
End Products	Methanol	Fatty alcohol	Hydrogen	Ethylene Glycol	Methanol	Higher alcohol	propylene glycol	Dimethyl ether	DMC

XRD=X-ray powder diffraction; SEM=Scanning electron microscope; FTIR=Fourier transform infrared spectroscopy; TPD=Temperature-programmed desorption; TEM=Transmission electron microscopy; CHNS=Elemental analysis; TGA=Thermogravimetric analysis; ICP-OES=Inductively coupled plasma atomic emission spectroscopy; XPS=X-ray photoelectron spectroscopy; EPR=Electron paramagnetic resonance.

Chapter – 3

EXPERIMENTAL

This chapter deals with the description of the materials and the experimental method adopted for the synthesis of dimethyl carbonate (DMC). The details of the materials and the methods related to the synthesis of various catalysts are also described in this chapter. The details of the instruments and operating conditions used for the characterization of the synthesized catalysts and the determination of propylene carbonate (PC), DMC, propylene glycol (PG), and methanol are also described. The experimental procedures used for DMC production using direct CO_2 conversion reaction are also discussed.

3.1. CHEMICALS AND REAGENTS

All chemicals used in the study were of analytical reagents (AR) grade DMC, methanol, PC and PG were purchased from Sigma Aldrich chemicals, Germany.

The reagents such as copper nitrate trihydrate ($Cu(NO_3)_2.3H_2O$), zinc nitrate hexahydrate ($Zn(NO_3)_3.6H_2O$), aluminum nitrate nonahydrate ($Al(NO_3)_3.9H_2O$), ferrous nitrate nona-hydrate ($Fe(NO_3)_3.9H_2O$) and cobalt nitrate hexahydrate ($CO(NO_3)_2{\cdot}6H_2O$) were purchased from Himedia Chemicals, India. Cerium nitrate hexahydrate ($Ce(NO_3)_3.6H_2O$), manganese nitrate tetrahydrate ($Mn(NO_3)_2{\cdot}4H_2O$), lanthanum nitrate hexahydrate ($La(NO_3)_3{\cdot}6H_2O$) and zirconium oxynitrate hydrate ($ZrO(NO_3)_2{\cdot}xH_2O$) were purchased from Sigma Aldrich chemicals, Germany. Sodium hydroxide (NaOH) and sodium carbonate (Na_2CO_3) were purchased from VWR chemicals, Germany. Ammonia solution (25 wt.% in H_2O) and nitric acid (65 wt.% in H_2O) were purchased from Rankem Chemicals, India. Al_2O_3 and TiO_2 were obtained grants by Evonik Degussa, Germany; SiO_2 was purchased from Thomas Baker Chemicals, India. Preactivated (24 h at 110°C) Polymer-based spherical activated carbon (PBSAC) spheres (Brunauer-Emmett-Teller (BET) surface area=1748 m^2/g; Barrett-Joyner-Halenda (BJH) volume=2 cm^3/g; diameter=0.45-0.5 mm) were obtained

grants from Blücher, GmbH, Germany. Pluronic F-127 was purchased from BASF, GmbH, Germany. Double distilled water and the Milli-Q water were obtained from the Milli-Q water filtration station (Millipore) in the laboratory. This was used in the synthesis of the catalyst, washing, etc.

3.2. SYNTHESIS OF CATALYSTS

3.2.1. DMC Synthesis using Transesterification of PC with Methanol

3.2.1.1. Ce-M catalysts (M=Co, Fe, Cu and Zn) mixed metal oxide using sol-gel method

Solid Ce-M catalysts (M=Co, Fe, Cu and Zn) were synthesized by complex decomposition method using $Ce(NO_3)_3.H_2O$, $Cu(NO_3).H_2O$, $Co(NO_3).H_2O$, $Fe(NO_3).9H_2O$, $Zn(NO_3).6H_2O$ as precursors of metals and citric acid as complexing agent. In a typical synthesis of CeCo, CeCu, CeFe and CeZn catalysts, a known amount of $Ce(NO_3)_3.H_2O$ and $M(NO_3).xH_2O$ (x=hydrated nitrates) were mixed with 100 mL of ethanol [0.5 mol/L, Ce/M=1.0 (molar ratio)] and put in to a 1000 mL beaker. Citric acid solution in ethanol (0.5 mol/L, 100 mL) was added drop-by-drop in the bulk solution over a period of 60 min under vigorous stirring condition. The mixture was further stirred for 12 h at the room temperature. The resulting solution was evaporated at 80°C for 18 h during which time the resulting sol was converted into the dried xerogel. After grinding the dried xerogel, it was calcined at 100°C for 30 min and then at 500°C for 4 h. Thereafter, the calcined samples were used as the catalysts for DMC synthesis using transesterification of PC with methanol.

3.2.1.2. Ceria-lanthanum mixed metal oxide using co-precipitation method

Ceria and lanthanum oxide solid solution were synthesized with different Ce/La molar ratio (0.2; 0.4; 0.6; and 0.8) by co-precipitation method using liquid ammonia solution as a precipitating agent. The cerium and lanthanum precursors namely $Ce(NO_3)_3.6H_2O$ and $La(NO_3)_3.6H_2O$, respectively, were first dissolved separately in 100 mL double distilled water at a given molar ratio and mixed together under continuous stirring at room temperature. Liquid ammonia solution was added drop-by-drop in the mixed metal solution

over a period of time until the pH of the solution reached ~8.5. The slurry which was obtained in light yellow/orange color was washed several times with double distilled water until it was free from anion impurities. The precipitate obtained was dried at 120°C under air atmosphere in an oven for 24 h and thereafter calcined at 500°C for 4 h under air atmosphere to obtain the ceria/lanthanum mixed oxides in solid phase.

3.2.1.3. CeO_2-ZnO-support mixed metal oxide using deposition-coprecipitation method

Ceria and zinc oxide were impregnated onto various individual oxide supports, namely Al_2O_3, TiO_2 and SiO_2. These catalysts were synthesized in the CeO_2:ZnO:support=1:1:2 molar ratio by a deposition-coprecipitation method using liquid ammonia as the precipitating agent [Reddy et al., 2008]. Metal precursors such as hexahydrates of cerium nitrate and zinc nitrate with a 1:1 molar ratio were dissolved separately in 100 mL of double distilled water and mixed together at room temperature. The supporting oxide was dispersed in 100 mL of water, stirred vigorously and thereafter metal precursor cerium-zinc solutions were mixed together in the molar ratio specified earlier. The prepared mixture was diluted with 100 mL of double distilled water and stirred for 1 h. Liquid ammonia was added drop by drop in the mixture under vigorous stirring condition until the pH reached 8.5. The mixture was filtered and the filtered precipitate was washed with double distilled water until it was free from all anion impurities. Thereafter, the solid precipitate was dried at 110°C for 24 h and calcined at 500°C under air atmosphere for 4 h. The composite oxides, thus formed, were denoted as CZA, CZT and CZS, where C, Z, A, T and S denote Ce, Zn, Al, Ti, and Si, respectively.

3.2.1.4. Copper-zinc-aluminum (HTLc) using co-precipitation method

Cu/Zn/Al (HTLc) catalyst was synthesized using co-precipitation method using $Cu(NO_3).3H_2O$, $Zn(NO_3).6H_2O$ and $Al(NO_3).9H_2O$ with molar ratio of Cu^{2+}:Zn^{2+}:Al^{3+} being 1:1:1. (8 g) NaOH (2 M) and (5.3 g) Na_2CO_3 (0.5 M) solution were mixed together and the mixed solution was added drop-by-drop in 100 mL water under vigorous stirring condition at room temperature and the pH was maintained ~9.5. The formed solution was aged for 24 h

under stirring condition, and then filtered and the precipitate on the filter paper was washed with double distilled water until the pH of the filtrate became neutral. The resulting precipitate was dried at 110°C for 24 h. This hydrotalcite material was calcined at 300, 500 and 800°C and was designated as CZA300, CZA500 and CZA800, respectively.

3.2.2. DMC Synthesis from Direct Conversion of CO_2 with Methanol

3.2.2.1. Ceria-zirconium based catalysts synthesized by hydrothermal method

CeO_2, $Ce_{0.5}Zr_{0.5}O_2$ and ZrO_2 catalysts were synthesized using hydrothermal method. $Ce(NO_3)_3.6H_2O$ (0, 6, 12 mmol), and $ZrOCl_2.8H_2O$ (12, 6, 0 mmol) were dissolved separately in 50 mL ethanol and then were mixed together in desired molar ratio under continuous stirring at room temperature. Liquid ammonia solution was added drop-by-drop in the mixed metal solution over a period of time until the pH became ~9.5. The resultant solution was aged under continuous stirring at the same speed for 4 h. This solution was introduced in a 100 mL teflon-lined autoclave and kept at 120°C for 24 h, then left to cool naturally to room temperature. The resulting slurry had yellow colour and it was centrifuged and the solid retained by the centrifuge was washed several times with double distilled water until the pH become neutral of the liquid. The resulting precipitate was dried at 110°C for 24 h in air. Finally, the fresh samples were calcined at 500°C for 4 h in air atmosphere to obtain CeO_2, $Ce_{0.5}Zr_{0.5}O_2$ and ZrO_2 catalysts.

3.2.2.2. Ceria-zirconium based catalysts synthesized by carbon templating method

Cerium-zirconium mixed oxide catalysts with different $Ce_{1-x}Zr_xO_2$ (x=0 to 1) molar ratios were synthesized using exo- and endo-templating method. For this, $Ce(NO_3)_2$ and $Zr(NO_3)_3$ were dissolved separately in 100 mL in double-distilled water and were further mixed together in the desired molar proportion $Ce_{1-x}Zr_xO_2$ (x=0 to 1) under continuous stirring at room temperature. Liquid ammonia solution was added drop-by-drop to the precursor solution over a period of 0.5 h until the pH reached ~9.5 and a white/light yellow precipitate was formed. The mixture was aged for 2 h under continuous stirring, and thereafter was filtered. The precipitate retained on the filter was washed with double-distilled

water until the pH of the filtrate became neutral. Finally, the filter cake was transferred to a 200 mL polypropylene (PP) bottle and double-distilled water was added to it until the total weight of the mixture become 30 g. Thereafter, 2.5 mL HNO_3 (65 wt.% in H_2O) was added to the mixture. The PP-bottle was transferred to an ultrasonic bath (Sonorex RK1, Fa. Bandelin) where it was kept for 4 h until a clear sol was formed. Pluronic F-127 as triblockcopolymer (TBC) was added such that the molar ratios of TBC to cerium along with zirconium (nTBC/nCe+Zr) become 0.017. This ratio was the optimum to the sol as a endo-template [With et al., 2010]. This mixture was again kept in the ultrasonic bath for 2 h for dissolving the Pluronic F-127. 4.42 g preactivated (for 24 h at 110°C) polymer-based spherical activated carbon (PBSAC) was added to the nanoparticle sol and was further dried at 60°C for 12 h. The carbon spheres were then calcined at 600°C for 5 h under air flow (40 cm^3/min) at a heating rate of 3°C/min from room temperature to 600°C with a holding time of 1 h at 100°C and 5 h at 600°C. After calcination, light yellow $Ce_{1-x}Zr_xO_2$ mixed oxide spheres were obtained. For characterization and catalytic experiments, $Ce_{1-x}Zr_xO_2$ mixed oxides were sieved to obtain the sphere in the size range of 0.2-0.4 mm.

3.2.2.3. Ceria-manganese-based catalysts synthesized by surfactant templating method

Ceria-manganese catalysts were synthesized by surfactant-template method with different molar ratios of Mn/Ce and hexadecyltrimethyl ammonium bromide (CTAB) as the template. In the synthesis of catalysts, CTAB, cerium nitrate and manganese chloride (CTAB/(Ce+Mn)=0.8 molar ratio were dissolved in 100 mL double distilled water under continuous stirring at room temperature. Liquid ammonia solution was added drop-by-drop in the mixed metal solution over a period of time until the pH reached ~11.5. After further stirring for 2 h, the resulting obtained suspension was transferred to a teflon-sealed autoclave and aged for 48 h at 120°C. Finally, a brown color slurry was filtered and the filter cake was obtained which was washed several times with double distilled 80% water with 20% acetone to remove the surfactant until pH became neutral [Liu et al., 2012]. The washed cake (in the form of particles) was dried at 120°C for 48 h and then calcined at 500°C for 5 h under air

flow (40 cm^3/min). The heating rate was 3°C/min from the room temperature to 600°C with a holding time of 1 h at 100°C and 5 h at 500°C. Synthesized catalyst particles were denoted as Ce_1-$Mn_{0.125}$, Ce_1-$Mn_{0.25}$ and Ce_1-Mn_1 with the Mn molar ratio of 10, 20 and 50%.

3.2.2.4. Ceria-calcium-based catalysts synthesized by surfactant templating method

CeO_2-CaO catalysts were synthesized by surfactant-template method and CTAB was used as the template. 1 M calcium nitrate and 1 M cerium nitrate solution were homogeneously mixed in various molar ratios of the catalyst samples. Synthesized catalysts were designated as Ce_1Ca_3, Ce_1Ca_1 and Ce_3Ca_1, respectively. In the synthesis of catalysts, CTAB, calcium nitrate and cerium chloride (CTAB/(Ce+Ca)=1) were dissolved in 100 mL ethanol under continuous stirring at room temperature. Liquid ammonia solution was added drop-by-drop in the mixed metal solution over a period of time until the pH became ~11.5. After further stirring for 2 h, the obtained suspension was transferred to a teflon-sealed autoclave and aged for 12 h at 120°C. Finally, a brown color slurry was filtered and the filtered solid particles were obtained which was washed several times with 80% double distilled water having 20% acetone mixture thoroughly to remove the surfactant [Zhao et al., 2010]. The resulting powder was dried at 120°C for 24 h and then calcined in air at 500°C for 5 h under air flow (40 cm^3/min). The heating rate was 3°C/min from the room temperature to 500°C with a holding time of 1 h at 100°C and 5 h at 500°C. The calcined catalyst particles were used as such in the experiments for their characterization and the DMC synthesis.

3.3. CHARACTERIZATION OF CATALYSTS

To understand the thermal and physcio-chemical characteristics of the synthesized catalysts, a number of characterization techniques were used as described below in this section.

3.3.1. X-ray Diffraction (XRD)

XRD was used to study the molecular structure, atoms and crystalline nature. For this purpose, Samples were crushed with a mortar before testing. X-ray diffractograms were

obtained with (Brueker AXS, Germany) diffractometer D8 operated at 40 kV and 30 mA with Cu Kα radiation (λ=1.5406Å) with step size of 0.02 over 2θ scan range 5≤ 2θ ≤100°. Crystalline phase was identified by PANalytical X'pert high score software with reference from International Centre for Diffraction Data (ICDD) database. Lattice parameter was calculated by standard cubic indexation method. Crystallite size were calculated from the Scherrer's equation:

$$L = \frac{K\lambda}{\beta cos\theta} \qquad (3.1.1)$$

where, K is the Scherrer's constant, which generally takes a value of 0.94, λ is the wavelength of X-ray radiation which is equal to 1.54051 Å, β is the full width of the reflection at half maximum (FWHM) in radian and θ is the scattering angle of the main reflection.

3.3.2. Surface Area and Pore Size Distribution

N_2 sorption isotherms utilize the principle of physical adsorption to get the information about BET surface area, pore size distribution and porosity of the solid materials. Textural properties were determined using multi point N_2-sorption measurements at -197°C, using Micromeritics ASAP 2020 apparatus. Samples were kept at 120°C for overnight in oven and then degassing was done for 6 h at 200°C under N_2 flow to remove any absorbed impurities. BET isotherm was used for calculating the surface area of the porous material by physical adsorption of N_2 gas at it's boiling temperature. The amount of gas adsorbed was measured by a continuous or volumetric flow procedure. BET isotherm is represented by following equitation [BET isotherm]:

$$\frac{1}{\left[V_a\left(\frac{P_o}{P}-1\right)\right]} = \frac{C-1}{V_m C} \times \frac{P}{P_o} + \frac{1}{V_m C} \qquad (3.1.2)$$

where, P is the partial vapour pressure of the adsorbate gas in equilibrium at the surface at 77 K, P_o is the saturated pressure of the adsorbate gas, V_m is the monolayer volume at the sample

surface, V_a is the volume of the gas adsorbed at the equilibrium pressure and temperature, and C is the dimensional constant which depends upon the heat of adsorption (Q_a) and the heat of liquefaction (Q_l) of nitrogen. Monolayer volume calculated from the adsorption isotherm was used for the calculation of specific surface area. Barrett-Joyner-Halenda (BJH) model given by following equitation was used to compute the pore size distribution from desorption branch of isotherm [Barrett et al., 1945]

$$\ln(P/P_o) = -2\sigma v \cos(\theta'/r_k R) \qquad (3.1.3)$$

where, R is the gas constant, θ` is the wetting angle, σ is the surface tension and r_k is the Kelvin radius.

BET surface areas of the catalysts were determined by using adsorption data obtained in the relative pressure (P/P_o) range of 0.05 to 0.35. Total pore volume was calculated from the amount of N_2 vapour adsorbed at a relative pressure of 0.99. BJH model was used for the determination of the pore volume and the pore area from the adsorption branches of the isotherm [Dhachapally et al., 2012].

Irregularity or roughness of the catalyst surface was compared by determining a factor called as fractal dimension (D). Value of D was estimated using N_2 desorption isotherm data of the catalysts using Frenkel-Halsey-Hill (FHH) equation [Halsey et al., 1948]:

$$\frac{q}{q_e} = K_{FHH} \ln\left(\frac{P_o}{P}\right)^{D-3} \qquad (3.1.4)$$

where, q is the amount of N_2 adsorbed at equilibrium pressure P, P_o is the saturated pressure, q_e is the amount adsorbed filling in micropore volume, K_{FHH} is a constant and D is the fractal dimension. Logarithmic plot of q/q_e versus P_o/P showed a linear behavior, and D was calculated from the slope (D-3) of the line. Surface roughness, irregular nature and smoothness of the surface depends upon the D value. If D=2, then the surface is perfectly smooth, whereas if D=3, then the surface is very irregular or rough.

3.3.3. Temperature Programmed Desorption (TPD)

TPD is used to study the binding interaction of adsorbates CO_2 or NH_3 on the catalyst surface and provides the information regarding the adsorbate bound on the surface. It is known that the high temperature desorption peak has stronger bonding of the adsorbates on the catalyst surface. In the TPD study, initially a sample is saturated with the reactant gas, and then physisorbed fraction of the reactant gas is desorbed with the help of inert an gas such as helium. After that the temperature of the sample is increased linearly at a particular heating rate. During this process, an inert carrier gas is passed through the sample at a particular flow rate. The amount of the desorbed CO_2 or NH_3 is quantified with the help of a thermal conductivity detector (TCD). The furnace should be antimagnetic so as to avoid the magnetic field which affect may on the sample.

Acidic and basic nature of the synthesized catalyst was determined by the TPD of NH_3 and CO_2, respectively, using Micromeritics Chemisorb 2720 instrument fitted with a TCD. A 50 mg sample was placed in a quartz U-tube which was activated/pretreated at 200°C under helium flow (20 cm^3/min) for 6 h. After cooling to 50°C, NH_3 adsorption was carried out by admitting 10% NH_3/He stream flow (20 cm^3/min) at 50°C up to saturation for the determination of acidity. Similarly, CO_2-TPD was performed for the determination of basicity using 100% CO_2 gas. Helium gas (20 cm^3/min at for 1 h at 50°C) was used for removing the physically bound NH_3 and CO_2 on the surface of the sample. Desorption profile was recorded from 50 to 900°C at a heating rate 10°C/min under helium flow (20 cm^3/min) and the evolved NH_3 and CO_2 were monitored with a TCD.

3.3.4. Thermogravimetric Analysis (TGA)

Thermogravimetric experiments were carried out for determining the thermo-physico-chemical properties of the catalysts. The weight loss of the sample was estimated as a function of temperature (or time) under atmospheric or inert gas atmosphere. TGA experiments were carried out using SII 6300 EXSTAR analyzer with a air flow rate of 200

cm^3/min in the temperature range of 30-1000°C with a heating rate 10°C/min. Aluminum was used as the reference material.

3.3.5. Fourier Transform Infrared Spectroscopy (FTIR)

FTIR spectroscopy was used to find out the surface functional groups of the synthesized catalysts. A FTIR spectrophotometer (Thermo Nicolet, Model Magna 760) in the wave number range of 400-4000 cm^{-1} was used for the purpose. The hand-pressed KBr pellet was used as the reference material.

3.3.6. Scanning Electron Microscope (SEM)

To investigate the morphology of the synthesized catalysts, scanning electron microscope (SEM) was used. Morphology and elemental composition of the synthesized materials were examined by using quanta 200 FEG from FEI Netherlands and special attachment of electron backscatter diffraction (EDBS). Initially, the prepared sample was spread on the sample holder and then the samples were gold coated using sputter coater (Edwards S150) to increase the conductivity of the preliminary materials. After that, the prepared samples were used for taking image using FE-SEM at 20 kV under vacuum. Thereafter, the energy-dispersive X-ray spectroscopy (EDX) was carried out find out the metal content of the sample. Elemental mapping was used for understanding the metal distribution in the prepared catalysts. Elemental composition determined by this method has a maximum of ±10% error.

3.3.7. Transmission Electron Microscopy (TEM)

To investigate the morphology of the catalysts using transmission electron microscopy (TEM) and the corresponding selected-area electron diffraction pattern were obtained using TECNAI G^2 20S-TWIN, FEI Netherlands with LaB_6 as cathode (resolution: point 0.24 nm and line 0.14 nm). For TEM analysis, catalysts were dispersed with ethanol solution and then sonicated for 30 min, and after that the sonicated catalysts were deposited on the TEM grids. Excess amount of solution was removed by tissue paper and then the grid was placed in a dark room for 30 min to evaporate the remaining moisture. Selected area

electron diffraction (SEAD) patterns were recorded to obtain the crystallographic information.

3.3.8. Atomic Force Microscopy (AFM)

Morphology of the catalysts was also studied using atomic force microscopy (AFM) (M/s Molecular Tools and Devices for Nanotechnology (NT-MDT)), equipped with NOVA software for the image analysis. Small amount (50 mg) of sample was dispersed in ethanol solution and sonicated for 120 min. Afterwards, (50 mg) small amount of solution dispersion was placed on a glass plate and dried at room temperature for 12 h. Then this glass plate was used for AFM analysis.

3.3.9. Atomic Absorption Spectroscopy (AAS) and Inductively Coupled Plasma-Optical Emission Spectroscopy (ICP-OES)

Metal loading on the catalysts was determined by AAS and ICP-OES. For determining the elemental ratio of the catalysts, 1 g of the catalyst was soaked in 10 ml 65% nitric acid for 24 h at room temperature so as to dissolve the metals from the catalysts. The solutions were filtered and the filtrate was used for the determination of the metal concentration by AAS (Avanta M by GBC Scientific Equipment Pvt Ltd.). ICP-OES supplied by OPTIMA 8000 von Perkin Elmer was also used for determining the amount of metals dispersed some catalysts. For sample preparation, the sample (50.0±0.1) was dissolved by a microwave assisted digestion (Multiwave 3000 from Anton Paar) using 2 ml HF (48 wt.%, Suprapur, Merck), 2 ml HNO_3 (69 wt.%, Supra, Roth), 2 ml HCl (35 wt.%, supra, Roth) and 3 ml H_2SO_4 (85 wt.%, suprapur, Merck). Microwave conditions were 1100 Watt/ramp for 20 min hold for 30 min cool for 15 min. After the microwave digestion, 12 ml H_3BO_4 (for complexation of HF) and 1 ml HlO_4 were added. Afterwards, the sample was digested for a second time using microwave conditions as used earlier. After the microwave treatment, H_2O was added until a volume of 50 ml was obtained. In units using these detector arrays, the intensities of all wavelengths (within the systems range) were measured simultaneously. The intensity of each line was then compared to previously measured intensities of known concentrations of the elements, and their concentrations were then computed by interpolation

along the calibration lines. The eight samples were prepared as known concentration for preparation of the calibration curve. Concentration of unknown solution was estimated using this calibration curve.

Techniques used for characterization of catalysts used for transesterification of PC with methanol and for direct conversion of CO_2 for DMC synthesis are listed in Table 3.3.1 and 3.3.2, respectively.

3.4. EXPERIMENTAL PROCEDURE FOR DMC SYNTHESIS

3.4.1. Experimental Procedure for DMC Synthesis using Transesterification of PC with methanol

Catalytic activity of the synthesized catalysts was checked for the synthesis of DMC from transesterification of PC and methanol in a stainless-steel autoclave reactor (700 mL) equipped with mechanical stirrer. The reactor was initially filled with required amounts of PC, methanol and the catalysts. Thereafter, the reactor was flushed with nitrogen and the temperature of the reactant mixture was increased to 170°C under autogenic pressure. After 4 h, the reactor was kept in an ice bath so as to cool down the product mixture quickly to 5-10°C. Thereafter, the catalyst was separated from the mixture by centrifugation.

In the present study, a slightly modified method with respect to that used by Holtbruegge et al. [2013] was used for the simultaneous estimation of DMC, PG, PC and methanol in the reaction mixture obtained after transesterification of PC with methanol reaction. The reaction mixture obtained after the completion of an experimental run was analyzed by a gas chromatograph (GC) (Perkin Elemer) equipped with flame ionization detector (FID) and a 30 m × 0.25 mm long elite-WAX capillary column with oven temperature of 220°C; and injector and detector temperatures of 220°C each. 1 µL sample was injected in split mode with initial column temperature of 40°C and the holding time of 5 min. After that the temperature was ramped to 100°C where it was held for 5 min, and then the temperature was further ramped to 220°C at the rate of 10°C/min where it was held for 5 min. Helium was used as the carrier gas and acetonitrile was used as the internal standard.

For DMC, the turn over frequency (TOF) was calculated using the following equation:

$$TOF = \frac{m_{PC} X_{PC} M_{PC}}{100 A_{Cat} t} \qquad (3.5.1)$$

where, m_{PC} is the initial mole of PC (mol), X_{PC} is the conversion of PC (%), M_{PC} is the molecular weight of PC (g/mol), A_{Cat} is the mass of catalyst used in the reaction (g) and *t* is the reaction time (h).

3.4.2. Experimental procedure for DMC synthesis from direct conversion of CO_2 with methanol

Catalytic direct conversion of CO_2 with methanol to produce DMC was performed in the reaction autoclave (i.e. batch reactor) made by Berghof, Germany (Model-BHL-800). A magnetic stirrer was used to make the reactant mixture homogeneous during the reaction. A rubber made O-ring was used in between the reaction autoclave and the head of the instrument panel to bind them smoothly and to make the reaction chamber air tight.

The reactor was initially filled with the required amounts of methanol and the catalysts. The reactor was heated to the reaction temperature (100-180°C) and pressurized with CO_2 up to a pressure of 150 bar and maintained for 6-48 h for the reactor to proceed. After (6-48 h), the reactor was kept in an ice bath so as to cool down the product mixture to (< −20°C), and thereafter, the catalyst was separated from the mixture by centrifugation. All the reactions were studied in the presence of activated molecular sieve 3A as a dehydrating agent and at constant stirrer speed of 600 revolutions/min. Catalyst was washed with methanol and dried at 150°C for 12 h and then was activated at 500°C for 4 h after each cycle. Similarly, molecular sieve was activated at 240°C for 4 h after each cycle.

Table 3.3.1. Techniques used for characterization of catalysts used for DMC production via transesterification of PC with methanol.

Catalyst	Methods	Characterization Techniques						
		XRD	N_2-sorption	SEM	NH_3-TPD	CO_2-TPD	FTIR	TG
Ce-Co	Sol-gel	Y	Y	Y	-	Y	-	-
Ce-Cu	Sol-gel	Y	Y	Y	-	Y	-	-
Ce-Zn	Sol-gel	Y	Y	Y	-	Y	-	-
Ce-Fe	Sol-gel	Y	Y	Y	-	Y	-	-
$Ce_{0.2}$-$La_{0.8}$	Co-precipitation	Y	Y	Y	Y	Y	-	-
$Ce_{0.4}$-$La_{0.6}$	Co-precipitation	Y	Y	Y	Y	Y	-	-
$Ce_{0.6}$-$La_{0.4}$	Co-precipitation	Y	Y	Y	Y	Y	-	-
$Ce_{0.8}$-$La_{0.2}$	Co-precipitation	Y	Y	Y	Y	Y	-	-
Ce-Zn /Al_2O_3	Deposition-coprecipitation	Y	Y	Y	Y	Y	Y	Y
Ce-Zn /SiO_2	Deposition-coprecipitation	Y	Y	Y	Y	Y	Y	Y
Ce-Zn /TiO_2	Deposition-coprecipitation	Y	Y	Y	Y	Y	Y	Y
CZA300	Co-precipitation	Y	Y	Y	Y	Y	Y	Y
CZA500	Co-precipitation	Y	Y	Y	Y	Y	Y	Y
CZA800	Co-precipitation	Y	Y	Y	Y	Y	Y	Y

Table 3.3.2. Characterization techniques for catalysts used direct conversion of CO_2 for DMC synthesis.

Catalyst	Method	Characterization Techniques					
		XRD	N_2-sorption	CO_2-TPD	NH_3-TPD	FTIR	SEM/TEM*
Zirconium	Carbon templating	Y	Y	Y	Y	Y	Y
Cerium	Carbon templating	Y	Y	Y	Y	Y	Y
Ce-Zr	Carbon templating	Y	Y	Y	Y	Y	Y
Ce-0.125Mn	Surfactant templating	Y	Y	Y	Y	Y	Y/Y*
Ce-0.25Mn	Surfactant templating	Y	Y	Y	Y	Y	Y
Ce-1.0Mn	Surfactant templating	Y	Y	Y	Y	Y	Y
1Ce-1Ca	Surfactant templating	Y	Y	Y	Y	Y	Y/Y*
3Ce-1Ca	Surfactant templating	Y	Y	Y	Y	Y	Y
1Ce-3Ca	Surfactant templating	Y	Y	Y	Y	Y	Y
Cerium	Hydrothermal	Y	Y	Y	Y	Y	Y
Zirconium	Hydrothermal	Y	Y	Y	Y	Y	Y
Ce-Zr	Hydrothermal	Y	Y	Y	Y	Y	Y

Chapter – 4

RESULTS AND DISCUSSION

This chapter presents the results and discussion on the catalyst characteristics and the transesterification reaction of propylene carbonate (PC) with methanol for the production of dimethyl carbonate (DMC) (given as part A). Part B of the chapter deals with the catalysts used, their characteristics and the results and discussion on the direct conversion of CO_2.

Part [A]. TRANSESTERIFICATION OF PC WITH METHANOL FOR THE PRODUCTION OF DMC: Characterization and catalytic activity for synthesis of DMC by transesterification reaction of PC with methanol using following catalysts:

- Ce-M (M=Co, Fe, Cu and Zn)
- Ceria-lanthanum mixed metal oxide i.e. $Ce_xLa_{1-x}O_{2-\delta}$ (x=0.2; 0.4; 0.6 and 0.8)
- Ceria–zinc catalysts impregnated onto various oxide supports, namely Al_2O_3, SiO_2 and TiO_2 (named as CZA, CZS and CZT)
- Copper-zinc-aluminum (CZA) hydrotalcite (HTLc) catalysts calcined at 300^oC, 500^oC and 800^oC (named as CZA300, CZA500 and CZA800)

Part [B]. DMC SYNTHESIS FROM DIRECT CONVERSION OF CO_2 WITH METHANOL: Characterization and catalytic activity for synthesis of DMC by direct conversion of CO_2 with methanol using following catalysts:

- Ceria-zirconium mixed oxide catalysts (CeO_2, $Ce_{0.5}Zr_{0.5}O_2$ and ZrO_2) prepared by hydrothermal method
- Ceria-zirconium mixed oxide catalysts $Ce_{1-x}Zr_xO_2$ (x=0 to 1) prepared by carbon templating method
- Ceria-manganese mixed oxide (CeO_2-MnO_x) catalysts
- Ceria-calcium mixed oxide (Ce_3-Ca_1, Ce_1-Ca_1 and Ce_1-Ca_3) catalysts

Part [A]. DMC SYNTHESIS USING TRANSESTERIFICATION OF PROPYLENE CARBONATE (PC) WITH METHANOL

DMC synthesis using transesterification of PC with methanol was carried out with four different sets of the catalysts, namely Ce-M (M=Co, Fe, Cu and Zn), ceria-lanthanum, CeO_2-ZnO supported mixed metal oxide and copper-zinc-aluminum hydrotalcites. These catalysts were synthesized following the methods given in chapter III. Synthesized catalysts were characterized by various techniques so as to determine their various physico-chemical properties such as crystalline nature, acidic-basic sites, surface area, pore volume, thermal stability and morphology. These catalysts were further tested and used in the DMC production via transesterification of PC with methanol.

4.1. Ce-M (M=Co, Fe, Cu and Zn) CATALYSTS: CHARACTERIZATION AND CATALYTIC ACTIVITY FOR TRANSESTERIFICATION OF PROPYLENE CARBONATE (PC) WITH METHANOL

Ce-M (M=Co, Fe, Cu and Zn) catalysts were synthesized by sol-gel method (details given in chapter 3) and were characterized using scanning electron microscope-energy dispersive atomic spectra (SEM-EDX), X-ray diffraction (XRD), particle size distribution, CO_2-temperature programmed desorption (CO_2-TPD) and atomic absorption spectrophotometer (AAS) in order to know their physico-chemical properties. These catalysts were further used in the DMC production; and the effects of the reaction conditions such as reaction temperature, catalyst dose, the composition of the reactants i.e. molar ratio of methanol/PC and reaction time and the reusability of catalysts were investigated.

4.1.1. Catalysts Characterization

4.1.1.1. X-ray diffraction

XRD pattern of Ce-M catalysts shows the presence of CeO_2 and other metal oxides (Figure 4.1.1). No additional impure phases were found in any of the synthesized catalysts. Most intensive peak was found at $2\theta \approx 28°$ due to CeO_2 in all the Ce-M catalysts and two weak peaks found at $2\theta \approx 35.5°$ and $2\theta \approx 38.7°$ were due to the diffraction peaks of other metals. Shift in these small peaks was due to the difference in the ionic radii of the host (Ce^{4+}=0.97 Å) and

guest (Co^{2+}=0.74 Å, Cu^{2+}=0.72 Å, Fe^{3+}=0.68 Å and Zn^{2+}=0.074 Å) ions [Kumar et al., 2011; Joe et al., 2012; Zhou et al., 2014; Banerjee et al., 2014]. The crystallite size of the catalysts was calculated using (111) crystalline plane diffraction peak of CeO_2 (Table 4.1.1). Crystallite sizes for CeCo, CeCu, CeFe and CeZn were found to be 19.4, 18.8, 9.6 and 21.6 nm, respectively.

4.1.1.2. N_2 adsorption–desorption

N_2 adsorption–desorption isotherms of the synthesized catalysts are shown in Figure 4.1.2 and the variation of pore volume and pore area with pore size is shown in Figure 4.1.2. Detailed textural characteristics are given in Table 4.1.1. All the catalysts exhibit type IV isotherms which corresponds to the porous substances with wide pore size distribution. Such porous substances show adsorption behavior extending from monolayer to multilayer and ultimately to capillary condensation [Brunauer et al., 1940; Zhou et al., 2013]. CeCo and CeCu catalysts exhibit negligible hysteresis, whereas CeFe and CeZn exhibit H_2 type hysteresis behavior corresponding to ink-bottle type of pores. Brunauer-Emmett-Teller (BET) surface area of CeCu, CeCu, CeFe and CeZn were found to be 40, 46, 34 and 38 m^2/g, respectively, whereas Barrett-Joyner-Halenda (BJH) pore volume and pore size were 0.078, 0.065, 0.046 and 0.051 cm^3/g; and 4.47, 5.85, 6.76 and 4.35 nm, respectively.

4.1.1.3. Scanning electron microscopy-energy dispersive atomic spectra

Morphology of the prepared Ce-M based catalysts was investigated by SEM, and these SEM micrographs are shown in Figure 4.1.3. CeCo exhibits a uniform surface morphology, whereas CeFe seems to be more heterogeneous as compared to other catalysts. EDX analysis of the catalyst was done to understand metal dispersion on the catalyst surface and to determine mass distribution (%) percentage of various elements in the catalysts. CeCo catalyst contained 42% O, 28% Ce and 30% Co; CeCu catalyst contained 34% O, 38% Ce, and 26% Cu; CeFe contained 35%O, 41%Ce and 24% Fe; and CeZn contained 16% O, 55% Ce and 29% Zn. Thus, the Ce mass percentage in various prepared catalysts followed the following order: CeZn > CeFe > CeCu > CeCo. These catalysts had other active metals in

following order: CeCo (Co=33%) > CeZn (Zn=29%) > CeCu (Cu=26%) > CeFe (Fe=24%) [Zeppieri et al., 2010].

4.1.1.4. CO_2-temperature programmed desorption (CO_2-TPD)

Basic properties of the catalysts were analyzed by CO_2-TPD analysis (Figure 4.1.4). The strength of the basic sites could be assigned according to the temperature at which peaks appear in CO_2-TPD profiles. Catalysts are supposed to possess weak, moderate and strong basic sites if the desorption peaks are in the range: < 200°C, 200-450°C and > 450°C, respectively [Kraleva et al., 2011]. All the catalysts used in the present study were found to possess weak and moderate basic sites (Figure 4.1.4). According to CO_2-TPD results as shown in Table 4.1.1, the total basicity of CeCo, CeCu, CeZn and CeFe catalysts were 0.083, 0.698, 0.424 and 0.492 mmol/g, respectively. Thus, the amount of basic sites and basic site density were found to be the highest in the CeCu catalyst.

4.1.1.5. Determination of leaching of metals

The leaching test for metals was calculated by refluxing the synthesized catalysts in methanol for 6 h using the optimum of catalyst dose for DMC yield. After the refluxing, the slurry was filtered/centrifuged and the filtrate/centrifuged supernatant solution was analyzed for Ce or M by various AAS. No Ce or metals (M=Co, Fe, Cu and Zn) were detected in the filtrate/supernatant solution. The recovered catalyst-free methanol (in place of direct pure methanol) was used along with PC at the methanol/PC molar ratio of 10 at 160°C for 4 h (as used in the optimum test condition) for testing the catalytic activity in terms of DMC synthesis. The absence of DMC at the end of the test ruled out any homogeneous reaction for DMC formation.

4.1.2. Catalytic Activity of Ce-M (M=Co, Fe, Cu and Zn)

The catalytic activity of Ce-M catalysts was tested in terms of for DMC synthesis from the transesterification of PC with methanol in a batch reactor. The results are shown in Figure 4.1.5. The activity of the CeCu catalyst was found to be the best-in comparision to that of CeCo, CeFe and CeZn catalysts. The turn over frequency (TOF) values of the CeCo, CeCu, CeFe and CeZn were found to be 1.09, 3.29, 2.47 and 2.90 h^{-1}, respectively. A catalyst

having higher BET surface area and higher density of basic sites is excepted to show higher yield of DMC from the transesterification of PC with methanol. Higher BET surface area and basicity are indirectly responsible for higher yield of DMC because of easy transport of the reactants and the products. The active basic sites increase PC conversion, TOF and DMC yield. It is found that the CeCu catalyst exhibits these characterizations. Therefore, further experiments on DMC production using transesterification were conducted with CeCu catalyst only.

Table 4.1.1. XRD, textural and CO_2-TPD analysis of catalysts.

	XRD	**Textural Properties**			**CO_2-TPD analysis**		
Catalyst	d-value[a]	Crystallite size (nm)[a]	Surface Area (m^2/g)	Pore volume (cm^3/g)[b]	Pore size (nm)[c]	Total CO_2 adsorption (mmol/g)	Basic site density ($\mu mol/m^2$)
CeCo	0.98	19.4	40	0.078	4.47	0.083	2.1
CeCu	0.96	18.8	46	0.065	5.85	0.698	15.2
CeFe	1.16	9.6	34	0.046	6.76	0.424	12.4
CeZn	0.84	21.6	38	0.051	4.35	0.492	12.9

[a]The unit cell parameter, crystallite size and the structure are calculated using Sherrer equation.
[b]BJH desorption cumulative pore volume in the percentage range of 17.00 to 3000 Å.
[c]BJH desorption average pore size.

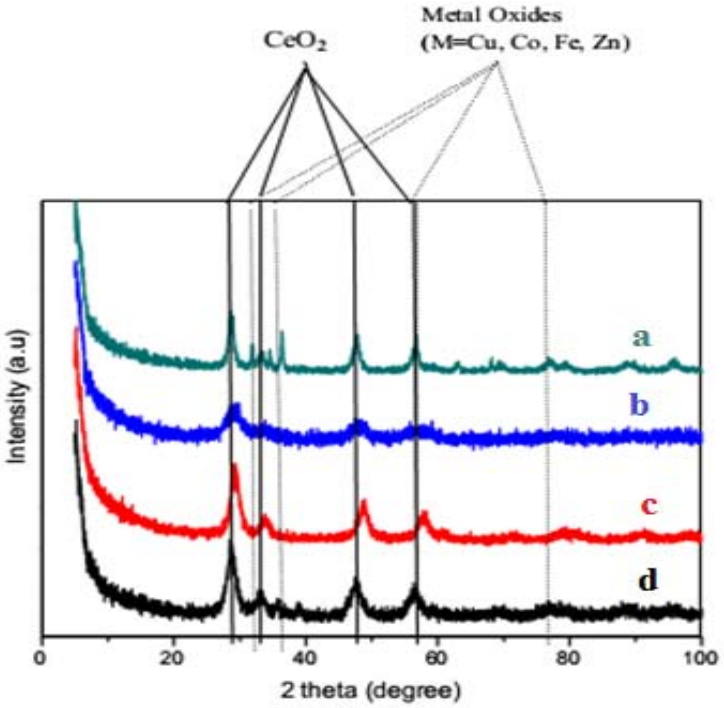

Figure 4.1.1. XRD patterns of Ce-M based catalysts (a) CeZn, (b) CeFe, (c) CeCo, and (d) CeCu.

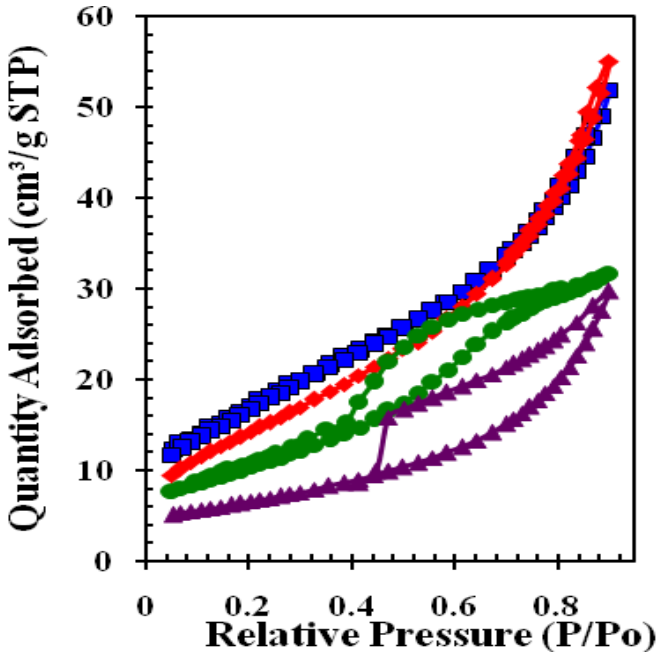

(a)

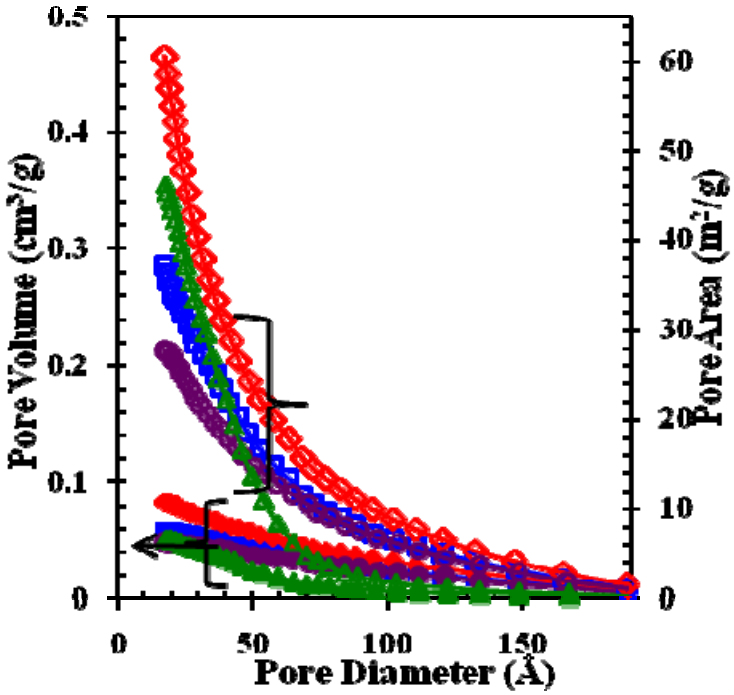

(b)

Figure 4.1.2. (a) Nitrogen adsorption-desorption isotherms; —■— CeCo, —♦— CeCu, —●— CeZn, —▲—CeFe. (b) Variation of cumulative pore volume and cumulative pore area with pore diameter for Ce-M (M=Co, Fe, Cu and Zn) catalysts; —■— CeCo-pore volume, —♦— CeCu-pore volume, —●— CeFe-pore volume, —▲—CeZn-pore volume, —□— CeCo-pore area, —◊— CeCu-pore area, —○— CeFe-Pore area, —△— CeZn-pore area.

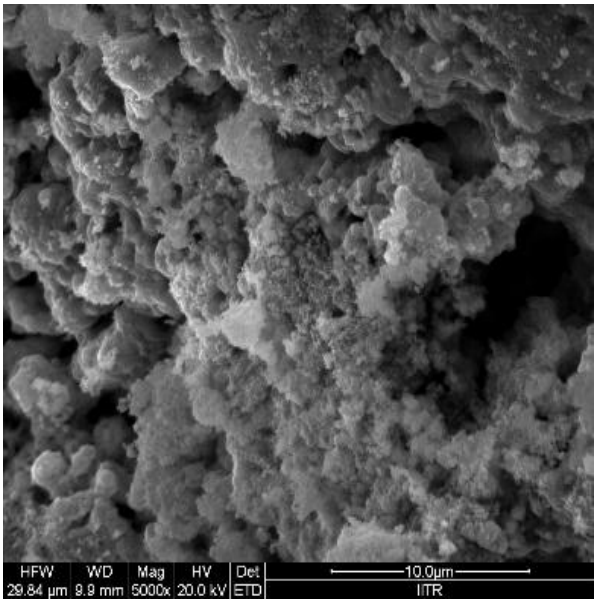

(a) CeZn

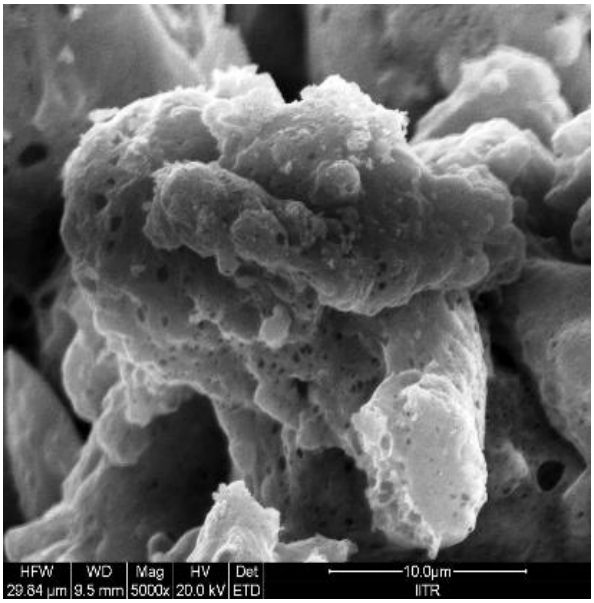

(b) CeFe

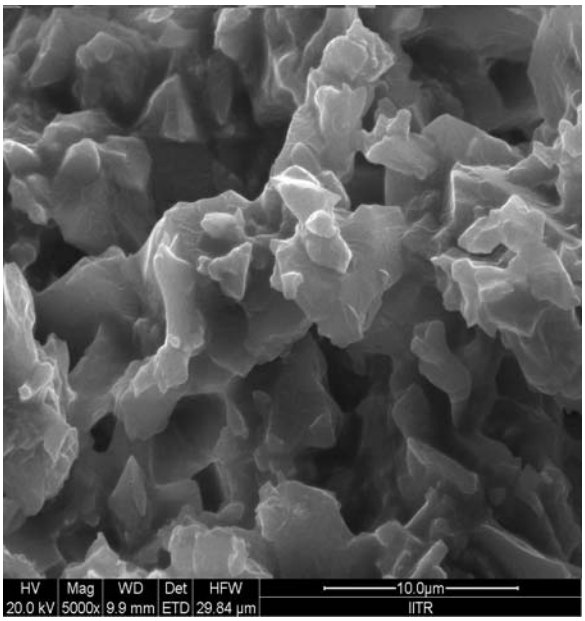

(c) CeCo

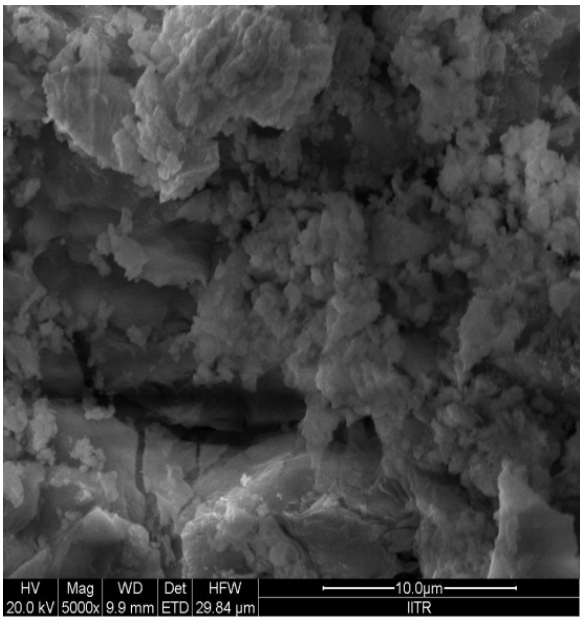

(d) CeCu

Figure 4.1.3. SEM micrographs of Ce-M based catalysts: (a) CeZn, (b) CeFe, (c) CeCo, and (d) CeCu.

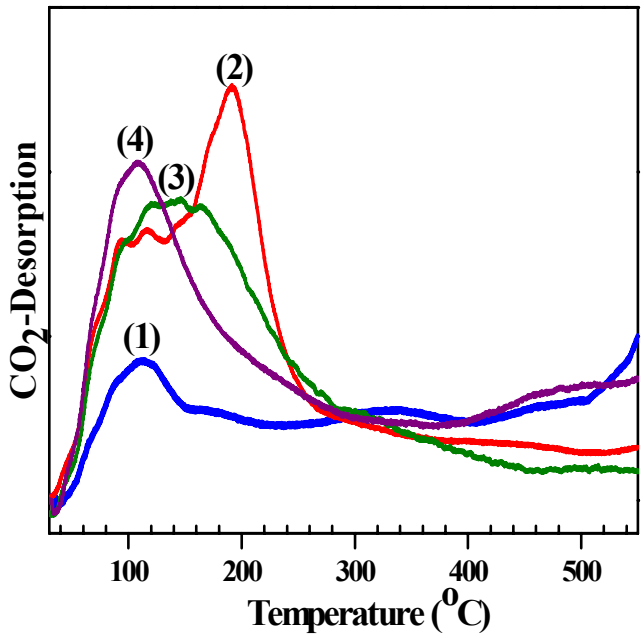

Figure 4.1.4. CO_2-TPD profile for Ce-M catalysts; (1) CeCo (2) CeCu (3) CeZn (4) CeFe

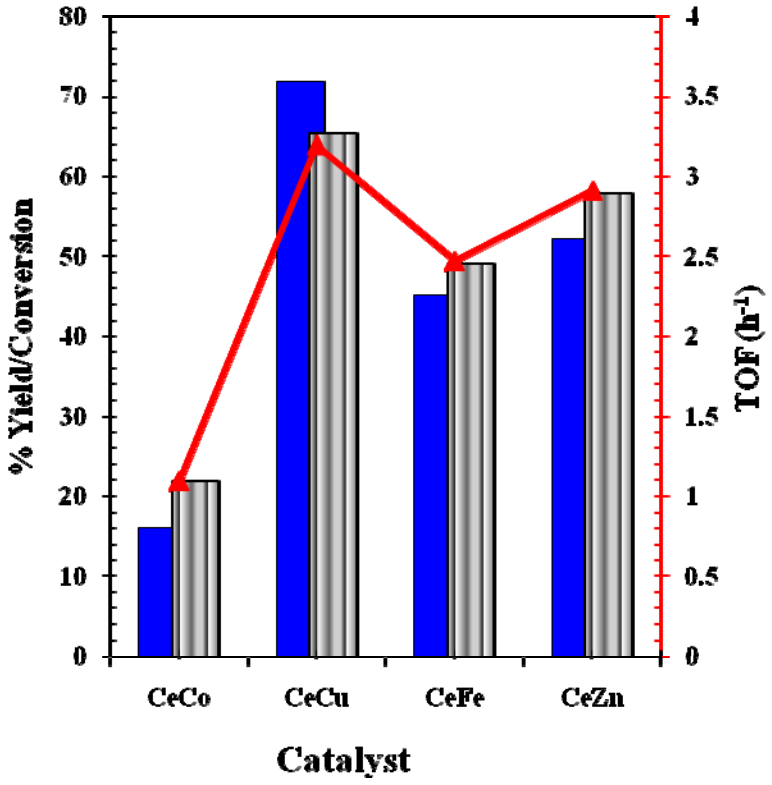

Figure 4.1.5. PC conversion, DMC yields and TOF values with different catalysts. Reaction condition: methanol/PC molar ratio=10, catalyst dose=5 wt.% of PC, temperature=160°C, reaction time=4 h; % DMC Yield, % PC conversion, —▲— % TOF.

4.1.2.1. Effect of operating parameters

The effect of such operating parameters as methanol/PC molar ratio, temperature, amount of catalyst and reaction time was studied one at a time (keeping all other parameters constant) for CeCu catalyst. The results are displayed in Figures 4.1.6 and 4.1.7.

The effect of methanol/PC molar ratio was studied in the range of 2 to 10 at the reaction temperature of 160°C, amount of catalyst being 5 wt.% of PC and 4 h of reaction time. The effect of methanol/PC ratio for DMC, PC conversion and TOF is shown in Figure 4.1.6a. It is seen that an increase in the molar ratio of methanol/PC from 2 to 10 increases the DMC yield from 15 to 71%, PC conversion from 12 to 65% and TOF and from 0.61 to 3.29. In transesterification reaction, 1 mole of PC reacts with 2 moles of methanol under equilibrium condition. If the molar ratio of methanol/PC is lower, the co-product will increase in the transesterification reaction. Higher methanol/PC ratio shifts the equilibrium towards product side [Sankar et al., 2006]. A number of investigators have reported methanol/PC molar ratio of 10 to be the optimum for the synthesis of DMC using Fe-Zn double-metal cyanide [Srivastava et al., 2006], KF/Al_2O_3 [Murugan et al., 2010], and the rare earth promoted Mg-Al hydrotalcite catalysts [Unnikrishnan and Srinivas, 2012]. Hence, methanol/PC molar ratio of 10 was considered as optimum.

Effect of temperature on the transesterification of PC with methanol for PC conversion and the yield of DMC is shown in Figure 4.1.6b. The optimum temperature is found to be 160°C with the maximum conversion of PC being 65.9%, yield of DMC being 70.1% and with TOF value is 3.31 h^{-1}. Beyond this temperature, the yield of the DMC decreases with an increase in the reaction temperature due to dehydrogenation and condensation of the byproduct methanol. However, at a higher reaction temperature, DMC decomposes and decomposition gets accelerated with an increase in temperature. The optimum reaction temperature were reported to be 160°C [Wei et al., 2003; Wang et al., 2006] and 170°C by Srivastava et al. [2006] by using various catalysts for DMC production.

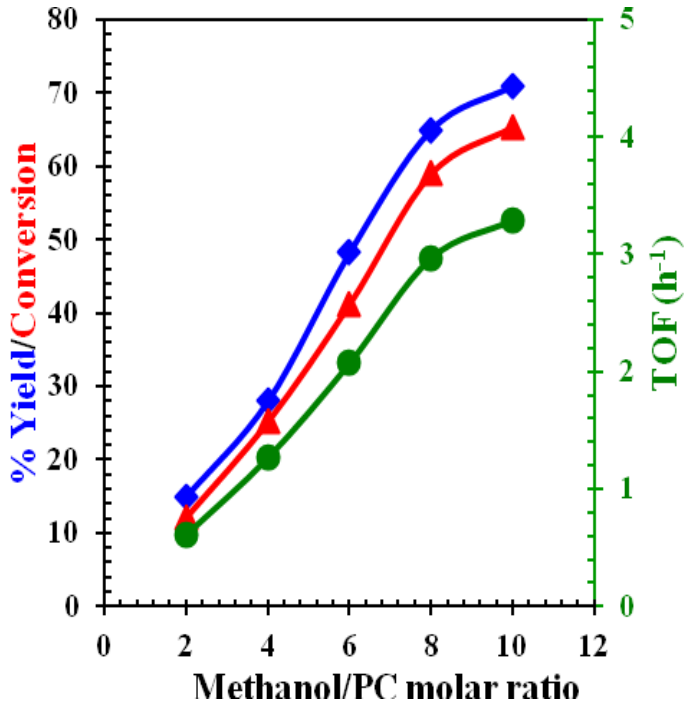

(a)

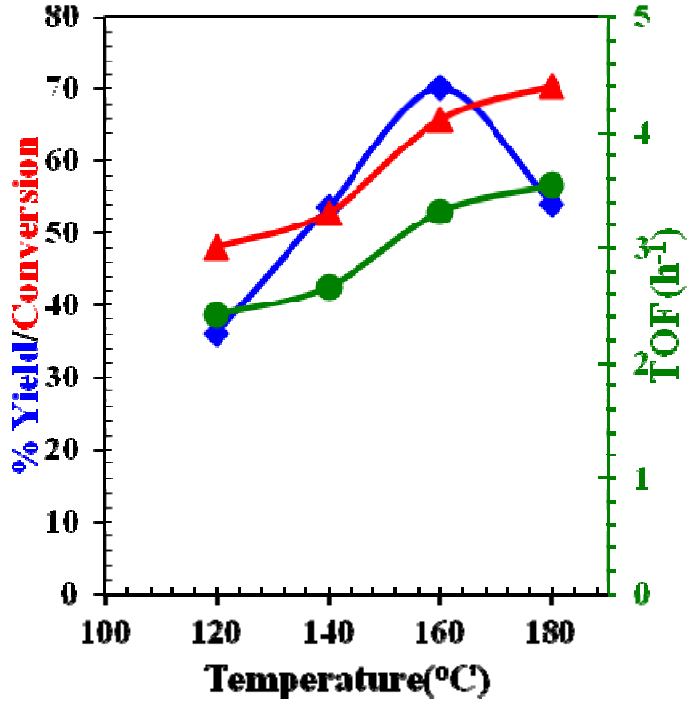

(b)

Figure 4.1.6. Effect of various parameters on transesterification of PC with methanol using CeCu catalyst; (a) effect of methanol/PC molar ratio: catalyst dose=5 wt.% of PC, reaction time=4 h, temperature=160°C; (b) effect of reaction temperature: methanol/PC molar ratio=10, catalyst dose=5 wt.% of PC, reaction time=4 h. —♦— % DMC Yield, —▲— % PC conversion, —●— TOF.

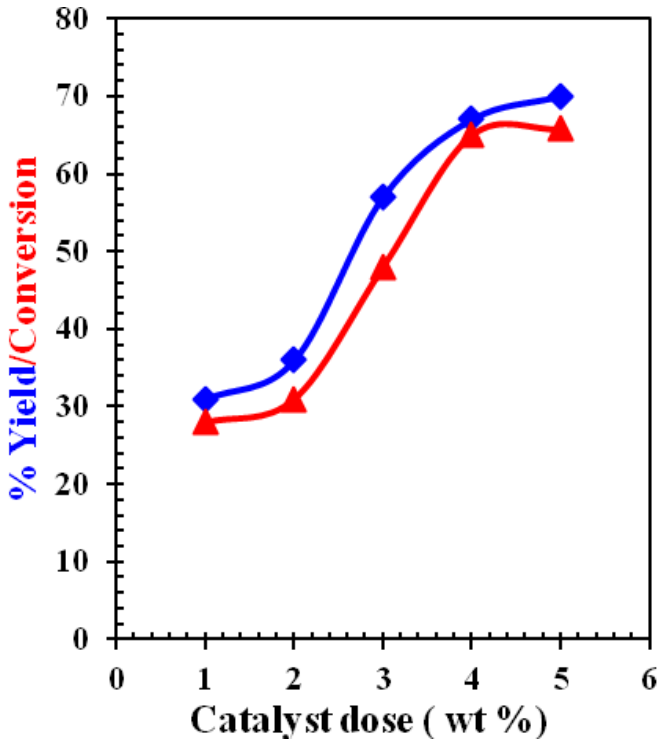

(a)

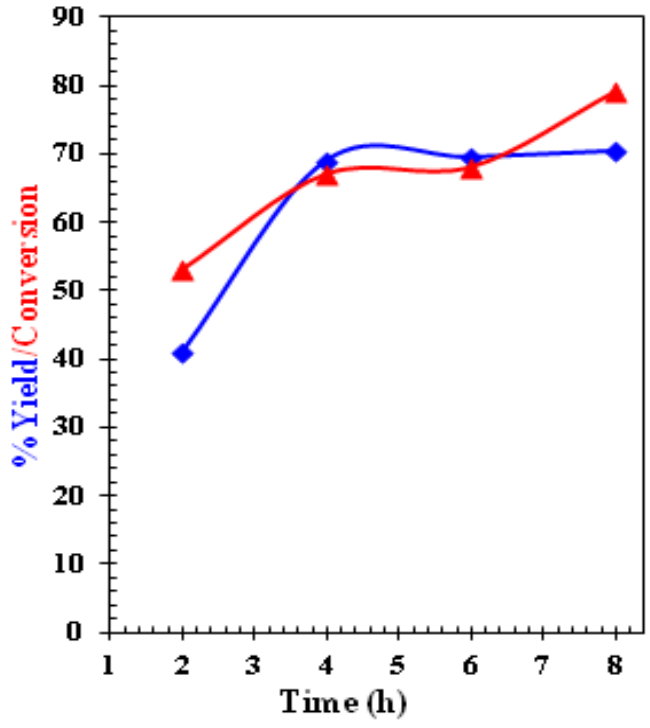

(b)

Figure 4.1.7. Effect of various parameters on transesterification of PC with methanol using CeCu catalyst; (a) effect of catalyst dose: methanol/PC molar ratio=10, reaction time=4 h, temperature=160°C; (b) effect of reaction time: catalyst dose=5 wt.% of PC, temperature=160°C, reaction time=4 h. —♦— % DMC Yield, —▲— % PC conversion.

The effect of catalysts dose conversion of PC and the on the yield of DMC are shown in Figure 4.1.7a. It can be seen that the conversion of PC and yield of DMC increase with an increases in the catalyst dose and that the highest yield of DMC was found at a catalyst dose of 5 wt.% of PC. A high dose of the catalyst promotes the decomposition of DMC to form PG in the reaction mixture. A higher catalyst dose can also the cause blockage of the active sites in the pores due to agglomeration of the catalyst particles. The effect of reaction time on the transesterification of PC with methanol for the synthesis of DMC is shown in Figure 4.1.7b. It was formed that the conversion of PC and yield of DMC increased up to t=4 h, after which the reaction time doesn't influence the formation of DMC as the reaction reaches the thermodynamic equilibrium. The equilibrium conversion time of 5-6 h for the formation of DMC has also been reported by Sankar et al. [2006] and Xu et al. [2013] by tungstate-based and graphitic carbon nitride-based catalysts, respectively for the transesterification of PC with methanol.

4.1.2.2. The catalyst of the reusability

The reusability of CeCu catalyst was investigated by utilizing it in four consecutive batches for the transesterification reaction. For each batch, the catalyst was recovered after the reaction by filtration and washed several times with methanol. Thereafter, it was dried in an air flushed oven at 120°C for 12 h and reactivated at 500°C for 4 h. Thereafter, the catalyst was reused in subsequent cycles of experiment under similar reaction conditions. The results of the conversion of PC and the yield of DMC are shown in Figure 4.1.8. It may be seen that upto 4 number of cycles, there is a 20% decreases the conversion of PC and 19% decreases the yield of DMC and 0.2 h^{-1} decreases the TOF. Results reveal that CeCu is reusable as catalyst with upto 20% decrease in its activity.

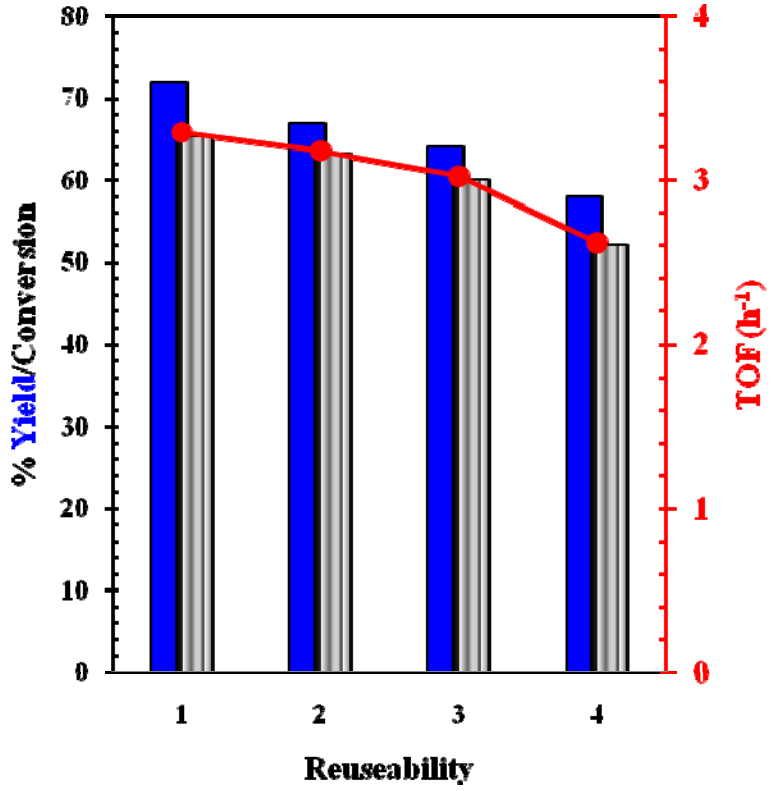

Figure 4.1.8. Reusability of CeCu catalyst. Reaction conditions: methanol/PC=10, catalyst dose=5 wt.% of PC, temperature=160°C, reaction time=4 h; % DMC Yield, % PC conversion, % TOF.

4.2. CERIUM–LANTHANUM OXIDES CATALYSTS: CHARACTERIZATION AND CATALYTIC ACTIVITY FOR TRANSESTERIFICATION OF PROPYLENE CARBONATE (PC) WITH METHANOL

In the present study, Ce-La mixed oxide catalysts (with different ratio of cerium and lanthanum) were synthesized by co-precipitation method and characterized by various techniques. Catalytic performance of these catalysts was further tested for the transesterification of PC with methanol to produce DMC and PG as a co-product. The effects of molar ratio of methanol/PC, catalyst dose, reaction time and temperature on the conversion of PC and yield of DMC was studied for all the synthesized catalysts.

4.2.1. Characterization of Ce-La Catalysts

4.2.1.1. X-ray diffraction

XRD patterns of synthesized $Ce_xLa_{1-x}O_{2-\delta}$ (x=0.2; 0.4; 0.6 and 0.8) catalysts are presented in Figure 4.2.1. XRD patterns of Ce_xLa_{1-x}(x=0.4, 0.6, and 0.8) exhibit peaks at 2θ=28°, 33°, 46°, 55°, 58°, 68° and 75°, corresponding to the (111), (200), (220), (311), (222), (400) and (331) planes of face-centered cubic (fcc) structure. These reflections indicate the presence of cubic fluorite structure of CeO_2 (JCPDS No. 810792) phase only. No reflections corresponding to La_2O_3 were observed in these three catalysts Ce_xLa_{1-x} (x=0.4, 0.6, and 0.8). Wang et al. [2010] also reported absence of La oxides in Ce-La mixed samples for La content as high as 75%. $Ce_{0.2}La_{0.8}$ showed minor reflection of hexagonal close-packed (hcp) structure of La_2O_3 (JCPDS No. 401284) phase along with CeO_2 (JCPDS No. 810792). In all the XRD pattern, (111) is the most intensive peak, therefore, it was used for calculation of unit cell parameters and crystalline size of all the prepared catalysts. Results are summarized in Table 4.2.1. XRD spectra shows that an increase in Ce content in $Ce_xLa_{1-x}O_2$ (x=0.2, 0.4, 0.6 and 0.8) shifts the peaks to higher diffraction angle [Bellière et al., 2010; Dai et al., 2012]. Ionic radius of La^{3+} (0.106 nm) is larger than that of Ce^{4+} (0.094 nm), therefore, an increase in lanthanum in the Ce_xLa_{1-x} catalysts results in an increase in the values of unit

cell parameters (Table 4.2.1) whereas an increase in cerium causes decrease in unit cell parameters [Wilkes et al., 2003; Zhang et al., 2010; Ma et al., 2005].

4.2.1.2. N_2 adsorption–desorption

Textural properties and pore size distribution of the synthesized catalysts (Table 4.2.1) were obtained from the nitrogen adsorption-desorption isotherms at 77 K (Figure 4.2.2). Isotherms belong to the "type IV" class in all cases and exhibit type "H4" hysteresis loop indicating that all Ce-La catalysts are mesoporous in nature. Synthesized catalysts were found to have the surface area in the range from 41-62 m^2/g, and it was found to be in the order: $Ce_{0.2}La_{0.8}$ < $Ce_{0.4}La_{0.6}$ < $Ce_{0.6}La_{0.4}$ < $Ce_{0.8}La_{0.2}$. Pore volume of the catalysts also increased in the same order. Thus, an increase the lanthanum content decreased the pore surface area and pore volume.

4.2.1.3. Scanning electron microscopy-energy dispersive atomic spectra

SEM studies were carried out so as to study the morphology of the synthesized catalysts (Figure 4.2.3). Synthesized $Ce_{0.8}La_{0.2}$ catalysts show spherical morphology with size of the crystal being 20-30 nm. All other catalysts have nanorod shape with length varying in the range of 50-300 nm. EDX elemental mapping shows even distribution and homogeneous dispersion of Ce and La in all synthesized catalysts shows in Figure 4.2.4. EDX of catalysts (Table 4.2.1) showed presence of the cerium, lanthanum and oxygen in all the catalysts.

4.2.1.4 CO_2-temperature programmed desorption

CO_2-TPD profile of synthesized $Ce_XLa_{(1-X)}$ catalysts is shown in Figure 4.2.5a. Distinct profiles are seen for different catalysts. Presence of weak basic sites in the catalysts allow low temperature desorption of the CO_2 gas whereas strong basic sites show the higher temperature desorption of CO_2 [Ma et al., 2005]. $Ce_{0.8}La_{0.2}$ catalyst show peaks corresponding to weak and moderate basic sites whereas all other catalysts shows peaks corresponding to weak, moderate and strong basic sites. Intensity of the low and moderate basic sites depends on the Lewis acid-basic paring and OH^- bond present on the surface, and higher basic nature is due to the low coordination of surface O^{2-} [Rossi et al., 1991].

Table 4.2.1. Crystallite size, textural properties and composition of cerium-lanthanum catalysts.

Catalyst	XRD		Textural Properties			Composition of Catalysts (From EDX)		
	Unit Cell Parameter (nm)[a]	Crystallite size (nm)[a]	Surface Area (m^2/g)	Pore volume (cm^3/g)[b]	Average Pore diameter (nm)[c]	Ce actual atomic%	La actual atomic%	O actual atomic%
$Ce_{0.2}La_{0.8}$	57.53	7.6	41	0.061	5.82	8	29	63
$Ce_{0.4}La_{0.6}$	55.98	9.5	42	0.080	6.67	18	26	56
$Ce_{0.6}La_{0.4}$	55.39	10.2	60	0.103	5.97	20	14	66
$Ce_{0.8}La_{0.2}$	54.52	11.7	62	0.128	6.57	25	9	66

[a]Scherrer equation used for the estimation of crystalline size peak (111);
[b]BJH desorption cumulative pore volume of pores in the range 17.00 to 3000 Å;
[c]BJH desorption average pore diameter (nm)

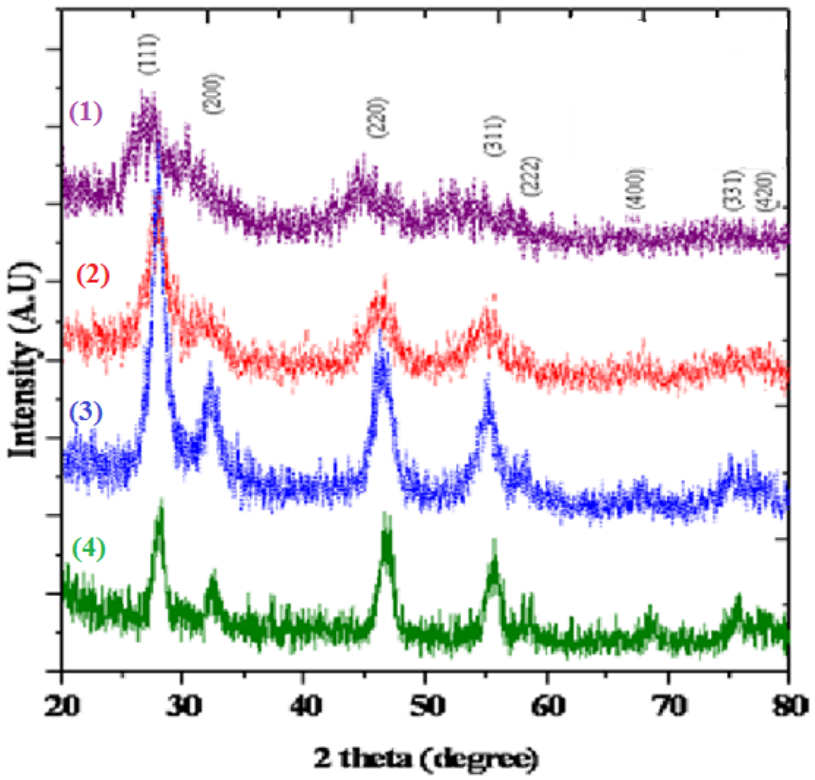

Figure 4.2.1. XRD profile of Ce-La based catalysts; (1) $Ce_{0.2}La_{0.8}$, (2) $Ce_{0.4}La_{0.6}$, (3) $Ce_{0.6}La_{0.4}$, (4) $Ce_{0.8}La_{0.2}$.

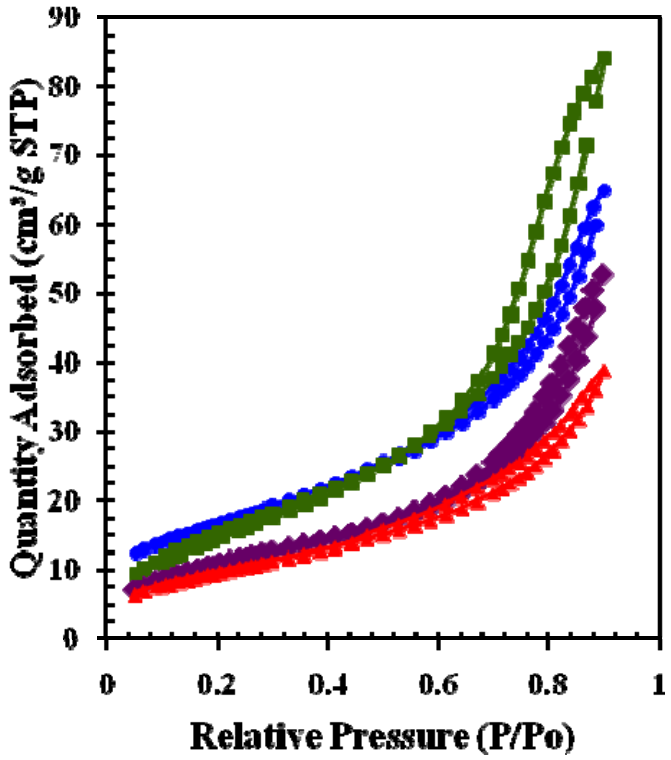

(a)

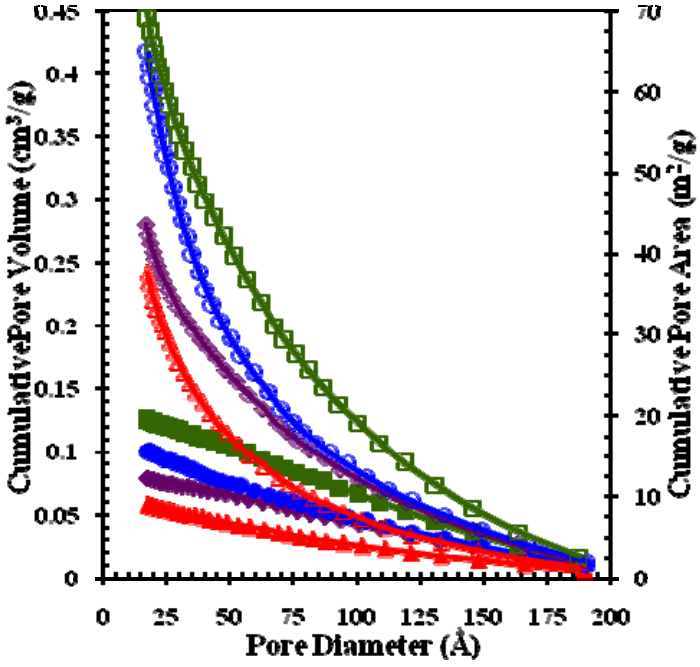

(b)

Figure 4.2.2. (a) Nitrogen adsorption isotherms, —♦— $Ce_{0.2}La_{0.8}$, —■— $Ce_{0.4}La_{0.6}$, —●— $Ce_{0.6}La_{0.4}$, —▲— $Ce_{0.8}La_{0.2}$. (b) variation of cumulative pore volume and cumulative pore area with average pore diameter for ceria-lanthanum based catalysts; —♦— $Ce_{0.2}La_{0.8}$-pore volume, —■— $Ce_{0.4}La_{0.6}$-pore volume, —●— $Ce_{0.6}La_{0.4}$-pore volume, —▲— $Ce_{0.8}La_{0.2}$-pore volume, —◊— $Ce_{0.2}La_{0.8}$-pore area, —Δ— $Ce_{0.4}La_{0.6}$-pore area, —○— $Ce_{0.6}La_{0.4}$-Pore area, —□— $Ce_{0.8}La_{0.2}$-pore area.

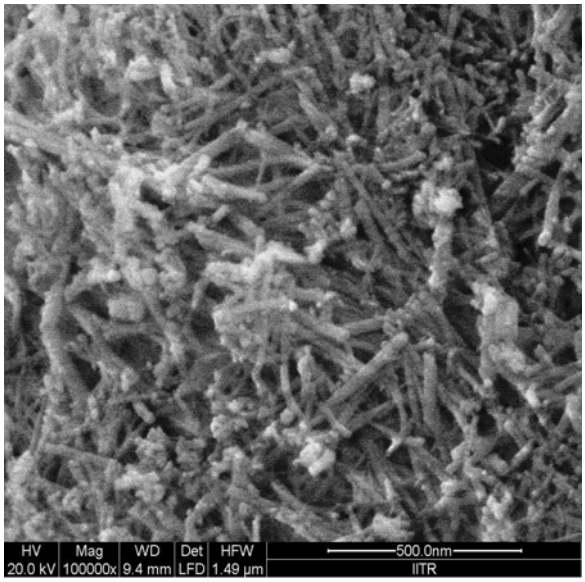

(a) $Ce_{0.2}La_{0.8}$

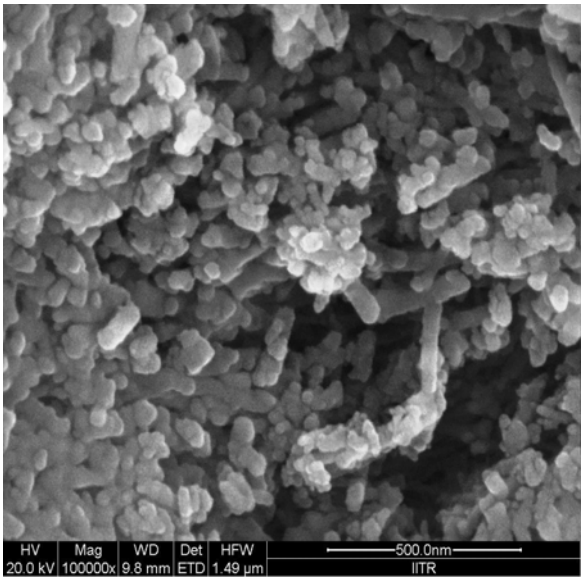

(b) $Ce_{0.4}La_{0.6}$

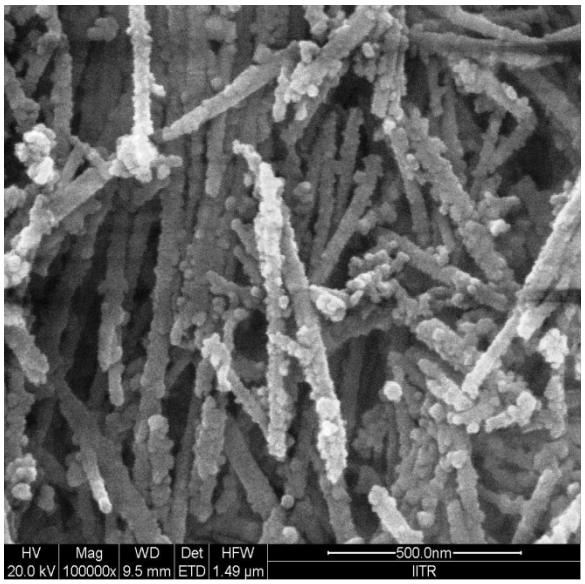

(c) $Ce_{0.6}La_{0.4}$

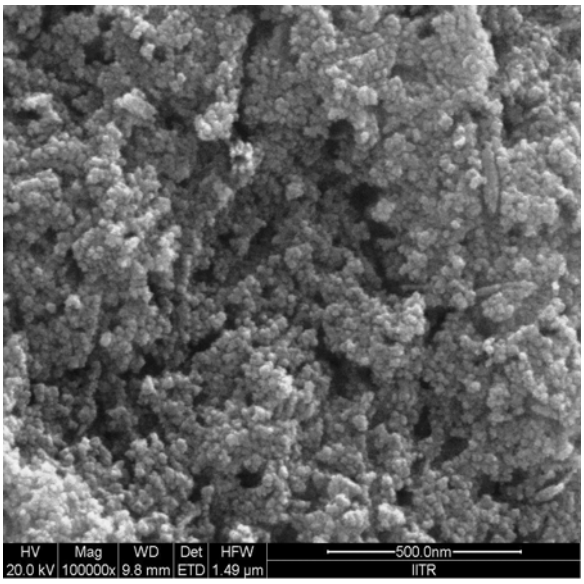

(d) $Ce_{0.8}La_{0.2}$

Figure 4.2.3. SEM micrographs of the cerium-lanthanum based catalysts (a) $Ce_{0.2}La_{0.8}$, (b) $Ce_{0.4}La_{0.6}$, (c) $Ce_{0.6}La_{0.4}$ and (d) $Ce_{0.8}La_{0.2}$.

Amount of total basic sites (per unit mass) for any catalyst was calculated by adding the amount of CO_2 desorbed from individual peaks. Thereafter, amount of total basic sites per unit surface area was calculated by dividing the amount of total basic sites per unit mass by the BET surface area. Distribution of basic sites in the synthesized catalysts followed the sequence (Table 4.2.2): $Ce_{0.2}La_{0.8}$ (66.90 µmol/m^2) > $Ce_{0.4}La_{0.6}$ (19.28 µmol/m^2) > $Ce_{0.6}La_{0.4}$ (11.66 µmol/m^2) > $Ce_{0.8}La_{0.2}$ (7.28 µmol/m^2). Results in Table 4.2.2 also show that an increase in the amount of lanthanum and a decrease in the amount of cerium in the catalysts increase the basic site density. This is due to more basic nature of lanthanum as compared to cerium [Wilkes et al., 2003].

4.2.1.5. NH_3-temperature programmed desorption

Results of NH_3-TPD analysis are shown in Figure 4.1.5b. All catalysts show desorption peaks of NH_3 corresponding to all regions over a temperature range of 50-950°C. NH_3 desorption temperature and the amount of acid sites are calculated and displayed in Table 4.2.2. Total amount of NH_3 desorbed from the $Ce_{0.2}La_{0.8}$, $Ce_{0.4}La_{0.6}$, $Ce_{0.6}La_{0.4}$, and $Ce_{0.8}La_{0.2}$ catalyst was 7.53, 5.85, 4.18 and 2.17 mmol/g, respectively. Respective value of acid site density was: 0.184, 0.139, 0.069 and 0.044 mmol/m^2 (Table 4.2.2). Acidic nature of the catalysts was as follows: $Ce_{0.2}La_{0.8}$ > $Ce_{0.4}La_{0.6}$ > $Ce_{0.6}La_{0.4}$ > $Ce_{0.8}La_{0.2}$. Similarly, for temperature range of 100-200°C, the total amount of NH_3 desorbed for $Ce_{0.2}La_{0.8}$, $Ce_{0.4}La_{0.6}$, $Ce_{0.6}La_{0.4}$, and $Ce_{0.8}La_{0.2}$ catalysts was 0.68, 0.41, 0.35 and 0.15 mmol/g, respectively. Respective value of acidic site density was: 16.58, 9.76, 5.84 and 2.42 µmol/m^2.

Thus, in the temperature range of 100-200°C, the total amount of NH_3 desorbed and acidic site densities follow the order: $Ce_{0.2}La_{0.8}$ > $Ce_{0.4}La_{0.6}$ > $Ce_{0.6}La_{0.4}$ > $Ce_{0.8}La_{0.2}$. The acidic nature of the catalysts and the amount of weak acidic sites (in the desorption temperature range of 100-200°C) increased with an increase in the amount of lanthanum and decreased with a decrease in the amount of cerium in the catalysts.

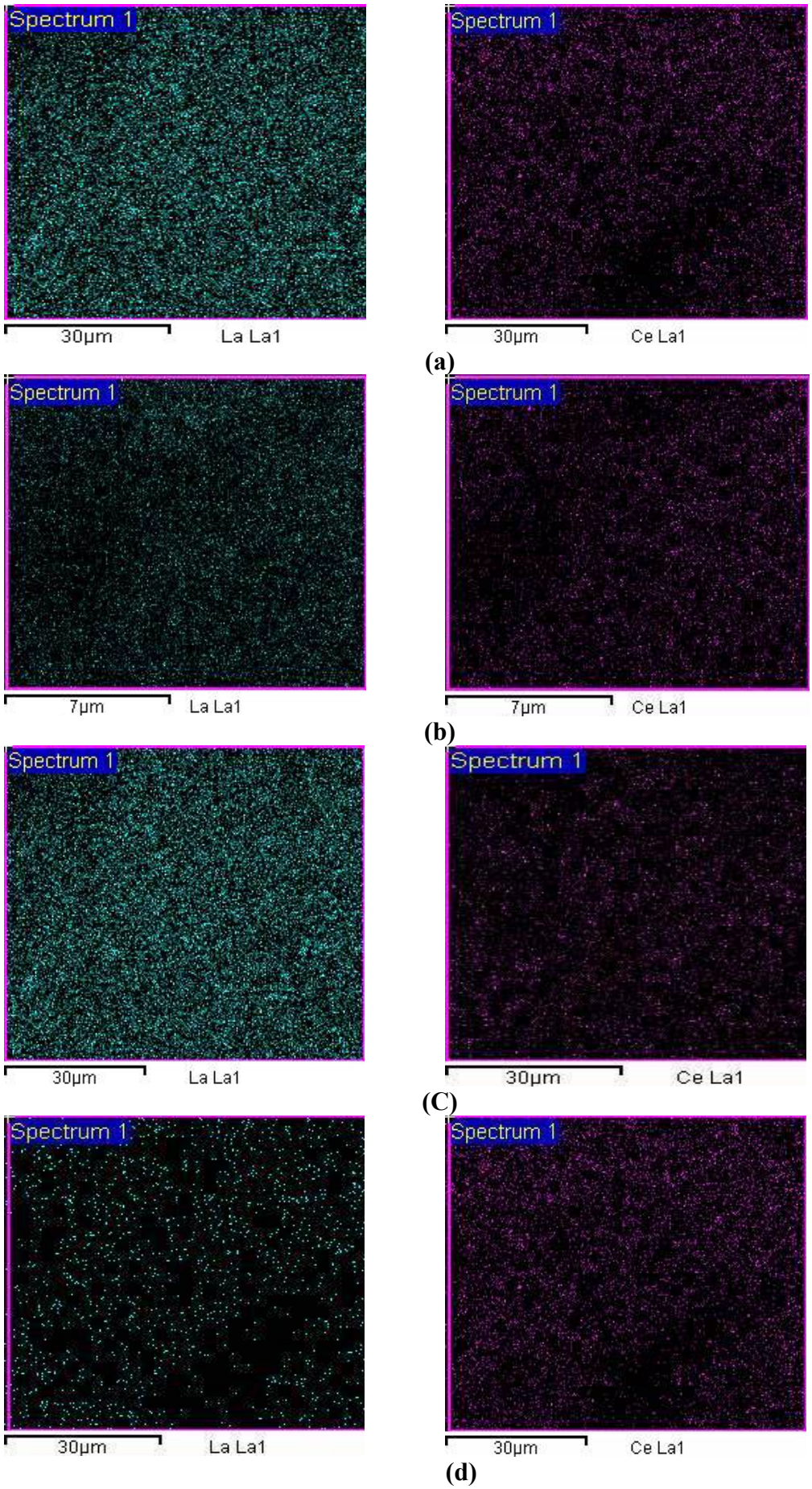

Figure 4.2.4. Mapping of La and Ce element of synthesized catalysts (a) $Ce_{0.2}La_{0.8}$, (b) $Ce_{0.4}La_{0.6}$, (c) $Ce_{0.6}La_{0.4}$ and (d) $Ce_{0.8}La_{0.2}$.

Table 4.2.2. TPD analysis using adsorbed CO_2 and NH_3 for determining basic and acidic properties of synthesized catalysts.

Catalyst	TPD analysis of adsorbed CO_2 (mmol/g)			Total evolved CO_2 (mmol/g)	Basic site density (µmol/m^2)
	Weak (< 200°C)	Moderate (200-450°C)	Strong (> 450°C)		
$Ce_{0.2}La_{0.8}$	0.17 (128)	0.15 (345)	2.29 (731)	2.61	66.90
$Ce_{0.4}La_{0.6}$	0.25 (113)	0.10 (363)	0.46 (746)	0.81	19.28
$Ce_{0.6}La_{0.4}$	0.42 (113)	0.06 (392)	0.22 (750)	0.70	11.66
$Ce_{0.8}La_{0.2}$	0.42 (123)	0.03 (343)	-	0.45	7.26

Catalyst	TPD analysis of absorbed NH_3 (mmol/g)			Total evolved NH_3 (mmol/g)	Acidic site density (mmol/m^2)
	Weak (< 200°C)	Moderate (200-450°C)	Strong (> 450°C)		
$Ce_{0.2}La_{0.8}$	1.38 (206)	0.97(387)	1.41 (533), 3.77 (727)	7.53	0.184
$Ce_{0.4}La_{0.6}$	0.50 (115)	0.03 (361)	1.35 (516), 3.97 (754)	5.85	0.139
$Ce_{0.6}La_{0.4}$	0.42 (115)	0.34 (416)	3.462 (631)	4.18	0.069
$Ce_{0.8}La_{0.2}$	0.96 (95)	0.72 (358)	0.13 (588), 0.90 (712)	2.71	0.044

Temperature (°C) at maxima is given in brackets.

4.2.2. Catalytic Activity of Ce-La Based Catalyst

DMC yield increases with an increase in the methanol/PC molar ratio (Figure 4.2.6a). At low methanol/PC molar ratio, the amount of PG formed increases during the transesterification reaction and thus, the DMC yield is lower. An increase in the methanol/PC molar ratio increases the DMC yield. For methanol/PC molar ratio > 10, the DMC yield remains constant. Higher methanol/PC molar ratio causes formation of DMC-methanol azeotrope due to excess methanol and shifts the equilibrium towards the product side [Murugan et al., 2010]. Hence, methanol/PC molar ratio of 10 was considered as the optimum. Figure 4.2.6b shows that the DMC yield increases with an increase in the catalyst amount in the reaction mixture until the catalyst amount was 5 wt.% of PC. Beyond this catalyst amount, DMC yield either decreased or remained constant with an increase in the catalyst amount for all the catalysts. This may be due to the blockage of the active sites in the

pores due to agglomeration of the catalyst. Also, high catalyst amount in the reaction can cause poor dispersion of the catalyst particle in the mixture, and the excess catalyst may inhibit the mass transfer of the reactants to the active site of the catalyst [Xian et al., 2014; Nawaratna et al., 2013]. It can be seen in Figure 4.2.7a that the $Ce_{0.2}La_{0.8}$ catalyst gave highest DMC yield (71%) and $Ce_{0.8}La_{0.2}$ showed lowest DMC yield (40%) after 6 h of reaction. Beyond 6 h of reaction time, DMC yield decreased indicating that the reaction reached equilibrium after 6 h of reaction. Equilibrium conversion time of 5-6 h has also been reported [Xian et al., 2014].

Effect of reaction temperature during transesterification of PC with methanol is shown in Figure 4.2.7b. DMC yield increases with an increase in reaction temperature up to 170°C and then decreases quickly as the temperature is increased beyond 170°C. Transesterification reaction is thermodynamically controlled and reaction temperature > 170°C shifts the equilibrium towards the reactant side [Wei et al., 2003]. Various investigators have also reported 160-170°C as the optimum reaction temperature for DMC synthesis by various catalysts [Wei et al., 2003; Srivastava et al., 2006; Wang et al., 2007].

It may be seen that the activity of the synthesized catalysts increases with an increase in the amount of lanthanum in the catalysts. Also, the transesterification of PC with methanol parallels the bi-functional nature (basic and acidic nature) of the catalysts and that catalytic activity, basic site density, acidic site density and amount of weak acidic sites (in the desorption temperature range of 100-200°C) follow the same order: $Ce_{0.8}La_{0.2} < Ce_{0.6}La_{0.4} < Ce_{0.4}La_{0.6} < Ce_{0.2}La_{0.8}$. It has been reported previously that the transesterification of PC with methanol for DMC synthesis strongly depends upon the basicity of the catalysts [Srivastava et al., 2006; Wang et al., 2007; Murugan and. Bajaj, 2010]. It may be mentioned that though the BET surface area is inversely proportional to the activity of the catalysts; it also affects the pore size and the acidic and basic site density of the catalysts which affect the catalytic activity [Murugan and. Bajaj, 2010].

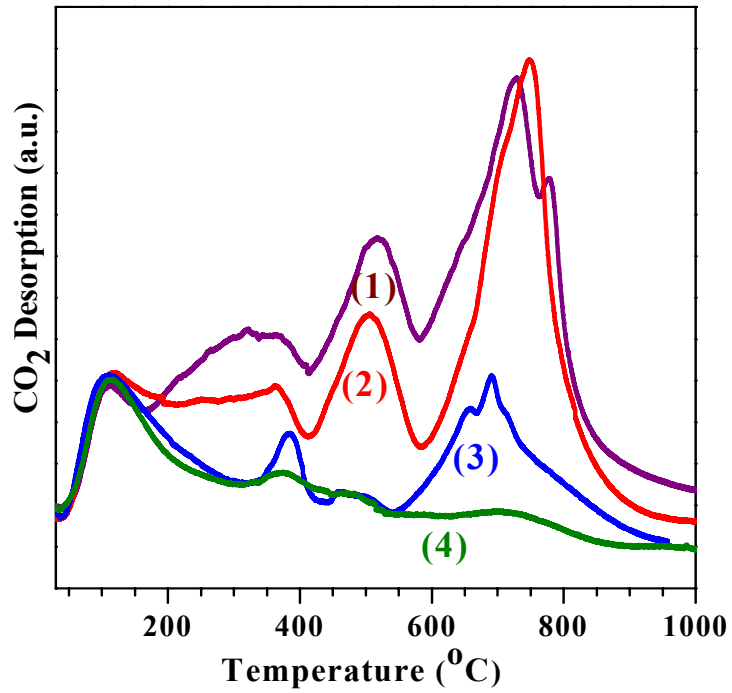

(a) CO_2-TPD profile

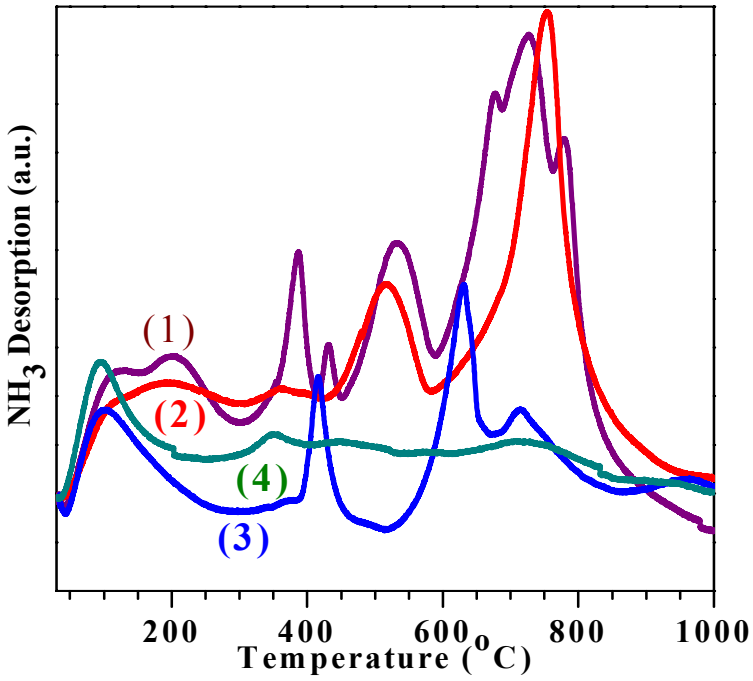

(b) NH_3-TPD profile

Figure 4.2.5. TPD profiles of cerium-lanthanum based catalysts (a) CO_2-TPD and (b) NH_3-TPD. (1) $Ce_{0.2}La_{0.8}$, (2) $Ce_{0.4}La_{0.6}$, (3) $Ce_{0.6}La_{0.4}$, (4) $Ce_{0.8}La_{0.2}$.

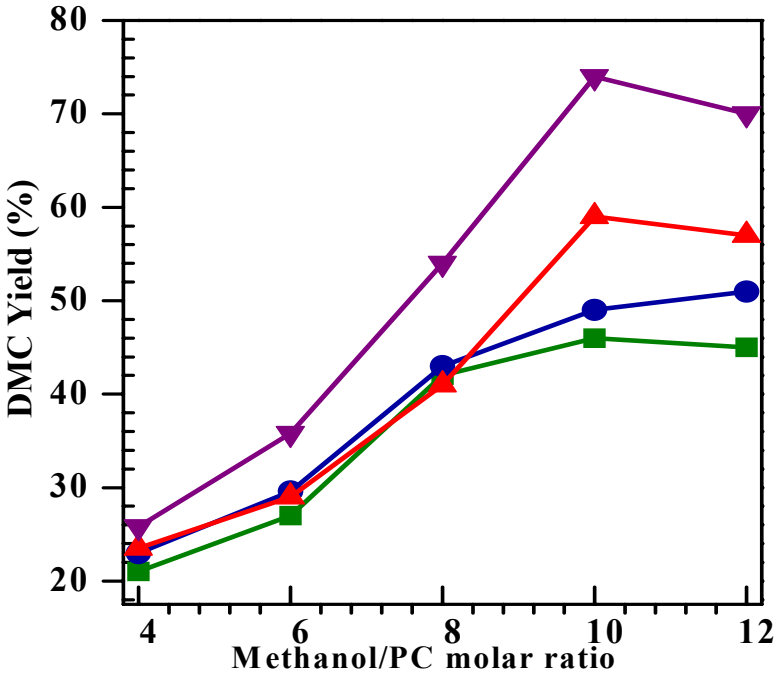

(a)

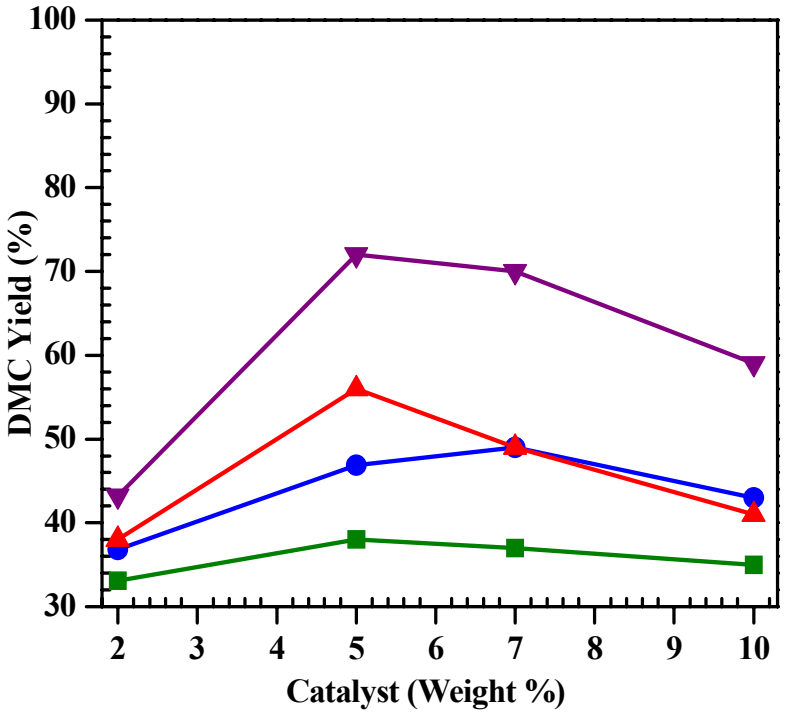

(b)

Figure 4.2.6. Effect of methanol/PC ratio and catalyst dose on transesterification of PC with methanol: (a) methanol/PC molar ratio: catalyst dose=5 wt.% of PC, reaction time=6 h, stirrer speed=550 rpm, temperature=170°C; (b) catalyst dose: methanol/PC molar ratio=10, reaction time=6 h, stirrer speed=550 rpm, temperature=170°C. —■— $Ce_{0.8}La_{0.2}$, —●— $Ce_{0.6}La_{0.4}$, —▲— $Ce_{0.4}La_{0.6}$, —▼—$Ce_{0.2}La_{0.8}$.

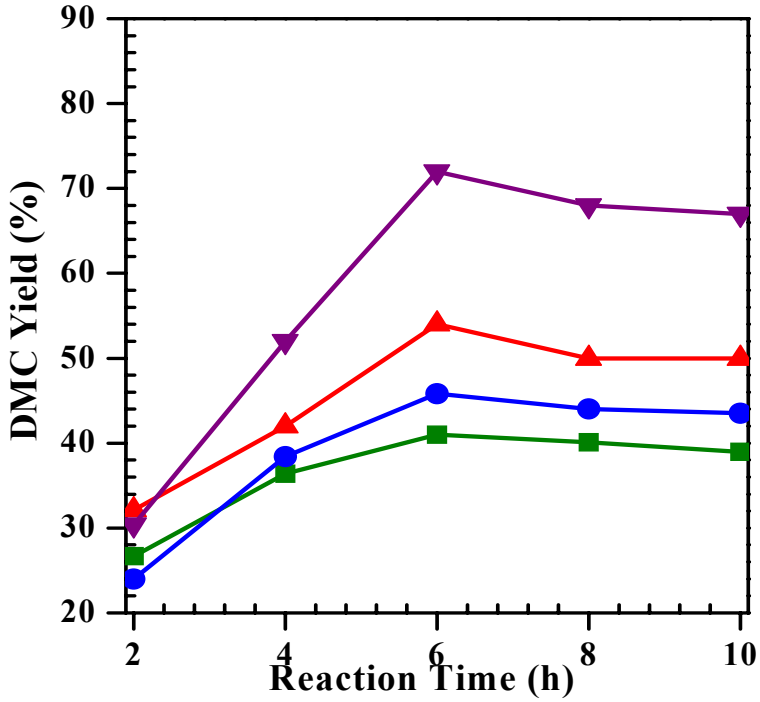

(a)

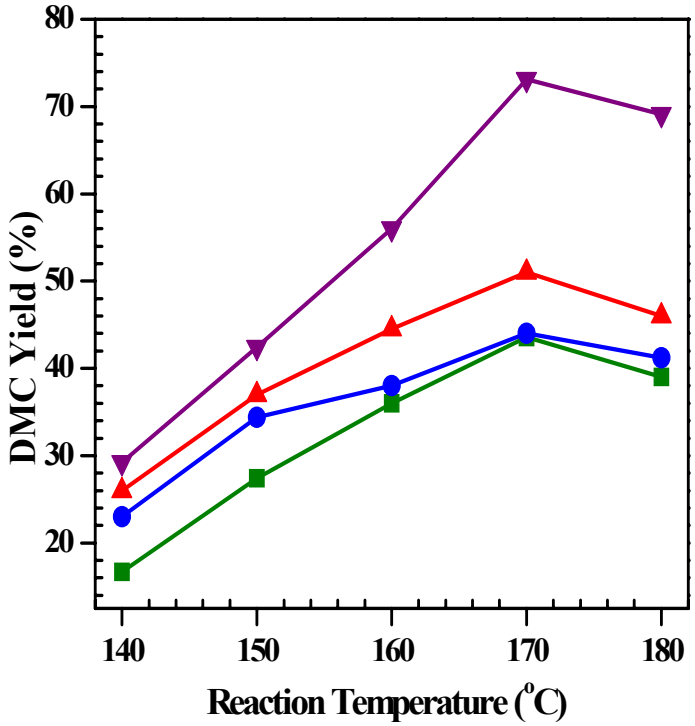

(b)

Figure 4.2.7. Effect of various parameters on transesterification of PC with methanol: (a) reaction time: catalyst dose=5 wt.% of PC, temperature=170°C, stirrer speed=550 rpm, reaction time=6 h; and (b) reaction temperature: methanol/PC molar ratio=10, catalyst dose=5 wt.% of PC, stirrer speed=550 rpm, reaction time=6 h. —■— $Ce_{0.8}La_{0.2}$, —●— $Ce_{0.6}La_{0.4}$, —▲— $Ce_{0.4}La_{0.6}$, —▼—$Ce_{0.2}La_{0.8}$.

4.3. CERIA–ZINC CATALYSTS: CHARACTERIZATION AND CATALYTIC ACTIVITY FOR TRANSESTERIFICATION OF PROPYLENE CARBONATE (PC) WITH METHANOL

The ceria-zinc composite oxide catalysts were impregnated onto various oxide supports, namely Al_2O_3, TiO_2 and SiO_2, individually by deposition-coprecipitation method (CZA, CZS and CZT having supports Al_2O_3, TiO_2 and SiO_2, respectively). These synthesized catalysts were characterized and tested for the synthesis of DMC.

4.3.1. Characterization of CeO_2-ZnO-Support Mixed Metal Oxide

4.3.1.1. Morphological characteristics

The SEM micrographs and the TEM images of the synthesized CZA, CZS and CZT catalysts are shown in Figure 4.3.1 and Figure 4.3.2, respectively. All the catalysts show spherical morphology, heterogeneous and crystalline structure. EDX image mapping of CZA, CZS and CZT catalysts are shown in Figure 4.3.3. Image maps show the distribution of Al, Si and Ti metals in CZA, CZS and CZT catalysts. In the CZA, the element Al is most scattered in CZA. Ti is well distributed and has least aggregation in CZT. EDX mapping also shows an almost even distribution of Ce and Zn in all the catalysts. Average particle size of the catalysts as determined from the FE-SEM studies are found to be in the range of 5-20 nm. TEM images show that all the particles are in the size range of ≈5-10 nm. AFM 3D images along with grain size distribution of the CZA, CZS and CZT are given in Fig.4.3.4. Average grain size (as estimated using AFM image) of CZA, CZS and CZT was found to 5.25 nm, 8.65 nm and 4.10 nm, respectively. Thus, the CZS was found to have larger average grain size than that of CZA or CZT.

4.3.1.2. Fourier transform infrared spectroscopy (FTIR) studies

FTIR spectra of CZA, CZS and CZT catalysts are shown in Figure 4.3.5. The origin of the vibration band seen at ~3430 cm^{-1} can be ascribed to the surface O-H stretching, absorbed water and N-H stretching amines groups. The peak at ~2925 cm^{-1} in all the catalysts is due to C-H stretching and the peak at ~1630 cm^{-1} is due to N-H bending. In CZA catalyst, vibrations appearing in the peak at 735 cm^{-1} is due to Al-O vibrations and that at 543 cm^{-1} is

due to Zn-O vibrations [Sankar et al., 2006; Shee et al., 2008; Potti and Srivastava, 2012; Priya et al., 2014]. Characteristic vibration band for Si-O-Si of the [SiO_4] tetrahedron vibration unit in CZS is observed at ~1100 cm^{-1} [Akondi et al., 2014]. The peaks at 463 and 805 cm^{-1} correspond to the ZnO and O-Si-O group, respectively [Cui et al., 2005]. The peaks at ≈500 cm^{-1} correspond to the TiO_2 in CZT [Dubey et al., 2015].

4.3.1.3 X-ray diffraction

XRD patterns of CZA, CZS, and CZT catalysts are shown in Figure 4.3.6. XRD peaks for CZA are found at 2θ angles of 28.629°, 33.042°, 47.577° and 56.545° corresponding to (111), (200), (220) and (311) planes, respectively, and representing face centered cubic lattice. XRD pattern of CZA indicates the presence of CeO_2 (PDF-ICDD 001-0800), Al_2O_3 (PDF-ICDD 004-00879), ZnO (PDF-ICDD 003-0888) and spinel form of $CeAlO_3$ (PDF-ICDD 021-0175). XRD peaks for CZS are found at 2θ angles of 28.804°, 33.267°, 47.451° and 56.594° corresponding to (111), (002), (022) and (113) planes, respectively, and representing face centered cubic lattice. These peaks indicates presence of ZnO (PDF-ICDD 00-003-0752), CeO_2 (PDF-ICDD 00-002-1306), SiO_2 (PDF-ICDD 008-0018), $Ce_2Si_2O_7$ (PDF-ICDD 048-1588) and Zn_2SiO_4 (PDF-ICDD 002-0813) in CZS. XRD peaks for CZT catalyst are seen at 2θ angle of 25.227°, 28.569°, 33.165°, 47.894°, and 56.58° corresponding to (111), (200), (210), (311) and (330) plane, respectively. CeO_2 (PDF-ICDD 001-0800), ZnO (PDF-ICDD 003-0752), TiO_2 (PDF-ICDD 001-0562) and Zn_4TiO_6 (PDF-ICDD 049-0687) are found to be present on CZT [Shee et al., 2010; Khobragade et al., 2012; Samiee et al., 2013]. All the CZA, CZS and CZT catalysts exhibit mixed peaks of ZnO and CeO_2 phases. Figure 4.3.6 also shows that the individual peak positions for CeO_2 and ZnO remain intact in the composite oxides. This is an indication that the composite oxides contain individual phases of ZnO, CeO_2 and some spinel forms of Zn, Ce within their supports. The CeO_2 peaks for catalysts CZA, CZS and CZT have been used in the Scherrer's equation to calculate the crystallite size of ceria. The data is summarized in Table 4.3.1**.** It is observed that the various types of supports (γ-Al_2O_3, SiO_2 and TiO_2) affect the particle size of the catalysts.

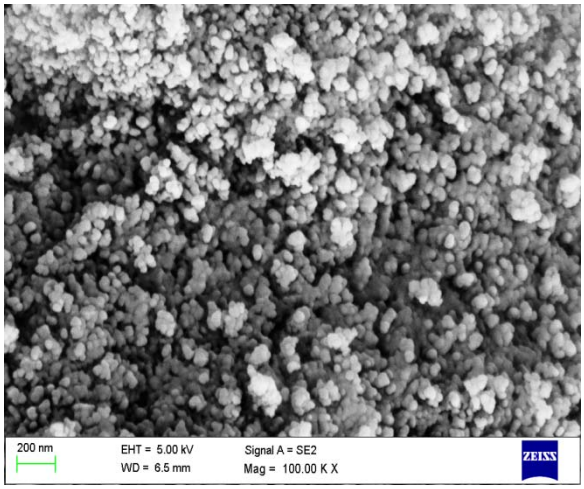

SEM-CZA

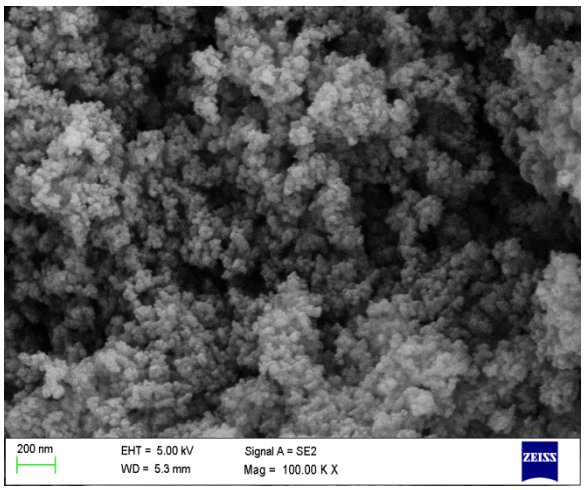

SEM-CZS

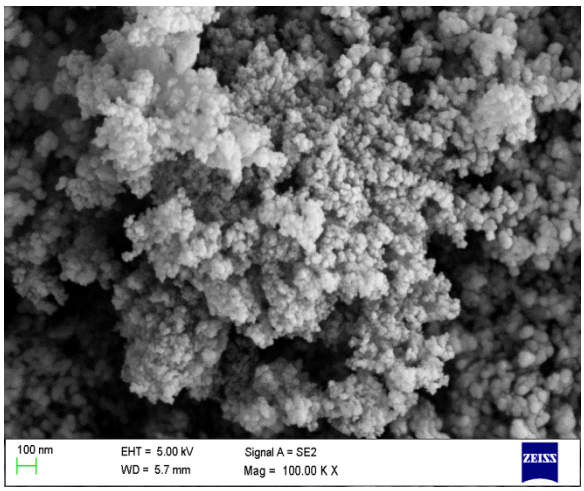

SEM-CZT

Figure 4.3.1. SEM of the CZA, CZS and CZT catalyst.

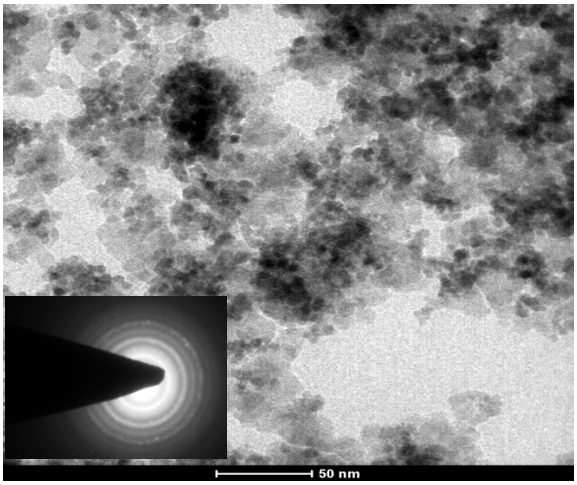

TEM-CZA

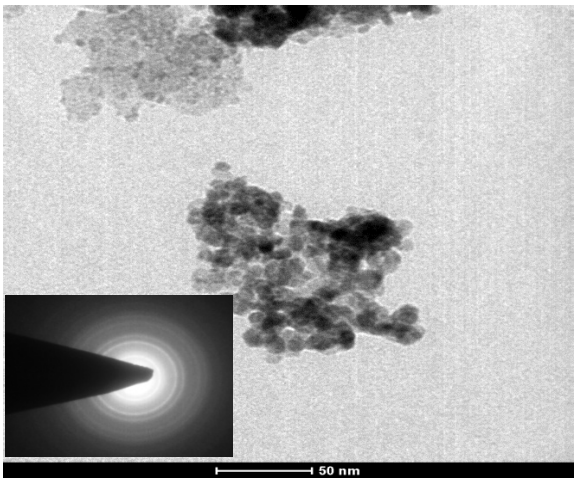

TEM-CZS

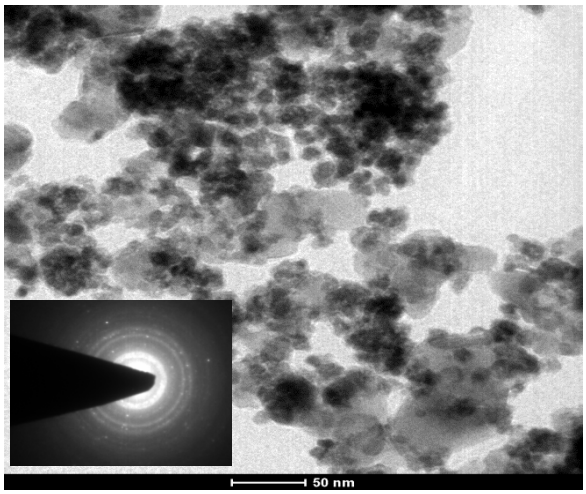

SEM-CZT

Figure 4.3.2. TEM of CZA, CZS and CZT catalyst.

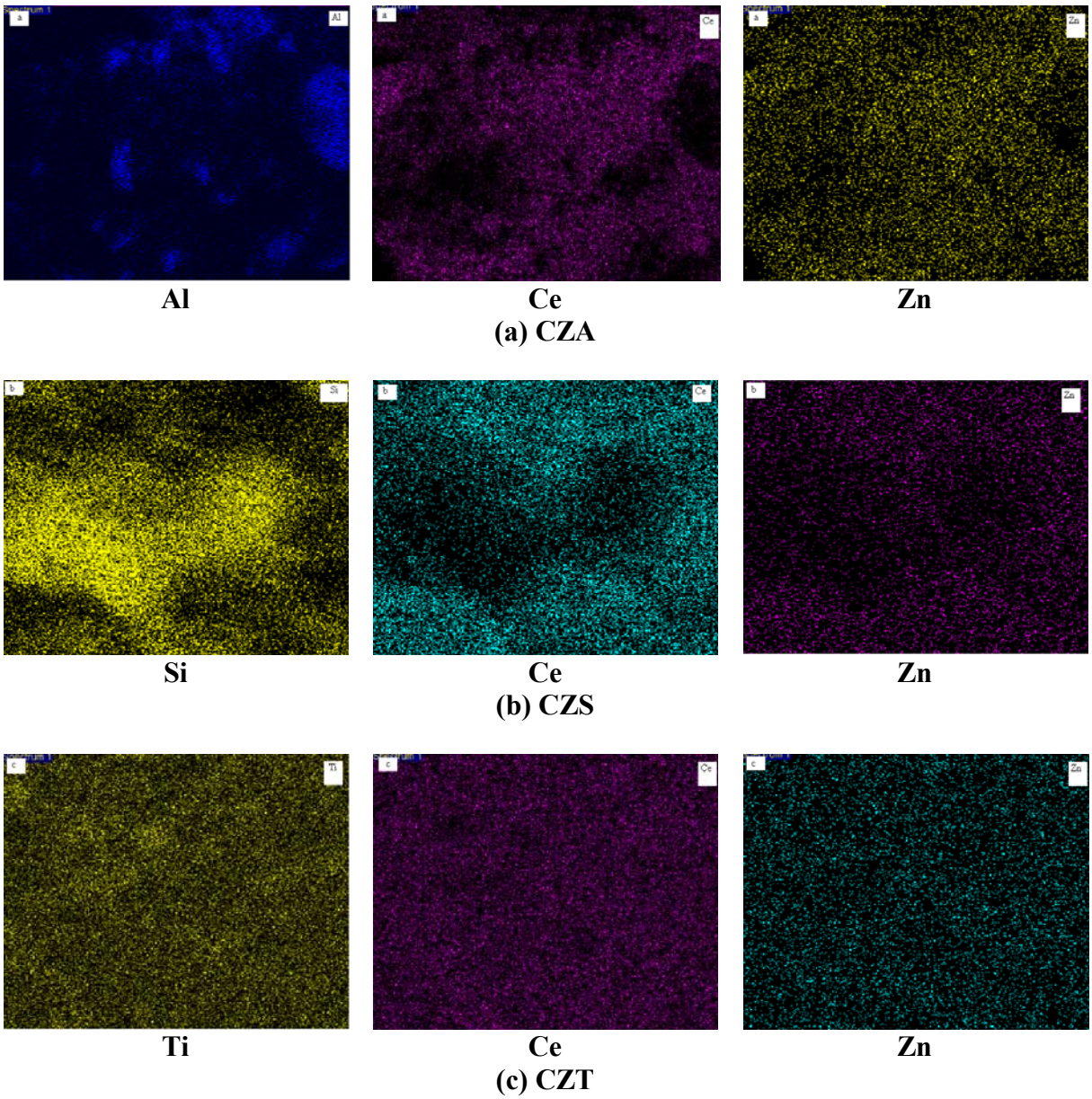

Figure 4.3.3. EDX image mapping of (a) Al, Ce, Zn element in CZA, (b) Si, Ce, Zn element in CZS, and (c) Ti, Ce, Zn element in CZT.

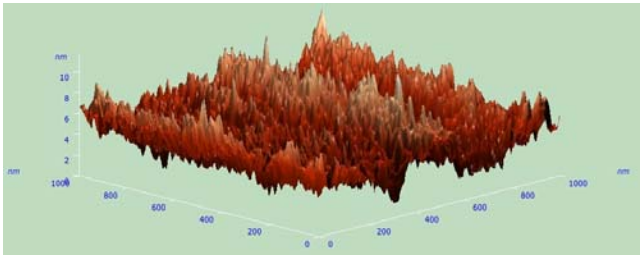

CZA

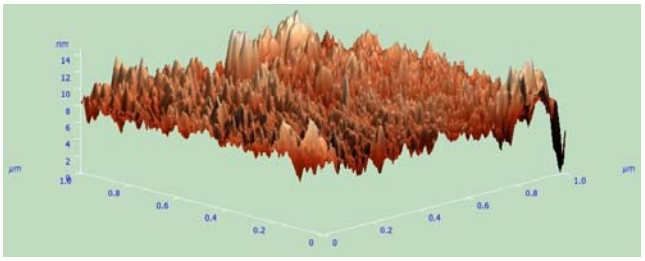

CZS

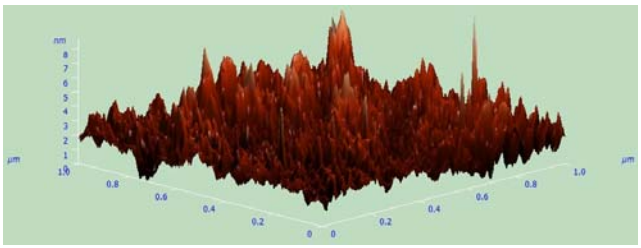

CZT

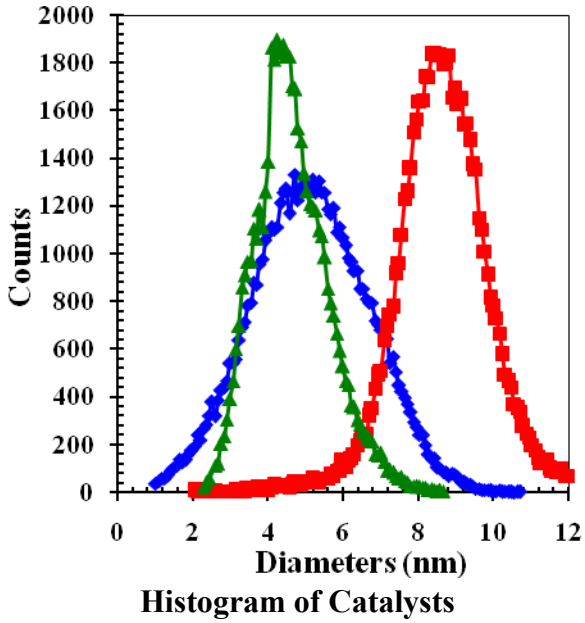

Histogram of Catalysts

Figure 4.3.4. 3D AFM-image and histogram of particle-size distribution in CZA, CZS and CZT catalysts; —♦— CZA, —■— CZS, —▲— CZT.

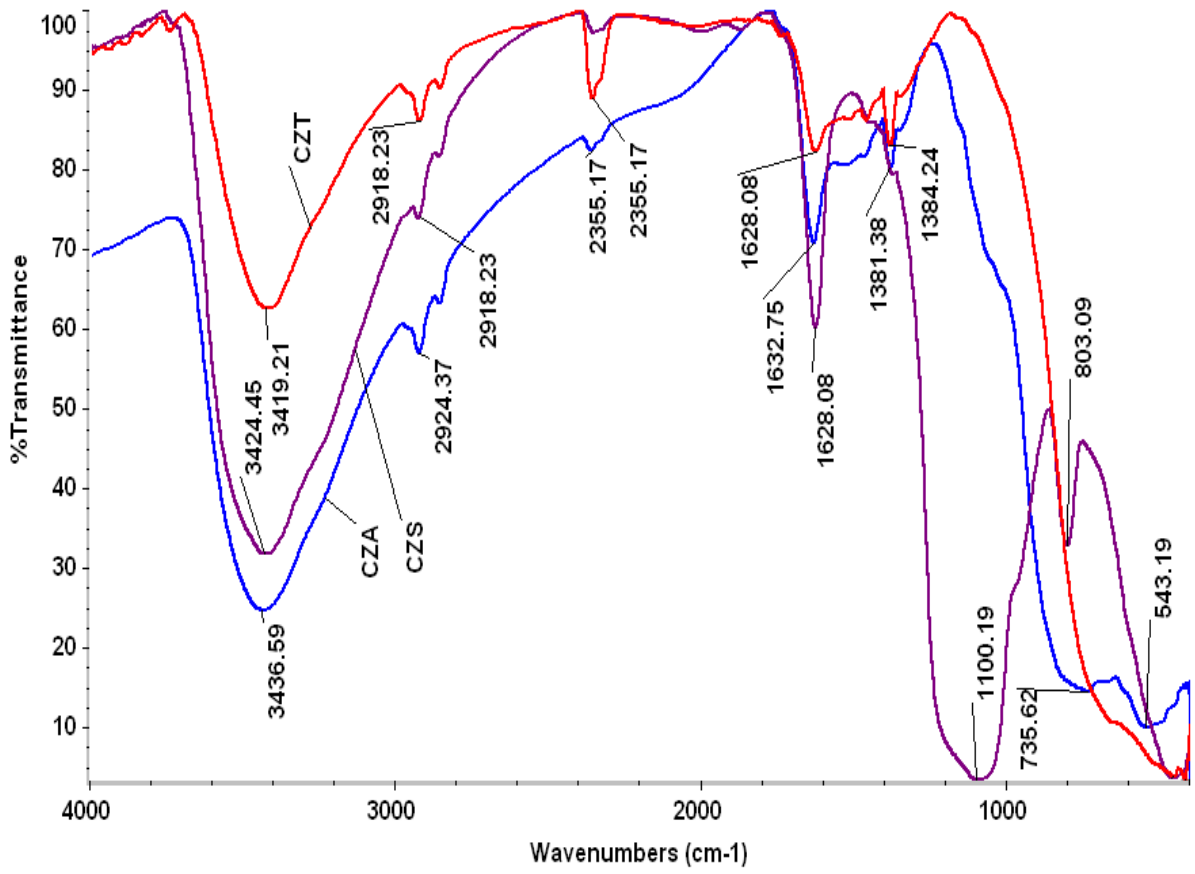

Figure 4.3.5. FTIR spectra of CZA, CZS and CZT catalysts.

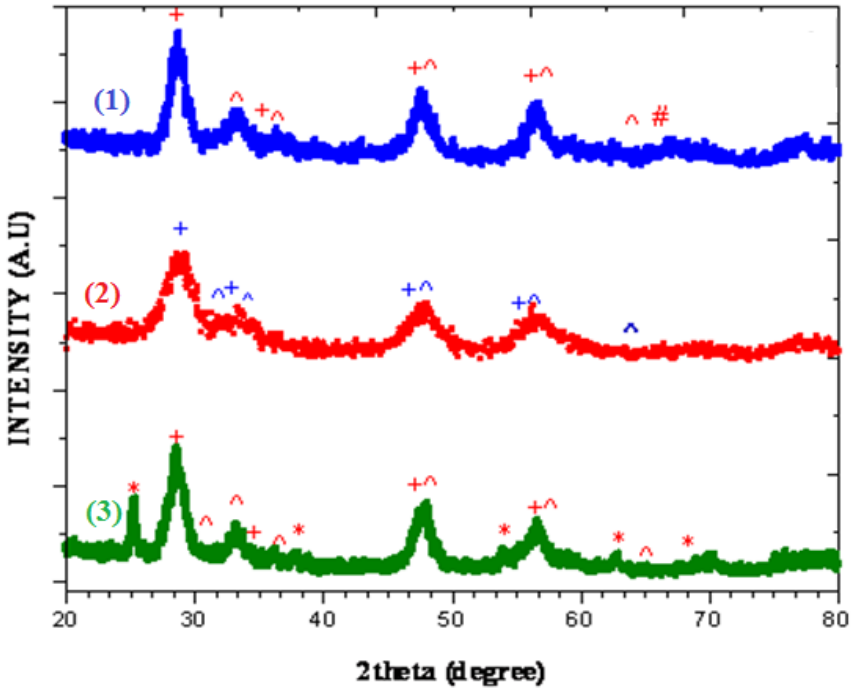

Figure 4.3.6. XRD patterns of CZA, CZS, and CZT catalysts at 500°C. (+) peaks due to CeO_2, (^) peaks due to ZnO, (#) peaks due to γ-Al_2O_3, (*) lines due to TiO_2 anatase. (1) CZA, (2) CZS and (3) CZT.

4.3.1.4. N_2-adsorption-desorption

BET surface area, pore size distribution and pore volume of all the catalysts are given in Figure 4.3.7 and the textural properties are summarized in Table 4.3.1. Synthesized catalysts have the surface area in the range of 61-104 m^2/g. Adsorption–desorption isotherms of the catalysts at 77.2 K confirm the generation of mesopores during their synthesis and the absence of micropores as shown in Figure 4.3.7. All the adsorption-desorption isotherms are of type III, according to the IUPAC interpretation and exhibit a H3 hysteresis loop [Sing et al., 1985; Rouquérol et al., 1994; Pandey et al., 2014; Goepel et al., 2014]. This confirms presence of mesopores and absence of micropores in the synthesized catalysts. If the relative pressure increases ($P/P_o > 0.60$), then the isotherms show the capillary condensation of nitrogen within the uniform mesopores, where the P/P_o position of the influence points is related to the diameter of the mesopores [Samiee et al., 2013]. Among silica, alumina and titania supports, specific surface area is as follows: silica > alumina > titania [Grun et al., 1996]. Therefore, metal oxides impregnated on these supports also follow the same trend. Voß et al. [2002] have reported similar trend of BET surface area for cobalt impregnated silica, aluminum and titania catalysts. Reddy et al. [2008] also observed similar BET surface area trend for aluminum, silica and titania supported ceria-zirconia catalyst. Fractal dimension which is used as an index for estimating the irregularity or roughness of the catalysts surface, was studied using the Frenkel-Halsey-Hill (FHH) equation [Halsey, 1948] for the CZA, CZS and CZT catalysts, to the adsorption isotherm of N_2 [Sato et al., 1997]:

$$\frac{q}{q_e} = K \ln\left(\frac{P_o}{P}\right)^{D-3} \qquad (4.3.1)$$

where, q is the amount adsorbed at equilibrium pressure P, P_o is the saturated pressure, D is the fractal dimension, q_e is the amount adsorbed filling micropore volume and K is a constant. The logarithmic plot of (q/q_e) verses (P_o/P) showed linear behavior, and D was calculated from the slope (D-3) of the straight line. Surface smoothness, irregular nature or roughness depends upon the D value. If D=2, then the surface is considered to be perfectly smooth,

whereas if D=3, then the surface is very irregular or very rough. For the synthesized catalysts, the fractal dimension was found to be 2.514 for CZA, 2.441 for CZS and 2.511 for CZT. This shows all the catalysts shows similar surface heterogeneity with a maximum deviation of 3%.

4.3.1.5. NH_3-temperature programmed desorption

To investigate the acid properties for the synthesized cerium-zinc with different supported catalysts, NH_3-TPD analysis was performed [Tanabe et al., 1989]. NH_3 desorption is temperature-dependent and can be classified in three stages, namely as weak (<200°C), moderate (200-450°C) and strong (> 450°C). Profiles of NH_3-TPD on the supported Ce-Zn catalysts are shown in Figure 4.3.8(a) and the acidity of catalysts (calculated form NH_3-TPD peak area) is given in Table 4.3.2. Two NH_3 desorption peaks at 131°C and 282°C were observed for CZA. Intensity of the peak was 0.691 mmol/g at 131°C and 0.116 mmol/g at 282°C. These peaks could be ascribed to the desorption of NH_3 from weak and moderate Lewis acid sites, respectively. CZS catalyst showed NH_3 desorption peaks at 113°C with 1.288 mmol/g intensity corresponding to weak Lewis acid site only. CZT catalyst showed NH_3 desorption peaks at 99°C with an intensity of 0.35 mmol/g in the weak region only. According to NH_3-TPD results, total acidity of the synthesized CZA, CZS and CZT catalysts were 0.81 mmol/g, 1.29 mmol/g and 0.35 mmol/g, respectively.

4.3.1.6. CO_2 -temperature programmed desorption

The profiles of CO_2-TPD on synthesized Ce-Zn with supported catalysts are shown in Figure 4.3.8b and the basicity of the catalysts calculated form CO_2-TPD peak area is summarized in Table 4.3.2. The CO_2-TPD can be classified as weak (< 200°C), moderate (200-450°C) and strong (> 450°C). CZT catalyst showed only weak basicity observed by peak around 145°C. CZA catalyst shows two distinct peaks at 242°C and 796°C in the moderate and strong region, respectively. For CZS catalyst, peaks are observed in all the three regions at 188, 459 and 763°C. According to the CO_2-TPD results, CZS catalyst showed the strong, moderate, and weak basic sites, with intensities of 1.951 mmol/g, 0.151 mmol/g and 0.719 mmol/g, respectively and the total basic amount being 2.821 mmol/g. CZA

showed desorption behavior at strong (> 450°C) and weak basic sites (< 200°C) with the basic amount being 0.795 mmol/g and 0.242 mmol/g, respectively. CZT catalyst showed only weak basic sites with intensity of 0.823 mmol/g.

Silanol groups in amorphous silica provide weak Bronsted acidity. Calcination of silica increases the Lewis acidity and basicity due to activation of siloxane groups by dehydration reaction. In comparison, alumina and titania supports develop lower amount of Lewis acidity and basicity during their calcination [Rouquérol et al., 1994; Gorrepati et al., 2010]. Synthesized Ce-Zn have both acidic and basic sites indicating that the catalysts can act as acid-base bifunctional catalysts, however, support materials varied the nature of the catalysts. A few investigators have reported that the presence of both acidic and basic sites help in the transesterification of PC with methanol used for DMC synthesis [Wei et al., 2003; Srivastava et al., 2006].

4.3.1.7. Thermal stability

Thermal stability of the CZA, CZS and CZT catalysts was determined by using thermogravimetric analysis (TGA), differential thermal gravimetery (DTG) and differential thermal analysis (DTA). Results are shown in Figure 4.3.9. TGA traces show mass loss of 7.3%, 8.03% and 4.4% for CZA, CZS and CZT catalysts, respectively, in the temperature range of 20-200°C. These mass losses may be due to vaporization of low boiling point organic molecules including moisture. Mass loss of 8% for CZA; 8.3% for CZS and 6.9% for CZT was observed in the range of 200-500°C. At 1000°C, the catalyst samples retained residual mass of 84.7%, 83.7% and 88.7% of the original mass for CZA, CZS and CZT catalyst, respectively. Thus, all the catalysts were found to be highly stable thermally.

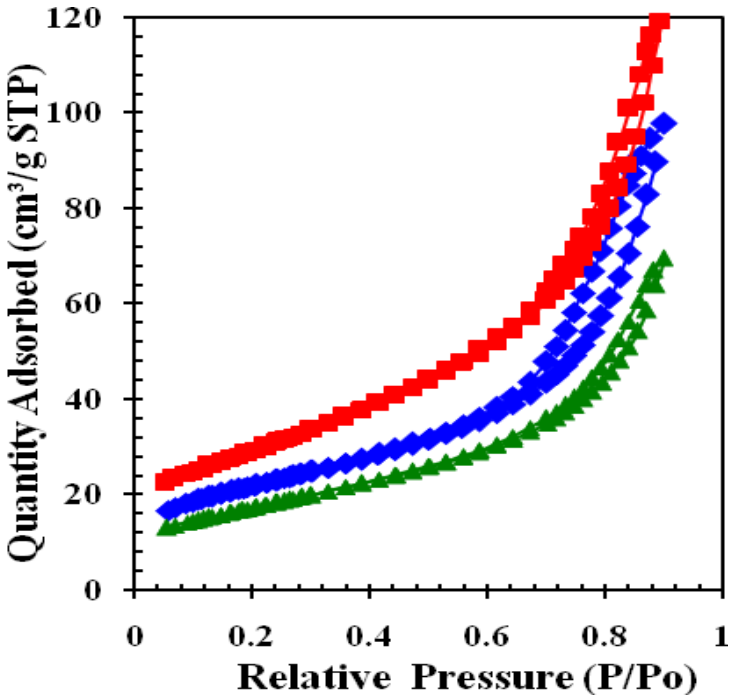

(a)

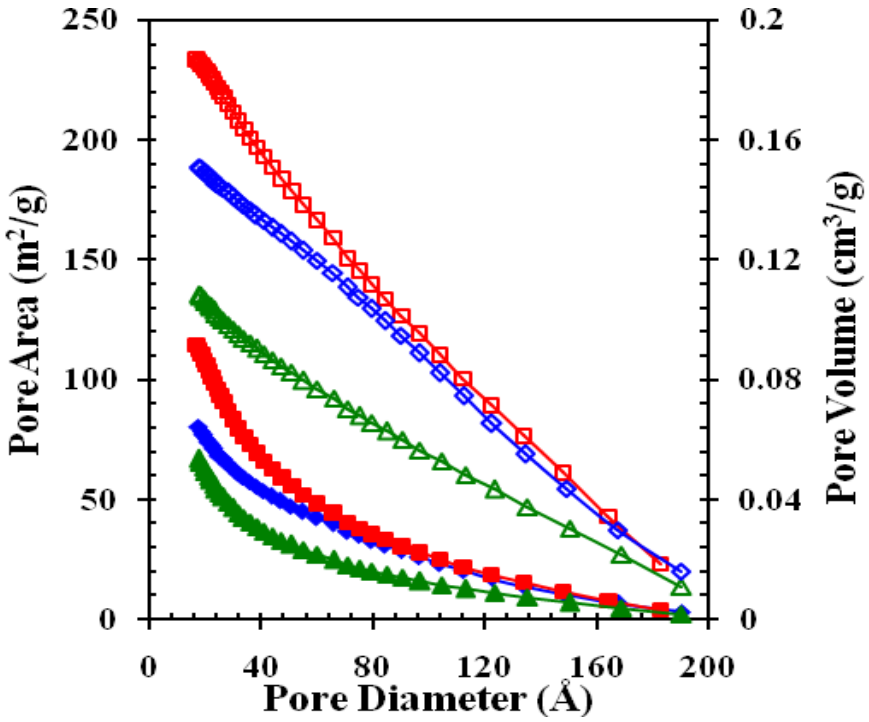

(b)

Figure 4.3.7. (a) Adsorption/desorption isotherms of N_2 at 77 K, —♦— CZA, —■— CZS, —▲— CZT. (b) Pore size distribution for CZA, CZS and CZT catalysts; —♦— CZA-pore volume, —■— CZS-pore volume, —▲— CZT-pore volume, —◊— CZA-pore area, —□— CZS-pore area, —Δ— CZT-pore area.

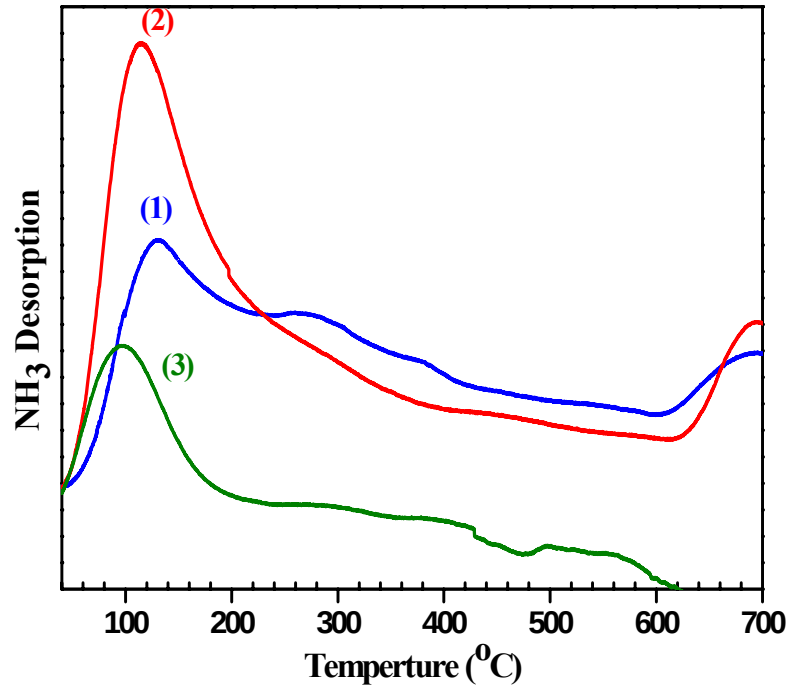

(a) NH_3-TPD

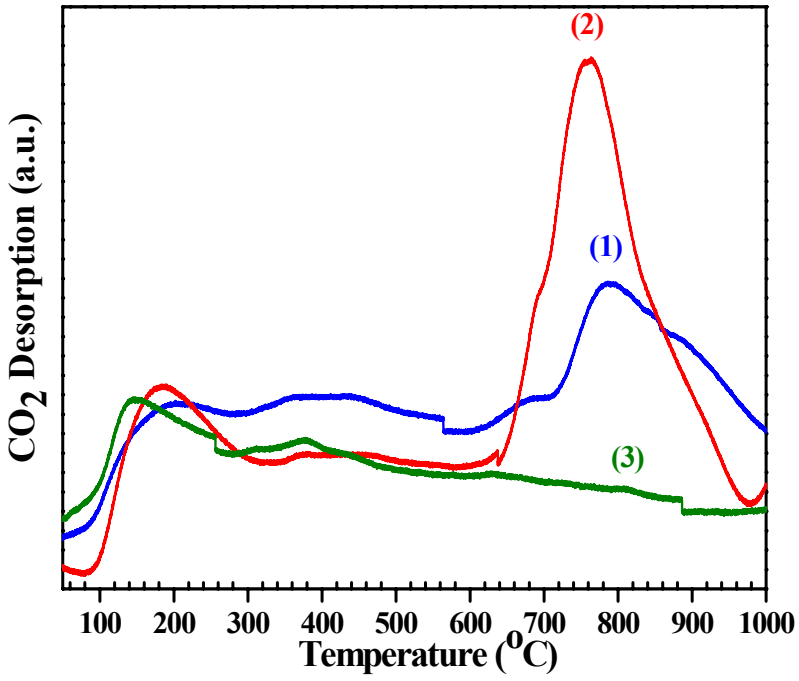

(b) CO_2-TPD

Figure 4.3.8. NH_3-/CO_2-TPD profile of synthesized catalysts; (1) CZA, (2) CZS, (3) CZT.

Table 4.3.1. Crystallite size and textural properties of CZA, CZS and CZT catalysts.

Catalyst	XRD			Textural properties		
	Unit Cell Parameter (nm)[a]	Crystallite size (nm)[a]	Structure[a]	Surface Area (m^2/g)	Pore volume (cm^3/g)[b]	Average Pore diameter (nm)[c]
CZA	54.2	3.70	Cubic	77	0.150	7.5
CZS	62.9	3.90	Cubic	104	0.187	6.3
CZT	53.8	3.05	Cubic	61	0.108	6.4

[a]The unit cell parameter, crystal size and structure is calculated using Sherrer's equation.
[b]BJH desorption cumulative pore volume of pores in the range 17 to 3000 Å.
[c]BJH desorption average pore diameter.

Table 4.3.2. TPD analysis using absorbed NH_3 and CO_2 for determining acidic and basic properties of synthesized catalysts.

Catalyst	TPD analysis of absorbed NH_3 (mmol/g)			Total NH_3 evolved (mmol/g)	Acid site density (µmol/m^2)
	Weak (< 200°C)	Moderate (200-450°C)	Strong (> 450°C)		
CZA	0.691 (131)	0.116 (282)	-	0.807	10.48
CZS	1.288 (113)	-	-	1.288	12.38
CZT	0.343 (99)	0.001 (296)	-	0.344	5.64
Catalyst	**TPD analysis of absorbed CO_2 (mmol/g)**			**Total CO_2 evolved (mmol/g)**	**Basic site density (µmol/m^2)**
	Weak (< 200°C)	**Moderate (200-450°C)**	**Strong (> 450°C)**		
CZA	0.242 (177)	-	0.795 (796)	1.037	13.47
CZS	0.719 (188)	0.151 (459)	1.951 (763)	2.821	27.12
CZT	0.713 (145)	-	-	0.713	11.69

Temperature (°C) at maxima is given in brackets.

4.3.2. Catalytic Activity of CeO_2-ZnO-Support Mixed Metal Oxide

The catalytic activity of the cerium-zinc oxide stabilized on the three supports was tested for the transesterification of PC with methanol. Activity measurement was performed at the initial pressure of 2-5 bar and the final pressure of 20-25 bar.

Effect of temperature on the formation of DMC was investigated over the temperature range of 120-200°C. The results are shown in Figure 4.3.10a. Maximum DMC yield of 77% was obtained at 170°C for CZS catalyst, whereas CZA and CZT gave 68% and 23% DMC yield, respectively at the same temperature. The DMC yield increases with an increase in temperature up to 170°C and, thereafter, decreases with an increase in the reaction temperature. At temperatures more than 170°C, side reactions and/or decomposition of DMC to PC and the formation of the byproduct PG were observed. Optimum synthesis temperature for DMC was found to be 170°C, giving an optimum yield of 77% with CZS catalyst.

The effect of molar ratio of methanol/PC on the synthesis of DMC using the three catalysts is shown in Figure 4.3.10. It is seen that the DMC yield increases with an increase in the mole ratio of methanol/PC. Maximum DMC yield is observed at a methanol/PC molar ratio of takes place producing PG, thereby adversely affecting the DMC formation. Higher methanol/PC ratio shifts the equilibrium towards the product side [Sato et al., 1997]. Maximum DMC yield of 77%, 69% and 23% for CZS, CZA and CZT, respectively was found at methanol/PC molar ratio of 10.

Overall, CZS catalyst exhibited better performance as compared to CZA and CZT catalysts. CZS has highest BET surface area, as also the acidic and basic sites per unit mass of the catalyst. Moreover, acid site densities (acidic sites per unit surface area) of the synthesized catalysts follow the sequence (Table 4.1.5): CZS (12.38 μmol/m^2) > CZA (11.48 μmol/m^2) > CZT (5.64 μmol/m^2). Similarly, the basic site density of the synthesized catalysts has the following sequence (Table 4.3.2): CZS (27.12 μmol/m^2) > CZA (13.47 μmol/m^2) > CZT (11.69 μmol/m^2). Thus, the basic and acidic site densities and the catalytic activity followed similar trend. CZS having higher basicity lowers the free energy of this reaction and enhances the yield of DMC by the transesterification reaction [Wei et al., 2003].

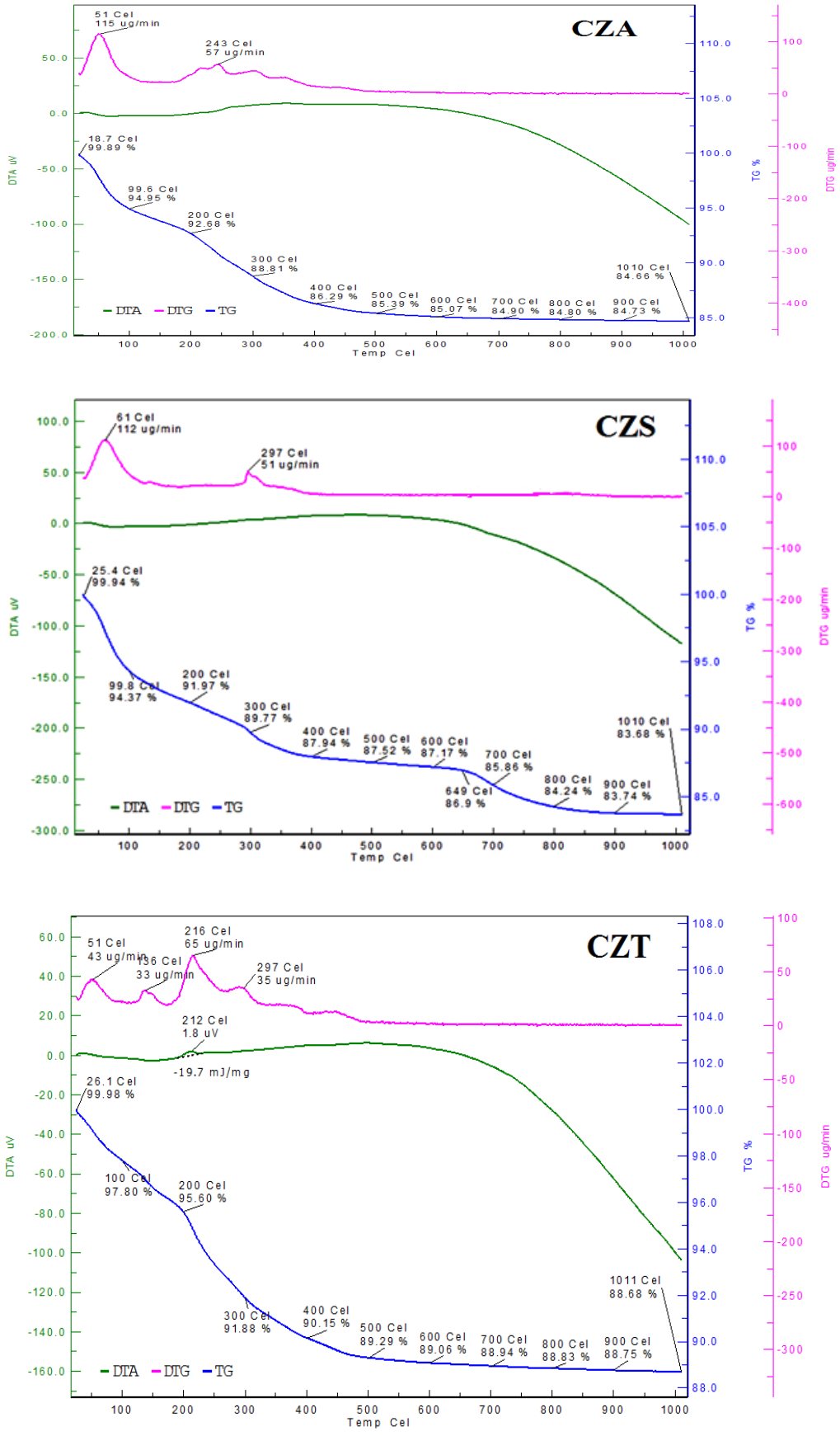

Figure 4.3.9. TG/DTA/DTG of synthesized CZA, CZS and CZT catalysts.

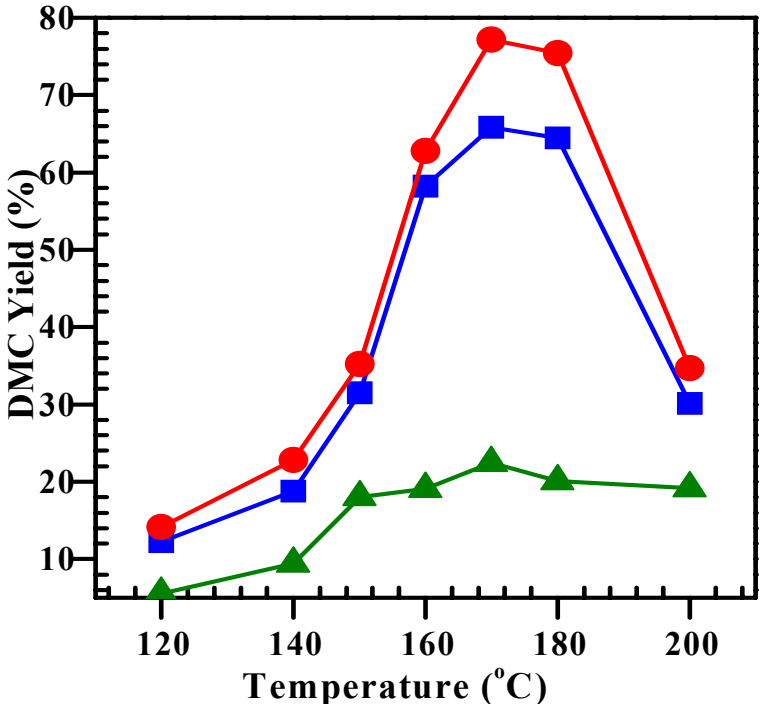

(a)

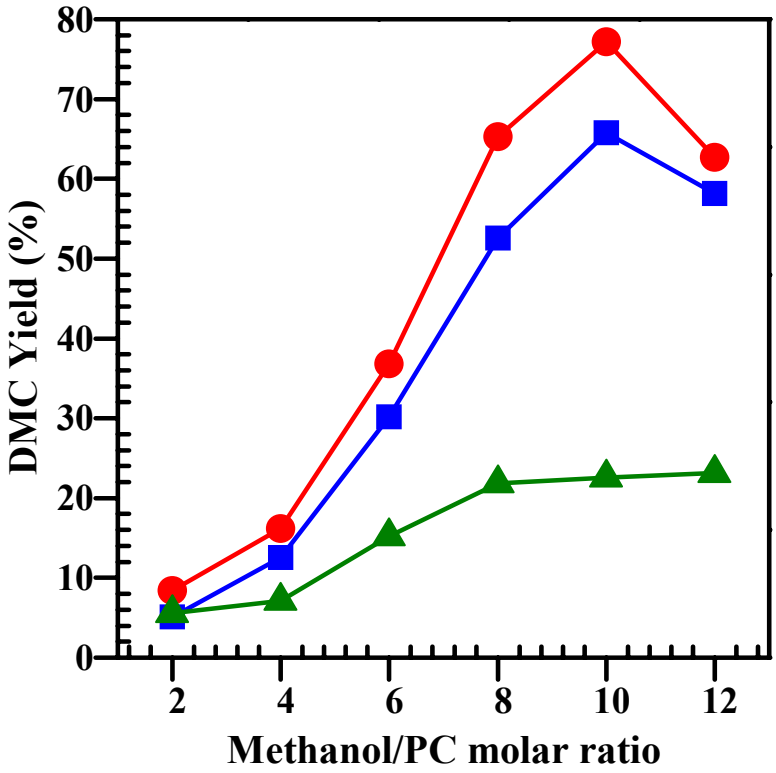

(b)

Figure 4.3.10. (a) Effect on reaction temperature on DMC formation using different catalysts; (b) Effect on PC to methanol molar ratio on synthesis of DMC using different catalysts at temperature 170°C; (Reaction condition: PC=0.25 mol, methanol=2.5 mol, catalyst=5 wt.% of reactant, reaction time=4 h). —■— CZA, —●— CZS, —▲— CZT.

4.4. Cu-Zn-Al HYDROTALCITE CATALYSTS: CHARACTERIZATION AND CATALYTIC ACTIVITY FOR TRANSESTERIFICATION OF PROPYLENE CARBONATE (PC) WITH METHANOL

In the present study, Cu-Zn-Al (CZA) hydrotalcite catalysts prepared by the co-precipitation method and calcined at 300^{o}C, 500^{o}C and 800^{o}C (named as CZA300, CZA500 and CZA800) were used for the synthesis of DMC from methanol and PC by transesterification reaction in a batch reactor. Further experiments were carried out with the best performing catalyst so as to optimize the operating conditions such as the reaction temperature, methanol/PC molar ratio, catalysts dose, reaction time and reuseability of the catalyst for the formation of DMC.

4.4.1. Characterization of Cu-Zn-Al Hydrotalcite

4.4.1.1. Thermal stability

Thermal stability of the synthesized Cu-Zn-Al hydrotalcite (before calcination) is shown in Figure 4.4.1. It shows that the thermal decomposition of the hydrotalcite occurs in three steps. Weight loss of 15%, 12% and 6% occur in three distinct regions over the temperature ranges of 50-250°C, 250-500°C and 500-800°C, respectively. The decomposition below 250°C was due to the removal of interlayer water molecules and physiosorbed water. The weight loss in the 250°C to 500°C region is due to the removal of interlayer anions like OH^- ions and CO_3^{2-} in the form of H_2O and CO_2, respectively [Dixit et al., 2013]. The third weight loss zone beyond 600°C may be due to the decomposition of Cu oxocarbonate of the synthesized hydrotalcite structure [Trujillano et al., 2006; Brito et al., 2009] Uncalcined Cu-Zn-Al hydrotalcite was further calcined at 300, 500 and 800°C and was designated as CZA300, CZA500 and CZA800, respectively. Gao et al. [2013] studied the TGA for Cu/Zn/Al HTLc after the calcination at 750°C under air atmosphere. They found three weight loss zones: below > 250°C (11.5%), 250-600°C (16.0%), 600-700°C (5.5%). Others authors have observed similar degradation zones [Kaluza et al., 2011; Cunha et al., 2012;]. These three mass loss zones are attributed to the decomposition of interlayer water molecules, collapse the layered structure and decomposition of Cu oxocarbonate.

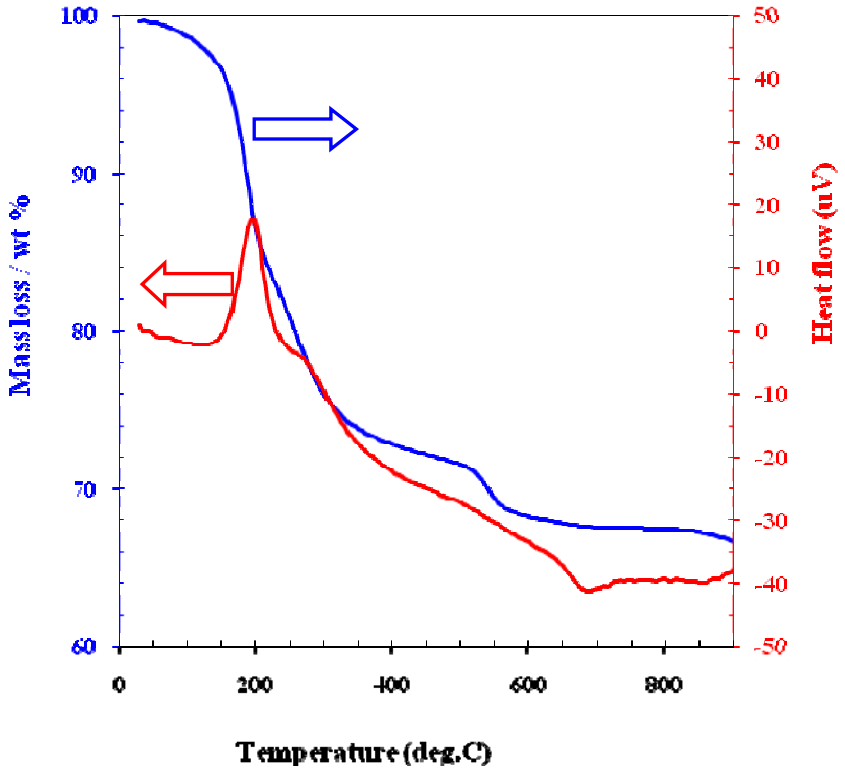

Figure 4.4.1. TGA profile of Cu-Zn-Al (HTLc).

4.4.1.2. X-ray diffraction

XRD spectrum of copper-zinc-aluminum HTLc (without calcination) is shown in Figure 4.4.2. It may be seen that this spectra is similar to that reported in the literature [Bahranowski et al., 2001; Gao et al., 2013; He et al., 2013]. This confirms that the synthesized material is HTLc. It is well known that the calcination temperature strongly affects the crystallinity of the catalysts. XRD patterns of the catalysts are shown in Figure 4.4.3. As shown in the figure, the crystallinity increases with an increase in the calcination temperature. XRD pattern of CZA300 indicated the presence of CuO (PDF-ICDD 00-041-0254); ZnO (PDF-ICDD 01-076-0704); Al_2O_3 (PDF-ICDD 01-086-1410); aluminum carbide nitride $Al_8C_3N_4$ (PDF-ICDD 01-085-0413). Source of nitrogen in CZA300 may be the small residue of nitrate ion left after washing. However, it was obtained only in CZA300. Other samples were free from nitrogen compound. CZA500 was found to contain ZnO (PDF-ICDD 01-079-0207); CuO (PDF-ICDD 01-080-1916); Al_2O_3 (PDF-ICDD 01-086-1410). Similarly,

CZA800 contained CuO, tenorite phase (PDF-ICDD 00-048-1548), ZnO (PDF-ICDD 01-080-0075) spinel $ZnAl_2O_4$, gahnite phase (PDF-ICDD 00-005-0669), $CuAl_2O_4$ (PDF-ICDD 00-033-0448) and $Cu_2Al_4O_7$ (PDF-ICDD 01-083-1476).

Thus, the XRD patterns of all the samples indicated the presence of diffraction peaks which may be attributed to CuO and ZnO in all the phases [Barroso et al., 2006]. It may be seen that the Al was present as Al_2O_3 in CZA300 and CZA500, however, it formed spinels like $ZnAl_2O_4$, $CuAl_2O_4$ and $Cu_2Al_4O_7$ in CZA800. Spinel $CuAl_2O_4$ is thermodynamically unstable below 600°C [Strohmeier et al., 1985]. This may be the reason of its absence in CZA300 and CZA500. However, CZA300 catalyst is least crystalline with weak intensity peaks as compared to CZA500 and CZA800. CZA800 exhibits sharp peaks indicating well-developed crystallinity. Busca et al. [2006], Souza et al. [2008], Meher et al. [2009] and Cunha et al. [2012] have shown similar phases of crystallinity in the catalysts calcined at similar temperatures.

4.4.1.3. Surface morphology and elemental analysis

The SEM micrographs were obtained to determine the morphologies of the synthesized CZA catalysts. The morphologies of the synthesized CZA catalysts calcined at 300, 500 and 800°C are shown in Figure 4.4.4. It can be observed that some of the pores get developed in the catalysts with an increase in the calcination temperature. Development of these pores is due to the removal of interlayer anions like OH^- and CO_3^{2-} as stated earlier. This was further confirmed by the EDX analysis (shown in Table 4.4.1). It may be seen that the percentage of Cu, Zn and Al continue to increase and that the percentage of C and O decreases with an increase in the calcination temperature.

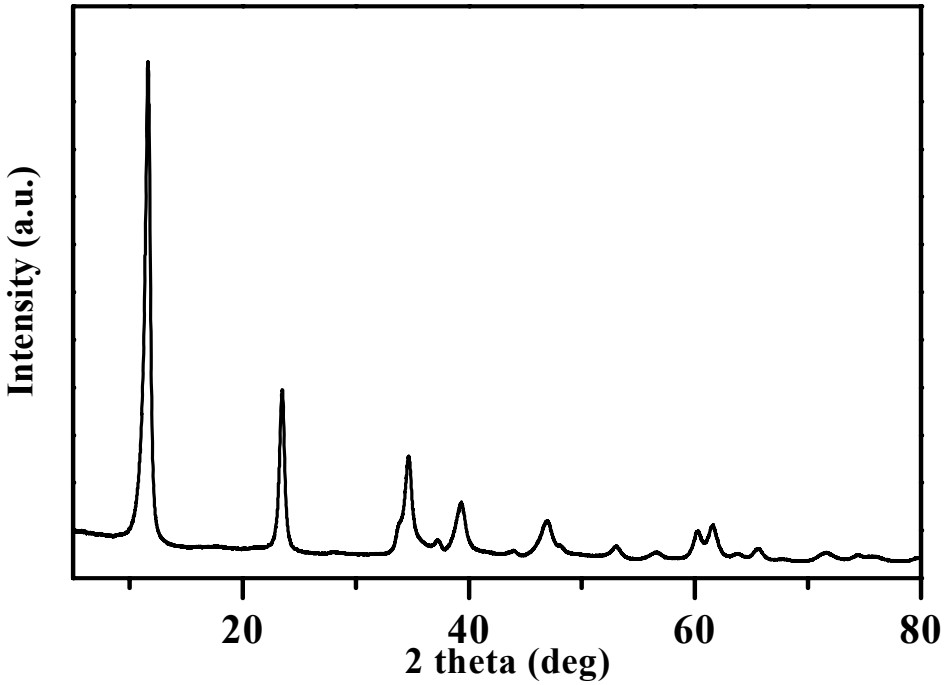

Figure 4.4.2. X-ray diffraction patterns of the CZA catalyst without calcination.

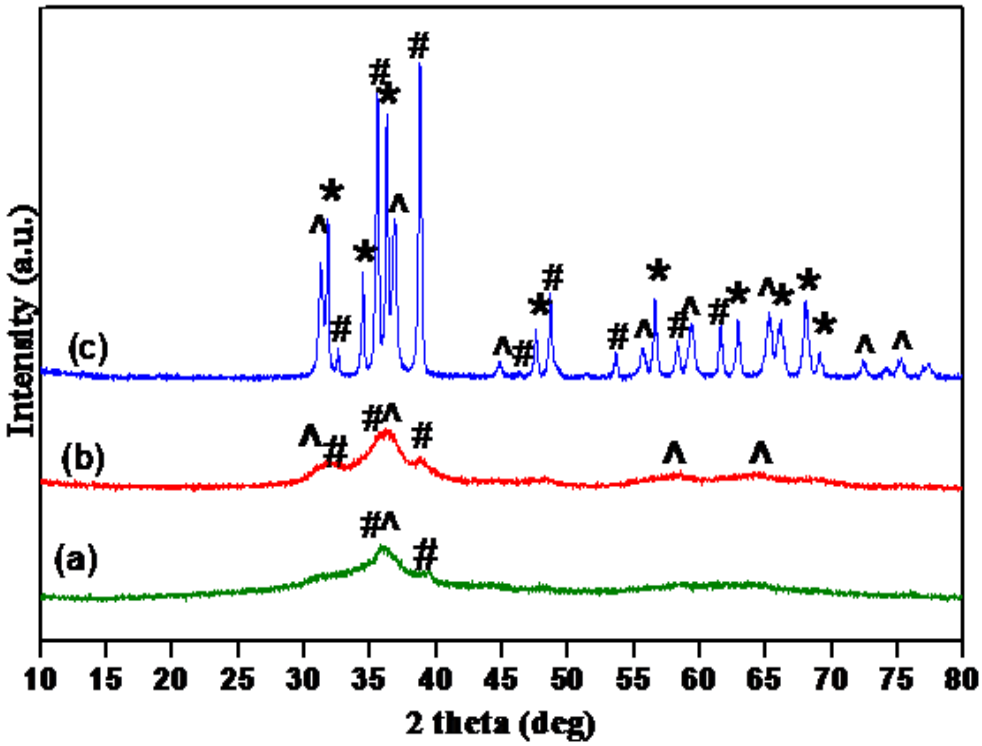

Figure 4.4.3. X-ray diffraction patterns of the CZA catalyst; (a) CZA300, (b) CZA500, (c) CZA800, (^$ZnAl_2O_4$, * ZnO, #CuO).

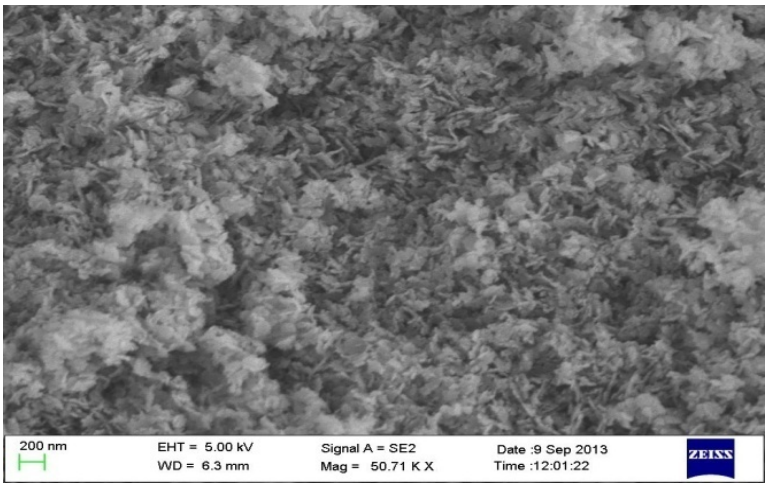

(a)

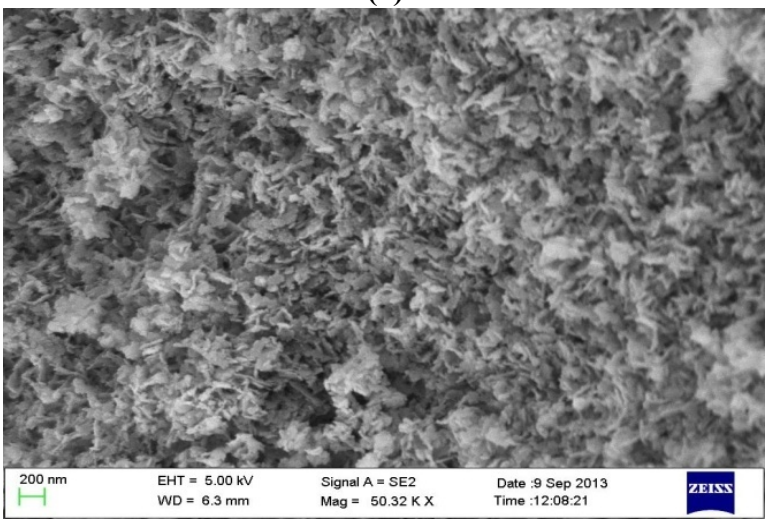

(b)

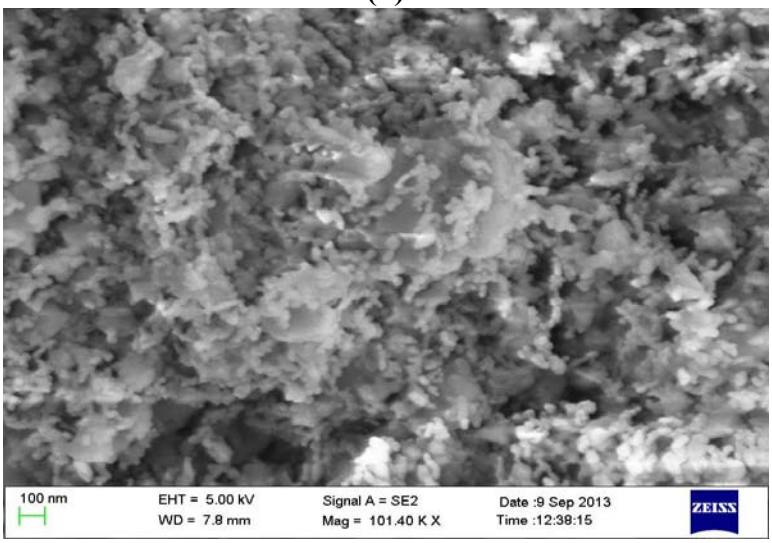

(c)

Figure 4.4.4. Scanning electron micrographs of (a) CZA300, (b) CZA500, (c) CZA800.

4.4.1.4. Textural characterization

Adsorption/desorption isotherms of N_2 at 77 K for all catalysts are given in Figure 4.4.5. Variation of cumulative pore volume and pore area with respect to pore diameter for different catalysts as obtained from liquid nitrogen adsorption-desorption experiments are shown in Figure 4.4.6a. BET surface area, total pore volume and average pore size are listed in Table 4.4.1. CZA300, CZA500 and CZA800 catalysts were found to possess BET surface area of 76, 84 and 14 m^2/g, respectively. Thus, samples of CZA calcined at 300 and 500°C were found to exhibit reasonably higher specific surface area as compared to that calcined at 800°C. Low surface area at higher calcination temperature may become of the sintering of the material. The average pore diameter of CZA300, CZA500 and CZA800 catalysts were found to be 55.6, 52.5 and 49.3 Å, respectively, which indicates a very marginal decrease in the pore size with an increase in calcination temperature.

Distribution of pore volume with respect to pore diameter is shown in Figure 4.4.6b. This figure reveals that CZA300 and CZA500 have bimodal pore distribution with pores centered at 36±1 Å and 131±2 Å. However, for peak centered at 131±2 Å, CZA300 has higher intensity than CZA500 whereas the reverse trend is observed for peak centered at 36±1 Å. Thus, overall CZA500 has slightly larger surface area than CZA300 and the average pore size of CZA300 (0.1086 cm^3/g) is slightly bigger than CZA500 (0.1076 cm^3/g). Also it is seen in Figure 4.4.6b that the surface area of CZA300 are dominated by the peak centered at 131±2 Å whereas it is nearly equally distributed among the two peaks for CZA500. CZA800 has a very small peak centered at 41 Å. Overall, CZA800 (0.00178 cm^3/g) has very less pore volume and surface area as compared to (0.1086 cm^3/g) CZA300 and (0.1076 cm^3/g) CZA500 catalysts. Based on structural, morphological and textural characterization, it can be said that CZA800 has high crystallinity because of sintering which leads to small pore surface area. Higher calcination temperature of 800°C destroys the hydrotalcite structure, decreases the surface area and pore size, though it increases the crystallinity [Sparks et al., 2008; Yi et al., 2011]. Zheng et al. [2007], Busca et al. [2006], Venugopa et al. [2009], Mehar et al. [2009] and Cunha et al. [2012] have reported BET surface area of 67, 67, 57, 73 and 96 m^2/g for CZA catalysts, respectively.

Table 4.4.1. Crystallite size, textural properties and composition of CZA catalysts.

Catalyst	XRD	Textural Properties			Atomic (%) using EDX[c]				
	Crystallite size (nm)	Surface Area (m^2/g)	Cumulative pore volume (cm^3/g)[a]	Average pore diameter (nm)[b]	Cu	Zn	Al	C	O
CZA300	15.9	76	0.1086	5.56	11	12	8	13	56
CZA500	18.6	84	0.1076	5.25	15	14	16	4	51
CZA800	123	14	0.0178	4.93	15	20	23	-	42

[a]BJH desorption cumulative pore volume of pores in the range 17.00 to 3000 Å.
[b]BJH desorption average pore diameter.
[c]Maximum possible error=±10%.

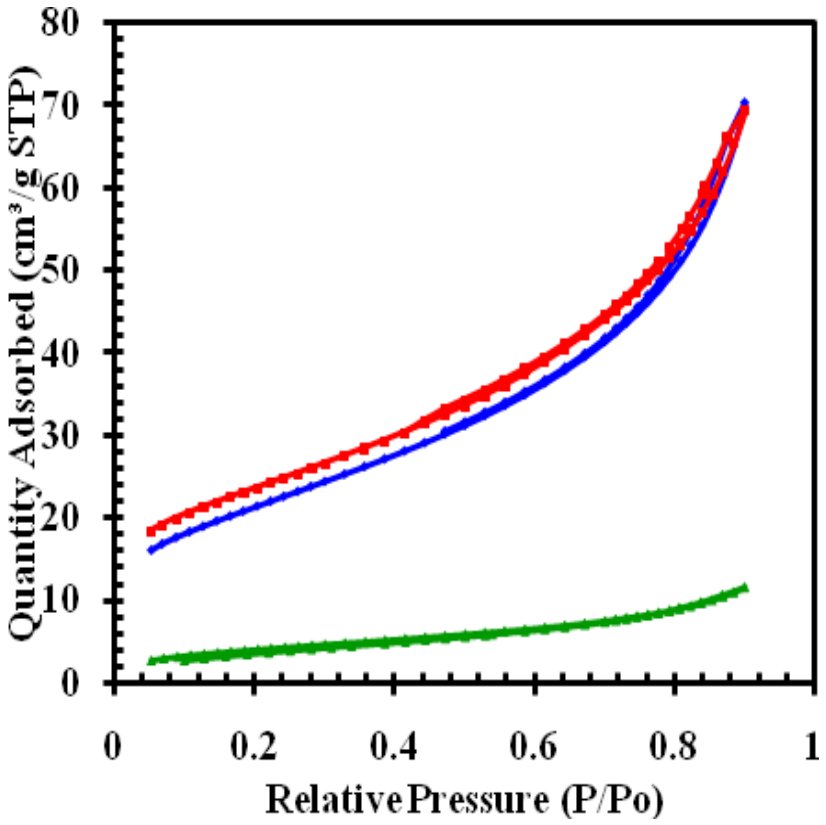

Figure 4.4.5. Adsorption/desorption isotherms of N_2 at 77 K of CZA300, CZA500 and CZA800; —♦— CZA300, —■— CZA500, —▲— CZA800.

4.4.1.5. Fourier transformed infrared spectroscopy

The presence of the functional groups on the catalysts surface was checked by FTIR spectra. Figure 4.4.7 shows the FTIR spectra of the prepared catalysts in the range of wave number 4000-400 cm^{-1}. The broad absorption peak observed at 3600-3200 cm^{-1} and 1620-1650 cm^{-1} are due to hydroxyl group of interlayer water molecules. Band at 1380-1390 cm^{-1} is due to interlayered nitrates [Blanch-Raga et al., 2013] and that at 757-779 cm^{-1} is due to the bending mode. Peaks in the range of 660-670 cm^{-1} are due to the interaction of carbonate within the layers. The peaks found in the range of 480-495 cm^{-1} are due to stretching mode of M-OH.

It may be seen that for wave numbers > 1600 cm^{-1}, CZA300 and CZA500 show peaks with similar intensity, whereas CZA800 has peaks with very low intensities as compared to those for CZA300 and CZA500, thereby confirming the removal of OH and CO_2 groups. Small persistence of these bands in CZA800 may be due to the presence of water moisture during the preparation of the samples for FTIR analysis [Blanch-Raga et al., 2013]. For peaks in the wave number range of 900-1600 cm^{-1}, the intensity of peaks were found to be in the order: CZA300 > CZA500 > CZA800. Therefore, functional groups within this wave number range decrease with an increase in the calcination temperature. For wave number < 900 cm^{-1}, the trend is reversed and the intensity of peaks was found to be in the order: CZA800 > CZA500 > CZA300. It is known that these peaks in HTLc's are due to metal-oxygen vibrations because of the presence of mixed metal oxides which get formed from HTLc phase [Aristizábal et al., 2011; Blanch-Raga et al., 2013], since high temperature calcination increases the percentage of metal oxides, therefore, the peak intensities were found to be in this order in the finger print region.

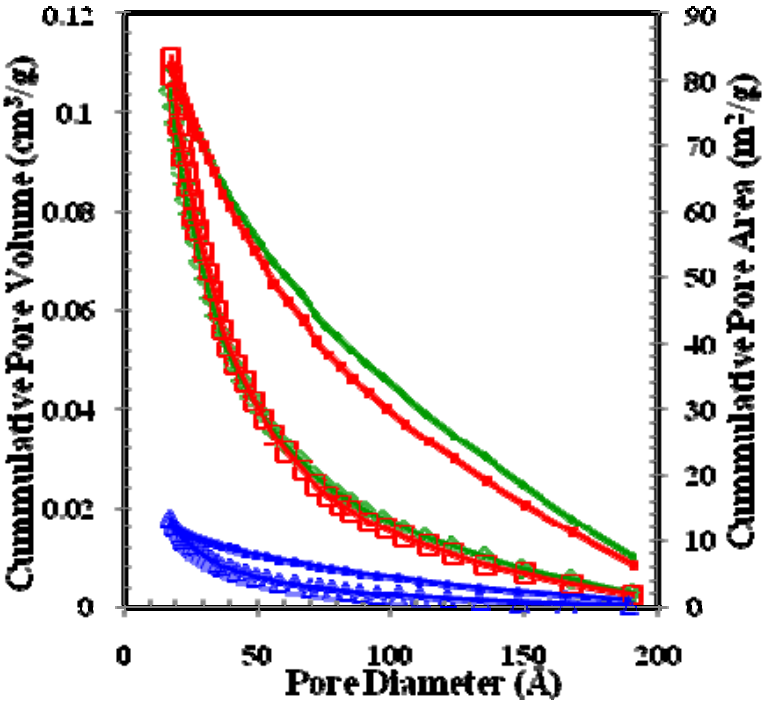

(a)

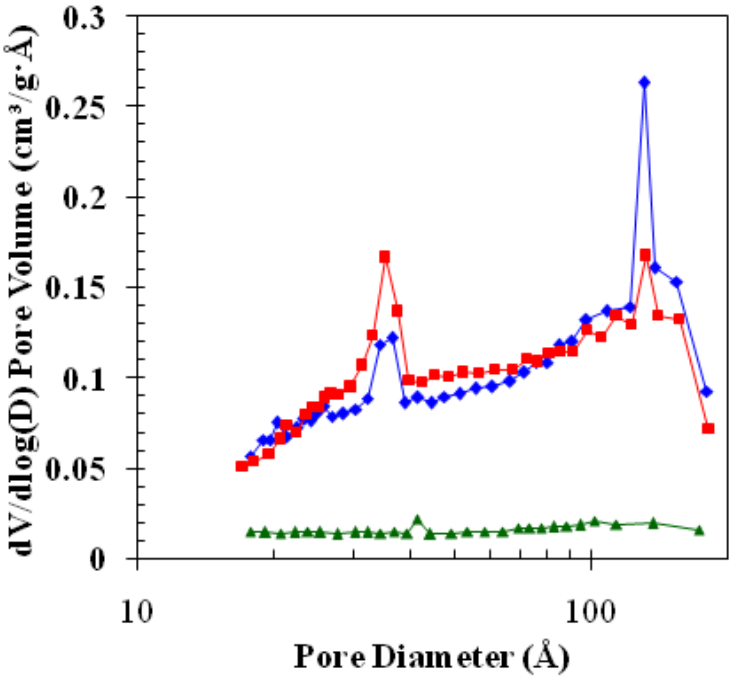

(b)

Figure 4.4.6. (a) Variation of cummulative pore volume and cummulative pore area with pore diameter; —♦— CZA300-pore volume; —■— CZA500-pore volume; —▲— CZA800-pore volume; —◊— CZA300-pore area; —□— CZA500-pore area; —Δ— CZA800-pore area. (b) pore size distribution for CZA300, CZA500 and CZA800 catalysts; —♦— CZA300; —■— CZA500; —▲— CZA800.

4.4.1.6. CO_2-temperature programmed desorption

It is known that calcined HTLc's has several types of active sites. Weak Bronsted basic sites are due to surface OH^- groups whereas the medium strength Lewis sites are due to M^{n+}-O^{2-} pairs. Strong basic sites are due to the presence of low-coordinated O^{2-} [Pavel et al., 2012]. The basic properties of CZA300, CZA500 and CZA800 catalysts were determined using CO_2 adsorption and the results are shown in Figure 4.4.8a. Since in the present study, there is weight loss during heating, therefore, CO_2 evolution during decomposition of the three synthesized HTLc was monitored as per the methods reported in the literature [Bergadà et al., 2007; Silva et al., 2010]. Actual basicity of the synthesized catalysts was obtained after subtracting the CO_2 desorption during decomposition of the three synthesized HTLc from their CO_2-TPD analysis.

It is well known that the base strength of the catalytic sites is represented by desorption temperature, whereas the quantity of CO_2 desorbed represents the basicity of the sites [Wei et al., 2003]. Desorption peaks observed in the figure in the temperature ranges of < 200°C, 200-400°C, > 400°C are attributed to the weak, moderate and strong basic sites, respectively [Wang et al., 2013]. The low temperature peaks can be ascribed to the adsorption at the surface weak basic site due to OH^- group and high temperature peaks are attributed to the strong Lewis basic sites of O^{2-} anions [Rabiah-Nizah et al., 2014]. The amount of CO_2 desorbed from the basic sites of the catalysts at various temperature range are shown in Table 4.4.2. Total basicity of CZA300 catalyst has highest amount of basic sites in all the weak and strong regions, whereas CZA500 catalyst has highest amount of basic sites in the moderate regions. CZA800 showed only strong basic sites with highest basic strength (desorption peaks at 928°C) among all the catalysts. Total basicity decreased with an increase in the calcination temperature, and CZA300 catalyst has the highest amount of total basic sites. The strength of the low and moderate basic sites depends on the Lewis acid-basic paring and OH^- bond on the surface and the higher basic strength are due to the coordination of surface O^{2-} [Rossi et al., 1991].

Table 4.4.2. TPD analysis using absorbed NH_3 and CO_2 for determining acidic and basic properties of synthesized catalysts.

Catalyst	TPD-CO_2 (mmol/g)	CO_2 released during decomposition experiment (mmol/g)	Difference of CO_2 (mmol/g)	TPD analysis of absorbed CO_2 (mmol/g) (Basic sites)		
				Weak (< 200°C)	Moderate (200-450°C)	Strong (> 450°C)
CZA300	4.615	1.96	2.655	2.60 (129)	0.02 (379)	0.035 (895)
CZA500	2.733	1.73	1.003	0.79 (103)	0.154 (356)	0.059 (898)
CZA800	0.9812	0.88	0.1012	0.0002 (115)		0.101 (929)

Catalyst	TPD analysis of absorbed NH_3 (mmol/g) (Acidic sites)			Total evolved NH_3 (mmol/g)
	Weak (< 200°C)	Moderate (200-450°C)	Strong (> 450°C)	
CZA300	1.73 (150)	1.63 (384)	1.58 (560) & 1.72 (882)	6.658
CZA500	1.44 (110)	0.24 (390)	1.44 (901)	3.123
CZA800	-	0.0363 (365)	1.23 (891)	1.255

Temperature (°C) at maxima is given in parenthesis.

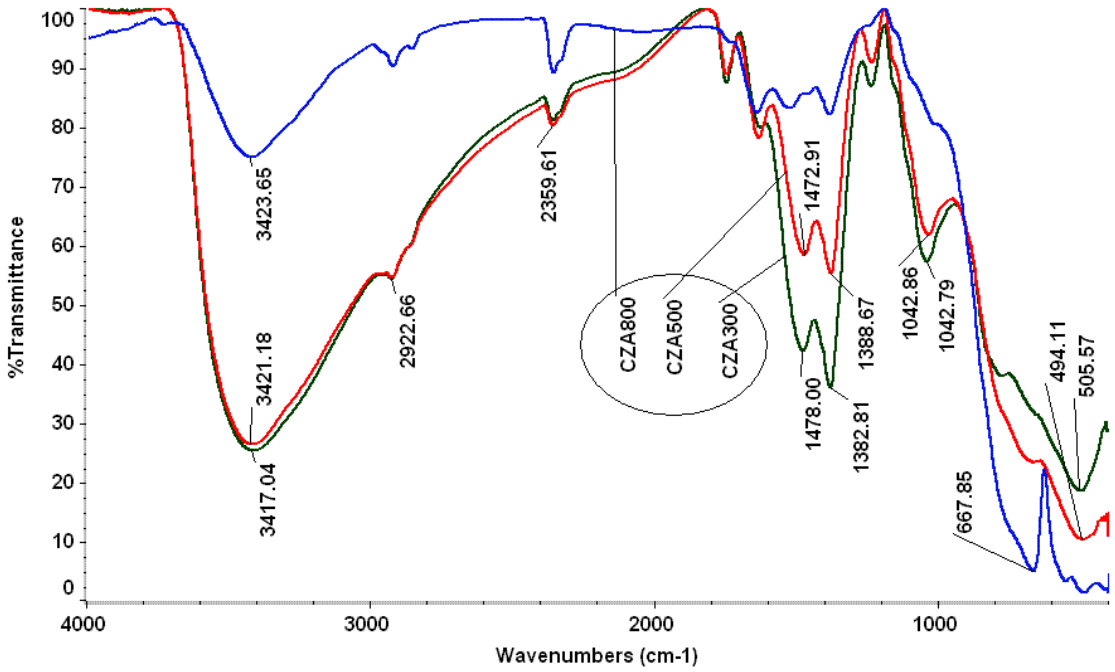

Figure 4.4.7. FTIR spectra of the CZA300, CZA500 and CZA800 catalysts.

4.4.1.7. NH_3-temperature programmed desorption

Variation of acidic properties of the synthesized catalysts was studied using NH_3-TPD and the results are shown in Figure 4.4.8b. Quantity of NH_3 desorbed from the weak (< 200°C), moderate (200-400°C) and strong (> 400°C) acidic sites are shown in Table 4.4.2. The peak in high temperature (> 700°C) is attributed to desorption of NH_3 from strong Bronsted acid sites [Rabiah-Nizah et al., 2014]. All the catalysts are having similar acidic strength as represented by very small variation in the highest desorption temperature (910±20°C). CZA300 catalyst has the highest amount of acidic sites in all the three regions. CZA800 was found to contain only medium and strong acidic sites. Total desorbed amount of NH_3 was found to be in the following order: CZA300 > CZA500 > CZA800. Therefore, the CZA300 has highest number of acidic sites whereas CZA800 has the lowest amount of the acidic sites. Overall, it is formed that an increase in the calcination temperature decrease amount the quantity of acidic sites in the catalyst.

It may be noted that the amount of basic and acidic sites are more in CZA300 and CZA500 which have higher specific surface area as compared to CZA800. Prepared CZA catalysts have both acidic and basic sites revealing that they can act as an acid-base bifunctional catalyst [Wang et al., 2013].

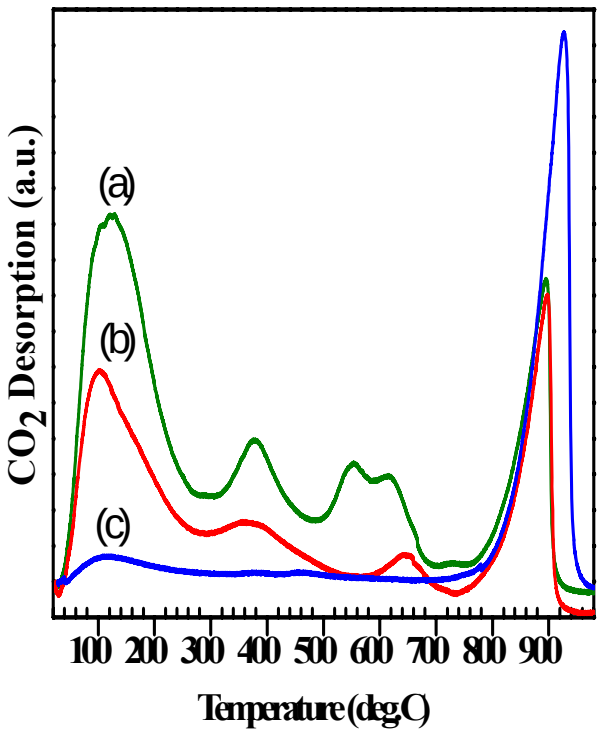

TPD-CO_2

(a) CZA300, (b) CZA500, (c) CZA800.

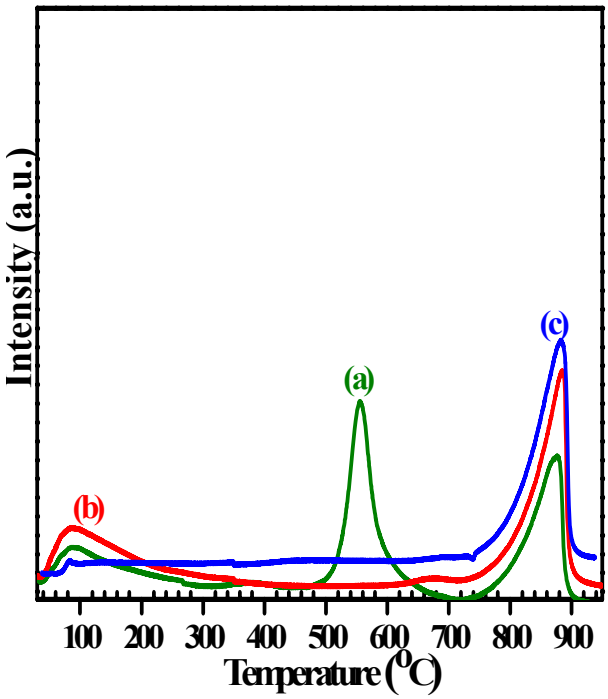

CO_2 evolution during decomposition of catalysts

(a) CZA300, (b) CZA500, (c) CZA800

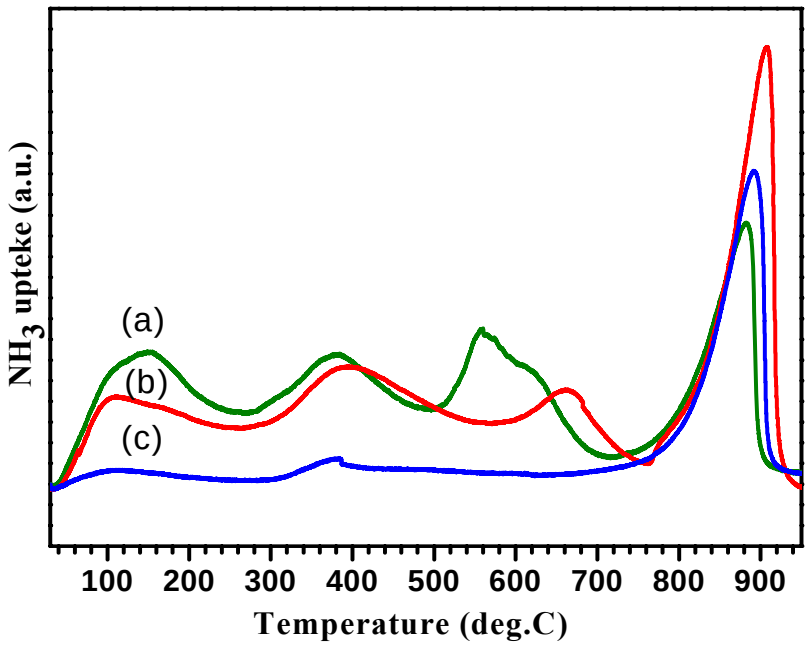

TPD-NH_3

(a) CZA300, (b) CZA500, (c) CZA800

Figure 4.4.8. TPD-CO_2, decomposition and TPD-NH_3 of catalysts CZA300, CZA500 and CZA800.

4.4.2. Catalytic Activity of Cu-Zn-Al Hydrotalcite Catalysts

One mole of PC reacts with two moles of methanol to produce one mole of DMC and one mole of PG. However, an excess amount of methanol drives the reaction towards the transesterified product [Nawaratna et al., 2012]. Performance of CZA catalyst with different calcination temperature was investigated for the formation of DMC from PC with methanol in a batch reactor and the results are presented in Figure 4.4.9. TOF values for CZA300, CZA500 and CZA800 were found to be 5.99, 5.61 and 1.50 h^{-1}, respectively.

The activity of the CZA300 catalyst was found to be better as compared to that of CZA500 and CZA800 catalysts. Catalyst characterization provides an insight as to why the CZA300 catalyst better results of transesterification of PC with methanol. Generally, the basicity of the catalysts facilitated the selectivity of DMC and conversion of PC. The transesterification activity and the basicity of the catalysts follow the same order: CZA300 > CZA500 > CZA800.

As shown in Table 4.4.2, the basicity and the base strength of the CZA catalysts calcined at 300, is much higher than that calcined at 500 and 800°C. Therefore, CZA300 lowers the free energy of this reaction and enhances the yield of DMC by the transesterification reaction [Wei et al., 2003; Filippis et al., 2005; Singh and Fernando, 2008]. Moreover, CZA300 has bimodal pore distribution with pores centered at 36±1 Å and 131±2 Å, and the surface area associated with peak 131±2 Å being much larger than the at surface area associated with peak at 36±1 Å. Thus, CZA300 exhibits highest meso-porosity in comparison to all the catalysts studied in the present work. Bigger size pores of CZA300 help in easy transport of reactants and products in and out from the active basic sites, and this increases conversion of PC, TOF and DMC selectivity. Overall, the combination of textural, acidic and basic properties manifest together in better catalytic activity of CZA300 (in terms of higher yield of DMC) as compared to CZA500 and CZA800 catalysts. Therefore, further experiments were conducted with CZA300 catalyst only.

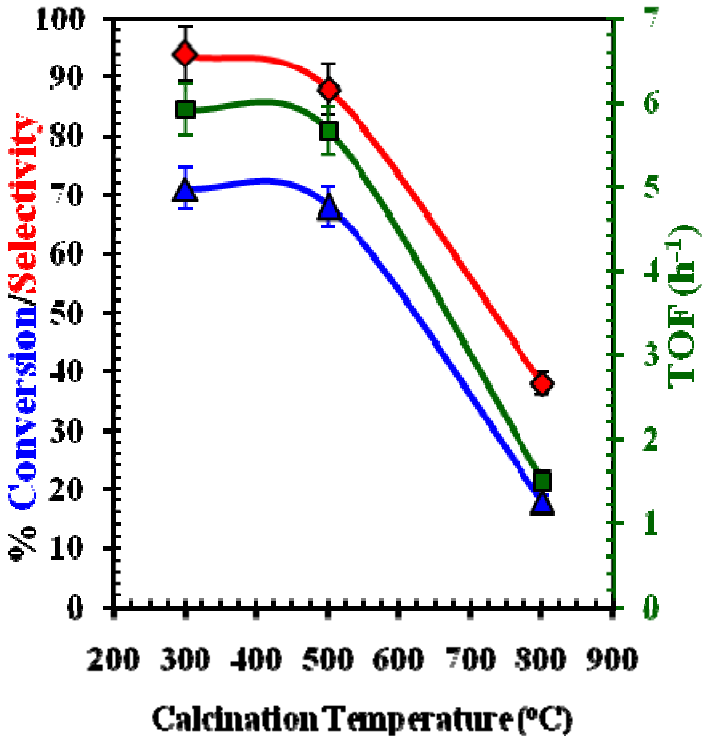

Figure 4.4.9. Conversion of PC and selectivity for DMC using CZA catalyst at 300, 500 and 800°C calcination temperature: Reaction condition: methanol/PC molar ratio=10, catalyst dose=3 wt.% of PC, initial pressure=2 bar, temperature=160°C. —♦— % Selectivity, —▲— % PC conversion, —■— TOF.

4.4.2.1. Effect of catalyst dose

In this study, CZA300 dose was varied between 0.5 to 5 wt.% with respect to PC at the reaction temperature of 160°C, molar ratio of methanol/PC molar ratio of 10. The reaction was carried out for 4 h. The results of Figure 4.4.10a, show that the addition of the catalysts enhances the conversion of PC and the DMC selectivity up to 3 wt.% catalyst dose. Further increase in the catalyst dose has no effect on the PC conversion and DMC selectivity. An increase in the CZA300 dose increases the number of acidic/basic sites, which in turn increase the PC conversion. For CZA300 dose > 3 wt.%, agglomeration of the catalysts and blockage of the pores and active sites occurs which do not allow any further increase in the conversion of PC. PC conversion of 68% and DMC selectivity of 94% were observed at CZA300 dose of 3 wt.% with respect to PC.

4.4.2.2. Effect of reaction time

To determine the optimum reaction time, transesterification of PC with methanol over CZA300 catalyst was studied at various reaction times with other parameters being maintained constant: temperature=160°C, catalyst dose=3 wt.% of PC and PC/methanol molar ratio=10. Variation of PC conversion, DMC selectivity and TOF with reaction time is shown in Figure 4.4.10b. PC Conversion and DMC selectivity increase with an increase in reaction time up to 4 h. Further increase in the reaction time did not increase the PC conversion. TOF value of 5.67 h^{-1} was found to be maximum for reaction time of 4 h, which decreased to 3.80 h^{-1} for the reaction time of 6 h. Thus, the reaction time of 4 h was taken as the optimum value for further experiments.

4.4.2.3. Effect of methanol/PC molar ratio

Effect of methanol/PC molar ratio was varied in the range of 4 to 12 and the results in terms of PC conversion, DMC selectivity and TOF are shown in Figure 4.4.11a. Since transesterification of PC with methanol is a reversible reaction, excess methanol is required to shift the equilibrium towards DMC formation. It can be seen that the PC conversion, DMC selectivity and TOF increase with an increase in the methanol/PC molar ratio from 4 to 10. Further increase in the ratio to 12 had no influence on the output parameters. Excessive amount of methanol at methanol/PC molar ratio > 10 decrease the adsorption of PC on the surface of CZA300, thus, decreasing its catalytic activity [Xu et al., 2013].

4.4.2.4. Effect of reaction temperature

Effect of reaction temperature for the transesterification of PC with methanol was investigated by carrying out the reaction at different temperatures in the temperature range of 120-180°C, reaction time=4 h, methanol/PC molar ratio=10 and catalyst dose=3 wt.% of PC. It may be seen from Figure 4.4.11b, that the PC conversion, TOF and DMC selectivity increase with an increase in temperature from 120 to 160°C, and thereafter, PC conversion and TOF become constant, whereas DMC selectivity decreases with an increase in temperature > 160°C. Unnikrishnan and Srinivas [2012] have reported similar effect of temperature on DMC synthesis.

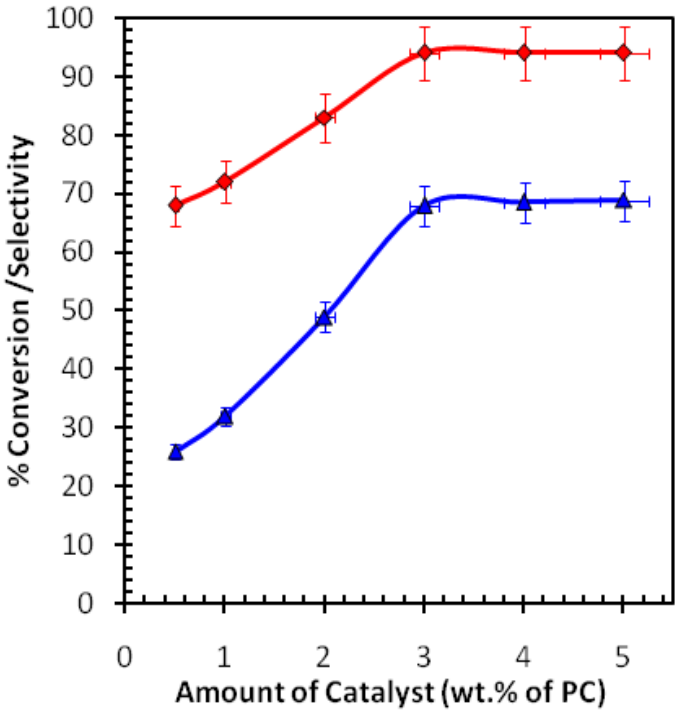

(a)

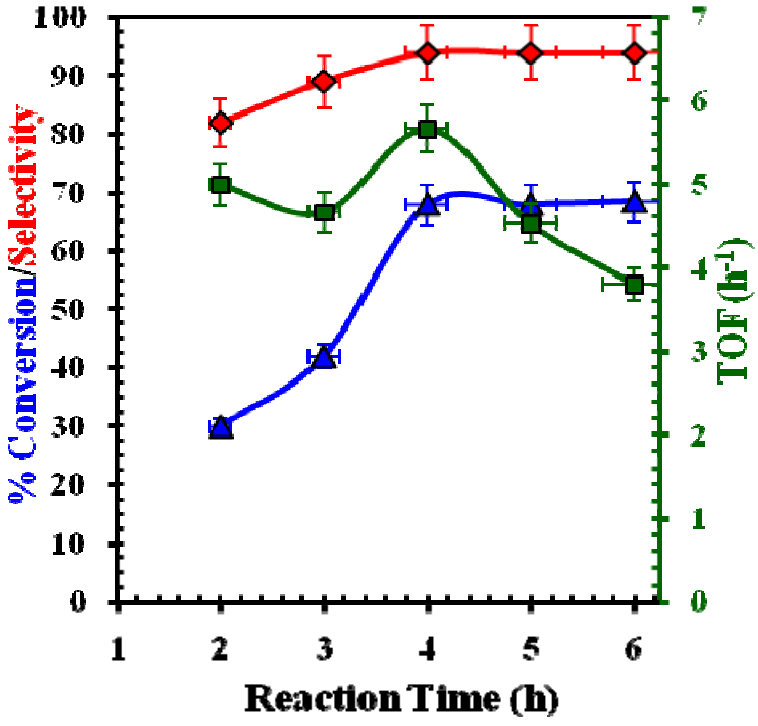

(b)

Figure 4.4.10 Effect of various parameters on transesterification of PC with methanol, (a) effect of catalyst dose: methanol/PC molar ratio=10, reaction time=4 h, temperature=160°C; (b) effect of reaction time: catalyst dose=3 wt.% of PC, temperature=160°C, methanol/PC molar ratio=10. —♦— % Selectivity, —▲— % PC conversion, —■— TOF.

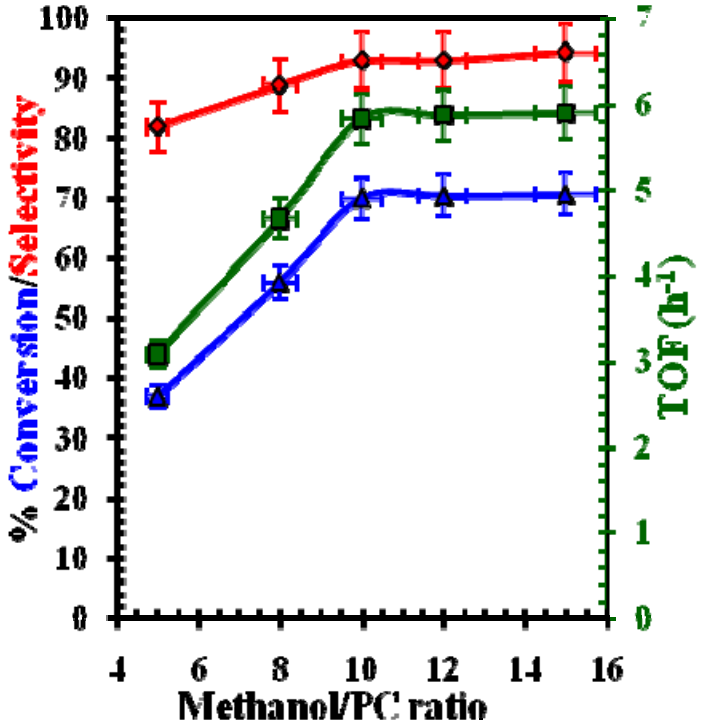

(a)

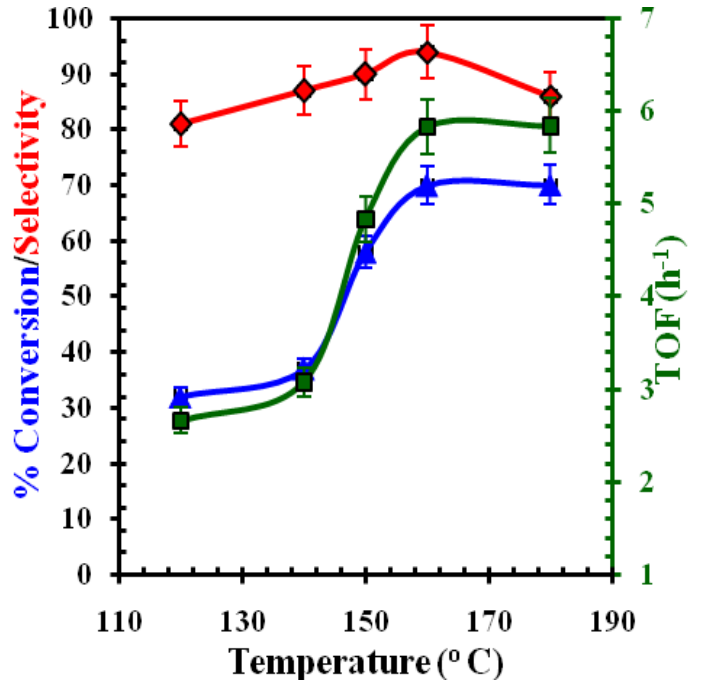

(b)

Figure 4.4.11. Effect of various parameters on transesterification of PC with methanol, (a) effect of methanol/PC molar ratio: catalyst dose=3 wt.% of PC, reaction time=4 h, temperature=160°C; and (b) effect of reaction temperature: methanol/PC molar ratio=10, catalyst dose=3 wt.% of PC, reaction time=4 h. —♦— % Selectivity, —▲— % PC conversion, —■— TOF.

4.4.2.5. Catalyst reusability

The reusability of CZA300 was examined by utilizing it in five consecutive batch reactions. The catalyst was recovered by filtration after the reaction and was washed several times with methanol. It was dried at 105°C for 24 h and reused for subsequent experiments under similar reaction conditions. The results are shown in Figure 4.4.12. It may be seen that there is no change in PC conversion although there is a marginal decrease in DMC selectivity and TOF. These results indicate that CZA300 can be reused in further cycles as a catalyst with no appreciable decrease in its activity.

Unnikrishnan and Srinivas [2012] and Murugan and Bajaj [2010] have used PC as a raw material for DMC synthesis, and that too on HTLc different than that used in the present study. In both of these studies, only selectivity is reported and the PC conversion is not reported. Few studies have reported better PC conversion and selectivity on other type of catalysts [Srivastava et al., 2006; Wang et al., 2007]. While many studies [Wang et al., 2006; Liu et al., 2007] have reported much lower PC conversion and selectivity than that observed in the present study. It is also well known that the direct comparison of catalytic activity of catalytic reactions varying in terms of catalysts, raw materials and optimum operational parameters such as initial concentration, catalysts dose, etc. is not possible.

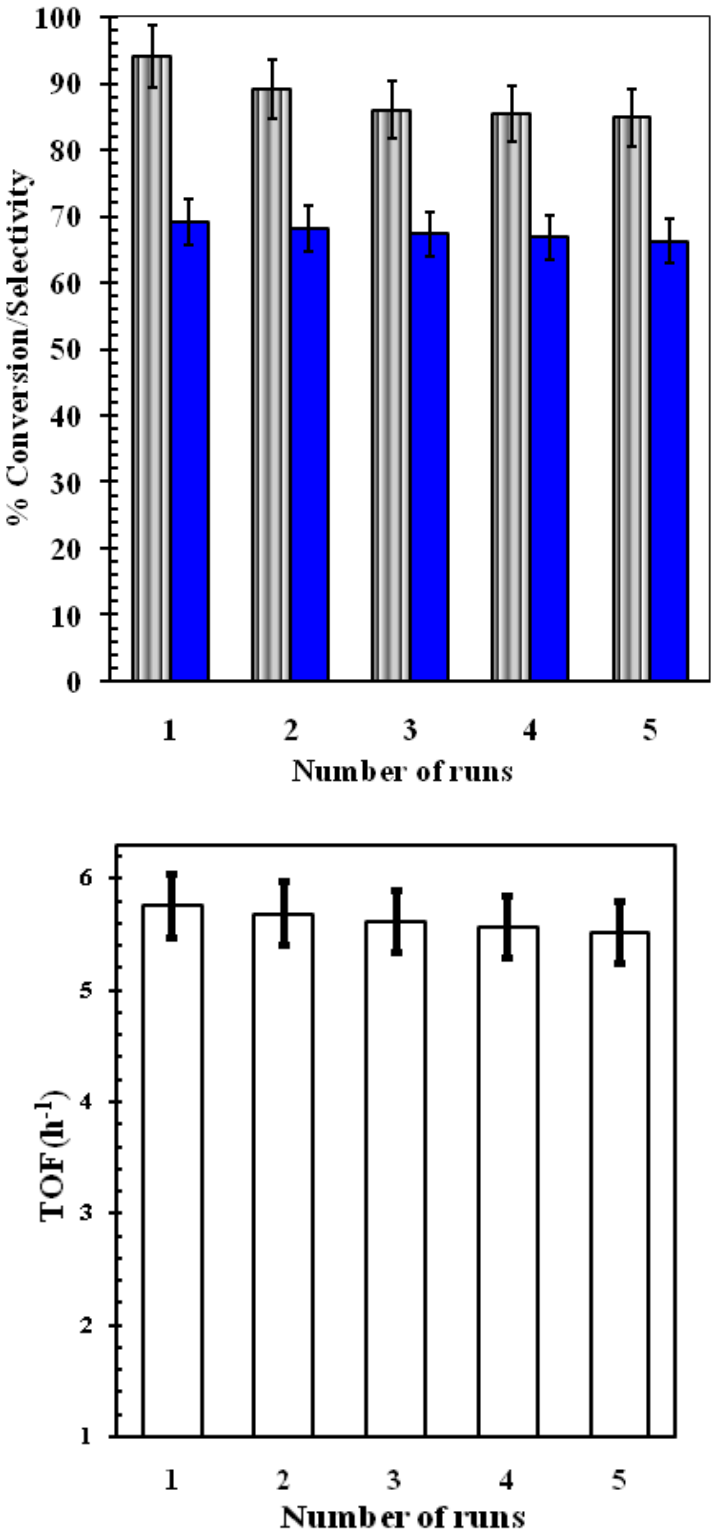

Figure 4.4.12. Conversion/Selectivity and TOF of CZA300 in a number of batch cycles: Reaction conditions: methanol/PC=10, catalyst dose: 3 wt.% of PC; reaction time=4 h temperature=160°C. % PC conversion, % DMC selectivity, ☐ TOF.

4.5. MECHANISM, KINETICS AND THERMODYNAMICS OF TRANSESTERIFICATION OF PC WITH METHANOL

4.5.1. Mechanism

Possible mechanism of synthesis of DMC from PC with methanol as produced by different investigators is shown in Figure 4.5.1 [Wei et al., 2003; Yang et al., 2010; Murugan and Bajaj, 2010; Wang et al., 2012; Xu et al., 2013]. Methanol gets activated in the presence of catalysts to form H^+ and CH_3O^-. CH_3O^- attracts the carbonyl C of the PC and forms CH_3O-CO-O-CH_2-CH (CH_3)-O^- as an intermediate which further reacts with H^+ to form 2-methyl-hydroxyethyl methyl carbonate (CH_3O-CO-O-CH_2-CH (CH_3)-OH) as an intermediate. This intermediate further reacts with CH_3O^- to form DMC and another intermediate, OH-CH_3-CH_2-CH_2-O^- which reacts with H^+ to form PG. The transesterification reaction of PC with methanol to produce DMC is exothermic in nature [Wei et al., 2003]. In this transesterification reaction, the main function of the solid catalyst is to assist in the abstraction of H^+ from methanol by the acid site so as to form CH_3O^-, which reacts with PC to produce DMC. Higher is the basic nature of the catalyst, more negative is the charge of MeO^- and lower is the free energy of reaction of MeO^- with PC.

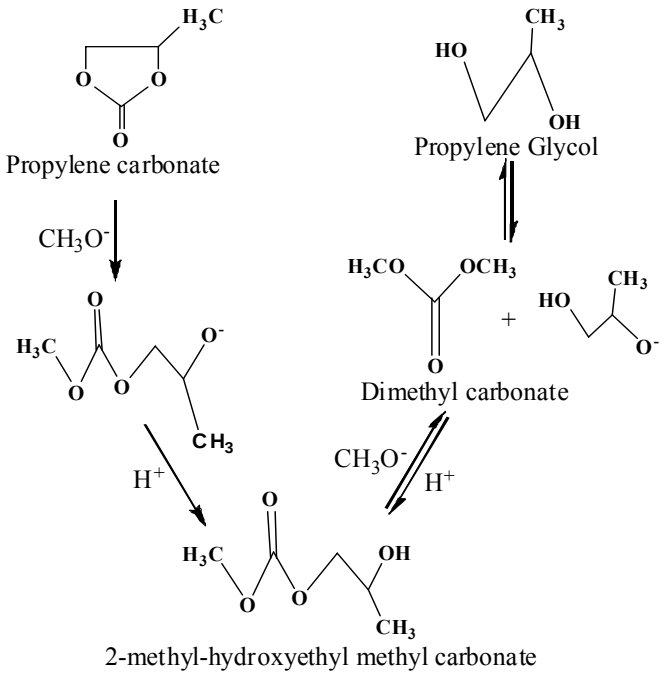

Figure 4.5.1. Mechanism of DMC formation from transesterification of PC with methanol [Wei et al., 2003].

4.5.2. Kinetic Study

Only few kinetics studies on the transesterification reaction of PC with methanol for DMC formation are reported in the literature [Jeong et al., 2005; Filippis et al., 2006; Williams et al., 2009]. In the present study, the following kinetic model, as proposed by Filippis et al. [2006], has been used for the kinetic analysis.

$$-\frac{dC_{PC,t}}{dt} = k'\left(C_{PC,t} - C_{PC,e}\right)\left(C_{MeOH,t} - C_{MeOH,e}\right) \tag{4.5.1}$$

where, $C_{MeOH,t}$ and $C_{PC,t}$ are the concentrations of methanol and PC at time t, respectively. $C_{MeOH,e}$ and $C_{PC,e}$ are the equilibrium concentration of methanol and PC, respectively. k' is the specific kinetic constant and t is the reaction time.

Considering that in the transesterification reaction, 2 moles of methanol (MeOH) react with 1 mole of PC, the actual concentration of methanol at any time during the reaction can be written as:

$$C_{MeOH,t} = C_{MeOH,o} - 2(C_{PC,o} - C_{PC,t}) \tag{4.5.2}$$

where, $C_{MeOH,o}$ and $C_{PC,o}$ are the initial concentration of methanol and PC, respectively. Using equitation (4.5.2) in equitation (4.5.1), we get

$$-\frac{dC_{PC,t}}{dt} = k'\left(C_{PC,t} - C_{PC,e}\right)\left[C_{MeOH,o} - 2(C_{PC,o} - C_{PC,t}) - C_{MeOH,e}\right] \tag{4.5.3}$$

Term $(C_{MeOH,o} - 2C_{PC,o} - C_{PC,e})$ constant, and therefore, the above equation can be written as:

$$\left[\frac{2dC_{PC,t}}{\left(M + 2C_{PC,t}\right)}\right] - \left[\frac{dC_{PC,t}}{\left(C_{PC,t} - C_{PC,e}\right)}\right] = k''dt \tag{4.5.4}$$

where, $M = (C_{MeOH,o} - 2C_{PC,o} - C_{PC,e})$ is constant, and $k'' = k'(M + 2C_{PC,e})$ (4.5.5)

Integration of the above and the substitution of M in accordance with its definition given the following equation:

$$\ln\left(\frac{(C_{MeOH,o} - C_{MeOH,e} - 2C_{PC,o} + 2C_{PC,t})(C_{PC,o} - C_{PC,e})}{(C_{MeOH,o} - C_{MeOH,e})(C_{PC,t} - C_{PC,e})}\right) = k''t \tag{4.5.6}$$

In the transesterification reaction, initial methanol concentration is kept high then the initial PC concentration i.e. $C_{MeOH,o}$ is much larger that $2(C_{PC,o}-C_{PC,t})$ and can be neglected. For CZA300 catalysts at 120°C, the ratio of $C_{MeOH,o}$ to $2(C_{PC,o}-C_{PC,t})$ at 2, 4 and 6 h was 22.81, 16.77 and 15.05, respectively. During the course of reaction there is no significant, change in $C_{MeOH,t}$, like for example, maximum 7.13% change in methanol concentration is observed for CZA300 catalysts at 120°C. Therefore, the above equation can be simplified as:

$$\ln\left(\frac{(C_{PC,o}-C_{PC,e})}{(C_{PC,t}-C_{PC,e})}\right)=k''t \qquad (4.5.7)$$

Values of k obtained by for CeCu and CZA300 catalysts are given in Table 4.5.1. For CeCu catalyst, the k values were found to be 0.105, 0.125 0.149 and 0.142 h^{-1} at 120, 140, 160 and 180°C, respectively. For CZA300 catalyst, the values of k were found to be 0.56, 0.58 and 0.65 h^{-1} at 120, 140 and 160°C, respectively. Jeong et al. [2005] have reported k value in the range of 0.1-0.165 h^{-1} at 120-140°C with methanol/PC molar ratio of 4 using quaternary ammonium salt as the catalyst. Similarly, Filippis et al. [2006] reported k values in the range of 0.22-1.068 h^{-1} for experiments carried out in the temperature range of 20-60°C with methanol/PC molar ratio of 8 using Na_3PO_4 as a catalyst. The values of k (h^{-1}) obtained in the present study are higher than those reported by Jeong et al. [2005] but lower than those reported by Filippis et al. [2006] lower temperature but with a different catalyst.

The rate constant (k) can be expressed mathematically as a function of temperature according to following Arrhenius equation:

$$k=k_o\exp\left(\frac{-E_a}{RT}\right) \qquad (4.5.8)$$

where, k_o is the frequency factor and E_a is the activation energy. Values of k_o and E_a were obtained from intercept and slope of plot of ln(k) versus (1/T), shown in Figure 4.5.2 and are given in Table 4.5.1. Zhang et al. [2012] calculated the values for E_a value of 31.29 kJ/mol using sodium ethoxide as catalyst.

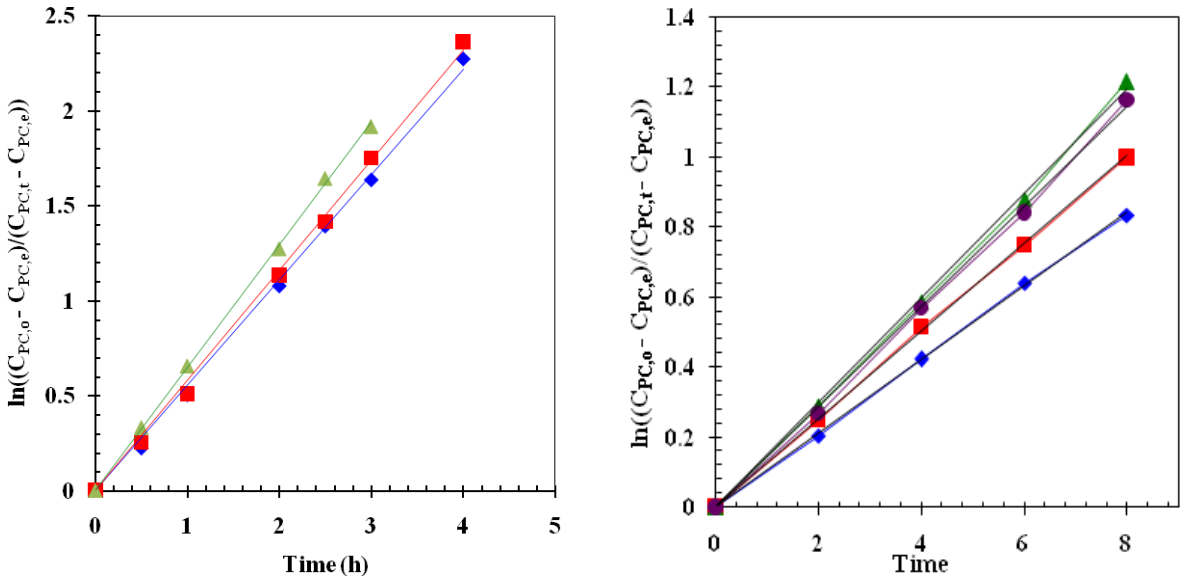

(a) (b)

Figure 4.5.2. (a) Rate of reaction for DMC synthesis using CZA300 catalyst at various temperature such as: 120°C, 140°C, 160°C; —◆— 120°C, —■— 140°C and —▲—160°C. (b) Rate of reaction for DMC synthesis using CeCu catalyst at various temperature such as: 120°C, 140°C, 160°C and 180°C; —◆— 120°C, —■— 140°C, —▲—160°C and —●— 180°C.

Table 4.5.1. Value of kinetic constant (k) at different temperatures for CeCu and CZA300 catalyst.

Catalyst	Temperature (°C)	k (h^{-1})	k_o and E_a
CeCu	120	0.105	k_o = 0.375 h^{-1}
CeCu	140	0.125	E_a= 2.294 kJ/mol
CeCu	160	0.149	
CeCu	180	0.142	
CZA300	120	0.56	k_o = 0.225 h^{-1}
CZA300	140	0.58	E_a= 12.72 kJ/mol
CZA300	160	0.65	

*k from equitation 4.5.6 to similarly k_o and E_a values too.

4.5.2. Thermodynamics Study

For liquid phase reactions, equilibrium constant (K_{eq}) can be written as [Sandler, 2006]:

$$K_{eq} = \prod_i (a_i)^{\nu_i} = \prod_i (x_i \gamma_i)^{\nu_i} \tag{4.5.9}$$

where, a_i is the activity, γ_i is the activity coefficient, x_i is the mole fraction, and υ_i the stoichiometric coefficient of various species at equilibrium. For the transesterification reaction of PC with methanol for the formation of DMC, the above equation can be written as:

$$K_{eq} = K_x K_\gamma = \left(\frac{x_{PG} x_{DMC}}{x_{PC} x_{MeOH}^2} \right) \left(\frac{\gamma_{PG} \gamma_{DMC}}{\gamma_{PC} \gamma_{MeOH}^2} \right) \tag{4.5.10}$$

Non-idealities in the liquid phase can be accounted for by the interaction between different molecules. The activity coefficient (γ_i) can be calculated using the (UNIversal QUAsi-Chemical) UNIQUAC equation g^E-model [Abrams and Prausnitz, 1975].

This model required van der Waals properties namely the area parameter (q_i) and the volume parameter (r_i) for the molecules participating in the reaction, and these may be used to describe the shape of the molecules. The pure-component parameters can be obtained from the literature, and are summarized in Table 4.5.2.

A binary interaction coefficient (τ_{ij}), which describes the interaction between components i and j, is used to quantify the effect of temperature on the activity coefficient in the UNIQUAC g^E-model. This binary interaction coefficient (τ_{ij}) is defined as [Holtbruegge et al., 2013]:

$$\tau_{ij} = \exp\left(a_{ij} + \frac{b_{ij}}{T} \right) \tag{4.5.11}$$

The two parameters a_{ij} and b_{ij} required to calculate τ_{ij} for each binary system are taken from the literature, and are given in Table 4.5.3 [Holtbruegge et al., 2013].

Equations 4.5.10 and 4.5.11; and equations of the UNIQUAC g^E-model were solved simultaneously using the parameters given in the Tables 4.5.2 and 4.5.3 to calculate the values of K_{eq} at various temperatures and pressures for different catalysts used in the present

work. Values of K_{eq} along with the operating conditions for CeCu and CZA300 catalysts are given in Table 4.5.4.

K_{eq} can be related to the temperature (T) by the classical van't Hoff equation:

$$\ln K_{eq,T} = -\frac{\Delta H_r^o}{RT} + \left(\frac{\Delta H_r^o - \Delta G_r^o}{RT^o} \right) \qquad (4.10.16)$$

The values of ΔH_r^o and ΔG_r^o for CeCu using the data points were found to be 69.99 kJ/mol and 36.96 kJ/mol, respectively. Similarly, for CZA300, the respective values were found to be 89.367 kJ/mol and 38.596 kJ/mol, respectively.

Table 4.5.2. Pure-component area parameter (q_i) and the volume parameter (r_i) of UNIQUAC g^E-model.

Component	q_i	r_i	Reference
PC	2.736	3.281	Gmehling et al., 1982b
MeOH	1.432	1.431	Gmehling et al., 1982a
DMC	2.816	3.061	Gmehling and Onken, 2007
PG	2.784	3.282	Gmehling et al., 1982a

Table 4.5.3. Binary interaction parameters a_{ij} and b_{ij} used in the UNIQUAC g^E-model.

Component 1	Component 2	i	j	a_{ij}	b_{ij} (K)	Reference
MeOH	PC	1	2	0.000	-42.880	Shi et al., 1999
		2	1	0.000	90.698	
DMC	PC	1	2	0.000	-209.935	Luo et al., 2001
		2	1	0.000	-2.664	
DMC	PC	1	2	0.000	-110.727	Luo et al., 2001
		2	1	0.000	41.865	
MeOH	DMC	1	2	-0.201	14.870	Rodríguez et al., 2002
		2	1	0.273	-306.550	
PG	PC	1	2	1.494	-958.829	Mathuni et al., 2011
		2	1	-1.418	674.112	
MeOH	PC	1	2	0.000	-38.031	Holtbruegge et al., 2013
		2	1	0.000	-205.152	

Table 4.5.4. Values of K_{eq} for the formation of DMC synthesis by transesterification reaction using CeCu and CZA300 catalysts at different temperatures.

T(K)	Selectivity (%)	PC Conversion (%)	x_{PC}	x_{MeOH}	x_{DMC}	x_{PG}	K_{eq} (l/mol)
CeCu							
393	75	48	0.051793	0.900398	0.035857	0.011952	0.001622
413	82.46154	65	0.036082	0.896907	0.055258	0.011753	0.004181
433	92.35837	75.9	0.025417	0.894537	0.073930	0.006117	0.004666
453	76.87943	70.5	0.030761	0.895725	0.056517	0.016997	0.008269
CZA300							
393	81	32	0.065637	0.903475	0.025019	0.005869	0.001103
413	87	37	0.061404	0.902534	0.031374	0.004688	0.002057
423	90	58	0.042683	0.898374	0.053049	0.005894	0.010235
433	94	70	0.03125	0.895833	0.068542	0.004375	0.026059
453	86	70.1	0.031152	0.895812	0.062811	0.010225	0.025739

It may be seen from Table 4.5.4 that the value of K_{eq} increases as the reaction temperature is increases from 393 K to 453 K. This means that the synthesis of DMC by transesterification reaction should be carried out at higher temperature.

4.5.4. Comparative Analysis

Table 4.5.5 compares various textural and acidic-basic properties and the catalytic activity of various catalyst used in the present study for the transesterification reaction of the PC with methanol for DMC synthesis. For different sets of catalysts (prepared by different methods), catalyst showing greater basic-acidic properties and higher surface area (with exception of $Ce_{0.2}$-$La_{0.8}$) showed higher PC conversion and DMC yield and TOF. Among all the catalysts, Cu-Zn-Al@300 showed highest basicity and acidity, however, its surface area was lower than that of Ce-Zn/SiO_2 catalyst. Among all the catalysts tested, Ce-Zn/SiO_2 showed highest PC conversion of 89% and DMC yield 78%. Overall supported catalysts

seem to be better option for use in the transesterification reaction of PC with methanol for DMC synthesis.

A number of previous investigators have shown the importance of basicity in the transesterification reactions. Juarez et al. [2009] used a series of metal oxide nanoparticles, namely MgO, ZrO_2, CeO_2 and Au/CeO_2 (1.5 wt.%) with acid or basic properties, exhibiting low to moderate activity towards the transesterification of PC with methanol. They reported that the strongly basic MgO increases the conversion of PC. ZrO_2, which is an acid metal oxide, showed low PC hydrolysis with better selectivity towards DMC. CeO_2 exhibited intermediate activity and selectivity towards DMC formation. Yield with CeO_2 was much better than MgO and ZrO_2 (in that order). Gold nanoparticles supported on nanocrystalline ceria (Au/CeO_2) exhibited much higher PC conversion better DMC selectivity with higher DMC yield than those with CeO_2.

Wang et al. [2011] used zinc-yttrium based catalysts used for the DMC via transesterification of ethyl carbonate (EC) with methanol. The yield of the DMC was well correlated with the BET surface area and the basicity of the catalysts. Cui et al. [2013] studied the synthesis of DMC through the transesterification of EC using MgO and mesoporous silica coated MgO ($MgO\text{-}SiO_2$) catalyst. BET surface area of $MgO\text{-}SiO_2$ (412.6 m^2/g) was much larger than that of the pure flower-like MgO (141.4 m^2/g). With MgO, EC conversion in the first run was 92% which dropped sharply to 52% in the second run because of the stability issues. For $MgO\text{-}SiO_2$, EC conversion was constantly over 80% for 10 consecutive runs. These authors didn't report basicity so it was not possible to correlate the results with basicity.

Xu et al. [2013] investigated various CeO_2-based catalysts (with different surface areas and basicity) for transesterification of EC with methanol for DMC synthesis. Catalyst CeO_2-meso-400 (182 m^2/g BET surface area and 212 µmol CO_2/g) had high surface area and high basicty as compared to CeO_2-meso-500 (149 m^2/g BET surface area and 178 µmol CO_2/g) and CeO_2-meso-600 (108 m^2/g BET surface area and 141 µmol CO_2/g). The highest

activity was observed with CeO_2-meso-400 with DMC yield of 73.3% as compared to CeO_2-meso-500 (63.8%) and CeO_2-meso-600 (57.1%). Therefore, it can be seen that the basicity and the BET surface area of the catalysts play an important role during the transesterification reactions for the formation of DMC. The catalytic activity of the supported catalyst depends upon the characterization of the support. The XRD patterns, CO_2-TPD, SEM and BET surface area provide interesting information about the synthesized catalysts with different supports that are used for the catalysts for the transesterification of PC with methanol to produce DMC.

Table 4.5.5. Comparative analysis of properties and catalytic activity of various catalysts used for transesterification reaction of PC with methanol for the production of DMC.

Catalyst	**Method of Preparation**	**Textural Properties**			**CO_2 & NH_3-TPD**		**% DMC Yield**	**TOF (h^{-1})**	**% PC Conversion**
		Surface Area (m^2/g)	Pore volume (cm^3/g)	Pore size (nm)	Total CO_2 adsorption (mmol/g)	Total NH_3 adsorption (mmol/g)			
Ce-Co	SG	40	0.078	4.47	0.083	-	16.1	1.097	21.8
Ce-Cu	SG	46	0.065	5.85	0.698	-	71.9	3.192	65.4
Ce-Zn	SG	34	0.046	6.76	0.424	-	45.2	2.47	49.1
Ce-Fe	SG	38	0.051	4.35	0.492	-	52.1	2.91	57.8
$Ce_{0.2}$-$La_{0.8}$	CP	41	0.061	5.82	2.61	7.53	74	3.72	74
$Ce_{0.4}$-$La_{0.6}$	CP	42	0.080	6.67	0.81	5.85	59	3.37	67
$Ce_{0.6}$-$La_{0.4}$	CP	60	0.103	5.97	0.70	4.18	49	2.97	59
$Ce_{0.8}$-$La_{0.2}$	CP	62	0.128	6.57	0.45	2.71	36	2.16	43
Ce-Zn/Al_2O_3	DCP	77	0.150	7.5	1.037	0.807	67	2.62	78
Ce-Zn/SiO_2	DCP	104	0.187	6.3	2.821	1.288	78	2.92	89
Ce-Zn/TiO_2	DCP	61	0.108	6.4	0.713	0.344	21	1.14	34
Cu-Zn-Al @300	CP	76	0.1086	5.56	4.615	6.658	66.8	5.92	71
Cu-Zn-Al @500	CP	84	0.1076	5.25	2.733	3.123	59.8	5.66	68
Cu-Zn-Al @800	CP	14	0.0178	4.93	0.9812	1.255	18	1.50	18

SG: Sol-gel; CP: Co-precipitation; DCP: Deposition-coprecipitation.

Part [B]. DMC SYNTHESIS USING DIRECT CONVERSION OF CO_2 WITH METHANOL

The synthesis of DMC from direct conversion of CO_2 with methanol was carried out using with four different sets of the catalysts namely: ceria-zirconium prepared by hydrothermal method, ceria-zirconium with carbon template method, CeO_2-MnO_2 by surfactant template method and ceria-calcium by surfactant template method. These catalysts were prepared as per procedure discussed in chapter III. These catalysts were characterized by various techniques, and were tested for the production of DMC.

4.6. CERIA-ZIRCONIUM OXIDES CATALYSTS: CHARACTERIZATION AND CATALYTIC ACTIVITY FOR DIRECT CONVERSION OF CO_2 TO DIMETHYL CARBONATE

In the present work, the synthesis of DMC from direct conversion of CO_2 with methanol was studied using ceria, zirconia and ceria-zirconia catalysts prepared by hydrothermal method. The catalysts were characterized by liquid nitrogen-sorption, XRD, AFM, SEM, and TEM. Acidity and basicity of the catalysts was investigated by NH_3- and CO_2-TPD methods. The effect of the reaction conditions such as catalysts dose, reaction temperature, reaction time the use of the catalysts in a number of cycles was studied using the best performing catalyst.

4.6.1. Catalysts Characterization

4.6.1.1. X-ray diffraction

The XRD profiles of CeO_2, $Ce_{0.5}Zr_{0.5}O_2$ and ZrO_2 catalysts are presented in Figure 4.6.1. The XRD pattern of CeO_2 catalysts shows the reflexes of cubic phase (JPDS File No. 01-074-1145) with space group Fm3m (225), ZrO_2 catalysts show reflexes of tetragonal phase (JPDS File No. 01-080-2155) with space group P42/nmc (137) and $Ce_{0.5}Zr_{0.5}O_2$ reflexes show tetragonal phase (JPDS File No. 00-038-1436) with space group P42/nmc (137). Only pure phases were found in CeO_2 and ZrO_2. $Ce_{0.5}Zr_{0.5}O_2$ catalysts showed the presence of $Ce_{0.5}Zr_{0.5}O_2$ (JPDS File No. 00-038-1436). XRD reflexes get shifted in the mixed solid

solution due to difference in the ionic radii of Ce^{4+} (0.097 nm) and Zr^{4+} (0.084 nm). Average crystallite sizes of CeO_2, ZrO_2 and $Ce_{0.5}Zr_{0.5}O_2$ were determined from the most intensive reflex at 2θ=28.5°, 30.2° and 29.2°, respectively [Dave and Pant, 2011]. Average crystallite sizes of the CeO_2, $Ce_{0.5}Zr_{0.5}O_2$ and ZrO_2 catalysts were found to be 9.48, 7.09 and 9.45 nm, respectively. Additionally, a TEM image of the $Ce_{0.5}Zr_{0.5}O_2$ catalyst shows spherical particles in the range of 7-12 nm. SAED indexing pattern confirms the presence of the crystalline phases identified using XRD of $Ce_{0.5}Zr_{0.5}O_2$. Several investigators have reported similar diffraction patterns for CeO_2, ZrO_2 and $Ce_{0.5}Zr_{0.5}O_2$. Chen et al. [2014] reported the cubic phase of CeO_2 and tetragonal phase of ZrO_2, whereas Zhang et al. [2009] reported both cubic and tetragonal phases in $Ce_{0.5}Zr_{0.5}O_2$ with average crystallite size of 2.6 nm. Fuentes and Baker [2009] reported both cubic and tetragonal phases of $Ce_{0.5}Zr_{0.5}O_2$ having P42/nmc space group with average crystallite size of 5.27 nm. Similarly, Si et al. [2007] reported average crystallite size of 5.34 nm with cubic and tetragonal mixed phase of $Ce_{0.5}Zr_{0.5}O_2$. In the present study, the Ce/Zr molar ratios in the $Ce_{0.5}Zr_{0.5}O_2$ mixed oxides catalyst were determined by ICP-OES analysis from which the chemical formula of the catalyst was calculated to be $Ce_{0.52}Zr_{0.48}O_2$.

4.6.1.2. Morphology

The SEM micrographs of CeO_2, $Ce_{0.5}Zr_{0.5}O_2$ and ZrO_2 catalysts are shown in Figure 4.6.2. All the catalysts show spherical morphology. Average particle size of the all the catalysts, as determined from FE-SEM was found to be in the range of 5-10 nm. ZrO_2 is of smaller size as compared to $Ce_{0.5}Zr_{0.5}O_2$ catalyst (Figure 4.6.2.). The surface morphology was further investigated by AFM. AFM (1D and 3D) images along with the grain size distribution of the $Ce_{0.5}Zr_{0.5}O_2$ catalyst is shown in Figure 4.6.3. Average grain size was found to be ~4.5 nm. Surface roughness value obtained from the AFM analysis was 0.945 nm.

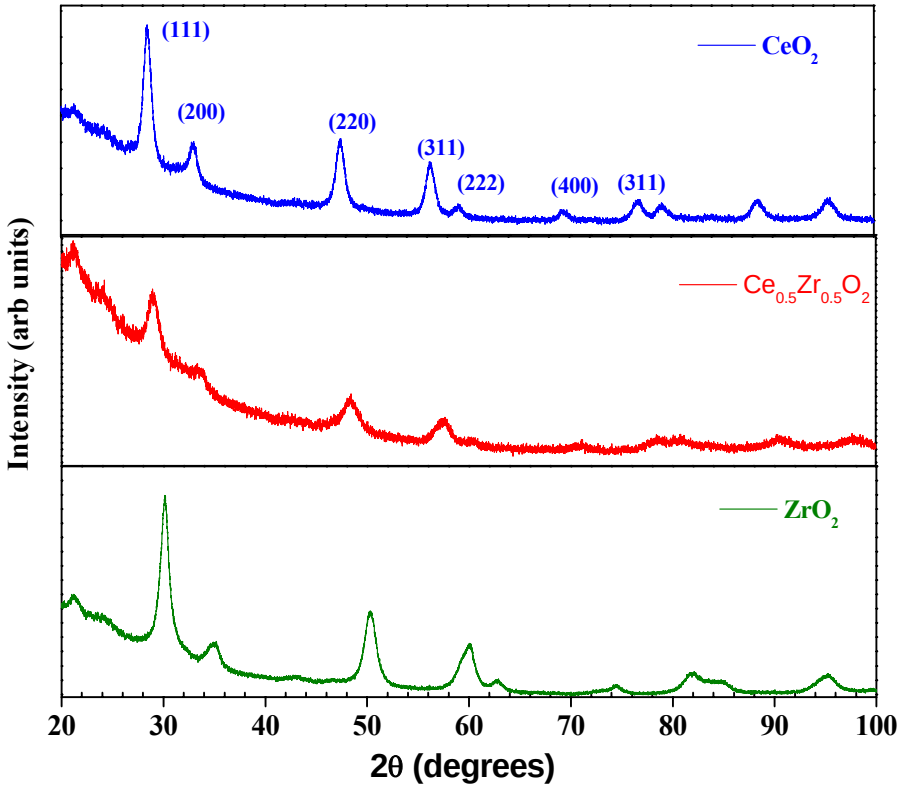

(a)

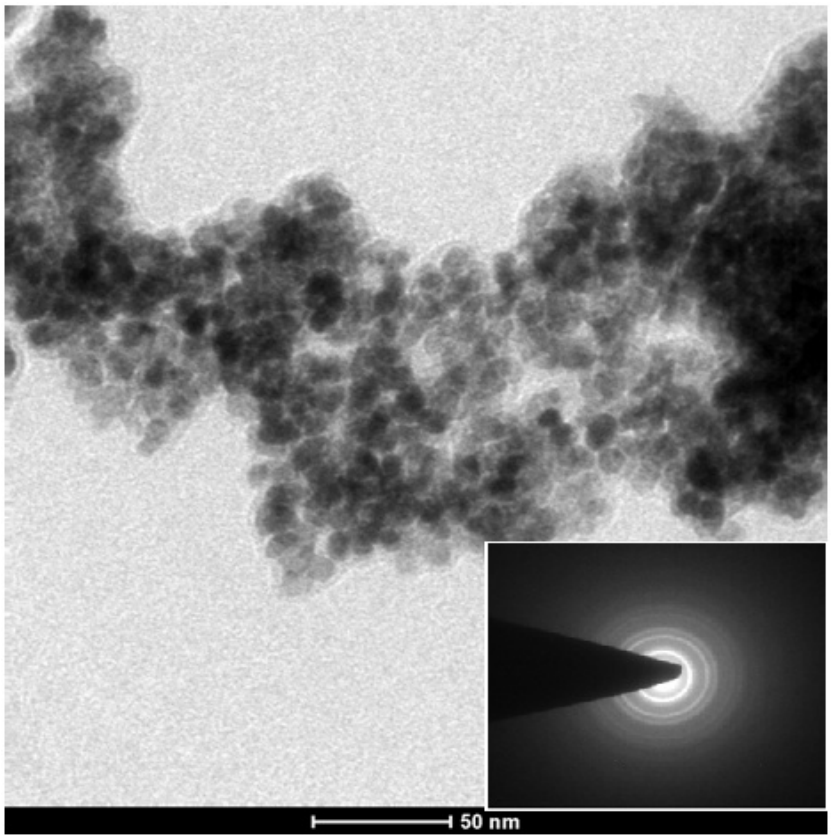

(b)

Figure 4.6.1. (a) XRD pattern of CeO_2, $Ce_{0.5}Zr_{0.5}O_2$ and ZrO_2 catalysts and; (b) TEM image of $Ce_{0.5}Zr_{0.5}O_2$ catalyst with SEAD patterns.

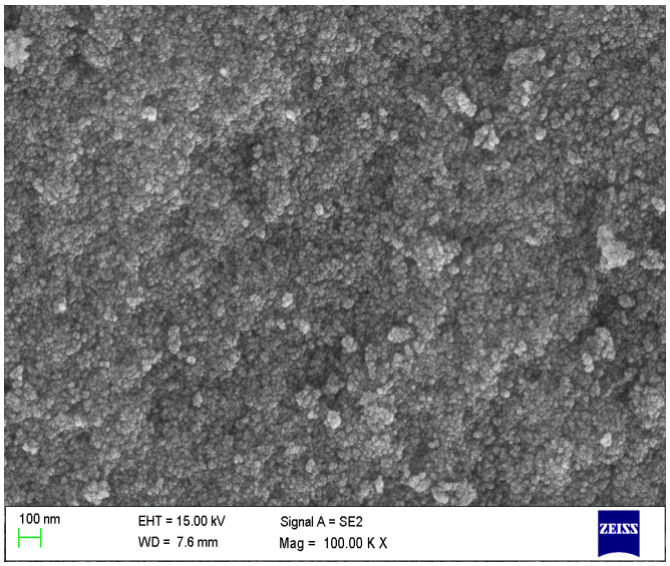

CeO_2

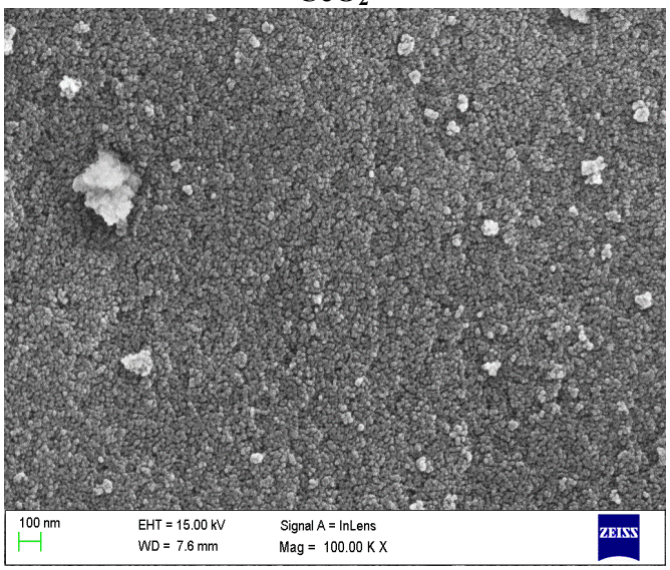

ZrO_2

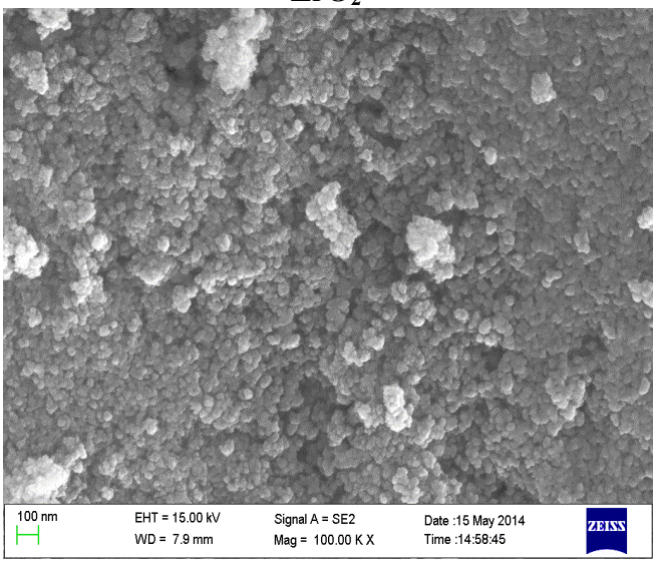

$Ce_{0.5}Zr_{0.5}O_2$

Figure 4.6.2. SEM micrographs of CeO_2, ZrO_2 and $Ce_{0.5}Zr_{0.5}O_2$ catalysts.

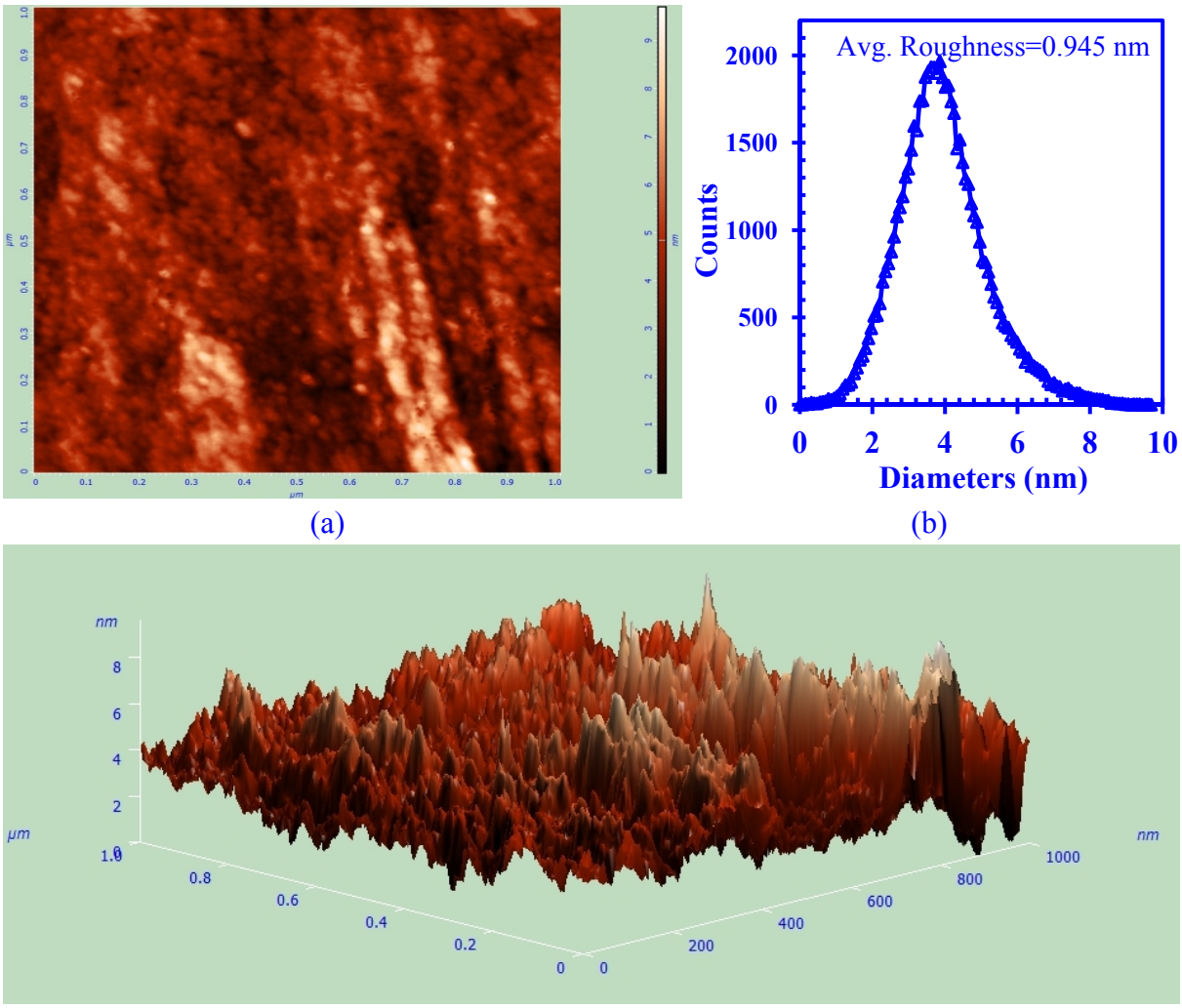

Figure 4.6.3. AFM micrographs (a) AFM 1D image of $CeZrO_2$ catalyst, (b) AFM roughness histogram, (c) AFM 3D micrograph of $CeZrO_2$ catalyst.

4.6.1.3. Textural properties

Pore surface area of the catalysts was calculated using BET model and pore size and pore volume was calculated by BJH model. N_2 adsorption-desorption isotherm and pore size distribution are shown in Figure 4.6.4. Textural data of the catalysts are given in Table 4.6.2. BET surface area of CeO_2, $Ce_{0.5}Zr_{0.5}O_2$ and ZrO_2 were found to be 88, 117 and 70 m^2/g, respectively, BJH desorption pore volume and the average pore diameter was in the range of 0.12-0.237 cm^3/g and 5-8.41 nm, respectively. $Ce_{0.5}Zr_{0.5}O_2$ catalyst was found to possess the highest surface area, specific pore volume and average pore diameter among all the catalysts. All catalysts showed type VI isotherms according to IUPAC classification: CeO_2 catalyst shows H_2 hysteresis loop, $Ce_{0.5}Zr_{0.5}O_2$ shows H_1 hysteresis loop and ZrO_2 catalyst shows H_2

hysteresis loop in the relative pressure (P/P_o) range of 0.4−0.95 which are characteristic of mesoporous materials [Preising et al., 2007; Kraiwattanawong et al., 2009; Wang et al., 2010; Ouyang et al., 2014]. Various researchers have reported BET surface area of $Ce_{0.5}Zr_{0.5}O_2$ catalysts in the range of 5-134 m^2/g [Zhang et al., 2009; Lee et al., 2012; Wang et al., 2013; Ouyang et al., 2014; Patel et al., 2013]. The $Ce_{0.5}Zr_{0.5}O_2$ catalyst in the present study, show its BET surface area in the higher side of the above range.

4.6.1.4. CO_2–TPD

Basic properties of the CeO_2, $Ce_{0.5}Zr_{0.5}O_2$ and ZrO_2 catalysts were characterized by CO_2-TPD experiments. The results are shows in Figure 4.6.5a. Basic properties of the catalysts depend upon the temperature profile in weak, moderate and strong range: < 200°C, 200−450°C, > 450°C, respectively [Priya et al., 2014a]. Since CeO_2, $Ce_{0.5}Zr_{0.5}O_2$ and ZrO_2 catalysts show main peaks in the range of 78−117°C, they contain predominantly week basic sites as shown in Figure 4.6.5a. Basic site density (per unit mass of catalysts) of the catalysts was in the order: ZrO_2 (0.2512 mmol/g) < CeO_2 (0.4154 mmol/g) < $Ce_{0.5}Zr_{0.5}O_2$ (0.6487 mmol/g). The basic site density per unit area also follows the same order (Table 4.6.2). Thus, the mixed metal oxides are found have similar basic site density as these by single oxide catalysts. Zheng et al. [2009] and Lee et al. [2012] reported maximum basic site density (per unit mass of catalysts) of 0.276 and 0.017 mmol/g, respectively, for $Ce_{0.6}Zr_{0.4}O_2$ catalysts.

4.6.1.5. NH_3–TPD

Acidic properties of CeO_2, $Ce_{0.5}Zr_{0.5}O_2$ and ZrO_2 catalysts were investigated using NH_3-TPD. NH_3 desorption peaks were found to be in the temperature region of 50-550°C Figure 4.6.5b. All the catalysts was found to contain only week acidic sites. Total desorbed amount of NH_3 was found to be in the following order: $Ce_{0.5}Zr_{0.5}O_2$ > CeO_2 > ZrO_2. The acidic site density (per unit mass) of synthesized catalysts was in the order: ZrO_2 (0.511 mmol/g) < CeO_2 (0.793 mmol/g) < $Ce_{0.5}Zr_{0.5}O_2$ (1.893 mmol/g). Respective value of acid site density (per unit area) were: ZrO_2 (7.3 $mmol/m^2$) < CeO_2 (9.012 $mmol/m^2$) < $Ce_{0.5}Zr_{0.5}O_2$ (16.18 $mmol/m^2$).

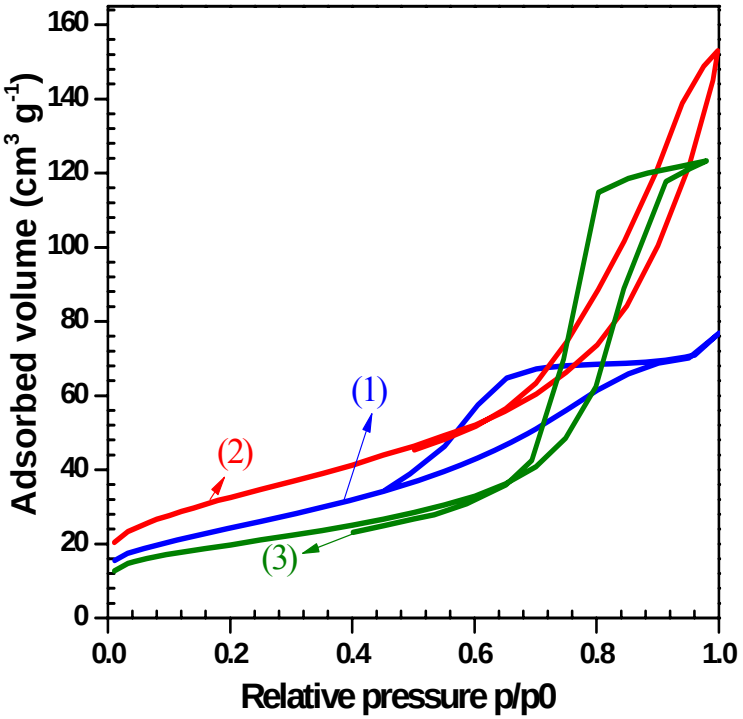

(a)

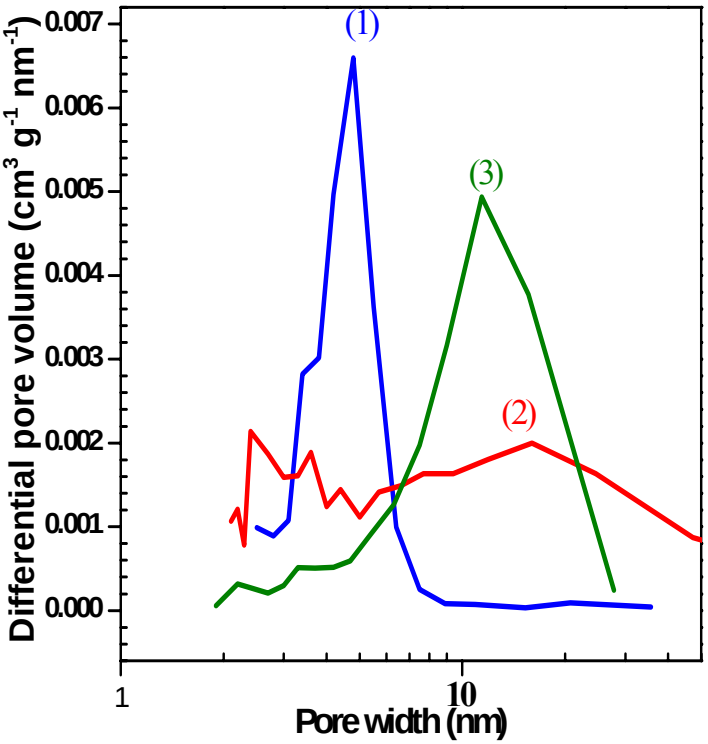

(b)

Figure 4.6.4. (a) Nitrogen adsorption-desorption isotherms, (b) Variation of pore volume and pore area with pore diameter of CeO_2, $Ce_{0.5}Zr_{0.5}O_2$ and ZrO_2 catalysts. (1) CeO_2, (2) $Ce_{0.5}Zr_{0.5}O_2$, (3) ZrO_2.

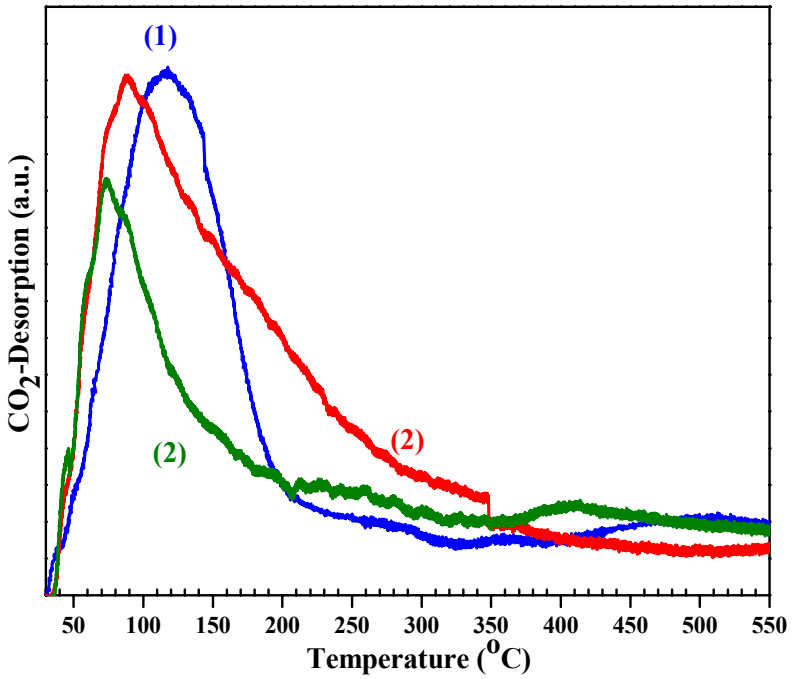

(a)

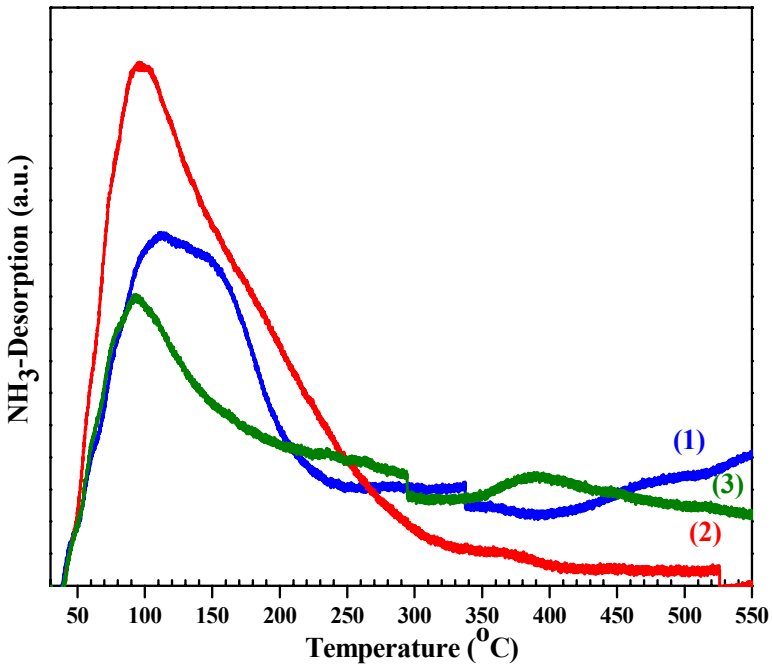

(b)

Figure 4.6.5. (a) CO_2-TPD and (b) NH_3-TPD of CeO_2, $Ce_{0.5}Zr_{0.5}O_2$ and ZrO_2 catalysts; (1) CeO_2, (2) $Ce_{0.5}Zr_{0.5}O_2$, (3) ZrO_2.

Thus, $Ce_{0.5}Zr_{0.5}O_2$ was found to have the highest acidic site density and ZrO_2 was found to have the lowest acidic site density in the catalyst. Lee et al. [2012] reported much lower NH_3 desorption of 0.0857 mmol/g for $Ce_{0.6}Zr_{0.4}O_2$ catalyst. It may be seen that the $Ce_{0.5}Zr_{0.5}O_2$ catalyst has highest surface area, acidic and basic site density (per unit mass/per unit area) as compared to other CeO_2 and ZrO_2 catalysts. Prepared $Ce_{0.5}Zr_{0.5}O_2$ catalyst possess both basic and acidic sites indicating that it can act as a base-acid bi-functional catalyst. It has been suggested both acidic and basic sites are required for direct conversion of CO_2 with methanol to produce DMC [Zhang et al., 2009; Lee et al., 2012; Chen et al., 2014].

Table 4.6.1. Characterization of CeO_2, $Ce_{0.5}Zr_{0.5}O_2$ and ZrO_2 catalysts.

Catalysts Properties	CeO_2	$Ce_{0.5}Zr_{0.5}O_2$	ZrO_2
Crystallite size (nm)[a]	9.48	7.09	9.45
Lattice constant d (nm)[a]	0.3124	0.3051	0.2950
BET surface area (m^2/g)	88	117	70
Specific pore volume (cm^3/g)[b]	0.12	0.237	0.202
Average Pore diameter (nm)[c]	5	8.41	7.89
CO_2 adsorption (mmol/g)[d]	0.4154 (117)	0.6487 (88)	0.2512 (78)
Basic site density ($\mu mol/m^2$) [d]	4.721	5.550	3.588
NH_3 adsorption (mmol/g)[e]	0.793 (110)	1.893 (96)	0.511 (93)
Acidic site density ($\mu mol/m^2$)[e]	9.012	16.18	7.3

[a]The unit cell parameter, crystal size and structure is calculated applying the Scherrer equation.

[b]BJH desorption cumulative pore volume of pores in the range 17 to 3000 Å.

[c]BJH desorption average pore diameter.

[d]CO_2-TPD for basicity and basic site and temperature (°C) at maxima is given in brackets.

[e]NH_3-TPD for acidity and acidic site and temperature (°C) at maxima is given in brackets.

4.6.2. Catalytic Activity of Catalysts for DMC Formation using CO_2

Direct conversion of CO_2 with methanol to form DMC was investigated under different conditions over CeO_2, ZrO_2 and $Ce_{0.5}Zr_{0.5}O_2$ catalysts. Non-catalytic conversion of CO_2 and methanol into DMC in 24 h was insignificant. The results are presented in Figure 4.6.6a. The activity of the catalysts was in the order $ZO_2 < CeO_2 < Ce_{0.5}Zr_{0.5}O_2$. The catalyst $Ce_{0.5}Zr_{0.5}O_2$ showed maximum formation of DMC (2.670 mmol DMC/g cat) in comparison to 0.456 mmol DMC/g cat by ZrO_2. The relationship between acidic-basic properties and the catalyst activity is shown in Figure 4.6.6b. ZrO_2 and CeO_2 have lower number of acidic and basic sites as compared to $Ce_{0.5}Zr_{0.5}O_2$. The DMC yield is found to depend directly upon the acidic-basic properties of the catalysts. Based on the preliminary test, $Ce_{0.5}Zr_{0.5}O_2$ catalyst was further used to study the effects of the reaction conditions such as amount of catalyst, reaction time and reaction temperature for the direct conversion of CO_2 and methanol to produce DMC.

4.6.2.1. Effect of operating parameters

The effect of reaction time was studied in the range of 6-48 h with all other conditions being constant. It can be seen from Figure 4.6.7a that an increase in the reaction time from 6 to 24 h increased the yield of DMC from 1.49 mmol/g cat to 2.67 mmol/g cat. After 24 h, the DMC yield remained constant, thus the optimum DMC yield was obtained after 24 h.The saturation of molecular sieve for the adsorption of water may be the reasons. The influence of catalysts dose was studied in the range of 0.62-2.19 g and the results are shown in Figure 4.6.7b. With an increase in the catalyst amount from 0.6-1.25 g, the DMC yield increased from 1.71 to 2.68 mmol/g cat. Thereafter, the DMC yield decreased with an increase in the catalyst amount from 1.86 to 2.19 g. Maximum DMC yield was found with 1.25 g of catalyst. The effect of reaction temperature was studied in the temperature range of 120-180°C (Figure 4.6.7(c)). It can be seen that an increase in the reaction temperature from 100 to 120°C increased the DMC yield from 1.249 to 2.682 mmol/g cat. With a further increase in temperature, the DMC yield decreased with the DMC yield being 0.129 mmol/g cat at 180°C.

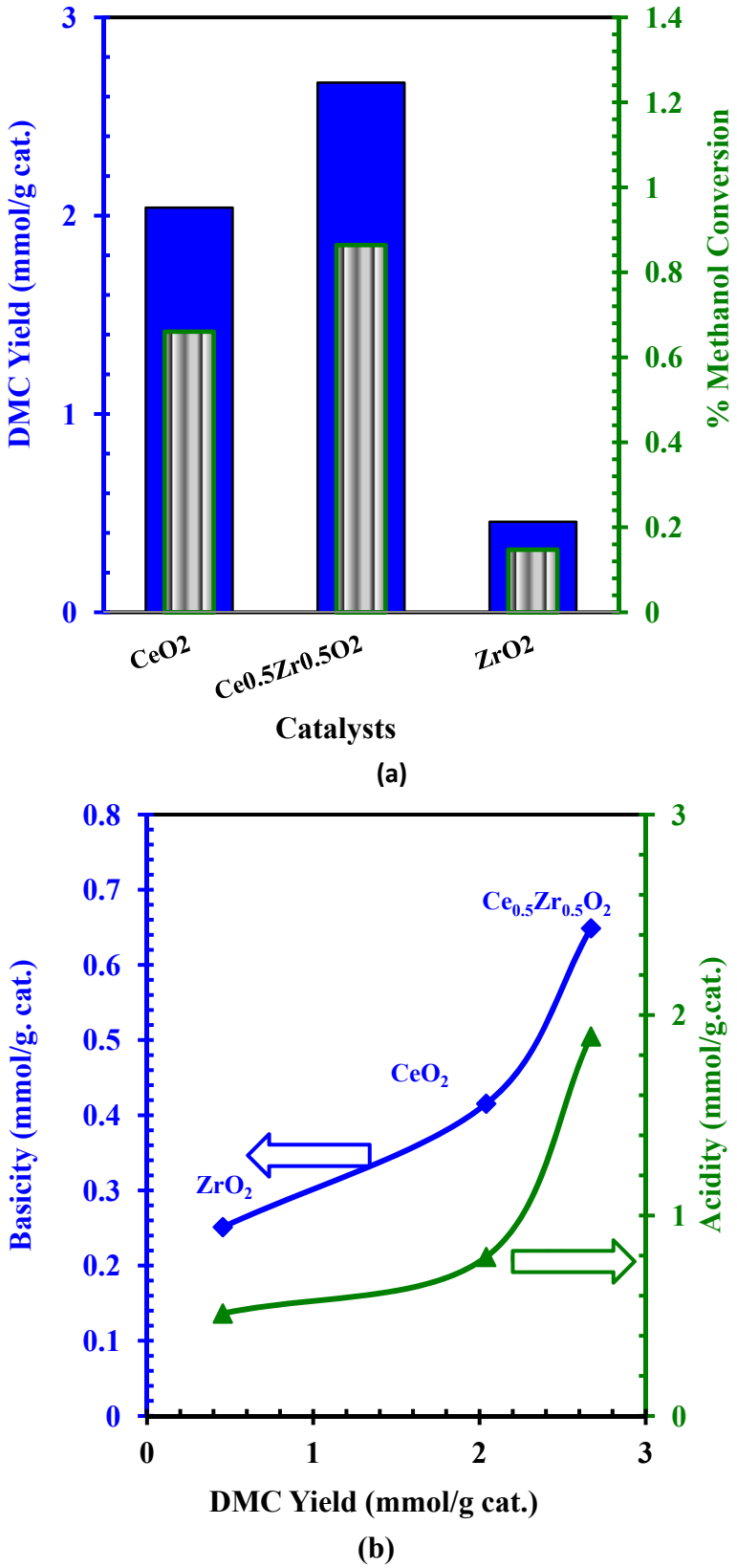

Figure 4.6.6. (a) Conversion of methanol and DMC yield over CeO_2, $Ce_{0.5}Zr_{0.5}O_2$ and ZrO_2 catalysts, ▬ DMC Yield (mmol/g cat.), ▮▮▮ % Methanol conversion. (b) Correlation between acidic-basic and catalytic activity of CeO_2, $Ce_{0.5}Zr_{0.5}O_2$ and ZrO_2 catalysts; Reaction conditions: (Methanol=25.03 mL, catalyst dose=1.25 g, P=150 bar, T=120°C, t=24 h); —♦— Basicity, —▲— Acidity.

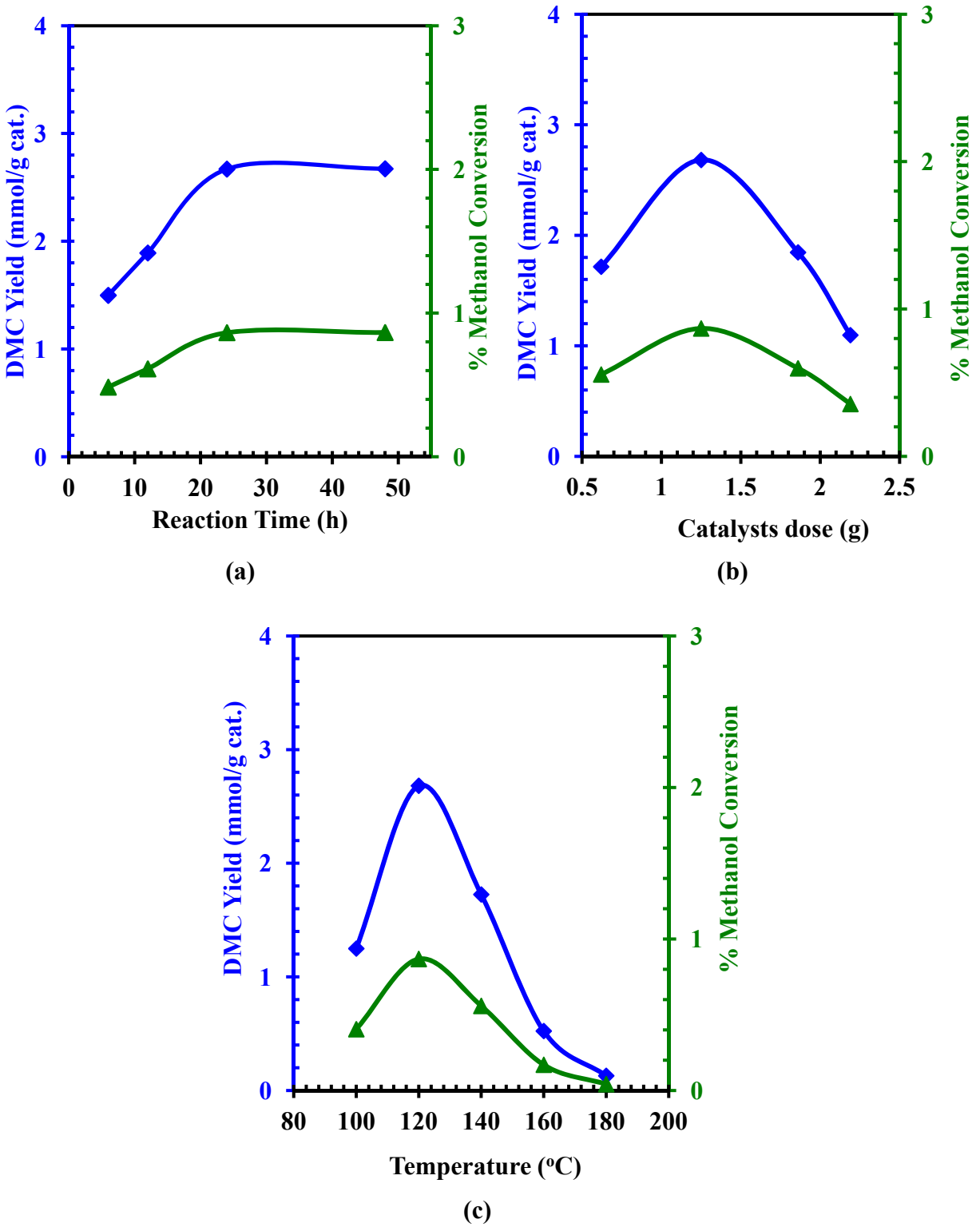

Figure 4.6.7. Effect of various parameters on the direct conversion of CO_2 with methanol for DMC synthesis. (a) effect of reaction time at Methanol=25.03 mL, catalyst dose=1.25 g, P=150 bar, T=120°C, (b) effect of catalyst dose at Methanol=25.03 mL, P=150 bar, T=120°C, t=24 h, (c) effect of temperature at Methanol=25.03 mL, catalyst dose=1.25 g, P=150 bar; —♦— Yield of DMC (mmol/g cat.), —▲— % Methanol conversion.

Thus, the optimum DMC yield was 2.682 mmol/g cat. at 120°C. The decrease in the DMC yield at temperature > 120°C is ascribed to the decrease in the solubility of CO_2 in methanol and the decomposition of DMC [Zhou et al., 2012].

4.6.2.2. Reusability of the catalyst

Reusability of $Ce_{0.5}Zr_{0.5}O_2$ catalyst was studied at optimum reaction conditions: catalyst amount=1.25 g, T=120°C and reaction time=24 h. The catalyst was used in five consecutive batch cycles (Figure 4.6.8). The DMC yield and the methanol conversion is found to have decreased marginally with an increase in the number of cycles. The DMC yield and the methanol conversion in fifth cycle was found to be 2.541 mmol/g cat. and 0.78454 mmol/g cat. as against 2.682 mmol/g cat. and 0.8643 mmol/g, respectively during the first batch of the reaction. This insignificant loss of activity of $Ce_{0.5}Zr_{0.5}O_2$ catalyst may be ascribed to the blockage of the pores and the deposition of reaction products at the active sites.

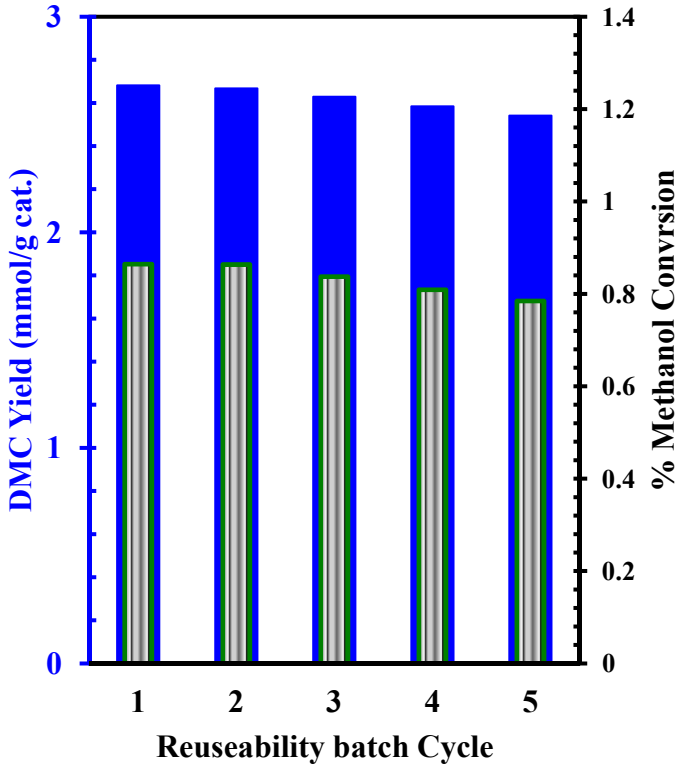

Figure 4.6.8. Reusability of $Ce_{0.5}Zr_{0.5}O_2$ catalyst for the DMC synthesis: (Methanol=25.03 mL, catalyst dose=1.25 g, P=150 bar, T=120°C, t=24 h). DMC Yield (mmol/g cat.), % Methanol conversion.

4.7. CERIA-ZIRCONIA BASED CATALYSTS: CHARACTERIZATION AND CATALYTIC ACTIVITY FOR DIRECT CONVERSION OF CO_2 TO DIMETHYL CARBONATE

4.7.1. Catalyst Characterization

4.7.1.1. X-ray diffraction

XRD profiles of $Ce_{1-x}Zr_xO_2$ (x=0 to 1) catalysts with molar ratios are given in Figure 4.7.1. No separate peak is found in the cerium-zirconium mixed oxide. Pure zirconia (x=0) tetragonal phase showed the characteristic (111) reflection at 2θ=30°. With an increase in ceria amount, the reflex at 2θ=30° shifted towards lower 2θ values. For pure ceria, a major peak at 2θ= 28° was observed, which is typical of the cubic fluorite structure of ceria [Epifani et al., 2012; Bharali et al., 2013]. For ceria content of 60 mol%, the crystal structure was tetragonal. The two peaks at 2θ=29° and 35° for the two samples of $Ce_{0.4}Zr_{0.6}O_2$ and $Ce_{0.5}Zr_{0.5}O_2$ showed much lower intensity than that for other mixed oxides. This is because of the crystallite formation for the samples having cerium/zirconium in the molar ratio ≈1 [Deshpande et al., 2007]. This would explain the sudden increase in the specific surface area of these two samples. XRD of $Ce_{0.5}Zr_{0.5}O_2$ synthesized using exotemplate and endo-/exo-template method (n_{TBC}/n_{Ce+Zr}=0.017) is shown in Figure 4.7.1b. It may be seen that the reflexes of $Ce_{0.5}Zr_{0.5}O_2$, synthesized with endo-/exo-template are more intense than that with exo-template. This suggests that in the presence of larger particles, endo-templates arise. This hypothesis is supported by the lower values of the specific surface and the specific pore volume (Table 4.7.1). At the same time, the mean pore diameter is larger.

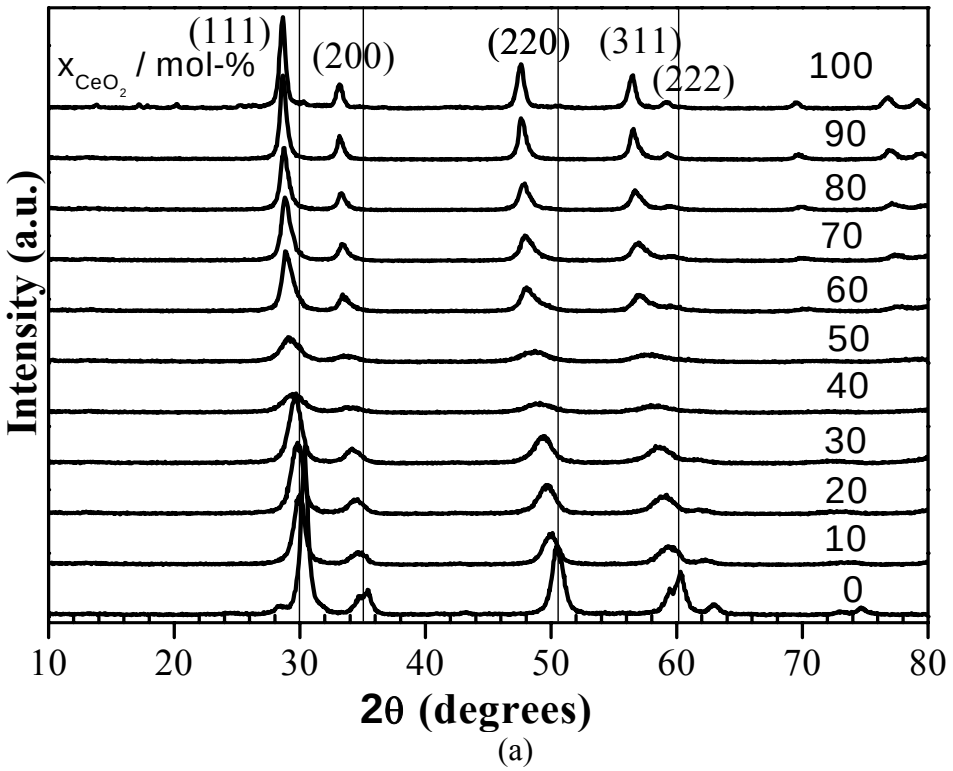

(a)

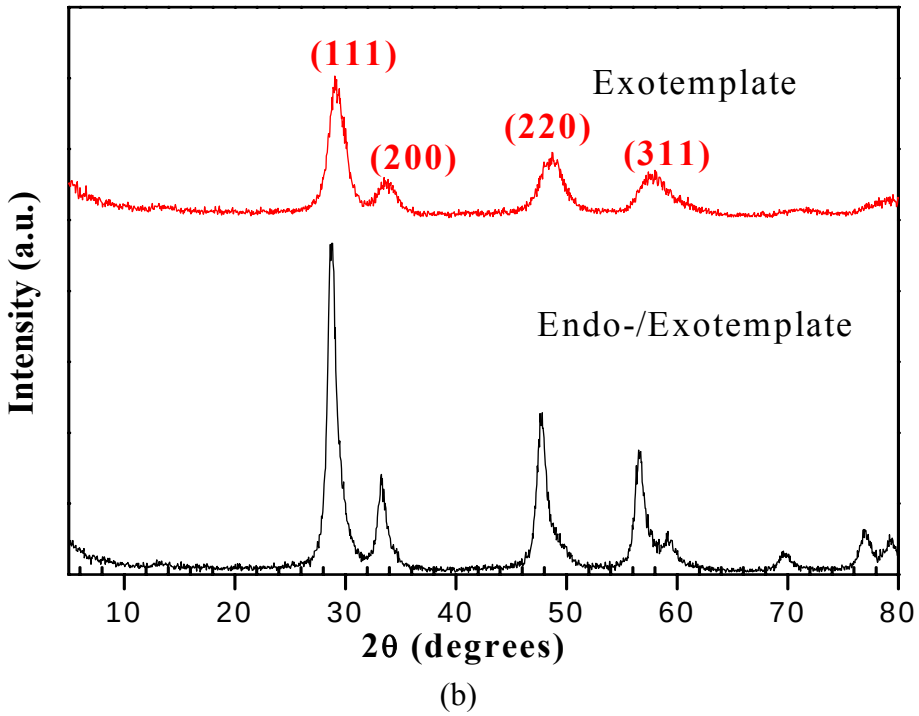

(b)

Figure 4.7.1. (a) XRD patterns $Ce_xZr_{1-x}O_2$ (x=0 to 1) with exotemplate, (b) XRD patterns of the $Ce_{0.5}Zr_{0.5}O_2$ with exotemplate and endo-/exotemplate (n_{TBC}/n_{Ce+Zr}=0.017).

4.7.1.2. Textural properties

The nitrogen sorption results of cerium-zirconium mixed oxides $Ce_{1-x}Zr_xO_2$ (x=0 to1) are summarized in Table 4.7.1. Among all the synthesized catalysts, $Ce_{0.4}Zr_{0.6}O_2$ and $Ce_{0.5}Zr_{0.5}O_2$ were found to possess highest BET surface area of 123 and 121 m^2/g and minimum pore diameter of 11.9 and 10.0 nm, respectively. It can be seen from the Figure 4.7.2, that the specific surface area of the mixed oxides is a function of the CeO_2 content in the synthesized catalyst. Adsorption/desorption isotherm and the pore volume distribution of CeO_2, $Ce_{0.5}Zr_{0.5}O_2$, ZrO_2 are shown in Figure 4.7.3a and Figure 4.7.3b, respectively. All the sorption isotherms of are type IV isotherm with the hysteresis loop, typical of mesoporous systems [Taubert et al., 2014]. Peak corresponding to maximum pore volume shifts towards higher pore with for mixed Ce-Zr oxide as compared to pure CeO_2 or ZrO_2. Mixed oxide exhibit specific surface areas between 112 m^2/g (pure zirconia) and 28 m^2/g (pure ceria). With an increase in the content of ceria, the specific surface area of the mixed oxide decreases. In addition, the average pore diameter increases with an increase in the ceria content, with the exception of the mixed oxides, $Ce_{0.4}Zr_{0.6}O_2$ and $Ce_{0.5}Zr_{0.5}O_2$: These two catalysts exhibit specific surface areas > 120 m^2/g with the mean pore diameter of ~10 nm. The plot of the specific surface area against the molar Ce ratio is shows in Figure 4.7.2.

Table 4.7.1. N2 sorption of cerium-zirconium mixed oxides catalysts

$Ce_{1-x}Zr_xO_2$	BET surface area (m^2/g)	Pore Volume (cm^3/g)	Pore diameter (nm)
x=0.0	28	0.20	30.4
x=0.1	31	0.21	30.6
x=0.2	49	0.36	30.1
x=0.3	54	0.35	28.7
x=0.4	59	0.39	24.8
x=0.5	123	0.40	11.9
x=0.6	121	0.33	10.0
x=0.7	71	0.47	24.3
x=0.8	69	0.43	22.9
x=0.9	81	0.42	21.5
x=1.0	112	0.42	15.4

4.7.1.3. CO_2–TPD

The basic properties of CeO_2, $Ce_{0.5}Zr_{0.5}O_2$ and ZrO_2 catalysts were determined from the CO_2-TPD profile (Figure 4.7.4a) and the results are given in Table 4.7.2. Basic properties of the catalysts depend upon the temperature profile in the weak region (< 200°C), moderate region (200−450°C) and the strong region (> 450°C). Weak basic sites are due to the interaction between the surface and the OH groups and the formation of bicarbonate; moderate basic sites are due to the sites M^{x+}–O^{2-} pairs and the formation of bidentate and bridged carbonates; and the strong basic sites are due to the low coordination O^{2-} ions and the formation of unidentate carbonates [Liu et al., 2013]. In the synthesized catalysts, basicity was found in the week and strong regions corresponding to ~115 and ~717°C. Basic site density of the synthesized catalysts was in the order: ZrO_2 (0.40 mmol/g) < CeO_2 (0.41 mmol/g) < $Ce_{0.5}Zr_{0.5}O_2$ (1.93 mmol/g), and the basic site density per unit area followed the same order (Table 4.7.2). Thus, the mixed metal oxides possess higher basic site density as compared to single oxide catalysts [La et al., 2007]. Lee et al. [2012] and Zheng et al. [2009] reported maximum basic site density of 0.017 and 0.276 mmol/g, respectively, for $Ce_{0.6}Zr_{0.4}O_2$ catalysts.

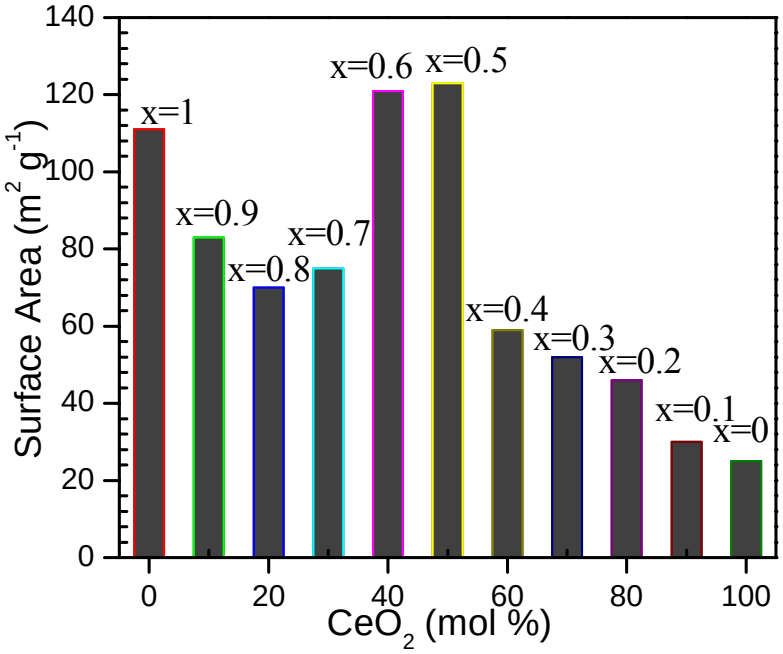

Figure 4.7.2. Surface area of the $Ce_{1-x}Zr_xO_2$ mixed oxides from the synthesis depending on the CeO_2-content.

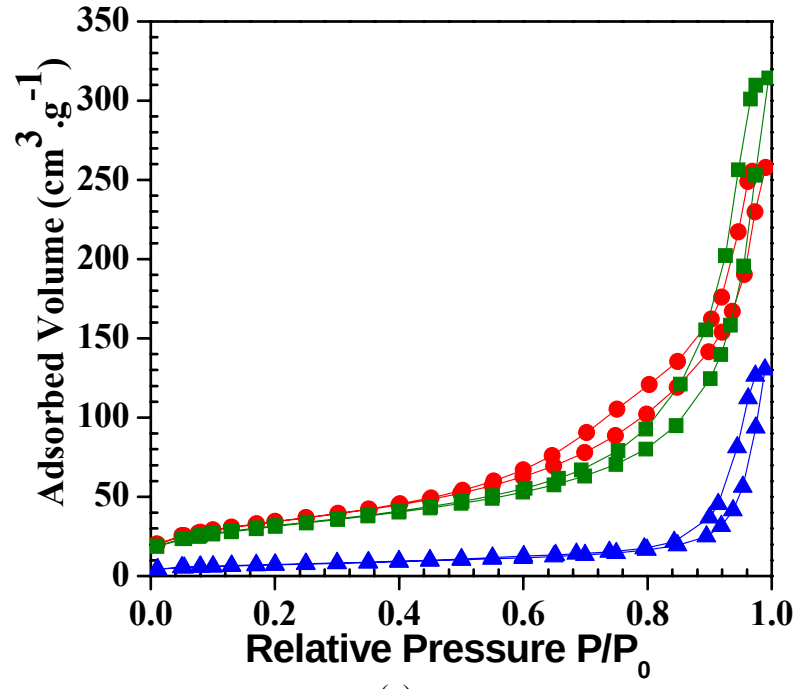

(a)

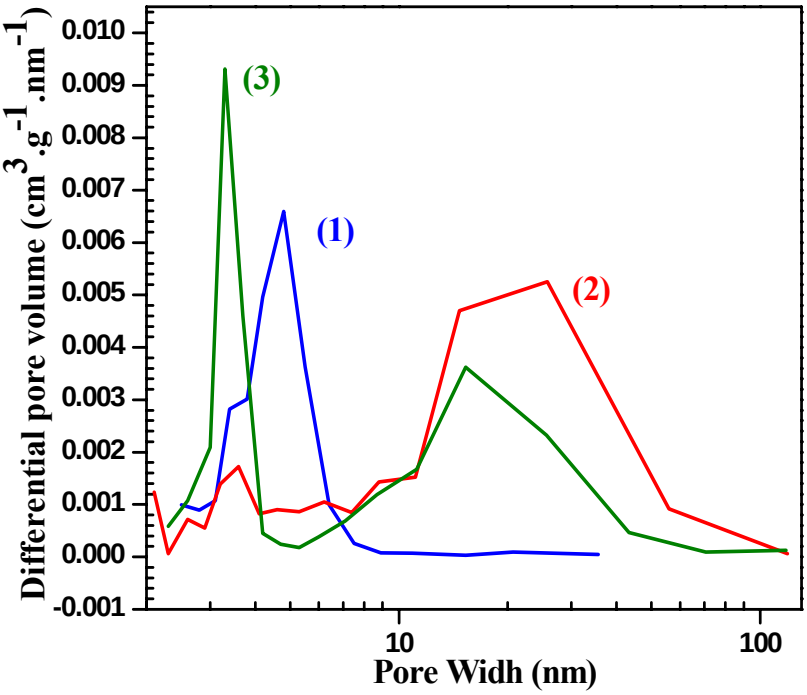

(b)

Figure 4.7.3. (a) N_2 adsorption/desorption isotherm CeO_2, $Ce_{0.5}Zr_{0.5}O_2$, ZrO_2; —■— ZrO_2, —●— $Ce_{0.5}Zr_{0.5}O_2$, —▲— CeO_2. (b) Pore diameter distributions of CeO_2, $Ce_{0.5}Zr_{0.5}O_2$, ZrO_2. (1) CeO_2, (2) $Ce_{0.5}Zr_{0.5}O_2$, and (3) ZrO_2.

4.7.1.4. NH_3–TPD

NH_3-TPD spectra of CeO_2, $Ce_{0.5}Zr_{0.5}O_2$ and ZrO_2 catalysts are shown in Figure 4.7.4b and the results are summarized in Table 4.7.2. Desorption peaks of NH_3 are in the temperature range of 50-900°C. The NH_3 desorption peaks at 110°C and 667°C for CeO_2 and 156°C and 643°C for ZrO_2 were observed in the week and strong regions. $Ce_{0.5}Zr_{0.5}O_2$ catalyst shows peaks in all the three regions at 106°C, 294°C and 666°C. Acidic site density of synthesized catalysts is found to be: CeO_2 (0.94 mmol/g) < ZrO_2 (1.52 mmol/g) < $Ce_{0.5}Zr_{0.5}O_2$ (2.48 mmol/g). Thus, the $Ce_{0.5}Zr_{0.5}O_2$ catalyst has the highest acidic site density and the CeO_2 has the lowest of acidic sites density. Thus, the $Ce_{0.5}Zr_{0.5}O_2$ catalyst has the highest density of basic and acidic sites and the BET surface area, as compared to other catalysts. Therefore, this catalyst can act as an acid-base bifunctional catalyst. It has been reported that both the basic and acidic sites are required for the direct conversion of CO_2 to produce DMC [Zhang et al., 2009; Lee et al., 2012; Chen et al., 2014].

4.7.1.5. Surface morphology and elemental analysis

SEM micrographs of CeO_2, ZrO_2 and $Ce_{0.5}Zr_{0.5}O_2$ with particles size distribution in the range of d_P=0.2-0.4 mm are shown in Figure 4.7.5. The EDX analysis of the $Ce_{0.5}Zr_{0.5}O_2$ catalyst is shown in the Figure 4.7.5. Analysis has also been carried out by ICP-OES. The structural chemical compositions of the $Ce_{0.5}Zr_{0.5}O_2$ and $Ce_{0.4}Zr_{0.6}O_2$ catalysts are shown in Table 4.7.3. The composition of the synthesized catalysts are similar as the desired initial metal composition.

Table 4.7.2. TPD analysis using absorbed CO_2 and NH_3 for determining basic and acidic properties of CeO_2, $Ce_{0.5}Zr_{0.5}O_2$ and ZrO_2.

Catalyst	TPD analysis of absorbed CO_2 (mmol/g)			Total evolved CO_2 (mmol/g)	Basic site density (µmol/m^2)
	Weak (< 200°C)	Moderate (200-450°C)	Strong (> 450°C)		
CeO_2	0.41 (117)	0	0	0.41	14.64
$C_{0.5}Zr_{0.5}O_2$	0.45 (113)	0.17(345)	1.31 (717)	1.93	15.69
ZrO_2	0.37 (100)	0	0.03(846)	0.40	3.89

Catalyst	TPD analysis of absorbed NH_3 (mmol/g)			Total evolved NH_3 (mmol/g)
	Weak (< 200°C)	Moderate (200-450°C)	Strong (> 450°C)	
CeO_2	0.81 (110)	0	0.13 (667)	0.94
$C_{0.5}Zr_{0.5}O_2$	0.99 (106)	0.27 (294)	1.49 (666)	2.48
ZrO_2	1.31 (156)	0	0.21 (643)	1.52

Temperature (°C) at maxima is given in brackets.

Table 4.7.3. Elemental analysis of $Ce_{0.5}Zr_{0.5}O_2$ and $Ce_{0.4}Zr_{0.6}O_2$ catalysts.

Catalysts	Nominal value of metals		Actual values of metals from ICP-OES analysis		Chemical formula
	Ce	Zr	Ce	Zr	
$Ce_{0.5}Zr_{0.5}O_2$	0.5	0.5	0.48	0.52	$Ce_{0.48}Zr_{0.52}O_2$
$Ce_{0.4}Zr_{0.6}O_2$	0.4	0.6	0.39	0.61	$Ce_{0.39}Zr_{0.61}O_2$

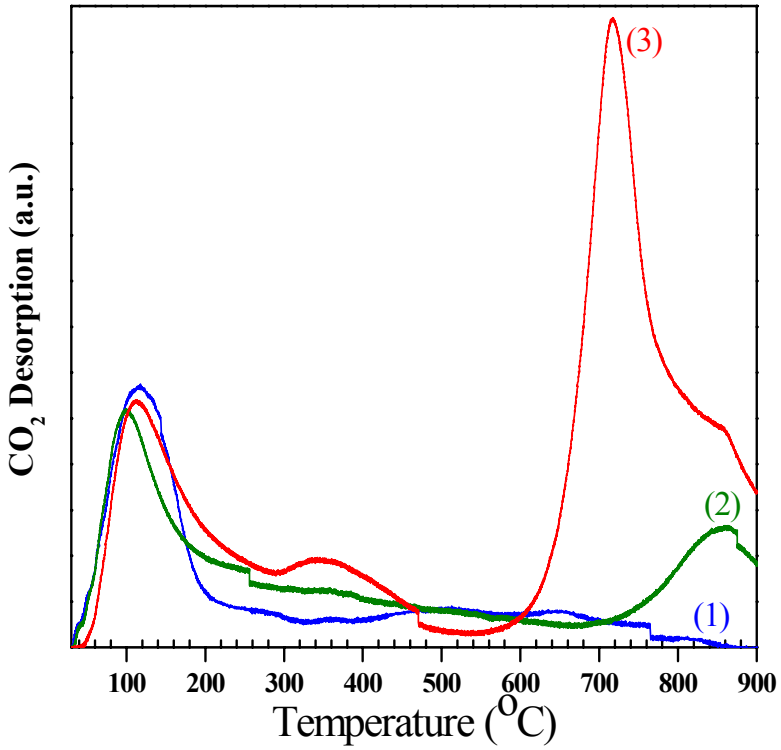

(a)

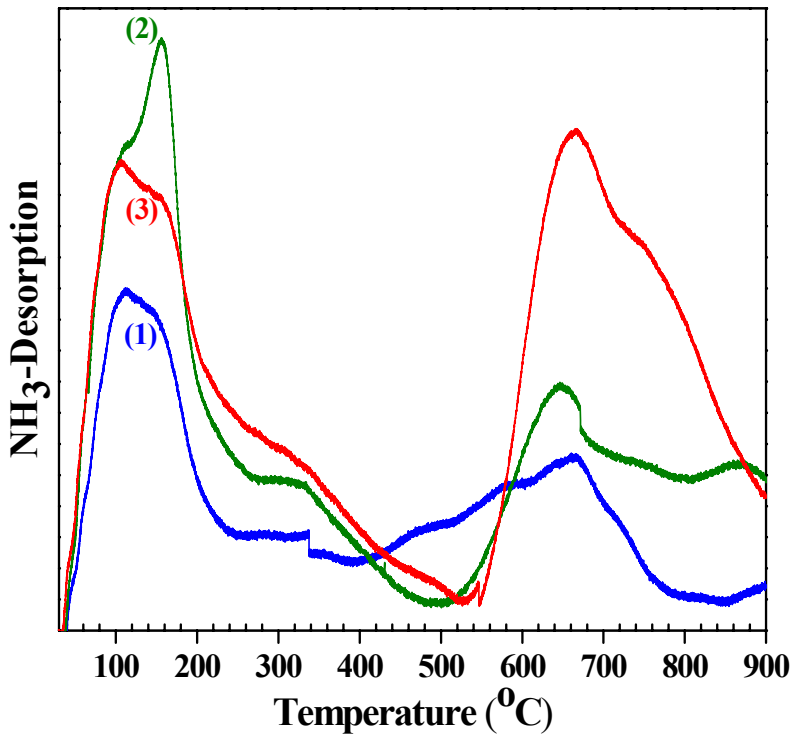

(b)

Figure.4.7. 4. (a) CO_2 –TPD of the synthesized CeO_2, $Ce_{0.5}Zr_{0.5}O_2$, ZrO_2 catalysts, (b) NH_3 –TPD of the synthesized CeO_2, $Ce_{0.5}Zr_{0.5}O_2$, ZrO_2 catalysts. (1) CeO_2, (2) ZrO_2, and (3) $Ce_{0.5}Zr_{0.5}O_2$.

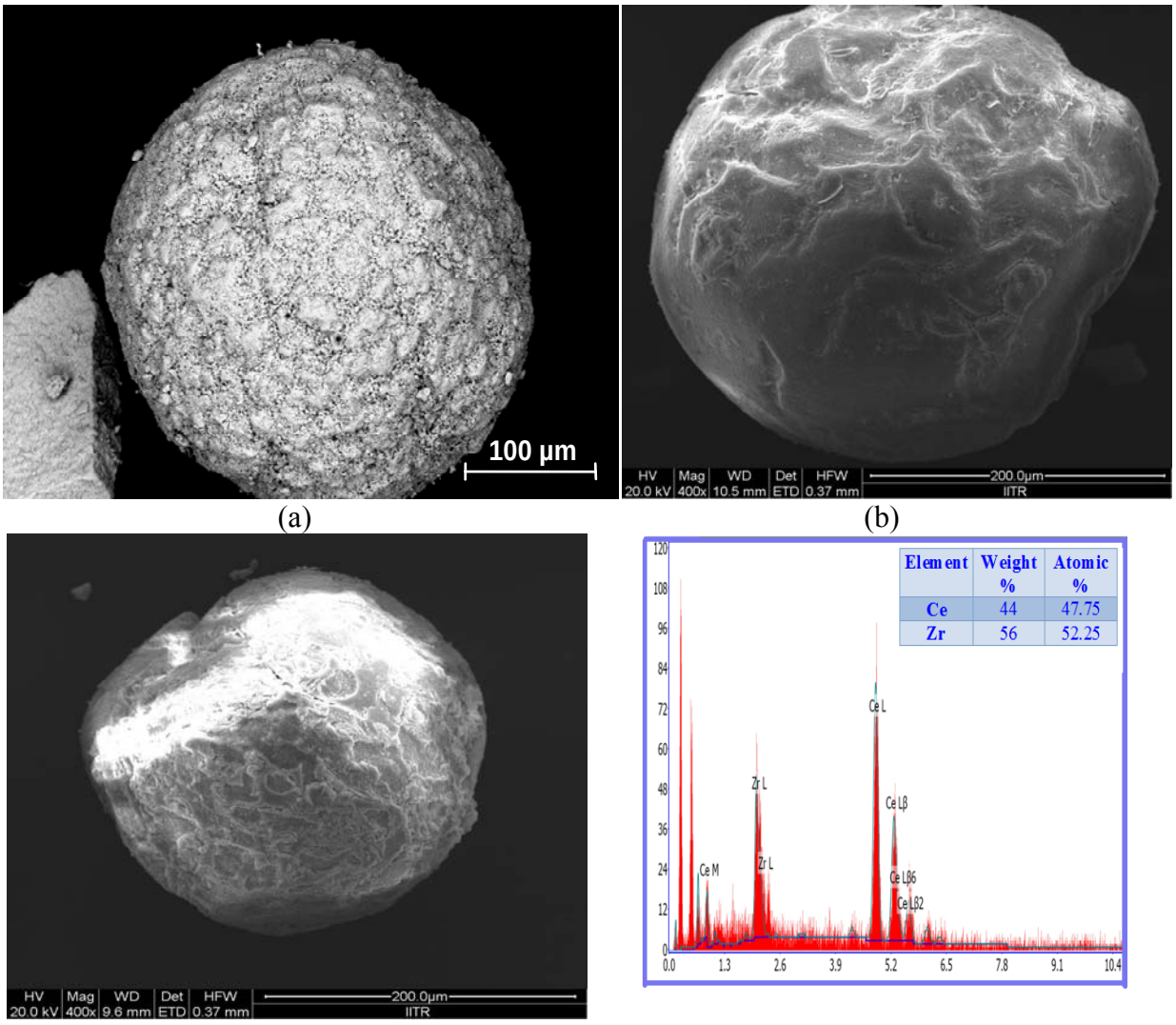

Figure 4.7.5. FE-SEM images and EDX of (a) CeO_2, (b) ZrO_2, (c) $Ce_{0.5}Zr_{0.5}O_2$, (d) EDX spectra of $Ce_{0.5}Zr_{0.5}O_2$.

4.7.2. Catalytic Activity of Catalysts for DMC Synthesis

The direct catalytic conversion of CO_2 with methanol for the synthesis of DMC was studied in the presence of CeO_2, ZrO_2 and $Ce_{0.5}Zr_{0.5}O_2$ catalysts. Negligible conversion of methanol/CO_2 to DMC after for 24 h at a pressure of 150 bar and 120°C temperature was observed in the blank experiment without any catalyst.

$Ce_{0.5}Zr_{0.5}O_2$ catalyst showed the best activity as compared to CeO_2, and ZrO_2 (Figure 4.7.6). The order of the activity of the catalysts followed: ZrO_2 (0.912 mmol DMC/g.cat.) < CeO_2 (1.384 mmol DMC/g.cat.) < $Ce_{0.5}Zr_{0.5}O_2$ (2.921 mmol DMC/g.cat.). Best active $Ce_{0.5}Zr_{0.5}O_2$ catalyst was further used for the optimization of the reaction conditions such as reaction temperature, catalyst dose and reaction time for CO_2 conversion.

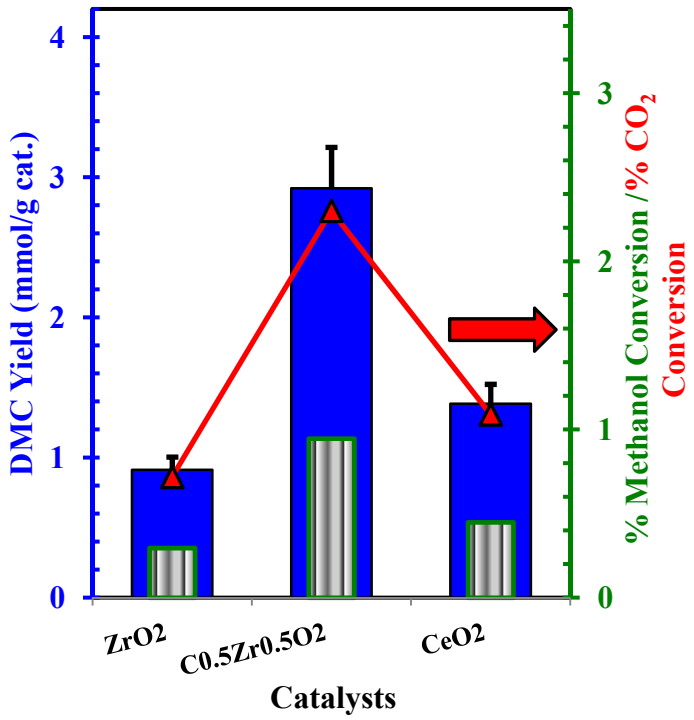

Figure 4.7.6. (a) Methanol Conversion and DMC yield over CeO_2, $Ce_{0.5}Zr_{0.5}O_2$ and ZrO_2 catalysts; Reaction conditions: (Methanol=25.03 mL, catalyst dose=1.25 g, P=150 bar, T=120°C, t=24 h); DMC Yield (mmol/g cat.), % Methanol conversion, —▲— % CO_2 conversion.

The influences of reaction time for DMC synthesis in the presence of $Ce_{0.5}Zr_{0.5}O_2$ catalyst is shown in Figure 4.7.7b. It can be seen from the Figure that the DMC formation (1.989-2.921 mmol/g.cat.), methanol conversion (0.644-0.945 mmol/g.cat.) and CO_2 conversion (1.567-2.310 mmol/g.cat.) increased with an increase in reaction time upto 24 h. Further increase in the reaction time showed a decrease in the DMC yield and CO_2/methanol conversion. It may be because of the saturation of the molecular sieves due to the adsorption of water.

The effect of catalyst dose on the DMC yield and the CO_2 conversion is shown in Figure 4.7.7b. It can be seen in that the maximum DMC yield and CO_2 conversion were obtained at a catalyst dose of 1.25 g. Further increase in the catalyst dose diminished the DMC yield. This may be because of the formation of agglomerates at higher catalyst doses in the reaction mixture.

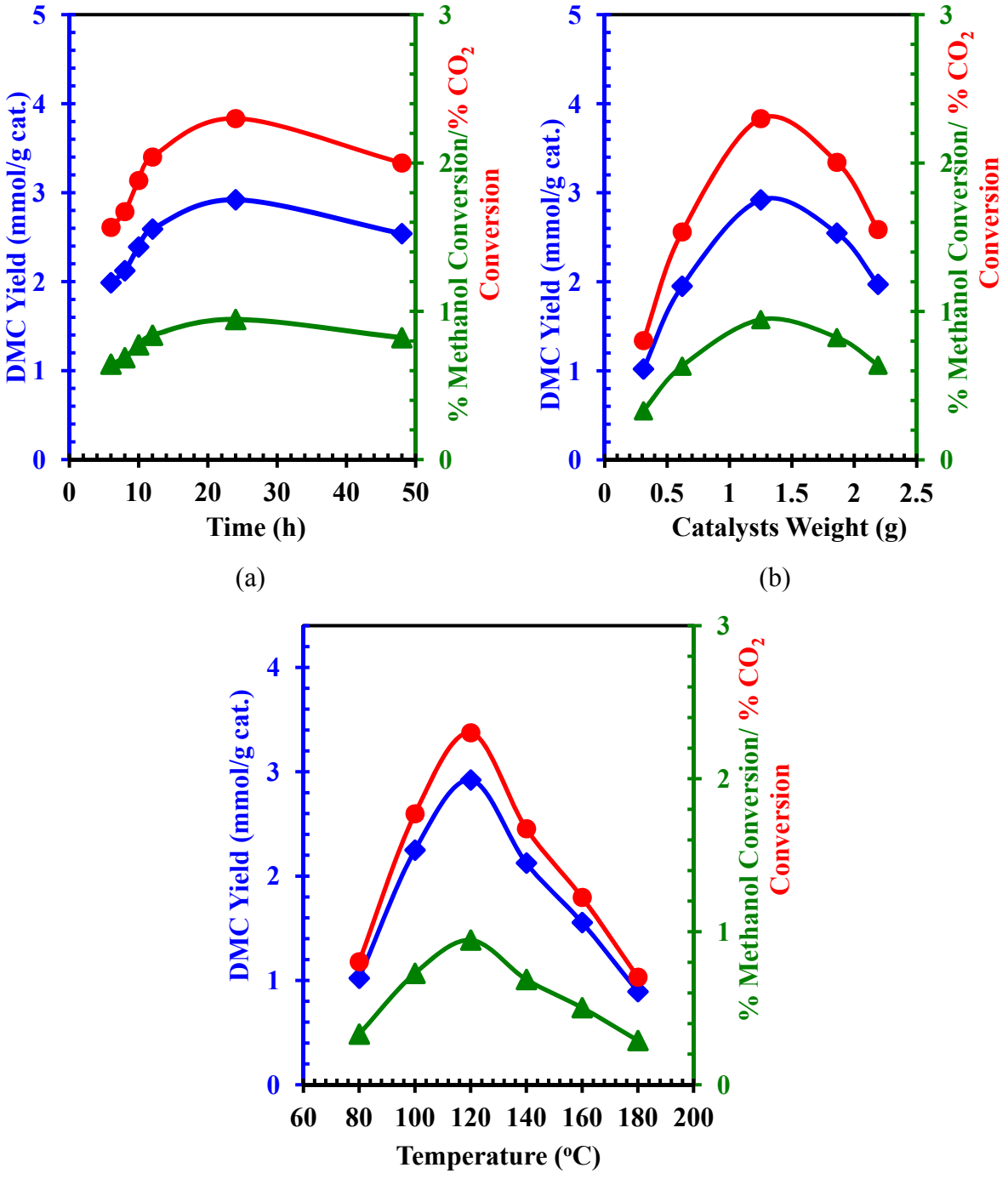

Figure 4.7.7. Effect of various parameters for direct conversion of CO_2 with methanol for DMC synthesis; (a) effect of reaction time at Methanol=25.03 ml, catalyst dose=1.25 g, P=150 bar, T=120 °C; (b) effect of catalyst dose at Methanol=25.03 ml, P=150 bar, T=120 °C, t=24 h; (c) effect of temperature at Methanol=25.03 ml, catalyst dose=1.25 g, P=150 bar. —●— CO_2 conversion, —♦— DMC yield, —▲— Methanol conversion.

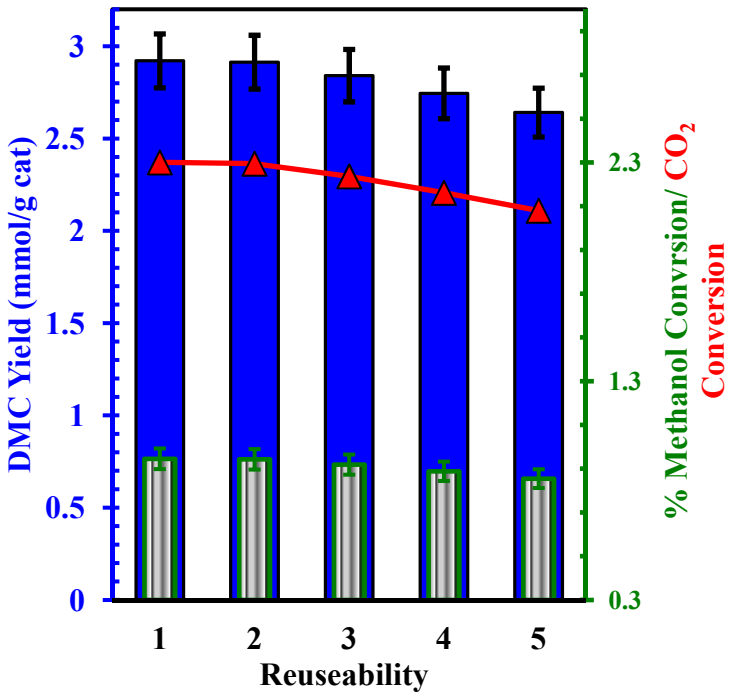

Figure 4.7.8. Reusability of $Ce_{0.5}Zr_{0.5}O_2$ catalyst DMC synthesis from direct conversion of CO_2 with methanol (methanol=25.03 mL, catalyst dose=1.25 g, P=150 bar, T=120°C, t=24 h); DMC Yield (mmol/g cat.), % Methanol conversion, —▲— % CO_2 conversion.

The influence of the reaction temperature for the DMC synthesis and CO_2/methanol conversion is shown in Figure 4.7.7c. Initially, the DMC yield (1.021-2.9212 mmol/g cat), methanol conversion (0.331-0.945 mmol/g cat) and CO_2 conversion (0.804-2.300 mmol/g cat.) increase with an increase in the reaction temperature in the range of 80-120°C. Above 120°C, an increase in the reaction temperature quickly decreased the DMC yield (2.125-0.8924 mmol/g cat), methanol conversion (0.687-0.2888 mmol/g cat) and the CO_2 conversion (1.673-0.7026 mmol/g cat). Thus, the optimum DMC yield was obtained at 120°C. The decrease in the DMC yield, methanol and CO_2 conversion may be because of the poor solubility of CO_2 in methanol and due to decomposition of DMC [Kumar and Jain, 2014].

The reuse of the $Ce_{0.5}Zr_{0.5}O_2$ catalyst was investigated at optimum reaction conditions (T=120°C, t=24 h and catalyst amount=1.25 g) in five consecutive batch cycles. Almost similar DMC yield was found in all the batch cycles. Thus, the $Ce_{0.5}Zr_{0.5}O_2$ catalyst is an effective catalyst with long life and can be used a number of times.

4.8. CERIA-MANGANESE OXIDES CATALYSTS: CHARACTERIZATION AND CATALYTIC ACTIVITY FOR DIRECT CONVERSION OF CO_2 TO DIMETHYL CARBONATE

In the present work, synthesis of DMC from direct conversion of CO_2 with methanol was studied using CeO_2-MnO_x composite catalysts prepared by surfactant-template method. Synthesized catalysts were characterized by various methods; and the catalytic activity and reusability of the best performing catalyst was studied for the formation of DMC.

4.8.1. Catalyst Characterization

4.8.1.1. X-ray diffraction

The XRD pattern of the synthesized catalysts with different Mn/Ce ratio is shown in Figure 4.8.1. The diffraction patterns corresponding to CeO_2 are obtained at 2θ values of 28.5, 33.1, 47.75 and 56.6 with the corresponding planes of CeO_2 being (111), (200), (220) and (311), respectively. CeO_2 was found to posses cubic fluorite structure (JCPDS- 43-1002). In all the synthesized catalysts, Mn or its other forms such as MnO_x species could not be detected. This means that the MnO_x species were highly dispersed or incorporated in the CeO_2 matrix. It is also possible that the Mn formed solid solution with the amorphous manganese oxides or cerianite structure [Chen et al., 2001]. According to Scherrer's equation, the crystallite size of Ce_1-$Mn_{0.125}$, Ce_1-$Mn_{0.25}$ and Ce_1-Mn_1 was found to be 9.83, 8.37 and 6.48 nm, respectively. The cationic size of Mn^{n+} (Mn^{4+}:0.053 nm; Mn^{3+}:0.065 nm; Mn^{2+}: 0.083 nm) is much smaller than that of Ce^{4+} (Ce^{4+}:0.097 nm; Ce^{3+}:0.114 nm). Therefore, an increase in Mn proportion in the synthesized catalysts decreased the crystalline size of the catalysts. In the synthesized catalysts, diffraction peaks at (111) shifts to the higher 2θ side due to the lower size of the cation Mn^{n+} with the replacement of Ce^{n+} by Mn^{n+} during partial dispersion of MnO_x in the combination matrix. The elemental composition of the synthesized catalysts was determined by ICP-OES (Table 4.8.1).

Table 4.8.1. Elemental composition of Mn/Ce catalysts.

Sample	Nominal values		Actual values from ICP-OES analysis		EDX analysis		Chemical formulae
	Ce	Mn	Ce	Mn	Ce	Mn	
Ce_1-$Mn_{0.125}$	1.0	0.125	0.997	0.128	0.95	0.130	$Ce_{0.997}Mn_{0.128}O_2$
Ce_1-$Mn_{0.25}$	1.0	0.25	0.991	0.259	0.982	0.268	$Ce_{0.991}Mn_{0.259}O_2$
Ce_1-$Mn_{1.0}$	1.0	1.0	0.99	1.01	0.94	1.06	$Ce_{0.99}Mn_{1.01}O_2$

It can be seen that the molar ratio of the Mn/Ce in the Ce-Mn-based solid solution are very close to the value as desired during the synthesis. These results show that the formed catalysts have homogenous composition. Similar phases in Ce-Mn catalysts were found by other investigators too [Delimaris and Loannides, 2008; Liu et al., 2013; Shen et al., 2014; Venkataswamy et al., 2014].

4.8.1.2. Raman spectroscopy

To investigate the type of species present on the catalyst surface and the nature of bonding between oxygen and the metal in the lattice, Raman spectroscopy was employed. Raman spectra of Ce-Mn mixed oxides for different Mn/Ce molar ratios are shown in Figure 4.8.1b. Two peaks at 460 and 577 cm^{-1} were observed for Ce_1-$Mn_{0.125}$, three peaks was observed at 256, 466 and 627 cm^{-1} for Ce_1-$Mn_{0.25}$, and four peaks at 261, 459, 537 and 646 for Ce_1-Mn_1 catalyst. Ce_1-$Mn_{0.125}$ and Ce_1-$Mn_{0.25}$ catalysts show strong peak at ≈460 cm^{-1} due to the cubic phase of CeO_2. Lower intensity of this peak in Ce_1-$Mn_{0.125}$ is due to the incorporation of MnO into the CeO_2 lattice and because of the homogeneous dispersion of Mn oxide to CeO_2 surface. The peaks identified in the Raman spectra are as follows: CeO_2 (460 and 577 cm^{-1}), MnO (247 cm^{-1}), MnO_2 (645 cm^{-1}) and Mn_2O_3 (698 cm^{-1}) [Pu et al., 2007; Chang et al., 2013]. These peaks show that the synthesized Ce-Mn catalysts has fluorite structure of CeO_2 and different phase of Mn oxides.

4.8.1.3. Textural properties

N_2 adsorption-desorption isotherms for Ce-Mn based catalysts are presented in Figure 4.8.2a and the BJH model for describing the pore size distribution which is based on the capillary condensation and is only valid for pore diameters of mesopores between 2-50 nm is shown in Figure 4.8.2b. BET surface area and the average pore diameter as determined from the desorption branch of isotherm are given in Table 4.8.2. BET surface area of the Ce_1-$Mn_{0.125}$, Ce_1-$Mn_{0.25}$ and Ce_1-Mn_1 catalyst are 97, 95 and 98, respectively. Ce_1-$Mn_{0.125}$ catalyst is found to have average pore diameter and pore volume of 9 nm and 0.39 cm^3/g. Ce_1-$Mn_{0.25}$ and Ce_1-Mn_1 catalyst have pore diameter of 19 nm and 14 nm, respectively, and the pore volume of 0.50 cm^3/g and 0.43 cm^3/g, respectively. All the catalysts exhibit type IV isotherms according to the IUPAC. The hysteresis loops showed sharp adsorption/desorption in the relative pressure (P/P_o) range of 0.68-0.98, showing a narrow size distribution. Predominantly mesoporous substances describe a hysteresis due to pore condensation processes and the adsorption and desorption isotherms do not coincide with each other. Following the IUPAC definition of hysteresis curves, they show a behavior corresponding to type H3 [Brunauer et al., 1938; Barret et al., 1951; Sing et al., 1985]. Venkataswamy et al. [2014] and Zhao et al. [2014] reported the BET surface area 58 m^2/g and 71.1 m^2/g, with the catalyst having Ce/Mn molar ratio of 1.2/1 and 2.33/1, respectively. Shen et al. [2014] reported BET surface area in the range of 3.7-86.9 m^2/g of Ce-Mn catalysts synthesized by different methods with a Ce/Mn molar ratio of 0.4/1. Liu et al. [2013] reported BET surface area in the range of 99-111 m^2/g for Ce-Mn catalysts synthesized using different preparation methods having 1/1 molar ratio. Li et al. [2012] reported BET surface area of 55-150 m^2/g for Ce-Mn having Ce-Mn catalysts having Ce:Mn molar ratio in the range of 1:1 to 1:4. Delimaris and Loannides [2008] reported BET surface area in the range of 38.2-59.4 m^2/g for Ce-Mn catalysts having Ce:Mn molar ratio in the range of 0.053:1 to 3:1.

Table 4.8.2. XRD and textural properties of synthesized catalysts.

Catalyst	XRD		Textural Properties		
	Lattice Strain	Crystallite size (nm)	Surface Area (m^2/g)	Cumulative pore volume (cm^3/g)	Average Pore diameter (nm)
Ce_1-$Mn_{0.125}$	0.0149	9.83	97	0.39	9
Ce_1-$Mn_{0.25}$	0.0174	8.37	95	0.50	19
Ce_1-Mn_1	0.0226	6.48	98	0.43	14

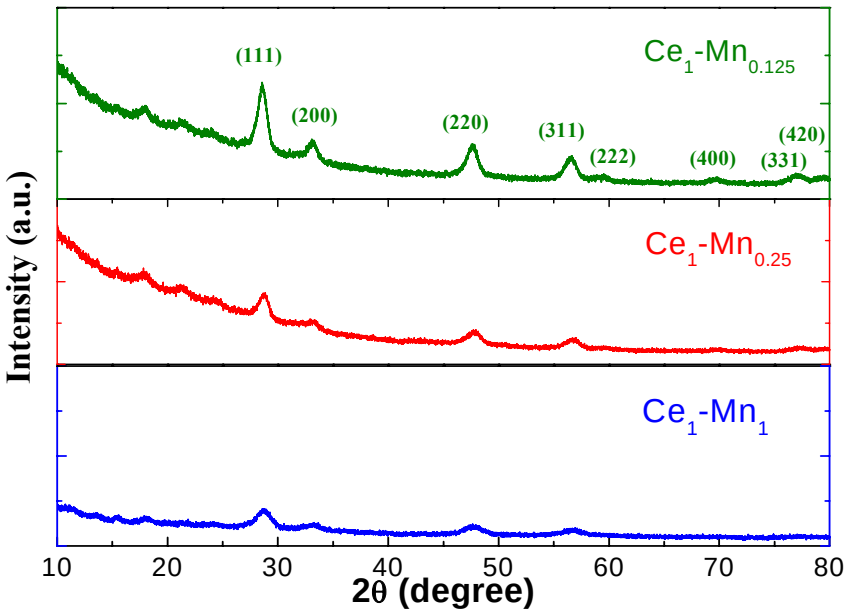

(a)

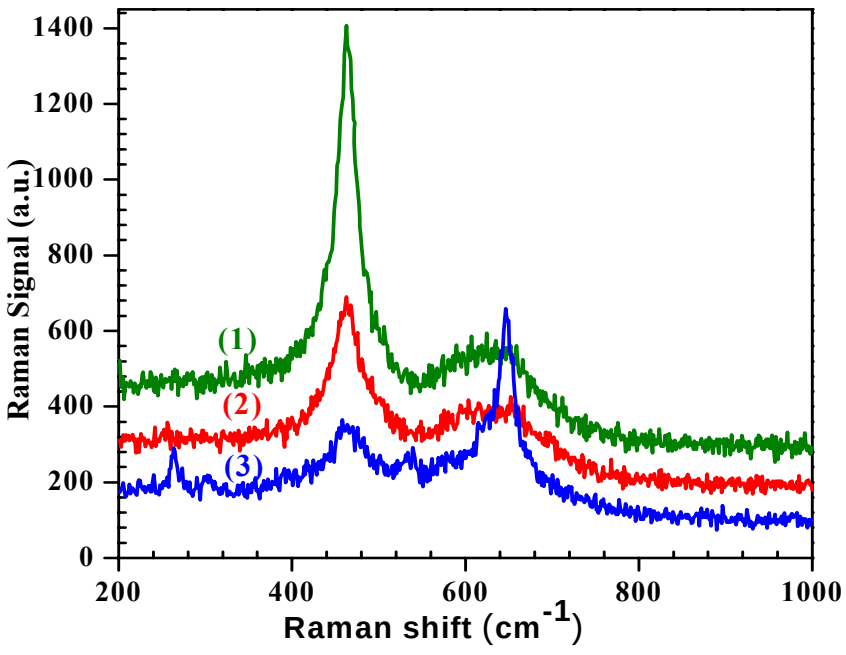

(b)

Figure 4.8.1. (a) XRD and (b) Raman spectroscopy of Ce_1-$Mn_{0.125}$, Ce_1-$Mn_{0.25}$ and Ce_1-Mn_1 catalysts; (1) Ce_1-$Mn_{0.125}$, (2) Ce_1-$Mn_{0.25}$, and (3) Ce_1-Mn_1.

4.8.1.4. Surface morphology

SEM micrographs were taken for the Ce_1-$Mn_{0.125}$, Ce_1-$Mn_{0.25}$ and Ce_1-Mn_1 catalysts in order to see the effect of Mn on the morphology of the catalysts. SEM image (Figure 4.8.3) shows spherical shape of the catalysts. Additionally, TEM images (Figure 4.8.4a and 4.8.4b) of the catalyst (Ce_1-$Mn_{0.125}$) show that the particles pore size in the range of 5-15 nm [Singh et al., 2007]. SAED pattern confirms the presence of the crystallite phases as observed by XRD patterns of Ce_1-$Mn_{0.125}$ catalyst.

4.8.1.5. CO_2–TPD

Basicity plays a crucial role in the conversion of CO_2 and formation of DMC. CO_2-TPD profiles are shown in Figure 4.8.5a. For the quantitative analysis of the basic centers all the peaks were integrated to evaluate their individual amounts. Numerical values of the basicity and the basic site density are given in Table 4.8.3. Ce_1-$Mn_{0.125}$ catalyst was found to possess highest basicity and basic site density as compared to Ce_1-$Mn_{0.25}$ and Ce_1-Mn_1 catalysts. Basicity of the catalyst was in the order: Ce_1-Mn_1 (0.314 µmol/g) < Ce_1-$Mn_{0.25}$ (0.518 µmol/g) < Ce_1-$Mn_{0.125}$ (0.868 µmol/g). Similar trend was observed and the order was same for basic site density as well. All the CO_2-TPD profiles have same shape, but the maximum desorption temperature decreased with an increase in the amount of Mn.

4.8.1.6. NH_3–TPD

Acidity and acidic site density of the Ce_1-$Mn_{0.125}$, Ce_1-$Mn_{0.25}$ and Ce_1-Mn_1 catalysts are shown in the Figure 4.8.5b. For the quantitative analysis of the acidic centers, all the peaks were integrated to evaluate the acidity and acid site density. Results are given in Table 4.8.3. Ce_1-$Mn_{0.125}$ and Ce_1-$Mn_{0.25}$ catalysts show week acidic sites, whereas the Ce_1-Mn_1 catalyst shows peaks in all the three regions. Ce_1-$Mn_{0.125}$ catalyst was found to possess highest acidity and acidic site density as compared to Ce_1-$Mn_{0.25}$ and Ce_1-Mn_1 catalysts. Acidity and acidic site density decreased with an increase in the Mn amount.

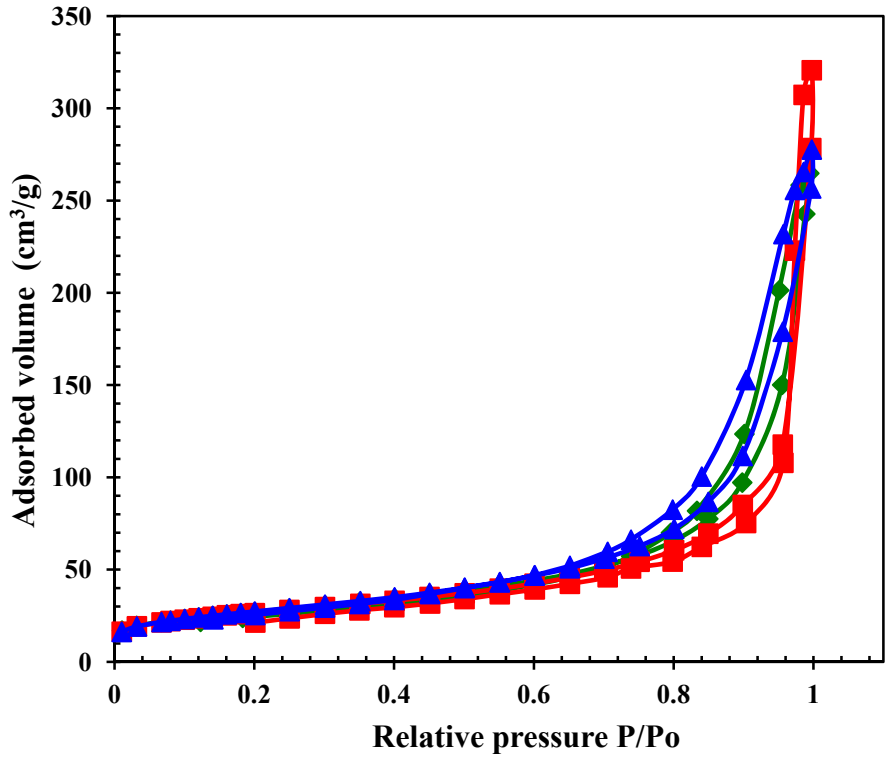

(a)

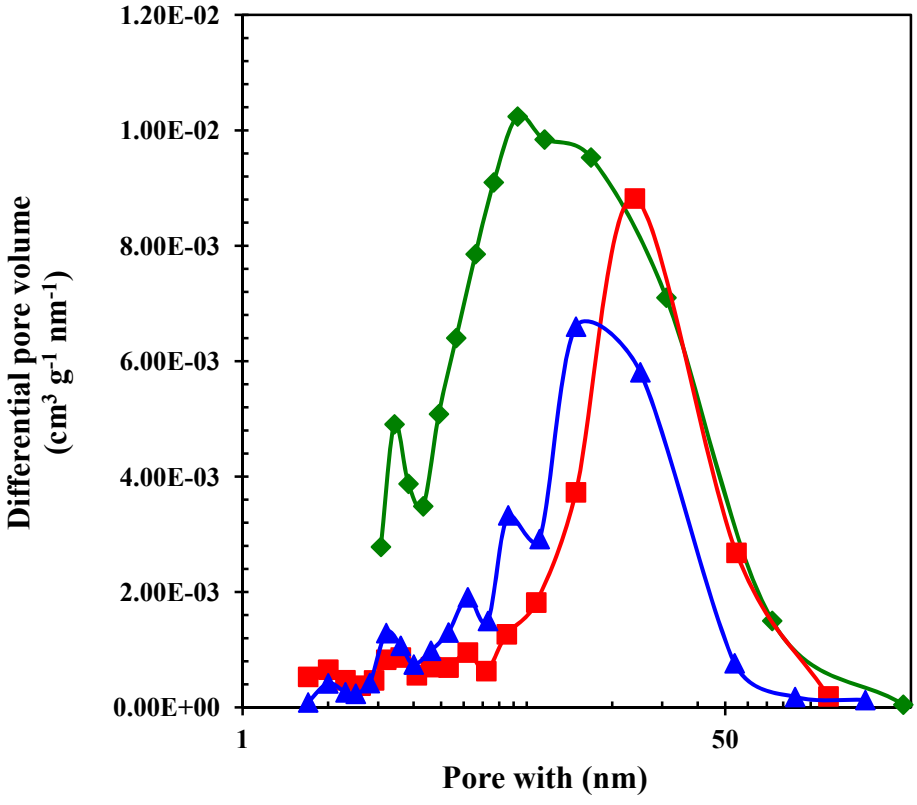

(b)

Figure 4.8.2. (a) N_2 sorption and, (b) Pore size distribution of Ce_1-$Mn_{0.125}$, Ce_1-$Mn_{0.25}$ and Ce_1-Mn_1 catalysts. —◆— Ce_1-$Mn_{0.125}$, —■— Ce_1-$Mn_{0.25}$, —▲— Ce_1-Mn_1.

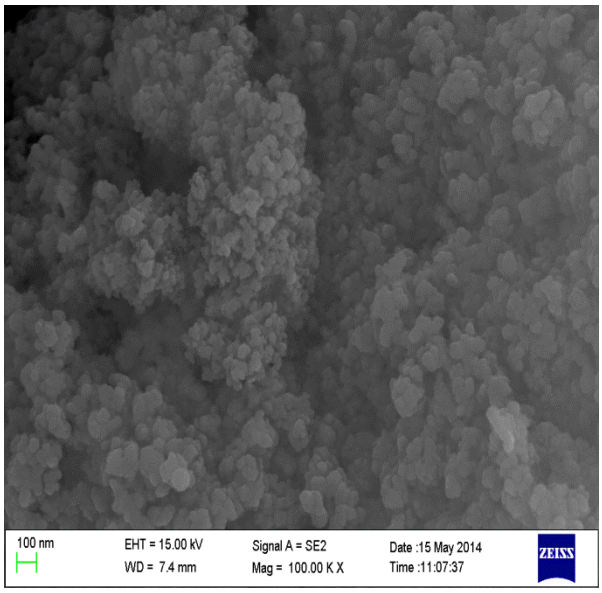

Ce_1-$Mn_{0.125}$

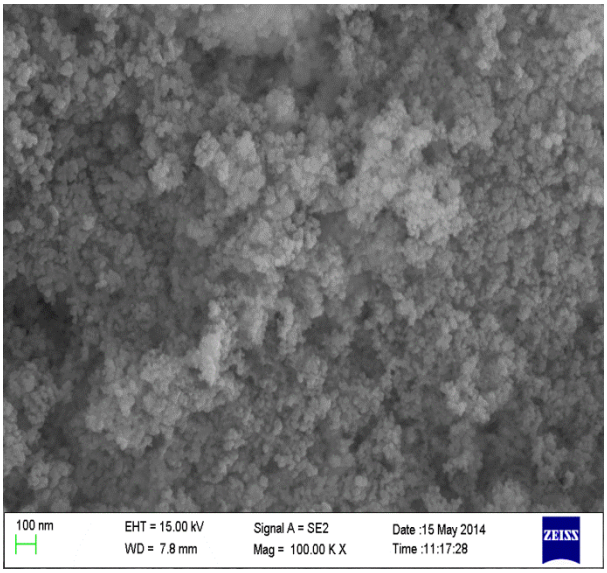

Ce_1-$Mn_{0.25}$

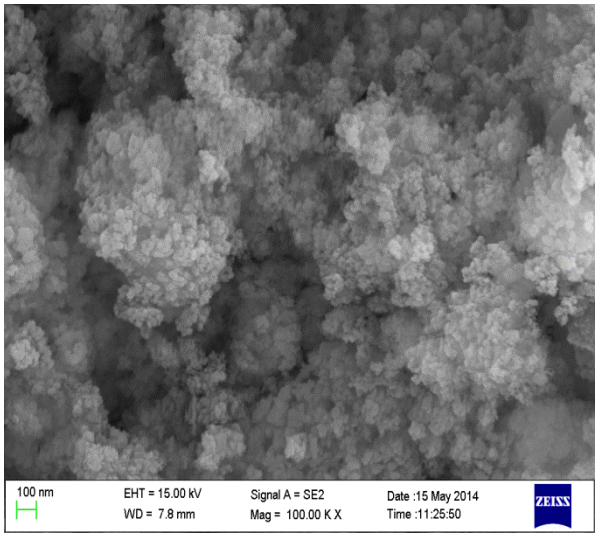

Ce_1-Mn_1

Figure 4.8.3. SEM micrographs of the synthesized Ce-Mn catalysts.

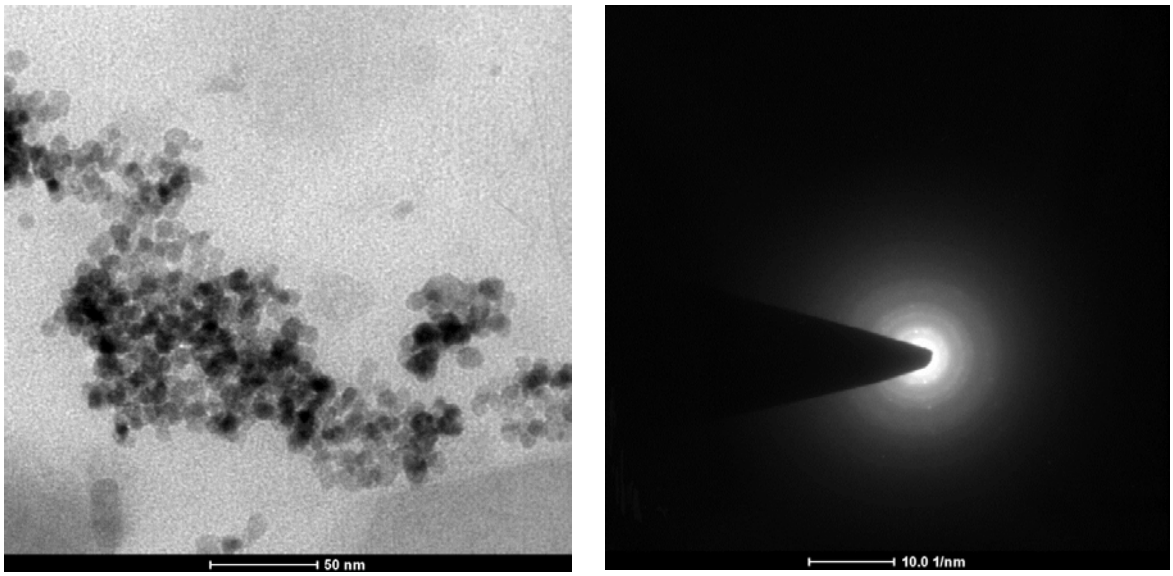

(a) (b)

Figure 4.8.4. TEM image with SEAD patterns of the Ce_1-$Mn_{0.125}$ catalyst.

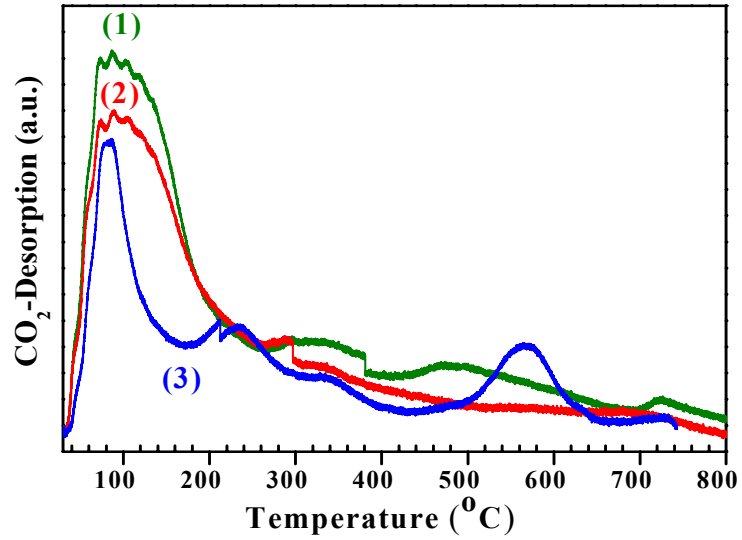

(a)

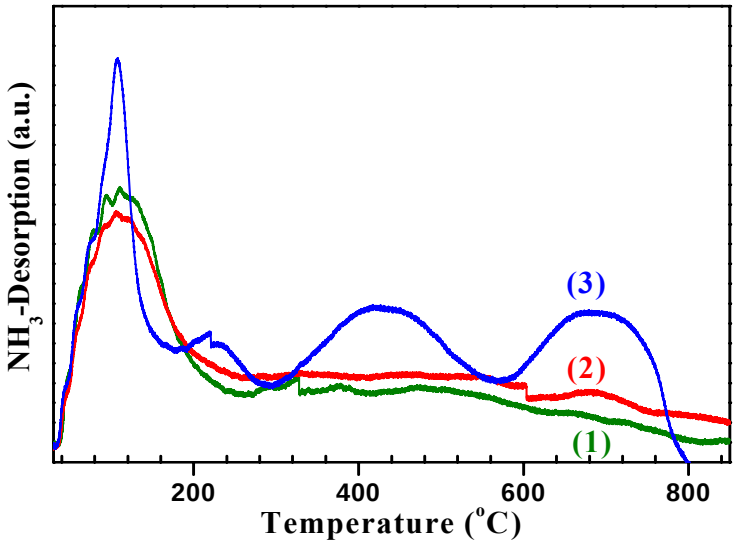

(b)

Figure 4.8.5. (a) CO_2-TPD and (b) NH_3-TPD measurement of the Ce_1-$Mn_{0.125}$, Ce_1-$Mn_{0.25}$ and Ce_1-Mn_1 catalysts with desorption at 90–800°C, (1) Ce_1-$Mn_{0.125}$, (2) Ce_1-$Mn_{0.25}$, and (3) Ce_1-Mn_1.

4.8.2. Catalytic Activity

Figure 4.8.6a shows CO_2 and methanol conversion, and the DMC yield over the Ce-Mn catalysts. Negligible CO_2/ methanol conversion and DMC formation were observed after 24 h reaction in the absence of the catalysts. The three catalysts showed different activity in the order of: Ce_1-$Mn_{0.125}$ > Ce_1-$Mn_{0.25}$ > Ce_1-Mn_1. The Ce_1-$Mn_{0.125}$ catalyst exhibited the best catalytic activity as compared to other catalysts (2.272 mmol DMC/g cat for Ce_1-$Mn_{0.125}$ and 0.7411 mmol DMC/g cat of Ce_1-Mn_1). Higher acidic and basic properties of the catalyst are responsible for larger CO_2 conversion and DMC synthesis with Ce_1-$Mn_{0.125}$ catalyst. It can be seen from Figure 4.8.6b, that the catalytic activity of the catalysts was directly influenced by the acidic-basic properties.

Table.4.8.3. TPD analysis using absorbed CO_2 and NH_3 for determining basic and acidic properties of the synthesized catalysts.

Catalyst	**TPD analysis of absorbed CO_2 (mmol/g)**			**Total evolved CO_2 (mmol/g)**	**Basic site density (µmol/m^2)**
	Weak (< 200 °C)	Moderate (200-450 °C)	Strong (> 450 °C)		
Ce_1-$Mn_{0.125}$	0.868 (102)	-	-	0.868	8.95
Ce_1-$Mn_{0.25}$	0.508 (90)	0.01 (344)	-	0.518	5.343
Ce_1-Mn_1	0.235 (86)	0.0236 (210)	0.055 (564)	0.3135	3.199
Catalyst	**TPD analysis of absorbed NH_3 (mmol/g)**			**Total evolved NH_3 (mmol/g)**	**Acidic site density (µmol/m^2)**
	Weak (< 200 °C)	Moderate (200-450 °C)	Strong (> 450 °C)		
Ce_1-$Mn_{0.125}$	0.881 (110)	-	-	0.881	9.079
Ce_1-$Mn_{0.25}$	0.729 (106)	-	-	0.729	7.671
Ce_1-Mn_1	0.688 (108)	0.0296 (202)	0.025 (738)	0.7421	7.572

Temperature (°C) at maxima is given in brackets.

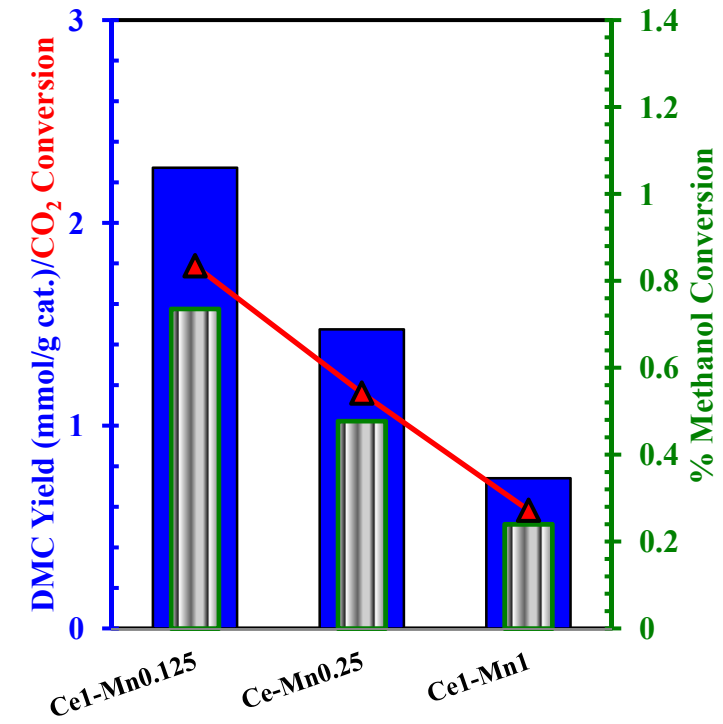

(a)

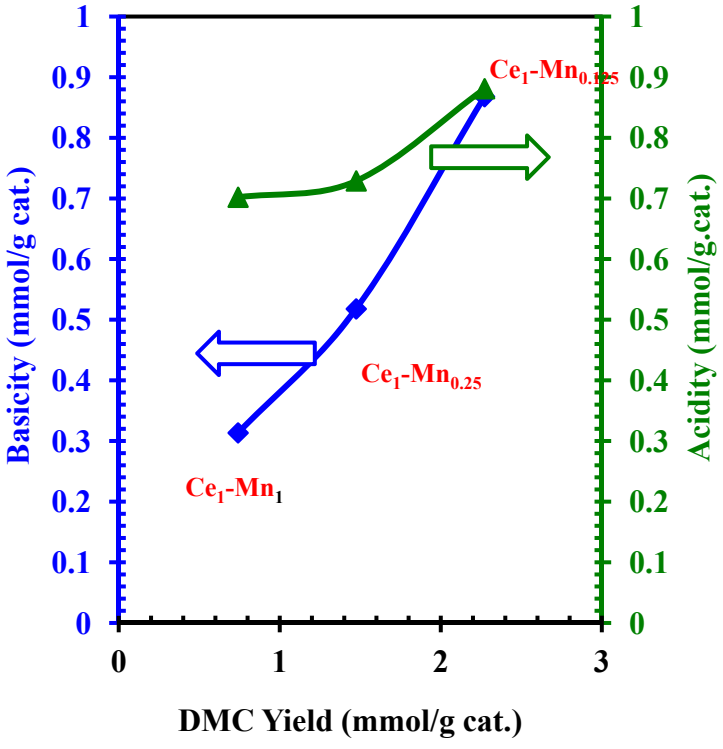

(b)

Figure 4.8.6. (a) CO_2/Methanol Conversion and DMC yield over Ce_1-$Mn_{0.125}$, Ce_1-$Mn_{0.25}$ and Ce_1-Mn_1 catalysts; DMC Yield (mmol/g cat.), % Methanol conversion, —▲— % CO_2 conversion. (b) Correlation between acidic-basic and catalytic activity of Ce_1-$Mn_{0.125}$, Ce_1-$Mn_{0.25}$ and Ce_1-Mn_1 catalysts; Reaction conditions: (Methanol=25.03 mL, catalyst dose=1.25 g, P=150 bar, T=120°C, t=24 h); —♦— Basicity, —▲— Acidity.

The reusability of Ce_1-$Mn_{0.125}$ catalyst was investigated for the direct conversion of CO_2 with methanol to form DMC with a optimum reaction conditions, catalyst dose=1.25 g, reaction pressure=150 bar, reaction temperature=120°C, and the reaction time=4 h. For this, the Ce_1-$Mn_{0.125}$ catalyst was used in five consecutive reactions (Figure 4.8.7). DMC yield and methanol conversion slightly decreased with an increase in the number of batch cycles. This slight loss of activity of Ce_1-$Mn_{0.125}$ catalyst may be due to the deposition on the active sites and the blockage of the pores due to reaction products.

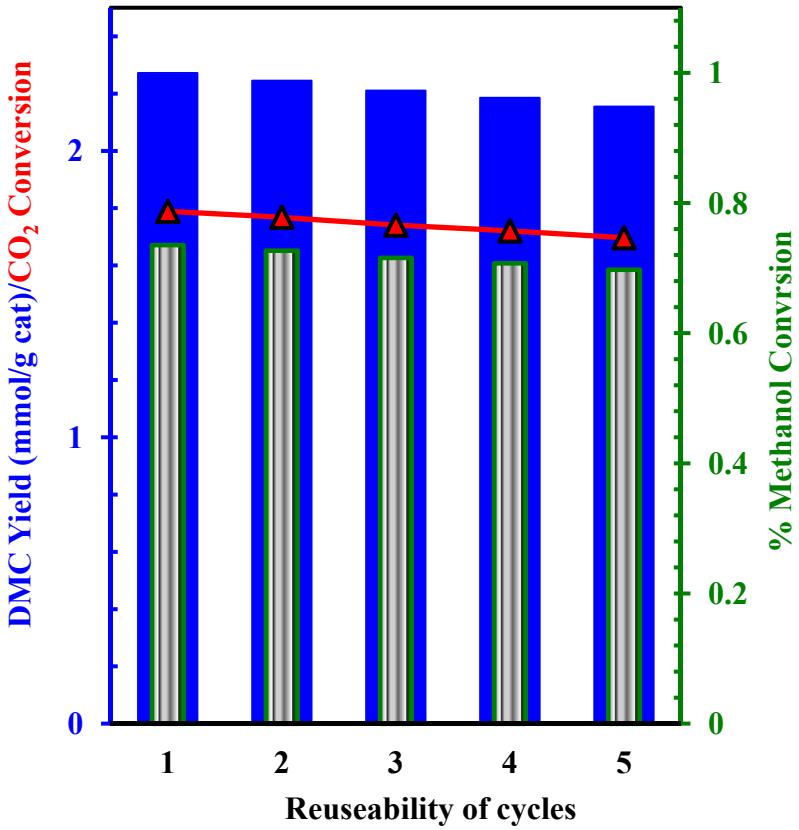

Figure 4.8.7. Reusability of Ce_1-$Mn_{0.125}$ catalyst DMC synthesis from direct conversion of CO_2 with methanol: (Methanol=25.03 mL, catalyst dose=1.25 g, P=150 bar, T=120°C, t=24 h). DMC Yield (mmol/g cat.), % Methanol conversion, —▲— % CO_2 conversion.

4.9. CERIA-CALCIUM OXIDE CATALYSTS: CHARACTERIZATION AND CATALYTIC ACTIVITY FOR DIRECT CONVERSION OF CO_2 WITH METHANOL TO DMC

Synthesis of DMC from the direct conversion of CO_2 with methanol was investigated with CeO_2-CaO_x composite catalysts prepared by the surfactant-template method.

4.9.1. Catalyst Characterization

4.9.1.1. X-ray diffraction

Figure 4.9.1 shows the XRD spectra of the synthesized Ce-Ca catalysts with varying molar ratio of Ce/Ca. Fluorite type phase of CeO_2 was observed in all the samples. Crystallite size was calculated according to Scherrer's equation and the values are given in Table 4.9.1. For the calculation of the crystallite size, the most intensive peak at 2θ=28.45 was chosen. It can be seen from Table 4.9.1, the Ce_3-Ca_1 has largest crystallite size (8.88 nm) and that Ce_1-Ca_3 has lowest crystallite size (6.85 nm). An increase in the Ce amount increases the crystallite size.

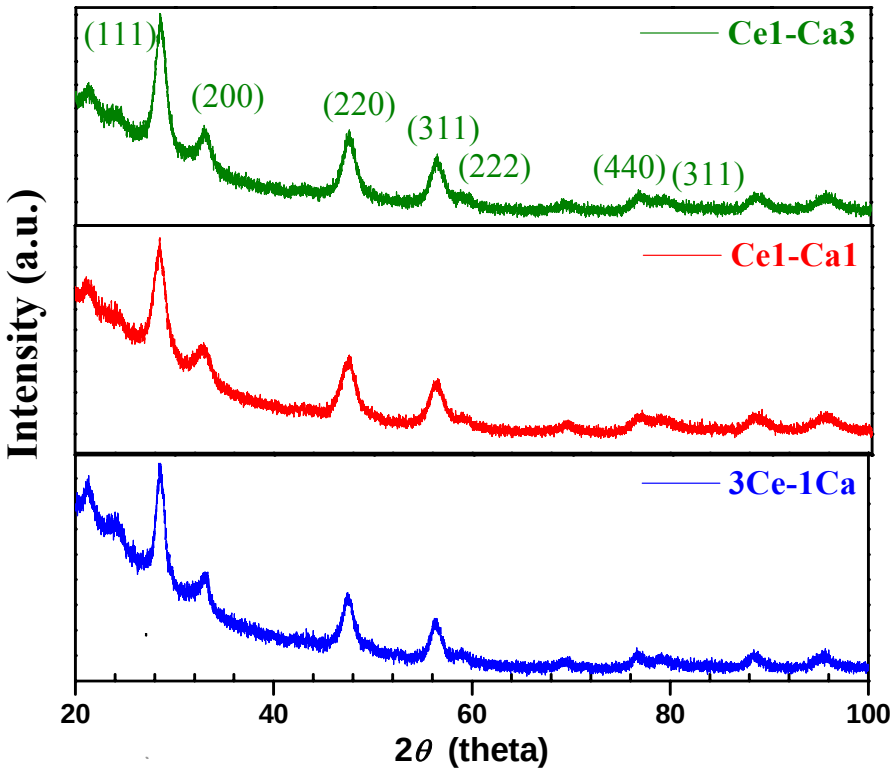

Figure 4.9.1. XRD spectra of the synthesized Ce-Ca catalysts.

4.9.2. Textural properties

Nitrogen sorption isotherms and particle size distribution of the catalysts are shown in Figure 4.9.2a and Figure 4.9.2b, respectively. Average specific surface area, pore volume and particle size diameter of the synthesized catalysts are given in Table 4.9.1. All catalysts showed stereo type VI isotherms according to IUPAC classification, and Ce_3-Ca_1 and Ce_1-Ca_1 with a H1 hysteresis loop and Ce_1-Ca_3 with H3 hysteresis loop were observed. Ce_1-Ca_3 is found to possess significantly different pore size distribution, as compared to Ce_1-Ca_1 and Ce_3-Ca_1. Due to the capillary condensation in the disordered pore structure, the adsorbed volume increases rapidly in the relative pressure (P/P_o) range of 0.4-0.95. BET surface area of Ce_1-Ca_3, Ce_1-Ca_1 and Ce_3-Ca_1 were found to be 109, 82 and 102 m^2/g, respectively, whereas BJH pore volumes were comparable, in the range of 0.17 to 0.26 cm^3/g. Thus, Ce_1-Ca_3 catalyst exhibited higher BET surface area as compared to Ce_3-Ca_1 and Ce_1-Ca_1 catalysts. Rodriguez et al. [2003], Yu et al. [2011] and Thitsartarn and Kawi [2011] reported BET surface area in the range of 78-130 m^2/g, 9-31 m^2/g and 12.6-25.7 m^2/g, respectively for Ce-Ca catalyst having different Ce/Ca ratio and prepared by using different methods.

Table. 4.9.1. Crystallite size, N2 sorption and acidic and basic properties of the catalysts

Catalysts Properties	Ce_3-Ca_1	Ce_1-Ca_1	Ce_1-Ca_3
Crystallite size (nm)[a]	8.80	7.02	6.85
Lattice constant d (nm)[a]	0.0165	0.0223	0.0202
BET surface area (m^2/g)	102	82	109
Specific pore volume (cm^3/g)[b]	0.26	0.25	0.17
Average Pore diameter (nm)[c]	9	12	5.0
CO_2 adsorption (mmol/g)[d]	0.883	2.277	0.835
Basic site density ($\mu mol/m^2$)	8.657	27.77	7.66
NH_3 adsorption (mmol/g)d	0.94	2.48	1.52
Acidic site density ($\mu mol/m^2$)	9.216	30.244	13.95

[a]The unit cell parameter, crystallite size is calculatedapplying the Scherrer equation.
[b]BJH desorption cumulative pore volume of pores in the range 1.7 to 300 nm.
[c]BJH desorption average pore diameter.
[d]CO_2 evolution during decomposition and maximum temperature given in brackets.
[e]CO_2-TPD values are calculated using the peak area at the maximum temperature given in brackets.
[f]NH_3-TPD values are calculated using the peak area at the maximum temperature given in brackets.

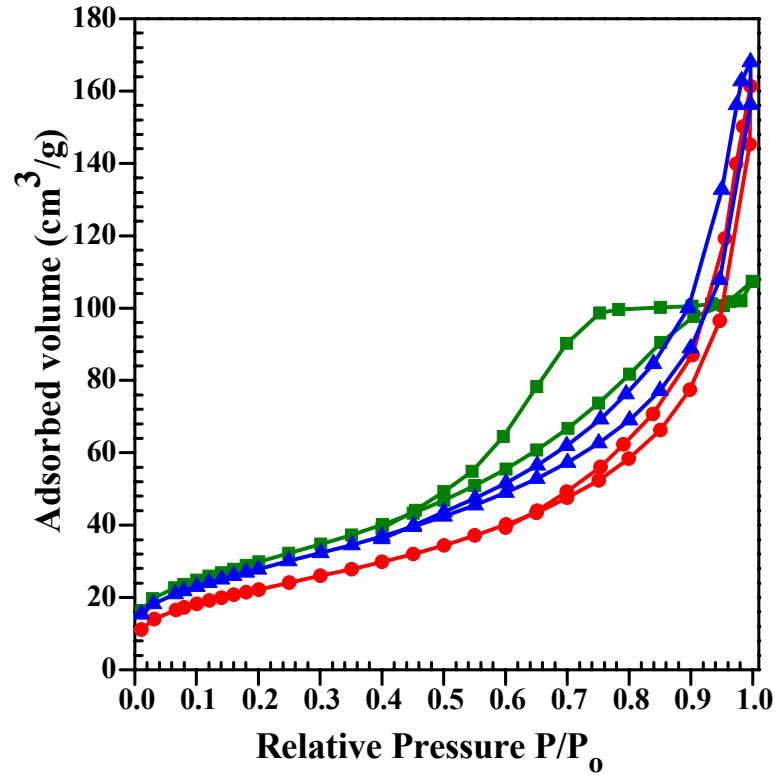

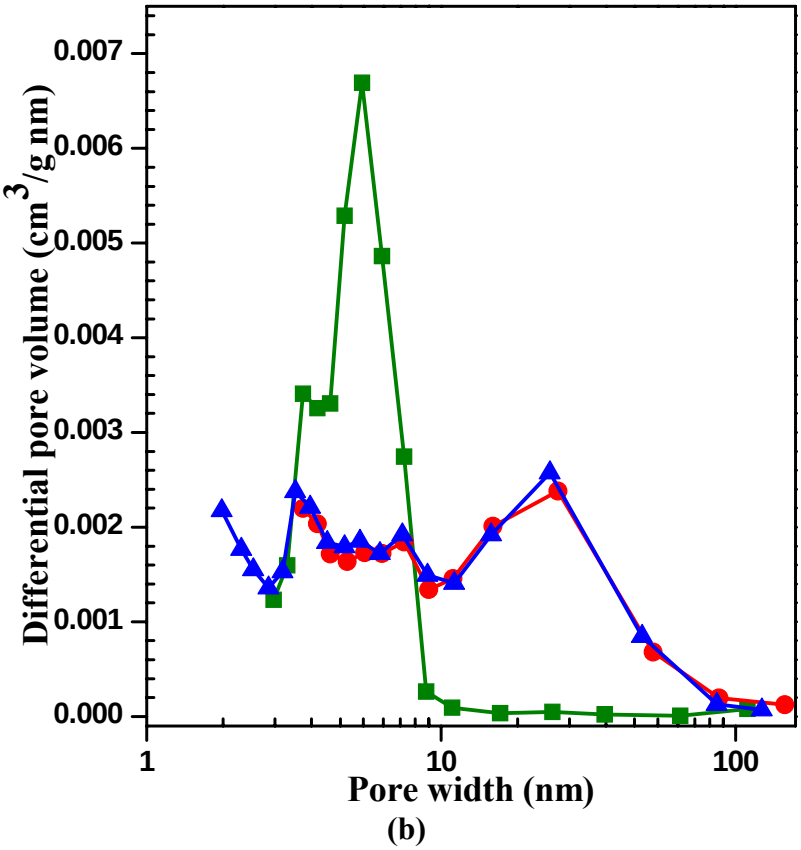

Figure 4.9.2. (a) N_2 sorption and, (b) Pore size distribution of Ce_3-Ca_1, Ce_1-Ca_1 and Ce_1-Ca_3 catalysts. —■— Ce_1-Ca_3, —●— Ce_1-Ca_1, —▲— Ce_3-Ca_1.

4.9.1.3. CO_2-TPD

CO_2-TPD profiles of the synthesized Ce_1-Ca_3, Ce_1-Ca_1 and Ce_3-Ca_1 catalysts are shown in Figure. 4.9.3a. The basic site densities of the catalysts were calculated from CO_2-TPD peak area and the results are shown in Table 2. Week basicity arises due to the interaction between CO_2 and the weak basic surface hydroxyl groups in the lower temperature range, and the strong basic sites arise due to CO_2 interaction between with low-coordination oxygen anions [Luo et al., 2013]. Week basic sites are found in all the catalysts. Ce_1-Ca_3, Ce_1-Ca_1 and Ce_3-Ca_1 catalysts show peaks in the weak region at 102°C, 116°C and 117°C, respectively. For Ce_1-Ca_3, Ce_1-Ca_1 and Ce_3-Ca_1 catalysts, total evolved CO_2 was 0.835 mmol/g , 2.277 mmol/g and 0.883 mmol/g, respectively, and the basic site density was 7.66 µmol/m^2, 27.77 and µmol/m^2, 8.657 µmol/m^2, respectively.

4.9.1.4. NH_3-TPD

Temperature programmed desorption of ammonia was studied in order to elucidate acidic surface properties of the catalysts and the results are shown in Figure 4.9.3b. The low temperature desorption peaks of ammonia indicate the presence of weak acidic sites in all the catalysts. The amount of the desorbed ammonia is shown in Table 4.9.2. Ce_1-Ca_1 catalyst is found to possess higher density of acid sites per unit mass as compared to Ce_1-Ca_3 and Ce_3-Ca_1 catalysts. According to the NH_3-TPD, Ce_1-Ca_3, Ce_1-Ca_1 and Ce_3-Ca_1 catalysts show total evolved NH_3 of 1.32 mmol/g, 2.48 mmol/g and 0.94 mmol/g, respectively and the acidic site density of 13.95 µmol/m^2, 30.24 µmol/m^2, 9.21 µmol/m^2, respectively. NH_3-TPD profile of the catalyst Ce_1-Ca_1 shows highest basic site density among all the synthesized catalysts.

4.9.1.5. Surface morphology

SEM micrographs (Figure 4.9.4) were taken in order to investigate the morphology and shape of the synthesized catalysts. All the catalysts showed the spherical morphology and with the average grain particle size to be in the range of 10–50 µm. An increase in the calcium content was found to effect a slightly increase in the size of the catalyst shown in the

TEM image (Figure 4.9.4). All the catalyst showed well homogenous dispersion of metals as was evident shows in the EDS elemental mapping (Figure 4.9.5).

4.9.2. Catalytic Activity

Figure 4.9.6 shows the methanol/CO_2 conversion and DMC yield for various Ce-Ca catalysts. The methanol/CO_2 conversion and the DMC formation in 48 h were found to be negligible in the absence of a catalyst. The three catalysts had their activity in the following order: Ce_1-Ca_1 > Ce_3-Ca_1 > Ce_1-Ca_3. Ce_1-Ca_1 catalyst exhibited highest catalytic activity as compared to Ce_1-Ca_1 and Ce_1-Ca_3 catalysts. The combination of textural, acidic and basic properties of Ce_1-Ca_1 catalyst effected larger CO_2/methanol conversion giving highest yield of DMC. When the catalyst Ce_1-Ca_1 was tested for a number of batch cycles, only a marginal loss of activity for methanol/CO_2 conversion and DMC formation was found. Figure 4.9.7 shows the activity of the catalyst for five consecutive runs carried out at a catalytic dose of 1.23 g, pressure P=150 bar and a temperature of 120°C for 24 h reaction time. The slight loss of activity can be ascribed to the blockage of pores due to the deposition of products during these runs.

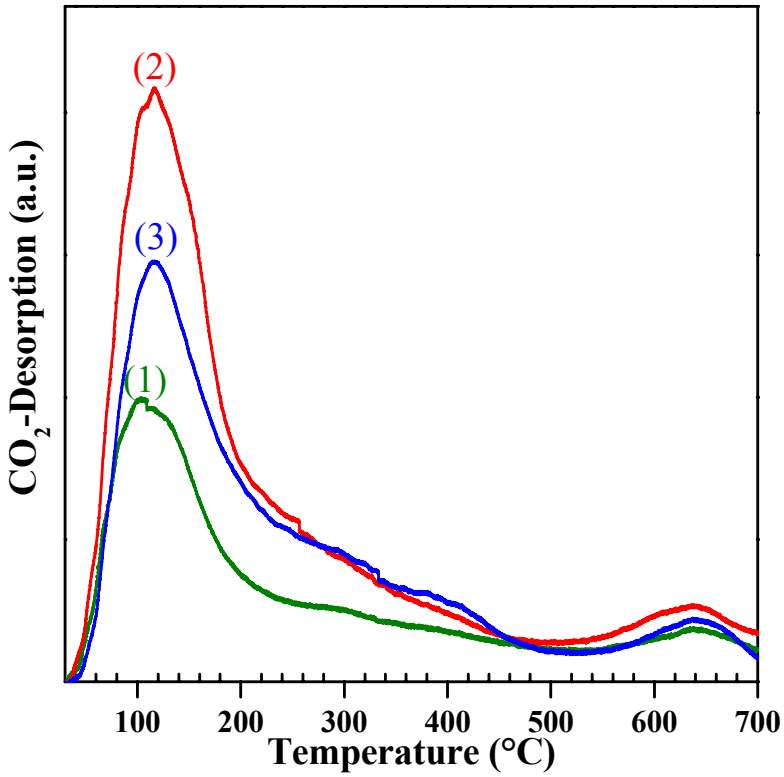

(a)

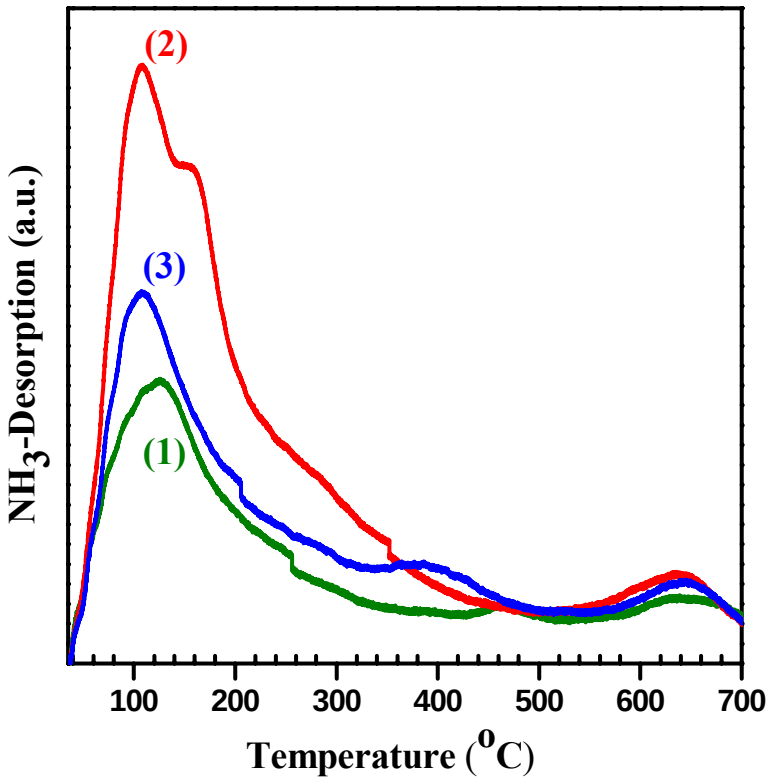

(b)

Figure 4.9.3. (a) CO_2-TPD and (b) NH_3-TPD plots for various Ce-Ca catalysts; (1) Ce_1-Ca_3, (2) Ce_1-Ca_1, and (3) Ce_3-Ca_1.

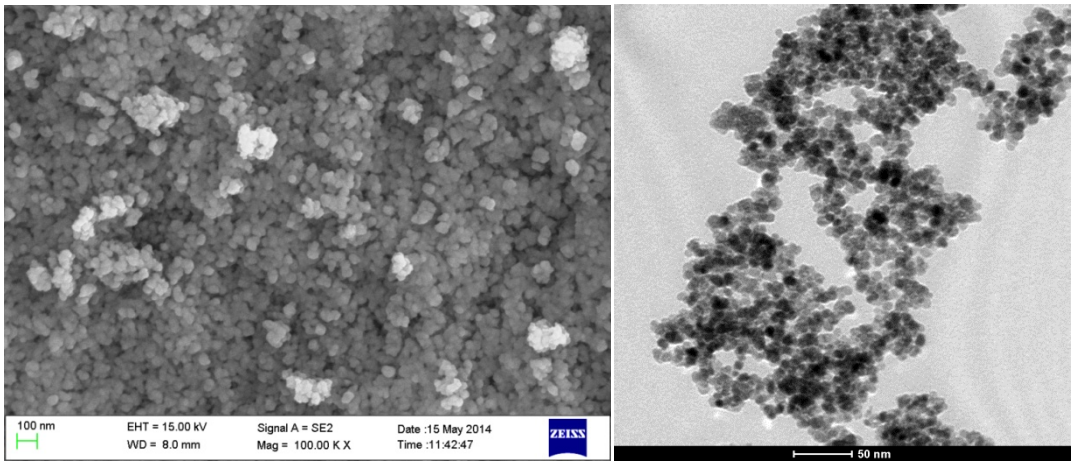

Ce1-Ca3

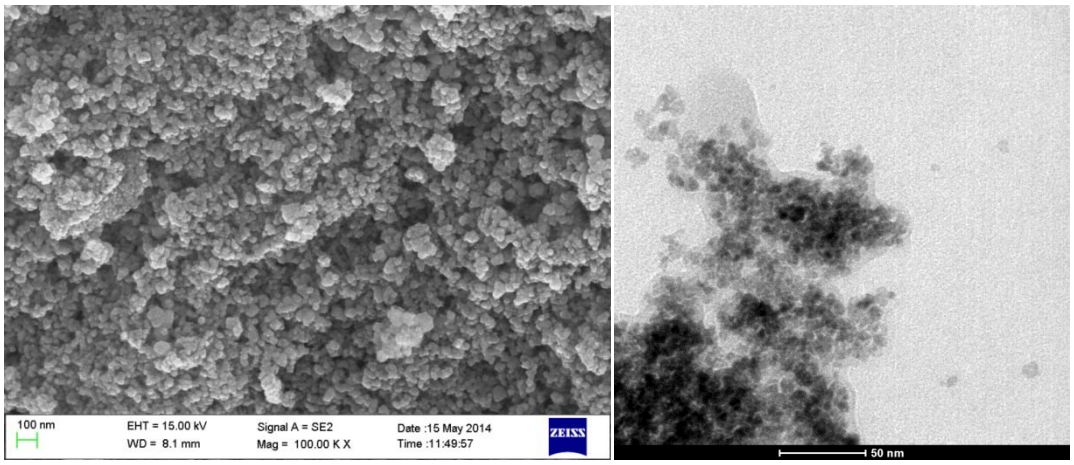

Ce1-Ca1

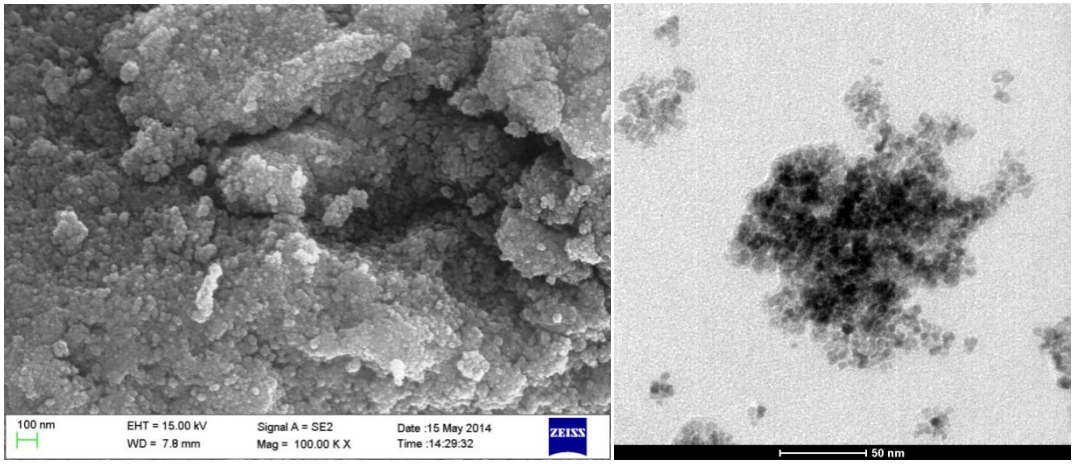

Ce3-Ca1

Figure 4.9.4 SEM and TEM micrographs of the Ce_3-Ca_1, Ce_1-Ca_1 and Ce_1-Ca_3 catalysts.

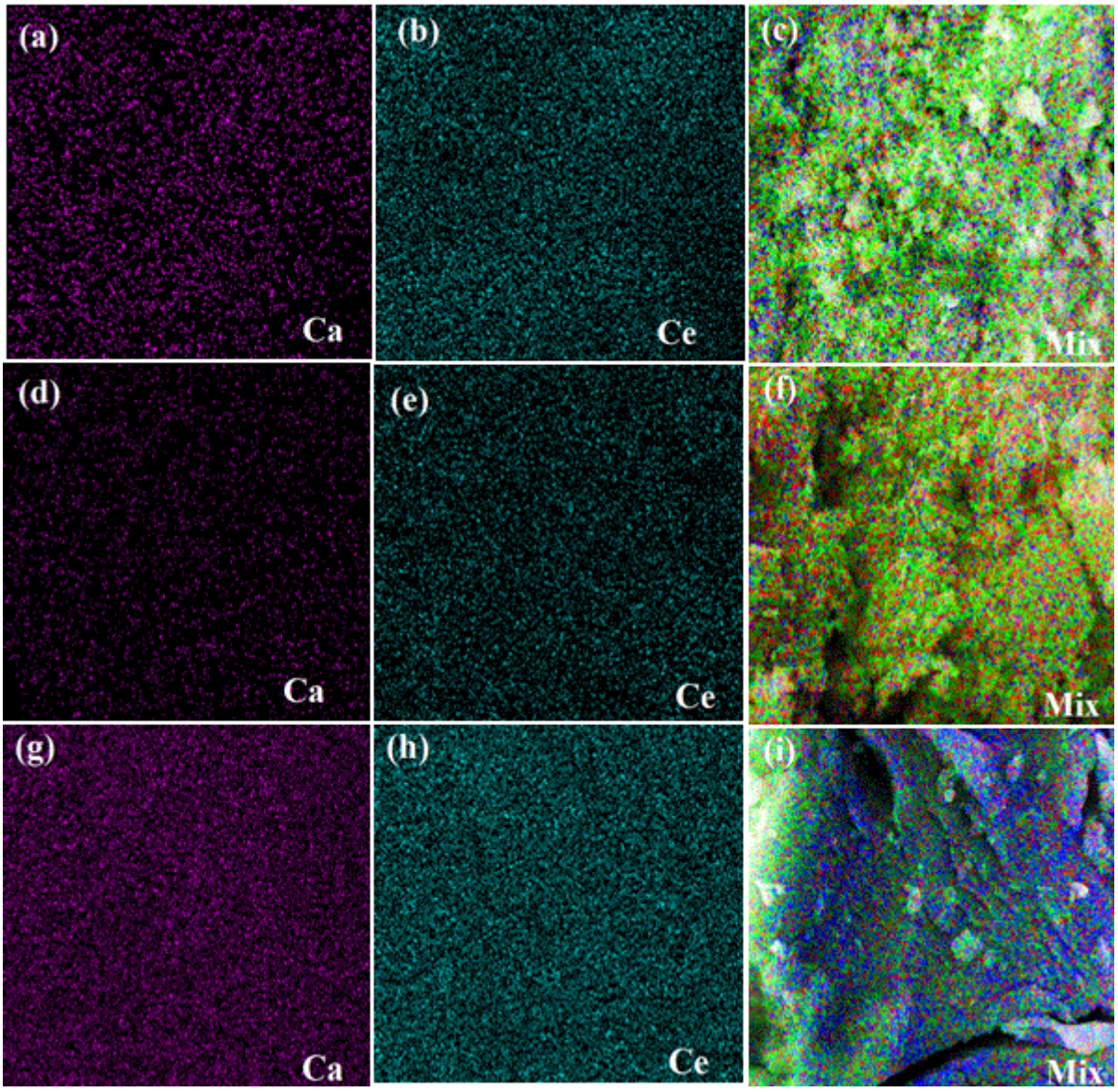

Figure 4.9.5. EDX elemental mapping of Ce_1-Ca_3 (a-c), Ce_1-Ca_1 (d-f) and Ce_3-Ca_1 (g-i).

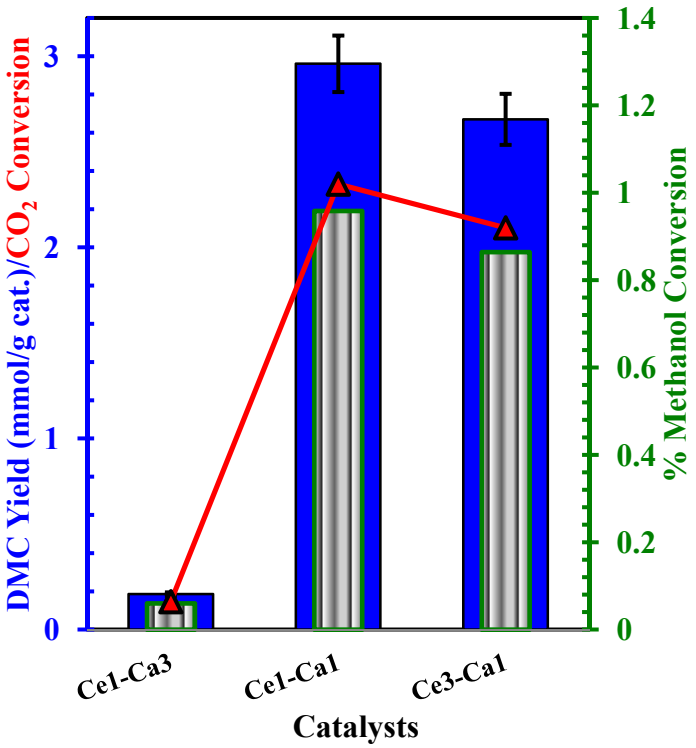

Figure 4.9.6. Catalytic activity of Ce_1-Ca_3, Ce_1-Ca_1, Ce_3-Ca_1 for DMC synthesis; DMC Yield (mmol/g cat.), % Methanol conversion, —▲— % CO_2 conversion.

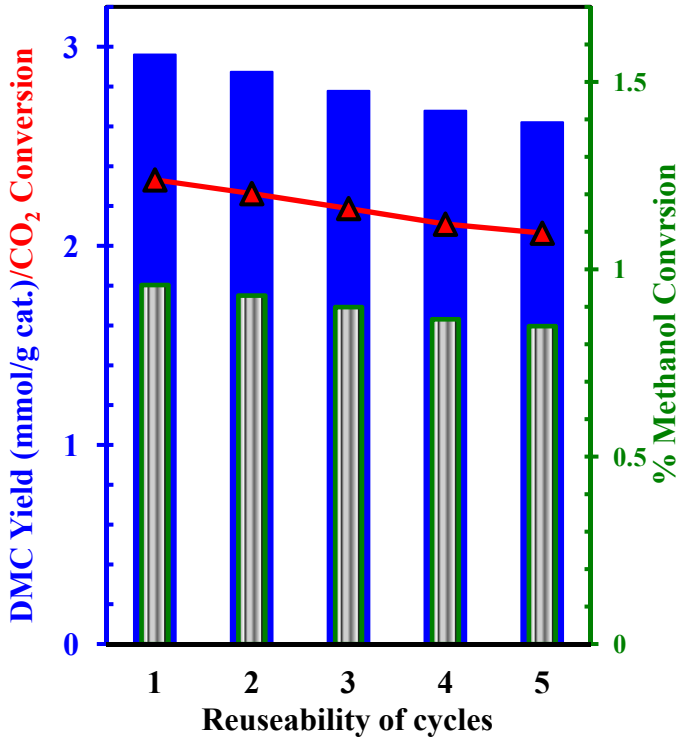

Figure 4.9.7. Reusability runs over 5 batch cycles for the Ce_1-Ca_1 catalyst; DMC Yield (mmol/g cat.), % Methanol conversion, —▲— % CO_2 conversion.

4.10. MECHANISM, KINETICS AND THERMODYNAMICS OF DIRECT CO_2 CONVERSION TO DMC

4.10.1 Mechanism

In the presence of a suitable catalyst ($Ce_{0.5}Zr_{0.5}O_2$, $CeZrO_2$, Ce_1-$Mn_{0.125}$ and Ce_1-Ca_1 in the present study), methanol is activated to form CH_3O^- and H^+. This activation depends upon the quantity of acidic and basic sites present on the surface of the catalysts. Methoxy species (CH_3O^-) reacts with CO_2 in the presence of basic site to form methoxyl carbonyl ions. Methanol at the acidic site forms CH_3^+ and OH^- ions. Methoxyl carbonyl ion reacts with CH_3^+ to form DMC, and OH^- reacts with H^+ to form water. As such, higher basicity and acidity in the catalysts facilitates DMC synthesis from CO_2 and methanol [La et al., 2007]. Reaction mechanism for DMC synthesis from direct conversion of CO_2 with methanol in the presence of catalyst is shown in Figure 4.10.1.

The relationship between acidic-basic properties and the activity of CeO_2, $Ce_{0.5}Zr_{0.5}O_2$ and ZrO_2 catalysts are shown in Figure 4.6.6b (and for other catalysts as observed and discussed in various sections). It can be seen that the acidic and basic properties directly influence the catalytic activity of DMC synthesis. Therefore, $Ce_{0.5}Zr_{0.5}O_2$, $CeZrO_2$, Ce_1-$Mn_{0.125}$ and Ce_1-Ca_1 catalysts which exhibit high basicity and acidity showed the best catalytic activity.

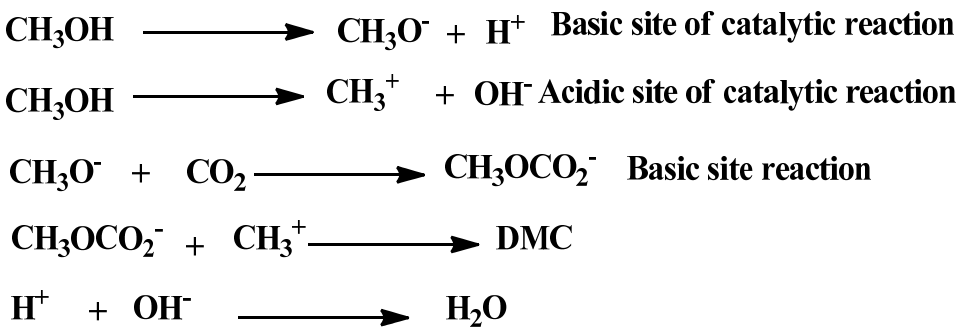

Figure 4.10.1. Mechanism of DMC synthesis from direct conversion of CO_2 and methanol.

4.10.2. Thermodynamics

4.10.2.1. Basic thermodynamic evaluation

The reaction of carbon dioxide and methanol to form DMC can be written as follows:

$$2\ CH_3OH + CO_2 \leftrightarrow DMC + H_2O \qquad (4.10.1)$$

Thermodynamic data on the change in heat of formation (ΔH_f^o), change in Gibbs function (ΔG_f^o) and heat capacity at constant pressure (C_p) of CO_2, methanol, DMC and H_2O for both gas and liquid phases are available in the literature and are compiled in Table 4.10.1 [Cai et al., 2009; Lide, 2010; Bustamante et al., 2012; Hofmann et al., 2012]. For the direct conversion of CO_2 and methanol carried out in the gaseous phase, the heat of reaction (ΔH_r^o) and Gibbs free energy change (ΔG_r^o) at 298 K were calculated using the stoichiometric coefficients, and ΔH_f^o and ΔG_f^o of the reactants and the products and were found to be −17.29 kJ/mol and 23.53 kJ/mol, respectively [Bustamante et al., 2012]. Similarly, for the reaction carried out at 298 K with methanol, DMC and H_2O being in the liquid phase and CO_2 being in the gaseous phase, the values of ΔH_r^o and ΔG_r^o are calculated as −27.90 kJ/mol and 26.21 kJ/mol, respectively [Cai et al., 2009]. These values indicate that both the gaseous and liquid phase reactions at room temperature (298 K) are exothermic and non-spontaneous.

Table 4.10.1. Thermodynamic data of pure substances involved in the direct synthesis of DMC from CO_2 and methanol.

Species	ΔH_f^o (kJ/mol)		ΔG_f^o (kJ/mol)		S^o (J/mol K)	C_p (J/mol K)[a]	
	Gas	Liquid	Gas	Liquid	Gas	Gas	Liquid
Methanol	−201	−239.10	−162.3	−166.6	239.9	44.1	81.59
CO_2	−393.51		−394.38	−	213.8	37.1	
H_2O	−241.8	−285.83	−228.6	−237.14	188.8	33.6	75.30
DMC	−571.0	−613.78	−466.85[b]	−464.23	366.01	128.12[b]	109.50

[a] Average between 298 and 500 K.

For avoiding temperature dependence of C_p, an average value of C_p over a temperature range of 273 - 400 K was taken. Then the equation for ΔH_r^o dependence on T can be written using Kirchhoff's law as:

$$\Delta H_{r,T}^o = \Delta H_{r,298}^o + C_p(T\text{-}298) = \text{-}23.29 - 0.0155T \qquad (4.10.2)$$

Above equation shows that ΔH_r^o becomes more negative when the temperature is increased. ΔG_r^o at different temperatures can be expressed by means of Gibb's–Helmholtz equation [Cai et al., 2009; Maqbool et al., 2011]:

$$d\left(\frac{\Delta G_r^o}{T}\right) = \left[\frac{23.29 + 0.0155T}{T^2}\right] dT \qquad (4.10.3)$$

On integrating both sides of the above equation, one gets following equation:

$$\Delta G_{r,T}^o = \frac{T\Delta G_{r,298K}^o}{298} - 23.29\left(\frac{1}{T} - \frac{1}{298}\right)T + 0.0155\,T\ln\left(\frac{T}{298}\right) \qquad (4.10.4)$$

This equation shows that the value of $\Delta G_{r,T}^o$ increases with an increase in T. For example, when the reaction temperature reaches to 393 K, $\Delta G_{r,393}^o$ becomes 43.65 kJ/mol in comparison to its value of 23.53 kJ/mol at 298 k. Thus, an increase in T is disadvantageous to the formation of DMC in terms of thermodynamics.

Since, dG=VdP – SdT, therefore, d(ΔG)=(ΔV) dP − (ΔS) dT. Assuming CO_2 to be an ideal gas, the $\Delta G_{r,T}$ with a change in pressure but at a constant temperature, can be written as:

$$d\left(\Delta G_{r,T}\right) = \Delta V\, dP = \left(V_l - V_g\right)dP = -V_g\, dP = -\left(RT/P\right)dP \qquad (4.10.5)$$

Since the volume of the gaseous reactant is very large than those of liquid $V_g >> V_l$, therefore, $\Delta V \approx -V_g$. By integrating both sides at constant T, one gets the following equation:

$$\Delta G_{r,P} = \Delta G_{r,P}^o - RT\ln\left(P/P^o\right) \qquad (4.10.6)$$

At 393 K, $\Delta G_{r,P} \leq 0$ for $P \geq 6.3\times10^4$ MPa. Therefore, the DMC synthesis from CO_2 and methanol at 393 K becomes spontaneous at $P \geq 6.3\times10^4$ MPa which is very difficult to achieve.

4.10.2.2. Chemical equilibrium modeling

For the direct synthesis of DMC, equilibrium conversion can be related to the equilibrium constant as shown below:

$$K_{eq}(T) = \frac{a_{DMC}a_{H_2O}}{a^2_{MeOH}a_{CO_2}}$$

$$= \frac{\frac{1}{2}X^2_{eq,MeOH}\left(1\text{-}0.5y_{MeOH,0}X_{eq,MeOH}\right)}{y_{MeOH,o}\left(1\text{-}X_{eq}\right)^2\left(\Theta_{CO_2}\text{-}\frac{1}{2}X_{eq}\right)} \times \left(\frac{\varphi_{DMC}\varphi_{H_2O}}{(\varphi_{MeOH})^2\varphi_{CO_2}}\right)_{eq}\left(\frac{(\varphi^0_{MeOH})^2\varphi^0_{CO_2}}{\varphi^0_{DMC}\varphi^0_{H_2O}}\right)\left(\frac{P^0}{P}\right) \quad (4.10.7)$$

where, $\Theta_{CO_2} = y_{CO_2,0}/y_{MeOH,o}$. The Peng–Robinson–Stryjek–Vera equation of state (PRSV-EoS) [Stryjek and Vera, 1986] along with the van der Waals one-fluid (1PVDW) mixing rule [Pinero et al., 2007], were used to calculate the rules fugacity coefficient of species in the mixture. PRSV-EoS is given as:

$$P = \frac{RT}{V-b} - \frac{a\alpha(T)}{V(V+b)+b(V-b)} \quad (4.10.8)$$

where,

$$a = 0.45724\ R^2T_c^2/P_c \quad (4.10.9)$$

$$b = 0.07780\ RT_c/P_c \quad (4.10.10)$$

$$\alpha = \left[1+m(\omega)\left(1-T_r^{1/2}\right)\right]^2 \quad (4.10.11)$$

$$m(\omega) = \kappa_0 + \kappa_1\left(1+T_r^{1/2}\right)\left(0.7-T_r\right) \quad (4.10.12)$$

$$\kappa_0 = 0.378893 + 1.4897153\omega - 0.1713184\omega^2 + 0.0196554\omega^3 \quad (4.10.13)$$

where, T_c and P_c are the critical temperature and pressure, respectively, ω is the accentric factor and κ is a specific pure compound parameter. The values of T_c, P_c, ω and κ as obtained from the literature are compiled in Table 4.10.2. van der Waals One- Fluid Model (1PVDW) gives the following sets of equations which were used to obtain data of the quadratic mixture:

$$a = \sum_i \sum_j y_i y_j \left(1 - k_{ij}\right)\left(a_i a_j\right)^{1/2} \tag{4.10.14}$$

$$b = \sum_i \sum_j y_i y_j \left(1 - l_{ij}\right)\left(\frac{b_i + b_j}{2}\right) \tag{4.10.15}$$

where, k_{ij} and l_{ij} are the single binary interaction parameters which are used to calculate the mixture parameters a, and b in the PRSV-EOS. Values of k_{ij} and l_{ij} were obtained from the literature and are given in Table 4.10.3.

Table 4.10.2. **Physical properties and the pure components parameters [Piñeroa et al., 2007].**

	CO_2	Methanol	DMC	H_2O
MW (g/mol)	44.01	32.042	90.60	18.02
T_c (K)	304.2	512.6	548.0	647.3
P_c (MPa)	7.382	8.096	4.500	22.09
ω	0.225	0.565	0.385	0.344
κ	0.04285	-0.16816	0.38462	-0.06635

Table 4.10.3. Temperature dependence of binary interaction parameters k_{ij} and l_{ij} [Bustamante et al., 2012].

System	k_{ij}	l_{ij}
CO_2 (1) +	k_{12}=−0.04889 + 0.000142 T	l_{12}=0.11655 − 0.00049 T
methanol (2)	k_{21}=−0.32186 + 0.001202 T	l_{21}=0.0034067 − 3×10^{-5} T
CO_2 (1) +	k_{12}=3.06296 − 0.009680 T	l_{12}=0
water (2)	k_{21}=−0.35981 + 0.000859 T	l_{21}=0
CO_2 (1) +	k_{12}=−0.00432 + 0.000010 T	l_{12}=8.2567×10^{-5} + 1.47×10^{-6} T
DMC (2)	k_{21}=−0.03110 + 0.000080T	l_{21}=0.0002787 − 2.67×10^{-6} T
methanol (1)	$k_{12=}$−0.61880 + 0.001570 T	l_{12}=0
+ water (2)	k_{21}=−0.39211 + 0.000815 T	l_{21} =0
DMC (1) +	k_{12}=−0.03545 + 0.000282 T	l_{12}=0
methanol (2)	k_{21}=0.03595 − 0.000035 T	l_{21} =0
DMC (1) +	k_{12}=−0.34043	l_{12}=-9.22×10^{-5}
water (2) a	k21=−0.0796	l_{21}=1.942×10^{-4}

Equations 4.10.7 to 4.10.15 were solved simultaneously using the parameters given in the Tables 4.10.2 and Tables 4.10.3 to calculate the values of K_{eq} at various temperatures and pressures for different catalysts. The values K_{eq} along with the operating conditions are given in Tables 4.10.4 and Tables 4.10.5.

Assuming that the heat of reaction ΔH_r^o is constant within the temperature range of 100-180°C, the equilibrium constant K_{eq} can be related to the T by the classical van't Hoff equation:

$$\ln K_{eq,T} = -\frac{\Delta H_r^o}{RT} + \left(\frac{\Delta H_r^o - \Delta G_r^o}{RT^o} \right) \qquad (4.10.16)$$

The values of ΔH_r^o and ΔG_r^o for $Ce_{0.5}Zr_{0.5}O_2$ (hydrothermal method) using the data points at T=120-160°C were found to be -45.66 kJ/mol and 25.04 kJ/mol, respectively. Similarly, for $Ce_{0.5}Zr_{0.5}O_2$ (templating method), the respective values were found to be -139.76 kJ/mol and 1.54 kJ/mol, respectively.

4.10.3. Comparative Analysis

Table 4.10.5 compares the textural and acidic-basic properties and the % CO_2 conversion and the DMC yield at P=150 bar and T=393 K. It may be seen that within different sets of catalyst, catalysts which exhibited higher acidity and basicity like $Ce_{0.5}Zr_{0.5}O_2$ (by hydrothermal and carbon templating methods), Ce_1-$Mn_{0.125}$ and Ce_1-Ca_1, showed better CO_2 conversion and DMC yield. Overall Ce_1-Ca_1 prepared by the surfactant templating method exhibited highest basicity, acidity and catalytic activity in terms of % CO_2 conversion and DMC yield.

Table 4.10.4. Values of K_{eq} for DMC synthesis by direct CO_2 conversion using $Ce_{0.5}Zr_{0.5}O_2$ catalyst prepared by hydrothermal and templating methods at different temperatures and a constant pressure, P=150 bar.

T (K)	$y_{o,MeOH}$	$y_{o,CO2}$	$X_{eq,MeOH,experimental}$	$y_{eq,MeOH}$	$y_{eq,CO2}$	$y_{eq,DMC}$	$y_{eq,H2O}$	K_{eq} (l/mol)
	$Ce_{0.5}Zr_{0.5}O_2$ (hydrothermal method)							
353	0.686055	0.313945	0.00330459	0.684985	0.313975	0.000519638	0.000519638	3.930×10^{-8}
373	0.697797	0.302203	0.0072792	0.695485	0.302307	0.001104294	0.001104294	2.221×10^{-7}
393	0.708692	0.291308	0.00945482	0.705748	0.291483	0.001384505	0.001384505	4.313×10^{-7}
413	0.718828	0.281172	0.00687782	0.716735	0.281324	0.000970785	0.000970785	2.608×10^{-7}
433	0.728283	0.271717	0.0050323	0.726785	0.271843	0.000685724	0.000685724	1.620×10^{-7}
453	0.737123	0.262877	0.00288836	0.736282	0.262957	0.000380307	0.000380307	6.370×10^{-8}
	$Ce_{0.5}Zr_{0.5}O_2$ (templating method)							
373	0.697797	0.302203	0.004043	0.696515	0.302261	0.000612258	0.000612258	6.811×10^{-8}
393	0.708692	0.291308	0.008680	0.705990	0.291469	0.001270488	0.001270488	3.629×10^{-7}
413	0.718828	0.281172	0.0055832	0.717130	0.281295	0.000787461	0.000787461	1.713×10^{-7}
433	0.728283	0.271717	0.0016944	0.727780	0.271759	0.000230430	0.000230430	1.823×10^{-8}
453	0.737123	0.262877	0.0004182	0.737002	0.262888	0.000054981	0.000054981	1.327×10^{-9}

Table 4.10.5. Values of K_{eq} for DMC synthesis by direct CO_2 reaction using various catalysts at P=150 bar, T= 393 K, Initial feed (Y_{MeOH})=0.708691585, Initial feed (Y_{CO2})= 0.29131.

Catalyst	$X_{eq,MeOH,experimental}$	$y_{eq,MeOH}$	$y_{eq,CO2}$	$y_{eq,DMC}$	$y_{eq,H2O}$	K_{eq} (l/mol)
Ceria	0.00660	0.70664	0.29143	0.0009655	0.0009655	3.565×10^{-7}
$Ce_{0.5}Zr_{0.5}O_2$	0.00864	0.70600	0.29147	0.0012651	0.0012651	6.124×10^{-7}
Zirconium	0.00148	0.70823	0.29134	0.0002152	0.0002152	1.752×10^{-8}
1Ce-3Ca	0.00060	0.70851	0.29132	0.0000876	0.0000876	2.901×10^{-9}
1Ce-1Ca	0.00958	0.70571	0.29149	0.0014035	0.0014035	7.541×10^{-7}
3Ce-1Ca	0.00864	0.70600	0.29147	0.0012649	0.0012649	6.124×10^{-7}
Ce_1-$Mn_{0.125}$	0.00735	0.70640	0.29144	0.0010755	0.0010755	4.421×10^{-7}
Ce_1-$Mn_{0.25}$	0.00477	0.70721	0.29140	0.0006971	0.0006971	1.852×10^{-7}
Ce_1-Mn_1	0.00240	0.70795	0.29135	0.0003499	0.0003499	4.652×10^{-8}
$C_{0.5}Zr_{0.5}O_2$	0.00945	0.70575	0.29148	0.0013845	0.0013845	7.341×10^{-7}
CeO_2	0.00448	0.70730	0.29139	0.0006541	0.0006541	1.632×10^{-7}

Table 4.10.6. Comparative analysis of properties and catalytic activity of various catalysts used for direct conversion of CO_2 to DMC.

Catalyst	Method of Preparation	Textural Properties			CO_2 & NH_3- TPD			% CO_2 conversion	DMC Yield (mmol/g)
		Surface Area (m^2/g)	Pore volume (cm^3/g)	Pore size (nm)	Total CO_2 adsorption (mmol/g)	Basic site density ($\mu mol/m^2$)	Total NH_3 adsorption (mmol/g)		
CeO_2	HT	87	0.12	4.52	0.42	4.72	0.79	1.82	2.04
$Ce_{0.5}Zr_{0.5}O_2$	HT	117	0.23	8.40	0.65	5.55	1.89	1.38	2.67
ZrO_2	HT	70	0.20	7.89	0.25	3.58	0.51	0.31	0.45
ZrO_2	CT	112	0.42	15.4	0.40	3.89	1.52	0.62	0.91
$Ce_{0.5}Zr_{0.5}O_2$	CT	123	0.4	11.9	1.93	15.69	2.48	1.98	2.92
CeO_2	CT	28	0.2	30.4	0.41	14.64	0.94	0.94	1.38
Ce_1-$Mn_{0.125}$	ST	97	0.39	9	0.86	8.95	0.88	1.79	2.27
Ce_1-$Mn_{0.25}$	ST	95	0.5	19	0.51	5.34	0.72	1.16	1.47
Ce_1-Mn_1	ST	98	0.43	14	0.31	3.19	0.70	0.55	0.74
Ce_1-Ca_3	ST	109	0.17	5	0.83	7.66	1.52	0.15	0.18
Ce_1-Ca_1	ST	82	0.25	12	2.27	27.77	2.48	2.33	2.96
Ce_3-Ca_1	ST	102	0.26	9	0.88	8.65	0.94	2.10	2.67

CT: Carbon Templating, HT: Hydrothermal; ST: Surfactant Templating.

CONCLUSIONS AND RECOMMENDATIONS

5.1 CONCLUSIONS

On the basis of results and discussion presented in chapter 4 for the dimethyl carbonate (DMC) synthesis from transesterification propylene carbonate (PC) with methanol and direct conversion of CO_2 with methanol, following major conclusions can be drawn for various sections of studies performed in the present work:

5.1.1. DMC Synthesis using Transesterification of PC with Methanol

5.1.1.1 Ce-M (M=Co, Fe, Cu and Zn) catalysts

- BET surface area of CeCo, CeCu, CeFe and CeZn catalysts synthesized by sol-gel method was found to be 40, 46, 24, and 37 m^2/g, respectively. CeCu catalyst having highest basicity was found to be most effective during transesterification of PC to form DMC.
- Highest DMC yield of 71.9% and PC conversion of 65.4% was obtained with CeCu catalyst at optimum reaction conditions of reaction temperature=160°C, reaction time = 4 h, catalyst dose=5 wt.% of PC and methanol/PC molar ratio =10.

5.1.1.2 Ceria-lanthanum mixed metal oxide i.e. $Ce_xLa_{1-x}O_{2-\delta}$

- A series of cerium-lanthanum catalysts prepared using co-precipitation method and characterized by various techniques have been tested for the transesterification.
- Total amount of NH_3 desorbed from the $Ce_{0.2}La_{0.8}$, $Ce_{0.4}La_{0.6}$, $Ce_{0.6}La_{0.4}$, and $Ce_{0.8}La_{0.2}$ catalyst was 7.53, 5.85, 4.18 and 2.17 mmol/g, respectively. Respective value of acid site density was: 0.184, 0.139, 0.069 and 0.044 $mmol/m^2$.
- Activity of synthesized catalysts increased with an increase in lanthanum content in the catalysts. Also, transesterification of PC with methanol parallels the bifunctional nature (basic and acidic nature) of the catalysts and that catalytic activity, basic site density, acidic site density and amount of weak acidic sites (in the desorption temperature range of 100-200°C) follow the same order: $Ce_{0.8}La_{0.2} < Ce_{0.6}La_{0.4} < Ce_{0.4}La_{0.6} < Ce_{0.2}La_{0.8}$.
- DMC yield of 74%, PG yield of 65% and PC conversion of 72% was obtained with $Ce_{0.2}$-$La_{0.8}$ catalyst at optimum reaction conditions of reaction temperature=170°C, reaction time=6 h and methanol/PC molar ratio=10.

5.1.1.3. Ceria–zinc catalysts impregnated onto various oxide supports, namely Al_2O_3, SiO_2 and TiO_2 (named as CZA, CZS and CZT)

- In the present study, ceria and zinc oxide catalyst were impregnated onto various oxide supports, namely Al_2O_3, TiO_2 and SiO_2, individually by deposition-coprecipitation method and characterized by various techniques and evaluated for transesterification reaction. Variation of support not only changed the structure and textural properties of the catalyst but also the basic strength and basic sites of the catalyst.
- Composite oxides (catalysts) were found to contain individual phases of ZnO, CeO_2 and some spinel forms of Zn, Ce along with their supports. CZS having highest basicity and surface area showed better catalytic activity as compared to CZA and CZT.
- CZS catalysts were found to possess higher catalytic activity due to high basic strength and high BET surface area in comparison to CZA and CZT catalysts.
- DMC yield of 77% was observed with CZS catalyst under optimal conditions (temperature = 170 ^{o}C and methanol/PC molar ratio = 1:10).

5.1.1.4. Copper-zinc-aluminum (CZA) hydrotalcite (HTLc) catalysts calcined at 300^{o}C, 500^{o}C and 800^{o}C (named as CZA300, CZA500 and CZA800)

- Cu-Zn-Al (CZA) hydrotalcite catalysts prepared by the co-precipitation method and calcined at 300^{o}C, 500^{o}C and 800^{o}C (named as CZA300, CZA500 and CZA800) were physico-chemical Characterization and use for synthesis of DMC.
- The activity of the CZA300 catalyst was found to be better as compared CZA500 and CZA800 catalysts due to the highest amount of basic sites and acidic sites. Transesterification of PC with methanol paralleled the amount of basic site density and acidic site density and increased in the same order.
- PC conversion of 70% and DMC selectivity of 94% was observed at the optimum operating condition of reaction time=4 h, methanol/PC molar ratio=10, catalyst dose=3 wt.% of PC and temperature=160 $^{\circ}$C.
- Values of specific rate of reaction with CZA300 catalysts at 120, 140 and 160 °C were found to be 0.56, 0.58 and 0.65 h^{-1}, respectively.

5.1.1.5. Comparative Assessment

Table 4.5.1 summarizes the optimum reaction parameters during transesterification of PC with methanol reaction by Ce-M (M=Co, Fe, Cu and Zn), Ceria-Lanthanum, Ceria-Zinc-support mixed metal oxide and copper-zinc-aluminum hydrotalcite catalysts. Values of the frequency factor (k_o) and the activation energy (E_a) were found to be 0.375 h^{-1} and 2.294

kJ/mol for CeCu catalyst, whereas respective values for CZA300 catalyst were found to be 0.225 h^{-1} and 12.72 kJ/mol. Overall, $Ce_{0.2}$-$La_{0.8}$ and Ce-Zn/SiO_2 were found to be the best catalysts for DMC production via transesterification of PC with methanol.

5.1.2. DMC Synthesis from Direct Conversion of CO_2 with methanol

5.1.2.1. Ceria-zirconium based catalysts (prepared by hydrothermal method)

- In this study, ceria-zirconia based catalysts (CeO_2, ZrO_2 and $Ce_{0.5}Zr_{0.5}O_2$) catalysts were synthesized by hydrothermal method and characterized by characterization techniques and tested for direct conversion of CO_2 with methanol in presence of activated molecular sieve 3A as dehydrating agent.
- CeO_2 catalysts showed reflexes of cubic phase with average crystalline sizes 7.09 nm, ZrO_2 catalysts showed reflexes of tetragonal phase with average crystalline sizes 9.45 nm and $Ce_{0.5}Zr_{0.5}O_2$ showed tetragonal phase with average crystalline sizes 7.09 nm.
- BET surface area, basic site density, acidic site density followed the order ZrO_2 < CeO_2 < $Ce_{0.5}Zr_{0.5}O_2$.
- DMC yield was found to be highly dependent upon the both basicity and acidity of catalysts. $Ce_{0.5}Zr_{0.5}O_2$ catalysts showed better activity as compared to CeO_2 and ZrO_2 catalyst.
- Under optimized reaction condition of reaction temperature=120 °C, reaction time=24 h, catalysts dose=1.25 g with pressure=150 bar, optimum yield of DMC was obtained as 2.56 mmol/g-cat for $Ce_{0.5}Zr_{0.5}O_2$.

5.1.2.2. Ceria-zirconium based catalysts (prepared by templating method)

- In this section of the work is, cerium-zirconium mixed oxides catalysts were prepared using with endo- and exotemplate to generate a hierarchically structured system. Polymer based activated carbon spheres were used as exo-template, and pluronic was used as endo-template.
- Basic site density of the synthesized catalysts was in the same order as catalytic activity: ZrO_2 (0.40 mmol/g) < CeO_2 (0.41 mmol/g) < $Ce_{0.5}Zr_{0.5}O_2$ (1.93 mmol/g), and the basic site density per unit area followed the same order of the activity of the catalysts such as: ZrO_2 (0.912 mmol DMC/g cat.) < CeO_2 (1.384 mmol DMC/g.cat.) < $Ce_{0.5}Zr_{0.5}O_2$ (2.921 mmol DMC/g cat.).
- The Ce_x-Zr_{1-x} (x=0.5) catalyst showed the highest basic sites and acidic site among all the catalysts, and giving the highest DMC yield.

5.1.2.3. Ceria-Manganese based catalysts (prepared by surfactant templating method)

- MnO_x-CeO_2 catalysts were synthesized by surfactant-template method with different ratio of Mn/Ce. Synthesized catalysts were characterized by various methods; and the

catalytic activity and reusability of the best performing catalyst was studied for the formation of DMC.

- Total basicity and acidity decreased with an increase in the manganese in the catalyst, and Ce_1-$Mn_{0.125}$ catalyst was found to possess the highest amount of total basic and acidic sites. Acidity and basicity of the catalyst was in the fallow same order such as: Ce_1-Mn_1 < Ce_1-$Mn_{0.25}$ < Ce_1-$Mn_{0.125}$.

5.1.2.4. Ceria- Calcium based catalysts (prepared by surfactant templating method)

- A series of CeO_2-CaO catalysts with different Ce/Ca ratio (Ce_3-Ca_1, Ce_1-Ca_1, and Ce_1-Ca_3) were synthesized by surfactant-template method. Hexadecyltrimethyl ammonium bromide (CTAB) was used as the template.
- Ce_1-Ca_1 catalyst was found to possess highest activity owing to its high surface area, acidity and basicity as compared to other catalysts.

5.1.2.5. Comparative Analysis

Table 4.5.2 summarizes the optimum reaction parameters for direct conversion of CO_2 with methanol reaction by Ce-Zr, Ce-Mn and Ce-Ca catalysts. The values of the heat of reaction (ΔH_r^o) and Gibbs free energy change (ΔG_r^o) for $Ce_{0.5}Zr_{0.5}O_2$ (hydrothermal method) using the data points at T=120-150^oC were found to be -45.66 kJ/mol and 25.04 kJ/mol, respectively. Similarly, for $Ce_{0.5}Zr_{0.5}O_2$ (templating method), the respective values were found to be -139.76 kJ/mol and 1.54 kJ/mol, respectively. Overall, Ce_1-Ca_1 and $Ce_{0.5}Zr_{0.5}O_2$ were the best catalysts for direct CO_2 conversion reaction for DMC production.

5.2. RECOMMENDATIONS

On the basis of the present research, some areas were identified that are worthy of further study so as to provide more support for the development of the technology at industrial scale. Following recommendations are made for future studies:

- Catalyst synthesis method strongly influences the physico-chemical properties of catalyst. It would therefore be of interest to explore other synthesis methods and catalytic materials that should maintain high activity for longer time.
- Experiments need to be carried out in continuous reactor for both transesterification reaction and CO_2 utilization reactions.
- Methods need to devised for enhance the CO_2 conversion despite the thermodynamic limitations of CO_2, utilization reactions for synthesizing DMC.

REFERENCES

Abrams D.S., Prausnitz J.M. Statistical thermodynamics of liquid mixture: A new expression for the excess Gibbs energy of partly or complete miscible systems. AIChE J. 1975, 21, 116−128.

Akondi A.M., Kantam M.L., Trivedi R., Sreedhar B., Buddana S.K., Prakasham R.S., Bhargava S. Formation of benzoxanthenones and benzochromenones via cerium-impregnated-MCM-41 catalyzed, solvent-free, three-component reaction and their biological evaluation as anti-microbial agents. J. Mol. Catal. A-Chem. 2014, 386, 49-60.

Almusaiteer K.A., Al-Mayman A.I., Alzeghayer Y.S.Z. Synthesis of dimethyl carbonate carbon dioxide and methanol. US20110196167A1.

Anderson S.A., Root T.W. Investigation of the effect of carbon monoxide on the oxidative carbonylation of methanol to dimethyl carbonate over Cu+X and Cu+ZSM-5 zeolites. J. Mol. Catal. A: Chem. 2004, 220, 247-255.

Aouissi A., Apbett A.W., Al-Othman Z.A., Al-Amro A. Direct synthesis of dimethyl carbonate from methanol and carbon dioxide using heteropolyoxometalates: the effects of cation and addenda atoms. Transition Met. Chem. 2010, 35, 927–931.

Aresta M., Galatola M. Life cycle analysis applied to the assessment of the environmental impact of alternative synthetic processes. The dimethylcarbonate case: part 1. J. Cleaner Production 1999, 7, 181-193.

Aristizábal A., Kolafa M., Contreras S., Dominguez M., Llorca J., Barrabes N., Tichit D., Medina F. Catalytic activity and characterization of Pt/calcined CuZnAl hydrotalcites in nitrate reduction reaction in water. Catal.Today 2011, 175, 370–379.

Bahranowski K., Dula R., Gąsior M., Labanowska M., Michalik A., Vartikian L.A., Serwicka E. Oxidation of aromatic hydrocarbons with hydrogen peroxide over Zn,Cu,Al-layered double hydroxides. Appl. Clay Sci. 2001, 18, 93-101.

Bain J., Wei X.W., Jin Y.R., Wang L., Luan D.C., Guan Z.P. Direct synthesis of dimethyl carbonate over activated carbon supported Cu-based catalysts. Chem. Eng. J. 2010, 165, 686-692.

Ballivet-Tkatchenko D., Chambrey S., Keiski R., Ligabue R., Plasseraud L., Richard P., Turunen H. Direct synthesis of dimethyl carbonate with supercritical carbon dioxide:

Characterization of a key organotin oxide intermediate. Catal. Today 2006, 115, 80-87.

Ballivet-Tkatchenko D., Santos J.H.Z.D, Philippot K., Vasreddy S. Carbon dioxide conversion to dimethyl carbonate: The effect of silica as support for SnO_2 and ZrO_2 catalysts. C.R. Chimie 2011, 14, 780-785.

Banerjee D., Jagadeesh R.V., Junge K, Pohl M.M., Radnik J., Brueckner A., Beller M. Convenient and mild epoxidation of alkenes using heterogeneous cobalt oxide catalysts. Angewandte Chemie-Int. Edi. 2014, 53, 4359-4363.

Barret E.P., Joyner L.G., Hanlenda P.P. The Determination of Pore Volume and Area Distributions in Porous Substances. I. Computations from Nitrogen Isotherms., J. Am. Chem. Soc.1951, 73, 373-380.

Barroso M.N., Gomez M.F., Gamboa J.A., Arrúa L.A., Abello M.C. Preparation and characterization of CuZnAl catalysts by citrate gel process. J. Phys. Chem. Solids. 2006, 67, 1583–1589.

Bellière V., Joorst G., Stephan O., Groot D.F.M.F., Weckhuysen B.M. Phase segregation in cerium−lanthanum solid solutions. J. Phys. Chem. B 2006, 110, 9984–9990.

Bergadà O., Vicente I., Salagre P., Ceteros Y., Medina F., Sueiras J.E. Microwave effect during aging on the porosity and basic properties of hydrotalcites. Micropor. Mesopor. Mat. 2007, 101, 363–373.

Bhanage B.M., Fujita S.I., He Y., Ikushima Y., Shirai M., Torii K., Arai M. Concurrent synthesis of dimethyl carbonate and ethylene glycol via transesterification of ethylene carbonate and methanol using smectite catalysts containing Mg and/or Ni. Catal. Lett. 2002, 83, 137-141.

Bhanage B.M., Fujita S.I., Ikushima Y., Arai M. Synthesis of dimethyl carbonate and glycols from carbon dioxide, epoxides, and methanol using heterogeneous basic metal oxide catalysts with high activity and selectivity. Appl. Catal. A: Gen. 2001, 219, 259–266.

Bharali P., Saikia P., Katta L., Reddy B.M. Enhancement in CO oxidation activity of nanosized $Ce_xZr_{1-x}O_2$ solid solutions by incorporation of additional dopants. J. Ind. Eng. Chem. 2013, 19, 327–336.

Bian J., Wei X.W., Wang L., Guan Z.P. Graphene nanosheet as support of catalytically active metal particles in DMC synthesis. Chinese Chem. Lett. 2011, 22, 57–60.

Bian J., Xiao M., Wang S., Lu Y., Meng Y. Direct synthesis of DMC from CH_3OH and CO_2 over V-doped Cu–Ni/AC catalysts. Catal. Commun. 2009, 10, 1142–1145.

Bian J., Xiao M., Wang S., Wang X., Lu Y., Meng Y. Highly effective synthesis of dimethyl carbonate from methanol and carbon dioxide using a novel copper–nickel/graphite bimetallic nanocomposite catalyst. Chem. Eng. J. 2009, 147, 287-296.

Blanch-Raga N., Palomares A.E., Martinez-Triguero J. Fetter G., Bosch P. Cu Mixed oxides based on hydrotalcite-like compounds for the oxidation of trichloroethylene. Ind. Eng. Chem. Res. 2013, 52, 15772–15779.

Brito A., Borges M.E., Garín M., Hernández A. Biodiesel production from waste oil using Mg−Al layered double hydroxide catalysts. Energ. Fuels 2009, 23, 2952–2958.

Brunauer S., Deming L.S., Deming W.E., Teller E. On a theory of the vanderwaals adsorption of gases. J Am Chem Soc 1940, 62, 1723-1732.

Brunauer S., Emmet P.H., Teller F. Adsorption of gases in multimolecular layers. J. Am. Chem. Soc. 1938, 60, 309-319.

Busca G., Costantiono U., Marnottini F., Montanari T., Patrono P., Pinzari F., Ramis G. Methanol steam reforming over ex-hydrotalcite Cu–Zn–Al catalysts. Appl. Catal. A: Gen. 2006, 310, 70-78.

Bustamente F., Orrego A.F., Villegas S., Villa A.L. Modeling of chemical equilibrium and gas phase behavior for the direct synthesis of dimethyl carbonate from CO_2 and methanol. Ind. Eng. Chem. Res. 2012, 51, 8945−8956.

Cai Q., Jin C., Lu B., Tangbo H., Shan Y. Synthesis of dimethyl carbonate from methanol and carbon dioxide using potassium methoxide as catalyst under mild conditions. Catal. Lett. 2005, 103, 3–4.

Cai Q., Lu B., Guo L., Shan Y. Studies on synthesis of dimethyl carbonate from methanol and carbon dioxide. Catal. Commun 2009, 10, 605–609.

Cao W., Zhang H., Yuan Y. $CuCl_2$ immobilized on amino-functionalized MCM-41 and MCM-48 as efficient heterogeneous catalysts for dimethyl carbonate synthesis by vapor-phase oxidative carbonylation of methanol. Catal. Lett. 2003, 91, 243-246.

Cao Y., Yang P., Yao C.Z., Yi N., Feng W.L., Dai W.L., Fan K.N. Impact of preparation strategy on the properties of carbon-supported Wacker-type catalysts in vapor-phase dimethyl carbonate synthesis. Appl. Catal. A: Gen.2004, 272, 15-22.

Centi G., Perathoner S. Catalysis by layered materials: A review. Micropor. Mesopor. Mat. 2008, 107, 3–15.

Chang H., Chen X., Li J., Ma L., Wang C., Liu C., Schwank J.W., Hao J. Improvement of activity and SO_2 tolerance of Sn-modified MnO_x−CeO_2 catalysts for NH_3-SCR at low temperatures. Environ. Sci. Technol. 2013, 47, 5294−5301.

Chang Y., Jiang T., Han B., Liu Z., Wu W., Gao L., Li J., Gao H., Zhao G., Huang J. One-pot synthesis of dimethyl carbonate and glycols from supercritical CO_2, ethylene oxide or propylene oxide, and methanol. Appl. Catal. A: Gen. 2004, 263, 179-186.

Chen H., Sayari A., Adnot A., Larachi F. Composition–activity effects of Mn–Ce–O composites on phenol catalytic wet oxidation. Appl. Catal. B: Environ. 2001, 32, 195–204.

Chen L., Wang S., Zhou J., Shen Y., Zhao Y., Ma X. Dimethyl carbonate synthesis from carbon dioxide and methanol over CeO_2 versus over ZrO_2: comparison of mechanisms. RSC Adv. 2014, 4, 30968-30975.

Chu G.H., Park J.B., Cheong M. Synthesis of dimethyl carbonate from carbon dioxide over polymer-supported iodide catalysts. Inorganica. Chimica. Acta 2000, 307, 131–133.

Cui H., Wang T., Wang F., Gu C., Wang P., Dai Y. Kinetic study on the one-pot synthesis of dimethyl carbonate in supercritical CO_2 conditions. Ind. Eng. Chem. Res. 2004, 43, 7732-7739.

Cui H., Zayat M. Levy D. Nanoparticle synthesis of willemite doped with cobalt ions ($Co_{0.05}Zn_{1.95}SiO_4$) by an epoxide-assisted sol−gel method. Chem. Mater. 2005, 17, 5562-5566.

Cui Z.M., Chen Z., Cao C.Y., Song W.G., Jiang L. Coating with mesoporous silica remarkably enhances the stability of the highly active yet fragile flower-like MgO catalyst for dimethyl carbonate synthesis. Chem. Commun. 2013, 49, 6093-6095.

Cunha A.F., Wu Y.Y., Santos J, Rodrigues A.E. Steam reforming of ethanol on copper catalysts derived from hydrotalcite-like materials. Ind. Eng. Chem. Res. 2012, 51, 13132-13143.

Dai Y., Wang X., Dai Q., Li D. Effect of Ce and La on the structure and activity of MnO_x catalyst in catalytic combustion of chlorobenzene. Appl. Catal. B: Environ. 2012, 111-112, 141-149.

Dave C.D., Pant K.K. Renewable hydrogen generation by steam reforming of glycerol over zirconia promoted ceria supported catalyst. Renew Energy 2011, 36, 3195-3202.

De C., Lu B., Lv H., Yu Y., Bai Y., Cai Q. One-pot synthesis of dimethyl carbonate from methanol, propylene oxide and carbon dioxide over supported choline hydroxide/MgO. Catal. Lett. 9, 128, 459-464.

Delimaris D., Loannides T. VOC oxidation over MnO_x-CeO_2 catalysts prepared by a combustion method. Appl. Catal. B: Environ. 2008, 84 303–312.

Delledonne D., Rivetti F., Romano U. Developments in the production and application of dimethylcarbonate. Appl. Catal. A: Gen. 2001, 221, 241–251.

Deshpande A.S., Niederberger M. Synthesis of mesoporous ceria zirconia beads. Micropor. Mesopor. Mat. 2007, 101, 413-418.

Dhachapally N., Kalevaru V.N., Brueckner A., Martin A. Metal vanadate catalysts for the ammoxidation of 2-methylpyrazine to 2-cyanopyrazine. Appl. Catal. A: Gen. 2012, 443, 111-118.

Dharman M.M., Ju H.Y., Shim H.L., Lee M.K., Kim K.H., Park D.W. Significant influence of microwave dielectric heating on ionic liquid catalyzed transesterification of ethylene carbonate with methanol. J. Mol. Catal. A: Chem. 2009, 303, 96–101.

Dhuri S.M., Mahajani V.V. Studies in transesterification of ethylene carbonate to dimethyl carbonate over Amberlyst A-21 catalyst. J. Chem. Tech. Biotech. 2006, 81, 62-69.

Ding X., Dong X., Kuang D., Wang S., Zhao X., Wang Y. Highly efficient catalyst $PdCl_2$–$CuCl_2$–KOAc/AC@Al_2O_3 for gas-phase oxidative carbonylation of methanol to dimethyl carbonate: Preparation and reaction mechanism. Chem. Eng. J. 2014, 240, 221-227.

Dixit M., Mishra M., Joshi P.A., Shah D.O. Physico-chemical and catalytic properties of Mg–Al hydrotelcite and Mg–Al mixed oxide supported copper catalysts. J. Ind. Eng. Chem. 2013, 19, 458-468.

Dong Q., Yin S., Guo C., Kimura T., Sato T. Hydrothermal synthesis of tin doped ceria-zirconia solid solutions with enhanced thermal stability and oxygen storage capacity. RSC Adv. 2012, 2, 12770–12774.

Dong W.S., Zhaou X., Xin C., Liu C., Liu Z. Ionic liquid as an efficient promoting medium for synthesis of dimethyl carbonate by oxidative carbonylation of methanol. Appl. Catal. A: Gen. 2008, 334, 100-105.

Drake I.J., Fujdala K.L., Bell A.T., Tilley T.D. Dimethyl carbonate production via the oxidative carbonylation of methanol over Cu/SiO_2 catalysts prepared via molecular

precursor grafting and chemical vapor deposition approaches. J. Catal. 2005, 230, 14-27.

Drake I.J., Zhang Y., Briggs D., Lim B., Chau T., Bell A.T. The local environment of Cu+ in Cu-Y zeolite and its relationship to the synthesis of dimethyl carbonate. J Phys. Chem. B 2006, 11654-11664.

Du G.F., Guo H., Wang Y., Li W.J., Shi W.J., Dai B. N-heterocyclic carbene catalyzed synthesis of dimethyl carbonate via transesterification of ethylene carbonate with methanol. J. Saudi Chemi. Soc. 2015, 19, 112–115.

Du M., Li Q., Dong W., Geng T., Jaing Y. Synthesis of glycerol carbonate from glycerol and dimethyl carbonate catalyzed by K_2CO_3/MgO. Res. Chem. Intermed. 2012, 38, 1069-1077.

Dubey P.K., Tripathi P., Tiwari R.S., Sinha A.S.K. Srivastava O.N. Synthesis of reduced graphene oxide–TiO_2 nanoparticle composite systems and its application in hydrogen production. Int. J. Hyd. Energ. 2014, 39, 16282–16292.

Engeldinger J., Domke C., Richter M., Bentrup U. Elucidating the role of Cu species in the oxidative carbonylation of methanol to dimethyl carbonate on CuY: An in situ spectroscopic and catalytic study. Appl. Catal. A: Gen. 2010, 382, 303-311.

Epifani M., Andreu T., Abdollahzadeh-Ghom S., Arbiol J., Morante J.R. Synthesis of ceria–zirconia nanocrystals with improved microstructural homogeneity and oxygen storage capacity by hydrolytic sol–gel process in coordinating environment. Adv. Funct. Mat. 2012, 22, 2867–2875.

Eta V., Maki-Arvela P., Salminen E., Salmi T., Murzin D.Y., Mikkola J.P. The effect of alkoxide ionic liquids on the synthesis of dimethyl carbonate from CO_2 and methanol over ZrO_2–MgO. Catal. Lett. 2011, 141, 1254–1261.

Fan B., Li H., Fan W., Zhang J., Li R., Organotin compound immobilized on mesoporous silicas as heterogeneous catalysts for direct synthesis of dimethyl carbonate from methanol and carbon dioxide. Appl. Catal. A: Gen. 2010, 372, 94–102.

Fan B., Zhang J., Li R., Fan W. In situ preparation of functional heterogeneous organotin catalyst tethered on SBA-15. Catal. Lett. 2008, 121, 297–302.

Fang S., Fujimoto K. Direct synthesis of dimethyl carbonate from carbon dioxide and methanol catalyzed by base. Appl. Catal. A: Gen. 1996, 142, L1-L3.

Filippis P.D., Borgianni C., Paolucci M. Rapeseed oil transesterification catalyzed by sodium phosphates. Energ. Fuels, 2005, 19, 2225–2228.

Filippis P.D., Scarsella M., Borgianni C., Pochetti F. Production of dimethyl carbonate via alkylene carbonate transesterification catalyzed by basic salts. Energ. Fuels 2006, 20, 17-20.

Fuentes R.O., Baker R.T. Synthesis of nanocrystalline CeO_2-ZrO_2 solid solutions by a citrate complexation route: A thermochemical and structural study. J. Phys. Chem. C 2009, 113, 914–924.

Funakawa A., Yamanaka I., Otsuka K. Active control of methanol carbonylation selectivity over Au/carbon anode by electrochemical potential. J. Phys. Chem. B 2005, 109, 9140-9147.

Gao P., Li P., Zhan H., Zhao N., Xaio F., Wei W., Zhong L., Wang H., Sun Y. Influence of Zr on the performance of Cu/Zn/Al/Zr catalysts via hydrotalcite-like precursors for CO_2 hydrogenation to methanol. J. Catal. 2013, 298, 51–60.

Gao Y., Xu C. Synthesis of dimethyl carbonate over waste eggshell catalyst. Catal. Today 2012, 190, 107-111.

Ge Y., Dong Y., Wang S., Zhao Y., Lv J., Ma X. Influence of crystalline phase of Li-Al-O oxides on the activity of Wacker-type catalysts in dimethyl carbonate synthesis. Front. Chem. Sci. Eng. 2012, 6, 415–422.

Ghirardini M., Nardo L.D., Novello E. Process for the production of high-purity dimethyl carbonate. US20120283464A1 and EP20100790588.

Gmehling J., Onken U., Alcohols. Dechema, Frankfurt am Main, 2007.

Gmehling J., Onken U., Arlt W. Organic Hydroxy Compounds: Alcoholsnkfurt am main, 1982a.

Gmehling J., Onken U., Grenzheuser P, Arlt W. Carboxylic acids, Anhydrides, Esters Dechema, Frankfurt am Main, 1982b.

Goepel M., Al-Naji M., With P., Wagner G., Oeckler O., Enke D., Glaser R. Hydrogenation of p-nitrophenol to p-aminophenol as a test reaction for the catalytic activity of supported Pt catalysts. Chem. Eng. Technol. 2014, 37,551-554.

Gorrepati E.A., Wongthahan P., Raha S., Fogler H.S. Silica precipitation in acidic solutions: mechanism, pH effect, and salt effect. Langmuir, 2010, 26, 10467–10474.

Grun M., Kurgabov A.A., Schacht S., Schuth F. Unger K.K. Comparison of an ordered mesoporous aluminosilicate, silica, alumina, titania and zirconia in normal-phase high-performance liquid chromatography. J. Chromatogr. A. 1996, 740, 1-9.

Halsey G.D. Physical adsorption on non-uniform surfaces, J. Chem. Phys. 1948, 16, 931–937.

Han M.S., Lee B.G., Ahn B.S., Kim H.S., Moon D.J., Hong S.I. The role of copper chloride hydroxides in the oxidative carbonylation of methanol for dimethyl carbonate synthesis. J. Mol. Catal. A: Chem. 2003, 203, 137-143.

Han M.S., Lee B.G., Ahn B.S., Park K.Y., Hong S.I. Kinetics of dimethyl carbonate synthesis from ethylene carbonate and methanol using alkali-metal compounds as catalysts. React. Kinet. Catal. Lett. 2001, 73, 33-38.

He L., Cheng H., Liang G., Yu Y., Zhao F. Effect of structure of $CuO/ZnO/Al_2O_3$ composites on catalytic performance for hydrogenation of fatty acid ester. Appl. Catal. A: Gen. 2013, 452, 88-93.

He X., Li Z., Su K., Cheng B., Ming J. Study on the reaction between bisphenol A and dimethyl carbonate over organotin oxide. Catal. Commun. 2013, 33, 20-23.

He Y., Yu X, Li T., Yan L., Yang B. Preparation of CeO_2/ZnO nanostructured microspheres and their catalytic properties. Powder Technol. 2006, 166, 72–76.

Heracleous E., Liakakou E.T., Lappas A.A., Lemonidou A.A. Investigation of K-promoted Cu-Zn-Al, Cu-X-Al and Cu-Zn-X (X=Cr, Mn) catalysts for carbon monoxide hydrogenation to higher alcohols. Appl. Catal. A: Gen. 2013, 455, 145–154.

Hofmann H.J., Brander A., Claus P. Direct Synthesis of dimethyl carbonate by carboxylation of methanol on ceria-based mixed oxides. Chem. Eng. Technol. 2012, 35, 2140–2146.

Holtbruegge J., Leimbrink M., Lutze P., Górak A. Synthesis of dimethyl carbonate and propylene glycol by transesterification of propylene carbonate with methanol: Catalyst screening, chemical equilibrium and reaction kinetics. Chem. Eng. Sci. 2013, 104, 347–360.

Honda M., Tamura M., Nakagawa Y., Nakao K., Suzuki K., Tomishige K. Organic carbonate synthesis from CO_2 and alcohol over CeO_2 with 2-cyanopyridine: Scope and mechanistic studies. J. Catal. 2014, 318, 95-107.

Honda M., Tamura M., Nakagawa Y., Sonehara S., Suzuki K., Fujimoto K.I, Tomishihe K. Ceria-catalyzed conversion of carbon dioxide into dimethyl carbonate with 2-cyanopyridine. ChemSusChem 2013, 6, 1341–1344.

Hou Z., Luo L., Liu K., Liu C., Wang Y., Dai L. High-yield synthesis of dimethyl carbonate from the direct alcoholysis of urea in supercritical methanol. Chem. Eng. J. 2014, 236, 415–418.

Houze E.C., Lewin L.A., Process for producing dimethyl carbonate containing compositions. US20100099806A1.

Hu J.C., Cao Y., Yang P., Deng J.F., Fan K.N. A novel homogeneous catalyst made of poly(N-vinyl-2-pyrrolidone)-$CuCl_2$ complex for the oxidative carbonylation of methanol to dimethyl carbonate. J. Mol. Catal. A: Chem. 2002, 185, 1-9.

Hua-yan Z., Jun R., Yuan Z., Yan-Yan N., Zhong L. Preparation of Cu^{+}/SiO_2-ZrO_2 catalysts for the oxidative carbonylation of methanol to dimethyl carbonate. J. Fuel Chem. Tech. 2011, 39, 282-286.

Ikeda Y., Asadullah M., Fujimoto K., Tomishige K. Structure of the active sites on H_3PO_4/ZrO_2 catalysts for dimethyl carbonate synthesis from methanol and carbon dioxide. J. Phys. Chem. B 2001, 105, 10653-10658.

Jagtap S.R., Bhor M.D., Bhanage B.M. Synthesis of dimethyl carbonate via transesterification of ethylene carbonate with methanol using poly-4-vinyl pyridine as a novel base catalyst. Catal. Commun. 2008, 9, 1928-1931.

Jentsch J.D., Klausenser A., Landscheidt H., Lenders B., Pennemann B., Wolters E., Zirngbiebl E. Process for the preparation of dimethyl carbonate. US005498744A.

Jeong E.S., Kim K.H., Park D.W., Park S.W., Lee J.W. Synthesis of dimethyl carbonate and propylene glycol from transesterification of propylene carbonate and methanol using quaternary ammonium salt catalysts. React. Kinet. Catal. Lett. 2005, 86, 241-248.

Jiang Q., Yang Y. The double component catalyst for the direct synthesis of dimethyl carbonate from carbon dioxide, propylene oxide and methanol. Catal. Lett. 2004, 95, 3-4.

Jiang R., Wang Y., Zhao X., Wang S., Jin C., Zhang C. Characterization of catalyst in the synthesis of dimethyl carbonate by gas-phase oxidative carbonylation of methanol. J. Mol. Catal. A: Chem. 2002, 185, 159-166.

Joe W., Lee H.J., Hong U.G., Ahn Y.S., Song C.J., Kwon B.J., Song I.K. Synthesis of dimethyl carbonate from urea and methanol over $ZnO(X)–CeO_2(1-X)$ catalysts prepared by a sol–gel method. J. Ind. Eng. Chem. 2012a, 18, 1018–1022.

Joe W., Lee H.J., Hong U.G., Ahn Y.S., Song C.J., Kwon B.J., Song I.K. Urea methanolysis to dimethyl carbonate over $ZnO–CeO_2–MO$ ($MO=La_2O_3$, Y_2O_3, Co_2O_3, Ga_2O_3 and ZrO_2) catalysts. J. Ind. Eng. Chem. 2012b, 18, 1730-1735.

Ju H.Y., Manju M.D., Lim K.H., Park S.W., Park D.W. Chemical fixation of carbon dioxide to dimethyl carbonate from propylene carbonate and methanol using ionic liquid catalysts. Korean J. Chem. Eng. 2007, 24, 917-919.

Juárez R., Corma A., García H. Gold nanoparticles promote the catalytic activity of ceria for the transalkylation of propylene carbonate to dimethyl carbonate. Green Chem. 2009, 11, 949-952.

Kaluza S., Behrens M., Schiefenhövel N., Kniep B., Fischer R., Schlögl R., Muhler M.A. Novel synthesis route for $Cu/ZnO/Al_2O_3$ catalysts used in methanol synthesis: combining continuous consecutive precipitation with continuous aging of the precipitate. ChemCatChem. 2011, 3, 189–199.

Keller N., Rebmann G., Keller V. Catalysts, mechanisms and industrial processes for the dimethylcarbonate synthesis. J. Mol. Catal. A: Chem. 2010, 317, 1–18.

Khobragade M., Majhi S., Pant K.K. Effect of K and CeO_2 promoters on the activity of Co/SiO_2 catalyst for liquid fuel production from syngas. Appl. Energy 2012, 94, 385-394.

Kim D.W., Kim C.W., Koh J.C., Park D.W. Synthesis of dimethyl carbonate from ethylene carbonate and methanol using immobilized ionic liquid on amorphous silica. J. Ind. Eng. Chem. 2010a, 16, 474-478.

Kim D.W., Lim D.O., Cho D.H., Koh J.C., Park D.W. Production of dimethyl carbonate from ethylene carbonate and methanol using immobilized ionic liquids on MCM-41. Catal. Today 2011, 164, 556-560.

Kim K.H., Kim D.W., Kim C.W., Koh J.C., Park D.W. Synthesis of dimethyl carbonate from transesterification of ethylene carbonate with methanol using immobilized ionic liquid on commercial silica. Korean J. Chem. Eng. 2010b, 27, 1441-1445.

Kishimoto Y., Ogawa I. Amine-catalyzed, one-pot coproduction of dialkyl carbonates and 1,2-diols from epoxides, alcohols, and carbon dioxide. Ind. Eng. Chem. Res. 2004, 43, 8155-8162.

Kizlink J. Synthesis of dimethyl carbonate from carbon dioxide and methanol in the presence of organotin compounds collect. Czech. Chem. Commun. 1993, 58, 1399-1402.

Kizlink J., Pastucha I. Preparation of dimethyl carbonate from methanol and carbon dioxide in the presence of Sn(IV) and Ti(IV) alkoxides and metal acetates collect. Czech. Chem. Commun. 1995, 60, 687-692.

Knifton J.F., Duranleau R.G. Ethylene glycol—dimethyl carbonate cogeneration. J. Mol. Catal. 1991, 67, 389–399.

Knifton J.F., Process for cosynthesis of ethylene glycol and dimethyl carbonate. US004661609.

Kobayashi K., Osora H., Seiki Y., Iijima M. Method and device for manufacturing dimethyl carbonate. US7605285B2, US20070037998A1and WO2004092109A1.

Kraiwattanawong K., Fogler H.S., Gharfeh S.G, Samir G. Singh P., Thomason W.H. Chavadej S. Effect of asphaltene dispersants on aggregate size distribution and growth. Energ. Fuel 2009, 23, 1575-1582.

Kraleva E., Palcheva R., Dimitrov L., Armbruster U., Brueckner A., Spojakina A. Solid acid catalysts for dehydration of glycerol to acrolein in gas phase. J Mat. Sci. 2011, 46, 7160-7168.

Kumar M., Awasthi R., Sinha A.S.K., Singh R.N. New ternary Fe, Co, and Mo mixed oxide electrocatalysts for oxygen evolution. Int. J. Hyd. Energy 2011, 36, 8831-8838.

Kumar S., Jain S.L. Polyethylene glycol enfolded KBr assisted base catalyzed synthesis of dimethyl carbonate from methanol and carbon dioxide. Ind. Eng. Chem. Res. 2014, 53 15798−15801.

Kumar S., Kumar P., Jain S.L. Graphene oxide immobilized copper phthalocyanine tetrasulphonamide: the first heterogenized homogeneous catalyst for dimethylcarbonate synthesis from CO_2 and methanol. J. Mater. Chem. A, 2014, 2, 18861-18866.

La K.W., Jung J.C., Kim H., Baeck S.H., Song I.K. Effect of acid–base properties of $H_3PW_{12}O_{40}/Ce_xTi_{1-x}O_2$ catalysts on the direct synthesis of dimethyl carbonate from methanol and carbon dioxide: A TPD study of of $H_3PW_{12}O_{40}/Ce_xTi_{1-x}O_2$ catalysts. J. Mole. Catal. A: Chem. 2007, 269, 41–45.

Landscheidt H., Wolters E., Wagner P., Klausenser A. Process for the preparation of dimethyl carbonate. US005543548A.

Laurenczy G., Picquet M., Plasseraud L. Di-n-butyltin(IV)-catalyzed dimethyl carbonate synthesis from carbon dioxide and methanol: An in situ high pressure 119Sn{1H} NMR spectroscopic study. J.Org. Chem. 2011, 696, 1904-1909.

Lee H.J., Joe W., Song I.K. Direct synthesis of dimethyl carbonate from methanol and carbon dioxide over transition metal oxide/$Ce_{0.6}Zr_{0.4}O_2$ catalysts: Effect of acidity and basicity of the catalysts. Korean J. Chem. Eng. 2012, 29, 317-322.

Lee H.J., Joe W., Song I.K. Direct synthesis of dimethyl carbonate from methanol and carbon dioxide over transition metal oxide/$Ce_{0.6}Zr_{0.4}O_2$ catalysts: Effect of acidity and basicity of the catalysts. Korean J. Chem. Eng. 2012, 29, 317-322.

Lee H.J., Park S., Song I.K., Jung J.C. Direct synthesis of dimethyl carbonate from methanol and carbon dioxide over $Ga_2O_3/Ce_{0.6}Zr_{0.4}O_2$ catalysts: effect of acidity and basicity of the catalysts. Catal. Lett. 2011, 141, 531-537.

Leino E., Mäki-Arvela P., Eta V., Murzin D.Y., Salmi T., Mikkola J.P. Conventional synthesis methods of short-chain dialkylcarbonates and novel production technology via direct route from alcohol and waste CO_2. Appl. Catal. A: Gen. 2010, 383, 1–13.

Li C.F., Zhong S.H. Study on application of membrane reactor in direct synthesis DMC from CO_2 and CH_3OH over Cu–KF/MgSiO catalyst. Catal. Today 2003, 82, 83–90.

Li J., Wang L., Shi F., Liu S., He Y., Lu L., Ma X., Deng Y. Quaternary ammonium ionic liquids as bi-functional catalysts for one-step synthesis of dimethyl carbonate from ethylene oxide, carbon dioxide and methanol. Catal. Lett. 2011, 141, 339–346.

Li R., Krcha M.D., Janik M.J., Roy A.D., Dooley K.M. Ce−Mn oxides for high-temperature gasifier effluent desulfurization. Energ. Fuel 2012, 26, 6765−6776.

Li Y., Zhao X.Q., Wang Y.J. Synthesis of dimethyl carbonate from methanol, propylene oxide and carbon dioxide over KOH/4A molecular sieve catalyst. Appl. Catal. A: Gen. 2005, 279, 205-208.

Lide D.R., Ed. Handbook of Chemistry and Physics. CRC Press, Taylor and Francis: Boca Raton, FL, 2010.

Liu Z., Yi Y., Zhang S., Zhu T., Zhu J., Wang J. Selective catalytic reduction of NO_x with NH_3 over Mn-Ce mixed oxide catalyst at low temperatures. Catal. Today 2013, 216, 76–81.

Luo H.P., Zhou J.H., Xiao W.D., Zhu K.H. Isobaric vapor−liquid equilibria of binary mixtures containing dimethyl carbonate under atmospheric pressure. J. Chem. Eng. Data, 2001, 46, 842–845.

Ma T.Y., Yuan Z.Y., Cao J.L. Hydrangea-like meso-/macroporous ZnO-CeO_2 binary oxide materials: synthesis, photocatalysis and CO oxidation. Eur. J. Inorg. Chem. 2010, 716–724.

Ma Z.Y., Yang C., Wei W., Li W.H., Sun Y.H. Surface properties and CO adsorption on zirconia polymorphs. J. Mol. Catal. A: Chem. 2005, 227, 119-124.

Maqbool T., Srikiratiwong P., Fogler H.S. Effect of temperature on the precipitation kinetics of asphaltenes. Energy Fuel 2011, 25, 694-700.

Mathuni T., Kim J.I., Park S.J. Phase equilibrium and physical properties for the purification of propylene carbonate (PC) and γ-butyrolactone (GBL). J. Chem. Eng. Data 2011, 56, 89–96.

Matsuzaki T. 99 Novel method for dimethyl carbonate synthesis using methyl nitrite. Stud. Surf. Sci. Catal. 2003, 145, 447-450.

Matsuzaki T., Nakamura. Dimethyl carbonate synthesis and other oxidative reactions using alkyl nitrites. Catal. Surv. Japan 1997, 1, 77-88.

Mehar L.C., Gopinath R., Naik S.N., Dalai A.K. Catalytic hydrogenolysis of glycerol to propylene glycol over mixed oxides derived from a hydrotalcite-type precursor. Ind. Eng. Chem. Res. 2009, 48, 1840-1846.

Meng X.L., Nie Y., Sun J., Cheng W.G., Wang J.Q., He H.Y., Zhang S.J. Functionalized dicyandiamide–formaldehyde polymers as efficient heterogeneous catalysts for conversion of CO_2 into organic carbonates. Green Chem. 2014, 16, 2771-2778.

Merza G., László B., Oszkó A., Pótári G., Baán K., Erdöhelyi A. The direct synthesis of dimethyl carbonate by the oxicarbonylation of methanol over Cu supported on carbon nanotube. J. Mol. Catal. A: Chem. 2014, 393, 117-124.

Mi J., Feng G., Han L., Guo T., Zhu Y., Wang J. Modified semi-coke-supported cerium oxide-doped zinc ferrites for the removal of H_2S from coal gas. Chem. Eng. Technol. 2012, 35, 9, 1626–1631.

Mishra B.G., Rao G.R. Promoting effect of ceria on the physicochemical and catalytic properties of CeO_2–ZnO composite oxide catalysts. J. Mol. Catal. A: Chem. 2006, 243, 204–213.

Mo W., Liu H., Xiong H., Li M., Li G. Preparation of CuCl/1,10-phenanthroline immobilized on polystyrene and catalytic performance in oxidative carbonylation of methanol. Appl. Catal. A: Gen. 2007, 333, 172-176.

Mo W., Xiong H., Li T., Guo X., Li G. The catalytic performance and corrosion inhibition of CuCl/Schiff base system in homogeneous oxidative carbonylation of methanol. J. Mol. Catal. A: Chem. 2006, 247, 227-232.

Murugan C., Bajaj H.C. Transesterification of propylene carbonate by methanol using Mg-Al-CO_3 hydrotelcite as solid base catalyst. Indian J. Chem. 2010b, 49A, 1182-1188.

Murugan C., Bajaj H.C., Jasra R.V. Transesterification of propylene carbonate by methanol using KF/Al_2O_3 as an efficient base catalyst. Catal. Lett. 137, 2010a, 224–231.

Nawaratna G., Fernando S.D. Reaction kinetics of transesterification with titanium alkoxide-based phase-transforming catalyst. Ind. Eng. Chem. Res. 52, 2013, 8392-8398.

Nawaratna G., Laceya R., Fernando S.D. Effect of hydrocarbon tail-groups of transition metal alkoxide based amphiphilic catalysts on transesterification. Catal. Sci. Technol. 2012, 2, 364-372.

Ono Y. Catalysis in the production and reactions of dimethyl carbonate, an environmentally benign building block, Appl. Catal. A: Gen. 1997, 155, 133–166.

Osora H., Kobayashi K., Seiki Y., Yasutake T., Iijima M. Methods for dimethyl carbonate synthesis. EP1623758B1.

Osora H., Kobayashi K., Seiki Y., Yasutake T., Iijima M., Oguchi A. Catalysts for dimethyl carbonate synthesis. US7674742B2.

Ouyang J., Jin J., Yang H., Tang A. A complex and de-complex strategy to ordered mesoporous $Ce_{0.5}Zr_{0..5}O_2$ with comprehensive pilot scale performances. Mat. Chem. Phy. 2014, 147, 1009-1015.

Pacheco M.A., Marshall C.L. Review of dimethyl carbonate (DMC) manufacture and its characteristics as a fuel additive. Energ. Fuel 1997, 11, 2-29.

Pandey D., Deo G. Promotional effects in alumina and silica supported bimetallic Ni-Fe catalysts during CO_2 hydrogenation. J. Mol. Catal. A: Chem. 2014, 382, 23-30.

Patel M., Jindal T.K., Pant K.K. Kinetic study of steam reforming of ethanol on Ni-based Ceria–Zirconia catalyst. Ind. Eng. Chem. Res. 2013, 52, 15763−15771.

Pavel O.D., Tichit D., Marcu I.C. Acido-basic and catalytic properties of transition-metal containing Mg–Al hydrotalcites and their corresponding mixed oxides. Appl. Clay Sci. 2012, 61, 52–58.

Piñeroa P., Garcíaa J., Sokolovab M., Cocero M.J. Modelling of the phase behaviour for the direct synthesis of dimethyl carbonate from CO_2 and methanol at supercritical or near critical conditions. The J. Chem. Thermodyn. 2007, 39, 536–549.

Potti P.R., Srivastava V.C. Comparative studies on structural, optical, and textural properties of combustion derived ZnO prepared using various fuels and their photocatalytic activity. Ind. Eng. Chem. Res. 2012, 51, 7948-7956.

Preising H., Enke D. Relations between texture and transport properties in the primary pore system of catalyst supports. Colloids and Surfaces A: Physicochem. Eng. Aspects, Colloid. Surf. A, 2007, 300, 21-29.

Priya S.S., Kumar P.V., Kantam M.L., Bhargava S.K., Chary K.V.R. Vapour-phase hydrogenolysis of glycerol to 1,3-propanediol over supported pt catalysts: the effect of supports on the catalytic functionalities. Catal. Lett. 2014, 144, 2129–2143.

Priya S.S., Kumar V.P., Kantam M.L., Bhargava S.K., Chary K.V.R. Catalytic performance of $Pt/AlPO_4$ catalysts for selective hydrogenolysis of glycerol to 1,3-propanediol in the vapour phase. RSC Adv. 2014a, 4, 51893-51903.

Priyanka, Subbaramaiah V., Srivastava V.C., Mall, I.D. Catalytic oxidation of nitrobenzene by copper loaded activated carbon. Sep. Purif. Technol. 2014, 125, 284–290.

Pu Z.Y., Lu J.Q., Luo M.F., Xie Y.L. Study of oxygen vacancies in $Ce_{0.9}Pr_{0.1}O_{2-\delta}$ solid solution by in situ X-ray diffraction and in situ Raman spectroscopy. J. Phys. Chem. C 2007, 111, 18695−18702.

Pyrlik A., Hoelderich W.F., Müller K., Arlt W., Strautmann J., Kruse D. Dimethyl carbonate via transesterification of propylene carbonate with methanol over ion exchange resins. Appl. Catal. B: Eviron. 2012, 125, 486-491.

Rabiah-Nizah M.F., Taufiq-Yap Y.H., Rashid U., Teo S.H., Nur Z.A.S., Islam A. Production of biodiesel from non-edible Jatropha curcas oil via transesterification using Bi_2O_3–La_2O_3 catalyst. Energ. Convers. Manage. 2014, 88, 1257-1262.

Rajgure A.V., Tarwal N.L., Patil J.Y., Chikhale L.P., Pawar R.C., Lee C.S., Mulla I.S., Suryavanshi S.S. Gas sensing performance of hydrothermally grown CeO_2–ZnO composites. Ceramic Int. 2014, 40, 5837-5842.

Ranade V.V., Kelkar A.A., Rane V.H., Kinage A.K., Shingote S.K., Roy L.S. Synthesis of dimethyl carbonate and related compounds. WO2014072802A2.

Reddy B.M., Saikia P., Bharali P. Highly dispersed $Ce_xZr_{1-x}O_2$ nano-oxides over alumina; silica and titania supports for catalytic applications. Catal. Surv. Asia 2008, 12, 214–228.

Ren J., Liu S., Li Z., Xie K. Oxidative carbony lation of meth anol to dimethyl carbonate over CuCl /SiO_2–TiO_2 catalysts prepared by microwave heating: The effect of support composition. Appl. Catal. A: Gen. 2009, 366, 93-101.

Ren J., Liu S., Li Z., Xie K. Structural feature and catalytic performance of Cu— SiO_2—TiO_2 cogelled xerogel catalysts for oxidative carbonylation of methanol to dimethyl carbonate. Catal. Commun. 2011, 12, 357-361.

Richter M., Fait M.J.G., Eckelt R., Schneider M., Radnik J., Heidemann D., Fricke R. Gas-phase carbonylation of methanol to dimethyl carbonate on chloride-free Cu-precipitated zeolite Y at normal pressure. J. Catal. 2007b, 245, 11-24.

Richter M., Fait M.J.G., Eckelt R., Schreier E., Schneider M., Pohl M.M., Fricke R. Oxidative gas phase carbonylation of methanol to dimethyl carbonate over chloride-free Cu-impregnated zeolite Y catalysts at elevated pressure. Appl. Catal. A: Environ. 2007a, 73, 269-281.

., Tojo J. Vapour–liquid equilibria of dimethyl carbonate with linear alcohols and estimation of interaction parameters for the UNIFAC and ASOG method. Fluid Phase Equilibria 2002, 201, 187–201.

Rodriguez - - . The behavior of mixed-metal oxides: Structural and electronic properties of $Ce_{1-x}Ca_xO_2$ and $Ce_{1-x}Ca_xO_{2-x}$. The J. Chem. Phys. 2003, 119, 5659-5669.

Roger J., Kailasam K., Thomas A. Covalent triazine frameworks as heterogeneous catalysts for the synthesis of cyclic and linear carbonates from carbon dioxide and epoxides. ChemSusChem 2012, 5, 1793-1799.

Romano U., Tesei R., Cipriani G., Micucci L. Method for the preparation of esters of carbonic acid. US 4218391 A.

Romano U., Tesel R., Mauri M.M., Rebora P. Synthesis of dimethyl carbonate from methanol, carbon monoxide, and oxygen catalyzed by copper compounds. Ind. Eng. Chem. Prod. Res. Dev. 1980, 19, 396–403.

Rossi P.F., Busca G., Lorenzelli V., Waqif M., Saw O., Lavalley J.C. Surface basicity of mixed oxides: magnesium and zinc aluminates. Langmuir 1991, 7, 2677-2681.

Rouquérol J., Avnir J.H., Fairbridge C.W., Everett D.H., Haynes J.H., Pernicone N., Ramsay J.D.F., Sing K.S.W., Unger K.K., Recomendation for the characterization of porous solids. Pure Appl. Chem. 1994, 66, 1739-1758.

Ruixia J., Shufang W., Xinqiang Z., Yanji W., Chengfang Z. The effects of promoters on catalytic properties and deactivation–regeneration of the catalyst in the synthesis of dimethyl carbonate. Appl. Catal. A: Gen.2003, 238, 131-139.

Sakakura T., Choi J.C., Yasuda H. Transformation of carbon dioxide. Chem. Rev. 2007, 107, 2365−2387.

Samiee L., Shoghi F. Vinu A. Fabrication and electrocatalytic application of functionalized nanoporous carbon material with different transition metal oxides. Appl. Surf. Sci. 2013, 265, 214-221.

Sandler S.I. Chemical, biochemical, and engineering thermodynamics. Wiley, Hoboken, 2006.

Sankar M., Nair C.M., Murty K.V.G.K., Manikandan P. Transesterification of cyclic carbonates with methanol at ambient conditions over tungstate-based solid catalysts. Appl. Catal. A: Gen. 2006, 312, 108–114.

Santos B.A.V., Pererira C.S.M., Silva V.M.T.M., Loureiro J.M., Rpdrigues A.E. Kinetic study for the direct synthesis of dimethyl carbonate from methanol and CO_2 over CeO_2 at high pressure conditions. Appl. Catal. A: Gen. 2013, 455, 219–226.

Sato M., Sukegawa T., Suzuki T. Kaneko K. Surface fractal dimension of less-crystalline carbon micropore walls. J. Phys. Chem. B. 1997, 101, 1845-1850.

Shee D., Deo G. Characterization and reactivity of TiO(2)/SiO(2) supported vanadium oxide catalysts. Catal. Lett. 2008, 124, 340-351.

Shee D., Deo G., Hirt A.M. Characterization and reactivity of sol–gel synthesized TiO_2–Al_2O_3 supported vanadium oxide catalysts. J. Catal. 2010, 273, 221-228.

Shen B., Wang F., Liu T. Homogeneous MnOx–CeO_2 pellets prepared by a one-step hydrolysis process for low-temperature NH_3-SCR. Powder Technol. 2014, 253, 152–157.

Shi Y., Li W., Tu J. Vapor-liquid equilibria for binary systems of methanol-isoamyl acetate, dimethyl carbonate-isoamyl acetate, and methanol-1,2-Propanediol at 101.325 kPa. J. Chem. Eng. Chinese Universities 1999, 13, 147-151.

Shiakh A.A.G., Sivaram S. Organic carbonates. Chem. Rev. 1996, 96, 951-976.

Si R., Zhang Y.W., Wang L.M., Li S.J., Lin B.X., Chu W.S., Wu Z.Y., Yan C.H. Enhanced thermal stability and oxygen storage capacity for $Ce_xZr_{1-x}O_2$ (x=0.4-0.6) solid solutions by hydrothermally homogenous doping of trivalent rare earths. J. Phys. Chem. C 2007, 111, 787-794.

Silva C.C.C.M., Ribeiro N.F.P., Souza M.V.M., Aranda D.A.G. Biodiesel production from soybean oil and methanol using hydrotalcites as catalyst. Fuel Process. Technol. 2010, 91, 205–210.

Sing K.S.W., Everett D.H., Haul R.A.W., Moscou L., Pierotti R.A., Rouquérol J., Siemieniewska T. Reporting physisorption data for gas/solid systems with special reference to the determination of surface area and porosity. Pure Appl. Chem. 1985, 57, 603-619.

Singh A.K., Fernando S.D. Transesterification of soybean oil using heterogeneous catalysts. Energ. Fuel 2008, 22, 2067–2069.

Singh D.P., Neti N.R., Sinha A.S.K., Srivastava O.N. Growth of different nanostructures of Cu_2O (nanothreads, nanowires, and nanocubes) by simple electrolysis based oxidation of copper. J. Phy. Chem. C 2007, 111, 1638-1645.

Souza M.M.V.M., Ferreira K.A., Neto O.R.D.M., Ribeiro N.F.P., Schmal M. Copper-based catalysts prepared from hydrotalcite precursors Hfor shift reaction at low temperatures. Catal. Today 2008, 133-135, 750-754.

Sparks D.E., Morgan T., Petterson P.M., Tackett S.A., Morris E., Crocker M. New sulfur adsorbent derived from layered double hydroxides I: synthesis and COS adsorption. Appl. Catal. B: Environ. 2008, 82, 190-198.

Srinivas D., Pulikkeel U. Process for making dimethyl carbonate. WO2013175510A1.

Srivastava R., Srinivas D., Ratnasamy P. Fe–Zn double-metal cyanide complexes as novel, solid transesterification catalysts. J. Catal. 2006, 241, 34-44.

Stoian D.C., Taboada E., Llorca J., Molins E., Medina F., Segarra A.M. Boosted CO_2 reaction with methanol to yield dimethyl carbonate over Mg–Al hydrotalcite-silica lyogels. Chem. Commun., 2013, 49, 5489-5491.

Stoica G., Abelló S., Pérez-Ramírez J. Synthesis of dimethyl carbonate by transesterification of ethylene carbonate over activated dawsonites. ChemSusChem 2009, 2, 301–304.

Strohmeier B.R., Levden D.E., Field R.S., Hercules D.M. Surface spectroscopic characterization of Cu/Al_2O_3 catalysts. J. Catal. 1985, 94, 514-530.

Sun J., Lu B., Wang X., Li X., Zhao J., Cai Q. A functionalized basic ionic liquid for synthesis of dimethyl carbonate from methanol and CO_2. Fuel Process. Technol. 2013, 115, 233–237.

Sun J., Yang B., Wang X., Wang D., Lin H. Synthesis of dimethyl carbonate from urea and methanol using polyphosphoric acid as catalyst. J. Mol. Catal. A: Chem. 2005, 239, 82-86.

Sun Y., Wei W., Zhao N., Sun B., Zhang B., Chen Y. Catalyst for the synthesis of dimethyl carbonate from urea and methanol, preparation and use thereof. US7271120B2, US2006004136A1 and EP1629888A1.

Sun Y.B., Cao C.Y., Yang S.L., Huang P.P., Wang C.R., Song W.G. C60 fullerenol as an active and stable catalyst for the synthesis of cyclic carbonates from CO_2 and epoxides. Chem. Commun. 2014, 50, 10307-10310.

Svec P., Olejník R., Padelková Z., Ruzicka A., Plasseraud L. C,N-chelated organotin(IV) trifluoromethanesulfonates: Synthesis, characterization and preliminary studies of its catalytic activity in the direct synthesis of dimethyl carbonate from methanol and CO_2. J. Organometallic Chem. 2012, 708-709, 82-87.

Tanabe K., Misono M., Ono Y., Hattori H. 2 Determination of acidic and basic properties on solid surfaces. Stud. Surf. Sci. Catal. 1989, 51, 5-25.

Taubert M., Beckmann J., Lange A., Enke D., Klepel O. Attempts to design porous carbon monoliths using porous concrete as a template. Micropor. Mesopor. Mat. 2014, 197, 58-62.

Thitsartarn W., Kawi S. An active and stable CaO-CeO_2 catalyst for transesterification of oil to biodiesel. Green Chem. 2011, 13, 3423–3430.

Tian J.S., Wang J.Q., Chen J.Y., Fan H.G., Cai F., He L.N. One-pot synthesis of dimethyl carbonate catalyzed by n-Bu_4NBr/n-Bu_3N from methanol, epoxides, and supercritical CO_2. Appl. Catal. A: Gen. 2006, 301, 215-221.

Tkatchenko D.B., Bernard F., Demoisson F., Plasseraud L., Sanapureddy S.R. Tin-based mesoporous silica for the conversion of CO_2 into dimethyl carbonate. ChemSusChem 2011, 4, 1316–1322.

Tomishige K., Ikeda Y., Sakaihori T., Fujimoto K. A novel method of direct synthesis of dimethyl carbonate from methanol and carbon dioxide catalyzed by zirconia. Catal. Lett. 1999b, 58, 225–229.

Tomishige K., Ikeda Y., Sakaihori T., Fujimoto K. Catalytic properties and structure of zirconia catalysts for direct synthesis of dimethyl carbonate from methanol and carbon dioxide. J. Catal. 2000, 192, 355-362.

Tomishige K., Kunimori K. Catalytic and direct synthesis of dimethyl carbonate starting from carbon dioxide using CeO_2-ZrO_2 solid solution heterogeneous catalyst: effect of H_2O removal from the reaction system. Appl. Catal. A: Gen. 2002, 237, 103-109.

Tomishige K., Sakaihori T., Sakai S.I., Fujimoto K. Dimethyl carbonate synthesis by oxidative carbonylation on activated carbon supported $CuCl_2$ catalysts: catalytic properties and structural change. Appl. Catal. A: Gen. 1999a, 181, 95-102.

Trujillano R., Holgado M.J., Pigazo F., Rives V. Preparation, physicochemical characterisation and magnetic properties of Cu–Al layered double hydroxides with CO_3^{2-} and anionic surfactants with different alkyl chains in the interlayer. Physica B, 2006, 373, 267–273.

Tundo P. New developments in dimethyl carbonate chemistry. Pure Appl. Chem. 2001, 73, 1117–1124.

Tundo P., Selva M. The chemistry of dimethyl carbonate. Acc. Chem. Res. 2002, 35, 706-716.

Uchiumi S., Ateka K., Matsuraki T. Oxidative reactions by a palladium–alkyl nitrite system. J. Organomet. Chem. 1999, 576, 279-289.

Unnikrishna P., Varhadia P., Srinivas D. Efficient, direct synthesis of dimethyl carbonate from CO_2 using a solid, calcined zirconium phenylphosphonate phosphite catalyst. RSC Adv., 2013, 3, 23993-23996.

Unnikrishnan P., Srinivas D. Calcined, rare earth modified hydrotalcite as a solid, reusable catalyst for dimethyl carbonate synthesis. Ind. Eng. Chem. Res. 2012, 51, 6356-6363.

Vélez R.P., González M.P.E., Bentrup U. Preparation and in situ spectroscopic characterization of Cu-clinoptilolite catalysts for the oxidative carbonylation of methanol. Micropor. Mesopor. Mat. 2012, 164, 93–98.

Venkataswamy P., Jampaiah D., Rao K.N., Reddy B.M. Nanostructured $Ce_{0.7}Mn_{0.3}O_{2-\delta}$ and $Ce_{0.7}Fe_{0.3}O_{2-\delta}$ solid solutions for diesel soot oxidation. Appl. Catal. A: Gen. 2014, 488, 1–10.

Venugopa A., Palgunadi J., Deog J.K., Joo O.S., Sjin C.H. Dimethyl ether synthesis on the admixed catalysts of Cu-Zn-Al-M (M=Ga, La, Y, Zr) and γ-Al2O3: The role of modifier. J. Mol. Catal. A: Chem. 2009, 302, 20-27.

Voß M., Borgmann D., Wedler G.J. Characterization of alumina, silica, and titania supported cobalt catalysts. Catal. 2002, 212, 10-21.

Wada S., Oka K., Watanable K., Izumi Y. Catalytic conversion of carbon dioxide into dimethyl carbonate using reduced copper-cerium oxide catalysts as low as 353 K and 1.3 MPa and the reaction mechanism. Front. Chem. 2013, 1, 1-8.

Wang D., Zhang X., Gao Y., Xiao F., Wei W. Sun Y. Synthesis of dimethyl carbonate from methyl carbamate and methanol over lanthanum compounds. Fuel Process. Technol. 2010, 91, 1081-1086.

Wang D., Zhang X., Gao Y., Xiao F., Wei W., Sun Y. Zn/Fe mixed oxide: Heterogeneous catalyst for the synthesis of dimethyl carbonate from methyl carbamate and methanol. Catal. Commun. 2010b, 11, 430–433.

Wang D., Zhang X., Wei W., Sun Y. Synthesis of dimethyl carbonate from methyl carbamate and methanol using a fixed-bed reactor. Chem. Eng. Technol. 2012a, 35, 2183-2188.

Wang D., Zhang X., Zhao W., Peng W Zhao N., Ziao F., Wei W., Sun Y. Synthesis of dimethyl carbonate from methyl carbamate and methanol catalyzed by mixed oxides from hydrotalcite-like compounds. J. Phys chem. Solids 2010d, 71, 427-430.

Wang H., Lu B., Wang X., Zhang J., Cai Q. Highly selective synthesis of dimethyl carbonate from urea and methanol catalyzed by ionic liquids. Fuel Process. Technol. 2009, 90, 1198–1201.

Wang H., Wang B., Liu C.L., Dong W.S. Oxidative carbonylation of methanol over copper ion-containing ionic liquids immobilized on SBA-15. Micropor. Mesopor. Mat. 2010a, 134, 51–57.

Wang H., Wang M., Liu S., Zhao N., Wei W. Sun Y. Influence of preparation methods on the structure and performance of $CaO–ZrO_2$ catalyst for the synthesis of dimethyl carbonate via transesterification. J. mol. Catal. A: Chem. 2006, 258, 308-312.

Wang H., Wang M., Zhang W., Zhao N., Wei W., Sun Y. Synthesis of dimethyl carbonate from propylene carbonate and methanol using $CaO–ZrO_2$ solid solutions as highly stable catalysts. Catal. Today 2006b, 115, 107-110.

Wang H., Wang M., Zhao N., Wei W., Sun Y. $CaO–ZrO_2$ Solid solution: A highly stable catalyst for the synthesis of dimethyl carbonate from propylene carbonate and methanol. Catal. Lett. 2005, 105, 253-257.

Wang H., Wang M., Zhao W., Wei W., Sun Y. Reaction of zinc oxide with urea and its role in urea methanolysis. Reac. Kinet. Mech. Cat. 2010e, 99, 381–389.

Wang J.Q., Cheng W.G., Sun J., Shi T.Y., Zhang X.P., Zhang S.J. Efficient fixation of CO_2 into organic carbonates catalyzed by 2-hydroxymethyl-functionalized ionic liquids. RSC Adv. 2014, 4, 2360-2367.

Wang J.Q., Sun J., Cheng W.G., Shi C.Y., Dong K., Zhang X.P., Zhang S.J. Synthesis of dimethyl carbonate catalyzed by carboxylic functionalized imidazolium salt via transesterification reaction. Catal. Sci. Technol. 2012b, 2, 600-605.

Wang L., Wang Y., Liu S., Lu L., Ma X. Deng Y. Efficient synthesis of dimethyl carbonate via transesterification of ethylene carbonate with methanol over binary zinc-yttrium oxides. Catal. Commun. 2011, 16, 45-49.

Wang M., Wang H., Zhao N., Wei W., Sun Y. Synthesis of dimethyl carbonate from urea and methanol over solid base catalysts. Catal. Commun. 2006a, 7, 6–10.

Wang M., Zhao N., Wei W., Sun Y. Synthesis of dimethyl carbonate from urea and methanol over metal oxides. Stud. Surf. Sci. Catal. 2004, 153, 197-200.

Wang M., Zhao N., Wei W., Sun Y. Synthesis of dimethyl carbonate from urea and methanol over ZnO. Ind. Eng. Chem. Res. 2005a, 44, 7596-7599.

Wang R., Crozier P.A., Sharma R. Nanoscale compositional and structural evolution in ceria zirconia during cyclic redox treatments. J. Mater. Chem. 2010, 20, 7497.

Wang R., Mutinda S. I., Fang M. One-pot hydrothermal synthesis and high temperature thermal stability of $Ce_xZr_{1-x}O_2$ nanocrystals. RSC Adv., 2013, 3, 19508-19514.

Wang S., Zhao L., Wang W., Zhao Y., Zhang G., Ma X., Gong J. Morphology control of ceria nanocrystals for catalytic conversion of CO_2 with methanol. Nanoscale, 2013, 5, 5582–5588.

Wang X.J., Xiao M., Wang S.J., Lu Y.X., Meng Y.Z. Direct synthesis of dimethyl carbonate from carbon dioxide and methanol using supported copper (Ni, V, O) catalyst with photo-assistance. J. Mol. Catal. A: Chem. 2007, 278, 92-96.

Watanabe Y., Tatsumi T. Hydrotalcite-type materials as catalysts for the synthesis of dimethyl carbonate from ethylene carbonate and methanol. Micropor Mesopor Mat. 1998, 22, 399–407.

Wei R.J., Zhang X.H., Du B.Y., Fan Z.Q., Qi G.R. Synthesis of bis(cyclic carbonate) and propylene carbonate via a one-pot carbonate via a one-pot coupling reaction of CO_2, bisepoxide and propylene oxide. RSC Adv. 2013, 3, 17307-17313.

Wei T., Wang M., Wei W., Sun Y., Zhong B. Effect of base strength and basicity on catalytic behavior of solid bases for synthesis of dimethyl carbonate from propylene carbonate and methanol. Fuel Process Technol. 2003b, 83, 175-182.

Wei T., Wang M., Wei W., Sun Y., Zhong B. Synthesis of dimethyl carbonate by transesterification over CaO/carbon composites. Green Chem. 2003a, 5, 343–346.

Wilkes M.F., Hayden P., Bhattacharya A.K. Surface segregation of lanthanum and cerium ions in ceria/lanthana solid solutions: comparison between experimental results and a statistical–mechanical model. Appl. Surf. Sci. 2003, 2006, 12-19.

Williams D.B.G., Sibiya M.S., Heerden P.S.V., Kirk M., Harris R. Verkade super base-catalysed transesterification of propylene carbonate with methanol to co-produce dimehyl carbonate and propylene glycol. J. Mol. Catal: Chem. 2009, 304, 147–152.

With P., Heinrich A., Lutecki M., Fichtner S., Böhringer B., Gläser R., Zirconia with defined particle morphology and hierarchically structured pore system synthesized via combined exo- and endotemplating. Chem. Eng. Technol. 2010, 33, 1712-1716.

Wu X., Kang M., Yin Y., Wang F., Zhao N., Xiao F., Wei W., Sun Y. Synthesis of dimethyl carbonate by urea alcoholysis over Zn/Al bi-functional catalysts. Appl. Catal. A: Gen. 2014a, 473, 13-20.

Wu X., Kang M., Zhao N., Wei W., Sun Y. Dimethyl carbonate synthesis over ZnO–CaO bi-functional catalysts. Catal. Commun. 2014b, 46, 46-50.

Wu X.L., Meng Y.Z., Xiao M., Lu Y.X. Direct synthesis of dimethyl carbonate (DMC) using Cu-Ni/VSO as catalyst. J. Mol. Catal. A: Chem. 2006, 249, 93–97.

Wu X.L., Xiao M., Meng Y.Z., Lu Y.X. Direct synthesis of dimethyl carbonate on H_3PO_4 modified V_2O_5. J. Mol. Catal. A: Chem. 2005, 238, 158-162.

Xian C.J., Bi J., Li D.W., Lin D., Ren C.L., Jie C.Z., Lian L.S., Biao L.X., Man T.X., Tong A.C. Catalytic fixation of CO_2 to cyclic carbonates over biopolymer chitosan-grafted quarternary phosphonium ionic liquid as a recylable catalyst. Appl. Catal. A: Gen. 2014, 484, 26-32.

Xie Q., Zhao Y., Guo H., Lu A., Zhang X., Wang L., Chen M.S., Peng D.L. Facile preparation of well-dispersed CeO_2−ZnO composite hollow microspheres with enhanced catalytic activity for CO oxidation. ACS Appl. Mater. Interfaces 2014, 6, 421−428.

Xu J., Long K.Z., Chen T., Xue B., Li Y.X., Cao Y. Meso-structured graphitic carbon nitride as a new base catalyst for the efficient synthesis of dimethyl carbonate by transesterification. Catal. Sci. Technol. 2013, 3, 3192-3199.

Xu J., Long K.Z., Wu F., Xue B., Li Y.X., Cao Y. Efficient synthesis of dimethyl carbonate via transesterification of ethylene carbonate over a new mesoporous ceria catalyst. Appl. Catal. A: Gen. 2014, 484, 1–7.

Yamamoto Y. Vapor phase carbonylation reactions using methyl nitrite over Pd catalysts. Catal. Surv. Asia 2010, 14, 103–110.

Yamamoto Y., Matsuzaki T., Tanaka S., Nishihira K., Ohdan K., Nakamura A., Okamoto. Catalysis and characterization of Pd/NaY for dimethyl carbonate synthesis from methyl nitrite and CO. J. Chem. Soc., Faraday Trans. 1997, 93, 3721-3727.

Yan C., Lu B., Wang X., Xhao J., Cai Q. Electrochemical synthesis of dimethyl carbonate from methanol, CO_2 and propylene oxide in an ionic liquid. J. Chem. Technol. Biotechnol. 2011, 86, 1413–1417.

Yang B., Wang D., Lin H., Sun J., wang X. Synthesis of dimethyl carbonate from urea and methanol catalyzed by the metallic compounds at atmospheric pressure. Catal. Commun. 2006, 7, 472-477.

Yang P., Cao Y., Hu J. C., Dai W.L., Dang J.F., Fan K.N. Effect of chemical treatment of activated carbon as a support for promoted dimethyl carbonate synthesis by vapor phase oxidative carbonylation of methanol over Wacker-type catalysts. Appl. Catal. A: Gen.2003b, 243, 323-331.

Yang P., Cao Y., Hu J.C., Dai W.L., Fan K.N. Mesoporous bimetallic $PdCl_2$-$CuCl_2$ catalysts for dimethyl carbonate synthesis by vapor phase oxidative carbonylation of methanol. Appl. Catal. A: Gen.2003a, 241, 363-373.

Yang Q., Wang H., Ding X., Yang X., Wang Y. One-pot synthesis of dimethyl carbonate from carbon dioxide, cyclohexene oxide, and methanol. Res. Chem. Intermed. 2015, 41, 4101-4111.

Yang Z.Z., He L.N., Dou X.Y., Chanfreau S. Dimethyl carbonate synthesis catalyzed by DABCO-derived basic ionic liquids via transesterification of ethylene carbonate with methanol. Tetrahedron Lett. 2010, 51, 2931–2934.

Yi, H., Zhao, S., Tang, X., Ning, P., Wang, H., He, D. Influence of calcination temperature on the hydrolysis of carbonyl sulfide over hydrotalcite-derived Zn–Ni–Al catalyst. Catal. Commun. 2011, 12, 1492–1495.

Ying L.A., Liu J., Mo L., Lou H., Zheng X. Hydrogen production by oxidative steam reforming of methanol over $Ce_{1-x}Zn_xO_y$ catalysts prepared by combustion method. Int. J. Hyd. Energy 2012, 37, 1002-1006.

Yoshida Y., Arai Y., Kado S., Kunimori K., Tomishige K. Direct synthesis of organic carbonates from the reaction of CO_2 with methanol and ethanol over CeO_2 catalysts. Catal. Today 2006, 115, 95-101.

Yu X., Wen Z., Li H., Tu S.T., Yan J. Transesterification of Pistacia chinensis oil for biodiesel catalyzed by $CaO–CeO_2$ mixed oxides. Fuel 2011, 90, 1868–1874.

Yuan D., Yan C., Lu B., Wang H., Zhong C., Cai Q. Electrochemical activation of carbon dioxide for synthesis of dimethyl carbonate in an ionic liquid. Electrochim. Acta 2009, 54, 2912-2915.

Zeppieri M., Villa P.L., Verdone N., Scarsella M., Filippis P.D. Kinetic of methane steam reforming reaction over nickel- and rhodium-based catalysts. Appl. Catal A: Gen 2010, 387, 147–154.

Zhang B., Li D., Wang X. Catalytic performance of La–Ce–O mixed oxide for combustion of methane. Catal. Today 2010, 158, 348-353.

Zhang C., Lu B., Wang X., Zhao J., Cai Q. Selective synthesis of dimethyl carbonate from urea and methanol over Fe_2O_3/HMCM-49. Catal. Sci. Technol. 2012, 2, 305–309.

Zhang J., Wang F., Wei W., Xiao F., SunY. Kinetics studies of dimethyl carbonate synthesis from urea and methanol over ZnO catalyst. Korean J. Chem. Eng. 2010, 27, 1744-1749.

Zhang S., Liu Q., Fan G., Li F. Highly-dispersed copper-based catalysts from Cu–Zn–Al layered double hydroxide precursor for gas-phase hydrogenation of dimethyl oxalate to ethylene glycol. Catal. Lett. 2012b, 142, 1121–1127.

Zhang Y., Bell A.T. The mechanism of dimethyl carbonate synthesis on Cu-exchanged zeolite Y. J. Catal. 2008, 255, 153-161.

Zhang Y., Briggs D.N., Smit E.D., Bell A.T. Effects of zeolite structure and composition on the synthesis of dimethyl carbonate by oxidative carbonylation of methanol on Cu-exchanged Y, ZSM-5, and Mordenite. J. Catal. 2007, 251, 443-452.

Zhang Y., Drake I.J., Briggs D.N., Bell A.T. Synthesis of dimethyl carbonate and dimethoxy methane over Cu-ZSM-5. J. Catal. 2006, 244, 219-229.

Zhang Z.F., Liu Z.T., Liu Z.W., Lu J. DMC formation over $Ce_{0.5}Zr_{0.5}O_2$ prepared by complex-decomposition method. Catal. Lett. 2009, 129, 428–436.

Zhang Z.F., Liu Z.W., Lu J. Liu Z.T. Synthesis of dimethyl carbonate from carbon dioxide and methanol over $Ce_xZr_{1-x}O_2$ and [EMIM]Br/$Ce_{0.5}Zr_{0.5}O_2$. Ind. Eng. Chem. Res. 2011, 50, 1981–1988.

Zhao B., Li G., Ge C., Wang Q., Zhou R. Preparation of $Ce_{0.67}Zr_{0.33}O_2$ mixed oxides as supports of improved Pd-only three-way catalysts. Appl. Catal. B: Environ. 2010, 96, 338–349.

Zhao H., Zhang G., Zhang Q. MnO_2/CeO_2 for catalytic ultrasonic degradation of methyl orange. Ultrason. Sonochem. 2014, 21, 991–996.

Zhao S., Yi H., Tang X., Song C. Low temperature hydrolysis of carbonyl sulfide using Zn–Al hydrotalcite-derived catalysts. Chem. Eng. J. 2013, 226, 161–165.

Zhao T., Han Y., Sun Y. Novel reaction route for dimethyl carbonate synthesis from CO and methanol. Fuel Process. Technol. 2000, 62, 187-194.

Zhao W., Wang F., Peng W., Zhao N., Li J., Xiao F., Wei W., Sun Y. Synthesis of dimethyl carbonate from methyl carbamate and methanol with zinc compounds as catalysts. Ind. Eng. Chem. Res. 2008, 47, 5913–5917.

Zheng X., Bell A.T. A theoretical investigation of dimethyl carbonate synthesis on Cu-Y zeolite. J. Phys. Chem. C 2008a, 112, 5043-5047.

Zheng X., Bell A.T. The mechanism of dimethyl carbonate synthesis on Cu-exchanged zeolite Y. J. Catal. 2008b, 255, 153-161.

Zheng, H.Y., Zhu, Y.L., Huang, L., Xiang, H.W. A new process for synthesis of γ-butyrolactone and cyclohexanone. Chem. Eng. Technol. 2007, 30, 621–627.

Zhong L., Ruiyu W., Huayan Z., Kechang X. Preparation of $Cu^{I}Y$ catalyst using $CuCl_2$ as precursor for vapor phase oxidative carbonylation of methanol to dimethyl carbonate. Fuel 2010, 89, 1339-1343.

Zhong S.L., Zhang L.F., Wang L., Huang W.X., Fan C.M., Xu A.W. Uniform and porous $Ce_{1-x}Zn_xO_{2-\delta}$ solid solution nanodisks: preparation and their CO oxidation activity. J. Phys. Chem. C 2012, 116, 13127−13132.

Zhou G., Lan H., Gao T., Xie H. Influence of Ce/Cu ratio on the performance of ordered mesoporous CeCu composite oxide catalysts. Chem. Eng. J. 2014, 246, 53-63.

Zhou G., Lan H., Yang X., Du Q., Xie H., Fu M. Effects of the structure of Ce–Cu catalysts on the catalytic combustion of toluene in air. Ceram. Int. 2013, 39, 3677-3683.

Zhou Y., Wang S., Xiao M., Han D., Lu Y., Meng Y. Novel Cu-Fe bimetal catalyst for the formation of dimethyl carbonate from carbon dioxide and methanol. RSC adv. 2012, 2, 6831-6837.

Zhu D., Mei F., Chen L., Li T., Mo W., Li G. Synthesis of dimethyl carbonate by oxidative carbonylation using an efficient and recyclable catalyst co-schiff base/zeolite. Energ. Fuel 2009, 23, 2359–2363.

PUBLICATIONS FROM THESIS

Papers Published in SCI (International) Journals

1. Praveen Kumar, Vimal Chandra Srivastava, Indra Mani Mishra. Synthesis and characterization of Ce–La oxides for formation of dimethyl carbonate by transesterification of propylene carbonate. Catalysis Communications 2015, 60, 27–31.
2. Praveen Kumar, Vimal Chandra Srivastava, Indra Mani Mishra. Dimethyl carbonate synthesis from propylene carbonate with methanol using Cu-Zn-Al catalyst. Energy Fuels 2015, 29, 2664–2675.
3. Praveen Kumar, Vimal Chandra Srivastava, Indra Mani Mishra. Synthesis and characterization of alumina, silica, and titania supported Ceria–Zinc catalysts for the production of dimethyl carbonate by transesterification of propylene carbonate. Korean Journal of Chemical Engineering 2015, DOI: 10.1007/s11814-015-0040-z.

Paper Communicated in SCI (International) Journals

1. Praveen Kumar, Vimal Chandra Srivastava, Indra Mani Mishra. Dimethyl carbonate synthesis by transesterification of propylene carbonate with methanol: comparative assessment of Ce-M (M=Co, Fe, Cu and Zn) Catalysts. Renewable Energy (Communicated, 2015).
2. Praveen Kumar, Patrick With, Vimal Chandra Srivastava, Roger Gläser, Indra Mani Mishra. Synthesis and characterization of Ceria-Zirconium oxides for dimethyl carbonate synthesis by direct conversion of CO_2. Journal of CO_2 utilization (Communicated, 2015).
3. Praveen Kumar, Vimal Chandra Srivastava, Kartikeya Shukla, Indra Mani Mishra. Direct conversion of carbon dioxide to dimethyl carbonate as green fuel over ceria nanocatalyst: Effect of active phase ratio on catalytic properties with different process conditions. Journal of Taiwan Inst. Chem. Eng. (Communicated, 2015).

Papers in Conferences

1. Vimal Chandra Srivastava, Praveen Kumar, Kartikeya Shukla, Indra Mani Mishra. Utilization of carbon-di-oxide for producing green alternative fuels: Environmentally sustainable method for producing energy. Paper presentation in 4th Annual International Conference on Sustainability (SUSCON-2015) at IIM Shilong; 11-13 March 2015. (Oral presentation).
2. Praveen Kumar, Vimal Chandra Srivastava, Indra Mani Mishra. Dimethyl carbonate synthesis catalyzed (Ce-Zn) with supported catalyst for transesterification of ethylene carbonate with methanol. Poster presentation in (CHEMFERENCE-2012) at IIT Bombay; 10-11 December 2012 (Poster presentation).
3. Praveen Kumar, Vimal Chandra Srivastava, Indra Mani Mishra; Preparation and Characterization of Ce-M (M=Co, Cu, Fe and Zn) catalysts for synthesis of dimethyl carbonate. Paper presentation in 65th Annual Session of the Indian Institute of Chemical Engineers (CHEMCON-2012) at NIT Jalandhar; 27-30 December 2012 (Oral presentation).
4. Praveen Kumar, Vimal Chandra Srivastava, Indra Mani Mishra; A critical review on production of dimethyl carbonate using various industrial processes. Paper presentation in 65th Annual Session of the Indian Institute of Chemical Engineers (CHEMCON-2012) at NIT Jalandhar; 27-30 December 2012 (Oral presentation).